A study of electrode-tissue impedances encountered in cardiac pacing

Volume two

Sub-title: Nonlinearity of the inter-electrode impedance and the study of electrode failures

ERIC THOMAS McADAMS BSc

Submitted in accordance with the requirements for the degree of Doctor of Philosophy

The University of Leeds,
Department of Medical Physics

June 1987

NOMENCLATURE

Subscripts

a	anodic
A	adsorption
ac	alternating current
ac+dc	small amplitude ac signal superimposed on variable dc bias
b	bulk
CPA	constant phase angle
CT	charge transfer
dc	direct current
dl	double layer
e	a) electrolyte
	b) electrical
f	faradaic
F	forward
HF	high frequency
i	interface
L	limiting
LF	low frequency
m	metal
M.T.	mass transfer
n.f.	non faradaic
O	oxidised
P	parallel
R	reduced
s	a) surface
	b) series
rev.	reversible
W	Warburg

Roman Symbols

A	area (cm^2)
a_i^{α}	activity of substance i in a phase α (M)
B	adsorption coefficient, potential independent
$\bar{B}$	adsorption coefficient, potential dependent
C	a) concentration (M, mol/cm^3)
	b) capacitance (μF)
C*	complex capacitance
C_A	adsorption pseudo capacitance (μF)
C_A^L	Langmuir's adsorption capacitance (μF)
C_D	capacitance of the diffuse layer (μF)
C_{dl}	double layer capacitance (μF)
C_i	a) integral capacitance (μF)
	b) series interfacial capacitance
C^j	concentration of species j (M, mol/cm^3)
C_b^j	bulk concentration of species j (M, mol/cm^3)
C_s^j	surface concentration of species j(M,mol/cm^3)
C_{HF}	limiting value of the capacitance at high frequencies (μF)
C_{LF}	limiting value of the capacitance at low frequencies (μF)
ΔC	an adsorption capacitance, where $\Delta C = C_{LF} - C_{HF}$ (μF)
C_{OHP}	Outer Helmholtz Plane capacitance (μF)
C_p	parallel capacitance (μF)
C_s	series capacitance (μF)
D_j	diffusion coefficient of species j (cm^2/sec)
d	distance (cm)

E	potential of an electrode versus a reference (V)
E^o	standard potential of an electrode (V)
E_{rev}	reversible potential of an electrode (V)
e	quantity of charge on the electron (C)
erf(x)	error function of x
erfc(x)	error function complement of x
F	the Faraday; charge on one mole of electrons (C)
f	a) F/RT (V^{-1})
	b) frequency (sec^{-1})
f_h	highest frequency component, $f_h = 1/t_s$
G	Gibbs free energy (kJ)
ΔG	Gibbs free energy change in a chemical process (kJ)
ΔG^o	standard Gibbs free energy of activation (kJ/mol)
$\bar{G}$	electrochemical free energy (kJ)
g	conductivity (Ω^{-1} cm^{-1})
I_{ac}	amplitude of ac current (A, mA)
I_o	Bessel function of order zero
i	current (A, mA)
i_a	anodic component current (A, μA)
i_{ac}	ac current (A, mA)
i_c	cathodic component current (A, μA)
i_{dc}	dc current (A, mA)
i_{dL}	diffusion limited current (A, mA)
i_f	faradaic current (A, mA)
i_L	limiting current of linearity (A, mA)
inf	nonfaradaic current (A, mA)

i_o	exchange current (A, μA)
i_{TOTAL}	total current = $i_{nf} + i_f$ (A, mA)
J_j	flux of species j (mol cm^{-2} sec^{-1})
j	a) current density (A/cm^2, A/cm^2)
	b) $\sqrt{-1}$
K	a) faradaic charge required to form a monolayer of adsorbed ions (C, μC)
	b) magnitude of Z_{CPA} impedance ($\Omega sec^{-\beta}$)
	c) potential dependent rate constant
K^o	standard, potential independent, rate constant (cm/sec)
K_F	potential dependent rate constant for the forward reaction
K_R	potential dependent rate constant for the reverse reaction
l	depth of surface pores (cm)
M	metal electrode in the reaction $M \rightleftharpoons M+e$
m	fractional power constant
n	electrons per molecule oxidised or reduced
O	oxidised form of the standard system $O+ne \rightleftharpoons R$
P	reciprocal of penetration depth (cm^{-1})
Q	charge (C, μC)
q^-	excess charge of anions (C, μC)
q^+	excess charge on phase cations (C, μC)
q_j	excess charge on phase j (C, μC)
$q_s^{(CA)}$	charge of ions coulombically adsorbed onto the surface (C, μC)
$q_s^{(SA)}$	charge of ions specifically adsorbed onto the surface (C, μC)

R	a) reduced form of the standard system, $O + ne \rightleftharpoons R$
	b) gas constant (J mol^{-1} K^{-1})
	c) resistance (Ω)
R_A	adsorption resistance (Ω)
R_{CT}	charge transfer resistance (Ω)
$R_{CT(ac)}$	charge transfer resistance measured under ac large signal conditions (Ω)
$R_{CT(dc)}$	charge transfer resistance measured under dc large signal conditions (Ω)
$R_{CT(ac+dc)}$	charge transfer resistance measured under 'ac + dc' large signal conditions (Ω)
$R_{ELECTROLYTE}$	resistance of electrolyte (Ω)
R_e	resistance of electrolyte per unit length of surface pore ($\Omega\,cm^{-1}$)
R_f	series interfacial resistance (Ω)
R_{LEAD}	resistance of leads (Ω)
R_p	parallel resistance (Ω)
R_s	series resistance (Ω)
R_{SALINE}	resistance of saline (Ω)
R_{TOTAL}	total series resistance (Ω)
R_o	resistance when $\omega = o$ (Ω)
R	resistance when $\omega = \infty$ (Ω)
r_o	radial distance from the centre of a spherical electrode (cm)
s	Laplacian operator, s = a+j
T	a) absolute temperature (°k)
	b) time period (sec)
T_p	total sampling period (sec)
t	time (sec.)

t_p	pulse duration (sec)
t_s	sample length (sec)
t	normalised time = t/T
v	a) volume (cm^3)
	b) Voltage (V)
V_{ac}	ac voltage amplitude (V)
V_{ecm}	electro capillary maximum voltage (V)
V_{dc}	dc voltage (V)
V_L	limit voltage of linearity (V)
V_j	flux of species j (mol cm^{-3} sec^{-1})
X	reactance (Ω)
X_i	series reactance of interfacial impedance (Ω)
X_s	series reactance (Ω)
Y	admittance (Ω^{-1})
Z	impedance (Ω)
Z_{CPA}	constant phase angle impedance (Ω)
Z_{CT}	charge transfer impedance (Ω)
Z_f	faradaic impedance (Ω)
Z_i	interface impedance (Ω)
Z_{MT}	mass transfer impedance (Ω)
$Z_{n.f.}$	nonfaradaic impedance (Ω)
Z_o	impedance of surface pore (Ω)
Z_W	Warbug impedance (Ω)
Z_{WA}	Adsorption pseudo Warburg impedance (Ω)

Greek symbols

α	transfer coefficient
β	fractional power dependence on fequency of z_{CPA}
Γ	gamma function
Γ_j	surface excess of species j at equilibrium (mol/cm)
Γ_s	saturation coverage
	a/ surface tension (dyne/cm)
	b/ activity coeffecient
δ	Nernst diffusion layer thickness (cm)
δ_o	maximum thickness of the Nernst diffusion layer (cm)
ε	dielectric constant
ε_{HF}	limiting value of permittivity at high frequencies
ε_{LF}	limiting value of permittivity at low frequencies
ε_o	dielectric constant of free space ($C^2N^{-1}m^{-2}$)
ε_r	dielectric constant of medium
ε_r^*	complex dielectric constant of medium
η	overpotential, $E - E_{rev}$ (V, mV)
η_{CT}	charge transfer overpotential (V, mV)
η_{MT}	mass transfer over-potential (V, mV)
θ_j	fractional coverage of an interface by species j
μ_j^{α}	chemical potential of species j in phase α (kJ/mol)

$\mu_j^{o\alpha}$ standard chemical potential of species j in phase α (kJ/mol)

$\bar{\mu}_j^{\alpha}$ electrochemical potential of species j in phase α (kJ/mol)

ρ resistivity (Ω cm)

diffusion coeffecient (Ω - $sec^{1/2}$)

τ time constant (sec)

τ_o coverage time constant (Sec)

ϕ_f a) electrostatic potential (V)

b) phase angle (degrees, radians)

ϕ phase angle of faradaic impedance (degrees,radians)

ψ loss angle, where $\psi = 90 - \phi^o = m\pi/2 = (1-\beta)/2$ rads

ω angular frequency (sec^{-1})

ω_o value of ω at which X_s has its maximum

$\omega_{10\%}$ angular frequency at which the impedance changes by 10% due to nonlinearities

Abbreviations

DDRT	Distribution of Dielectric Relaxation Times
DR	Decay Ratio
DRT	Distribution of Relation Times
ECM	ElectroCapillary Maximum
FFT	Fast Fourier Transform
IHP	Inner Helmholtz Plane
OHP	Outer Helmholtz Plane
PZC	Potential of Zero Charge
RHE	with Reference to the Hydrogen Electrode

Table of Contents

List of Diagrams

Page No

Chapter 4

DIAGRAMS CONTINUED

DIAGRAMS CONTINUED — Page No

Chapter 5

DIAGRAMS CONTINUED Page No

Chapter 6

DIAGRAMS CONTINUED

List of Tables

TABLES CONTINUED Page No

Chapter 6

Chapter 7

Chapter 4

Ac Nonlinearity of the electrode-electrolyte interface impedance

4.1 THEORETICAL SECTION

-Introduction

In this chapter the complex problem of the ac nonlinearity of the interfacial impedance is reviewed, and, it is hoped, clarified.

Many investigations of the electrode system's nonlinearity have been made using large amplitude signals (eg Schwan 1968). Although empirical expressions have been proposed which describe the observed relationships between frequencies at which 'distortions' are observed and the applied signal amptitude, no adequate physical model has been put forward to date capable of explaining this behaviour.

Before studying experimentally the ac nonlinearity of the electrode system, predictions will be made based on the proposed equivalent circuit model (figure 2.2.1) and the physical interpretion of its component elements. It will be shown that the equivalent circuit model successfully models the observed nonlinear behaviour.

The nonlinearity of each element of the equivalent circuit will initially be investigated in order to derive that of the overall circuit.

4.1.1 Nonlinearity of Individual Circuit Elements

The simplest equivalent circuit model of the interface impedance comprises the parallel combination of a nonfaradaic, constant phase angle impedance, Z_{CPA}, and a faradaic charge transfer resistance, R_{CT}.

4.1.1.1 Nonlinearity of the nonfaradaic, Z_{CPA}, impedance

- Introduction

It was shown in chapter one that the high frequency interfacial impedance in the presence of specific adsorption effects was well modelled empirically over a wide frequency range by a constant phase angle impedance, Z_{CPA}, where $Z_{CPA} = K(j\omega)^{-\beta}$

In electrochemical circles, however, the high frequency electrical properties of the electrode-electrolyte interface in the presence of adsorption effects are more commonly expressed in terms of a "pseudo capacitance", C_A, which has been found to be frequency and voltage dependent . One can write C_A in terms of K and β, ie

$$C_A = (1/K)(j\omega)^{\beta-1}$$

and deduce that K must also be potential dependent.

The derivation from first principles of expressions for C_A in terms of voltage and frequency will be reviewed in order to give some insight into the physical processes responsible for the experimentally observed Z_{CPA} behaviour and to give an appreciation of

the nonlinearity of the non-faradaic impedance.

- Surface excesses

The properties of the interface are governed by excesses and deficiencies in the concentrations of ions at the interface relative to their concentrations in the bulk of the electrolyte. These differences, due to coulombic and specific adsorption, are termed "surface excesses", Γ.

Gibbs (1877) suggested a means of measuring the total adsorption at an interface by considering laminae of the solution near the electrode surface, calculating the number of ions in them and subtracting the number of ions which would have been there in the absence of adsorption. He then summed the excesses of each of the laminae to obtain the total surface excess. This sum of the excesses is termed the Gibbs surface excess and is expressed as,

$$\begin{aligned} \Gamma &= \int_o^\infty [C(d) - C_b] \, d(d) \\ &= {}^1/_A \int_o^\infty [C(d) - C_b] \, dv \\ &= {}^1/_A \int_o^{n-n^b} d(\Delta n) \\ &= {}^n/_A - {}^{n^b}/_A \end{aligned} \qquad 4.1$$

Where $C(d)$ is the concentration as a function of distance d,

C_b is the bulk concentration,

n is the actual number of moles of a species in the interface region,

n^b is the number of moles that would have been present in the absence of adsorption,

d is distance from the interface,

v, the volume of the laminae and

A, the area of the interface.

Note: the amount of adsorbed material per unit area, $^n/_A$, is not equal to the surface excess, Γ, but to the sum of the surface excess and the amount of material present in the absence of adsorption.

Unfortunately the surface excess can only be measured directly with difficulty eg using radio active isotopes. One can however measure the surface excess indirectly by measuring some property which depends on the surface excess.

One such way of calculating the surface excess is by measuring the surface tension, γ, as it is related to surface excess. This is due to work having to be done against surface tension in order to increase the area of coverage of the electrode and hence create a surface excess.

- Nonfaradaic impedance in the absence of specific adsorption.

As an example let us first consider the case where there is no specific adsorption of ions present. A plot of surface tension, γ, (obtained by electro-capillary measurements) versus voltage, V, is in this case found to be almost parabolic (Bockris and Drazic, 1972) - see figure 4.1.

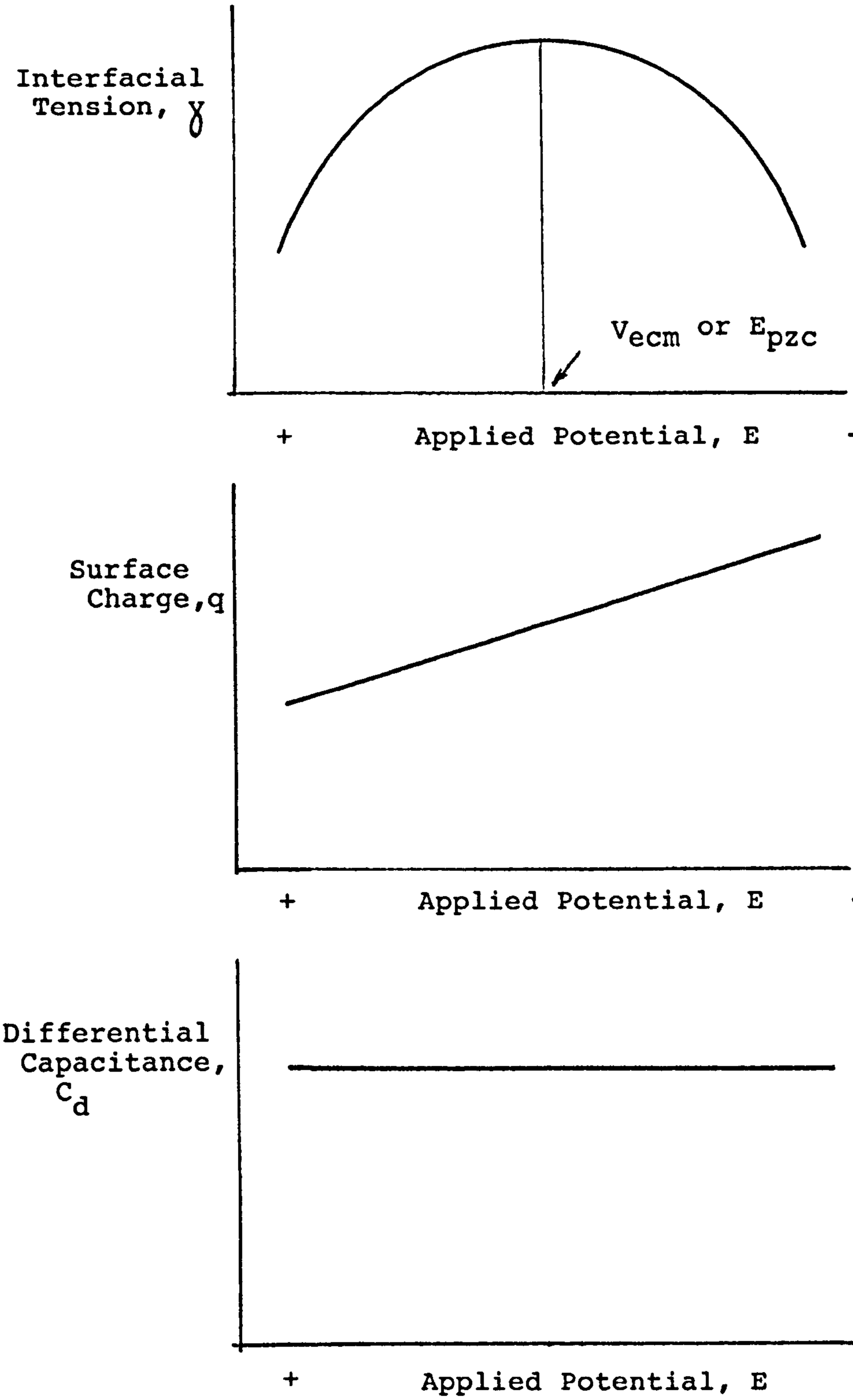

PLOTS OF γ, q AND C_d VS. APPLIED POTENTIAL
IN THE ABSENCE OF SPECIFIC ADSORPTION

Figure 4.1

The potential at which the surface tension is a maximum is known as the electrocapillary maximum voltage, V_{ecm}.

The relationship between interfacial tension and voltage is given by Gibbs adsorption equation and from this one can calculate the surface charge density and surface excesses of adsorbed species.

If no faradaic reaction occurs the Gibbs equation is (Sluyters-Rehbach and Sluyters, 1970)

$$- d\gamma = q_m \, dV + \sum_i \Gamma_i \, d\bar{\mu}_i \qquad 4.2$$

Where $\bar{\mu}i$ are the electrochemical potentials and q_m is the charge on the metal electrode.

For a solution of fixed composition $d\bar{\mu}_i = o$ and equation 4.2 becomes

$$d\gamma = q_m \, dV \qquad 4.3$$

Hence the slope of the electro capillary curve at a given potential is equal to the charge on the metal, q_m

$$\text{i.e.} \quad q_m = -\left(\partial\gamma/\partial V\right)_{\text{const. comp.}} \qquad 4.4$$

Equation 4.4 is termed the Lippmann equation.

Note: The gradient at V_{ecm} is zero and hence the charge, q_m, must be zero at this voltage / potential. For this reason V_{ecm} is often referred to as the Potential of Zero Charge, PZC.

As $q_m \lesseqgtr 0$ for $V \lesseqgtr V_{ecm}$, there is electrostatic attraction of anions by the electrode for $q > o$ and attraction of cations for $q < o$. Ions which are attracted to the electrode surface are repelled from each other and hence the work needed to expand the layer is smaller than in the absence of electrostatic

interaction with the electrode i.e. when q = o and V = V_{ecm}. Hence the interfacial tension decreases as /q/ increases, or as the voltage is moved to either side of V_{ecm} and ions are adsorbed. V_{ecm} tends to represent the dividing line between the adsorption and desorption for a given ion at the electrode and it is the voltage at which there is no excess charge upon the metal electrode.

For the above simple example where the electrocapillary curve is a perfect parabola, q_m is found to vary linearly with potential (figure 4.1).

As these charges are accumulated or depleted at the interface relative to the bulk of the electrolyte, the interface has the ability to store charge and act as a capacitance. This capacitance may not necessarily be constant and independent of the potential, and hence the differential capacitance, C_d, will be used, where

$$C_d = \left(\frac{\partial q_m}{\partial V}\right)_{\text{const. comp}} \qquad 4.5$$

C_d is used instead of the integral capacitance, C_i, which is the ratio of the total charge q_m at a potential E to the total potential difference putting it there (Bard and Faulkner 1980),

that is, $C_i = q_m / (V - V_{ecm})$ 4.6

A drawback with the integral capacitance is that V_{ecm} must be known in order to determine its value and it therefore cannot be measured directly.

From equation 4.5 it is obvious that C_d is given by the slope of the plot of q_m versus V at any point

and can be obtained by differentiating equation 4.4.

In the simple case where there is no specific adsorption of ions and hence where the γ - V curve is an ideal parabola and the q_m - V plot is linear, the differential capacitance, C_d, will be constant and independent of V (figure 4.1). This constant, voltage independent capacitance is the Helmoltz double layer capacitance, C_{dl}, in the absence of specific adsorption effects.

It can be shown mathematically that a constant, potential independent capacitance, such as C_{dl}, gives rise to a perfent parabola on the γ - V plot (Bockris and Drazic, 1972).

For the Helmoltz model (equation 1.5)

$$V = \frac{4\pi d}{\varepsilon} q_m$$

(where voltage is referred to V_{ecm}, i.e. V = o at V_{ecm})

$$\text{hence} \quad dV = \frac{4\pi d}{\varepsilon} \, d\, q_m \qquad 4.7$$

As $\partial\gamma/\partial V = - q_m$ (equation 4.4)

$$\text{then} \quad \int d\gamma = \int q_m \, dV \qquad 4.8$$

therefore (substituting equation 4.7 into eqn 4.8)

$$\int d\gamma = - \frac{4\pi d}{\varepsilon} \int q_m \, dq_m \qquad 4.9$$

Integrating equation 4.9 gives

$$\gamma + \text{const.} = - \frac{4\pi d}{\varepsilon} \, {}^1/_2 \, q^2_m$$

As q_m = o when $\gamma = \gamma$ max,

therefore

$$\gamma = \gamma \text{ max} - \frac{4\pi d}{\varepsilon} \, q^2_m / 2$$

or (using equation 1.5)

$$\gamma = \gamma_{max} - \frac{\mathcal{E}}{4\pi d} \quad 1/2 \quad v^2 \qquad 4.10$$

This is the equation of a parabola symmetrical about γ_{max} or V_{ecm}).

- Nonfaradaic impedance in the presence of specific adsorption

Unfortunately the electrocapillary curve is generally not a perfect parabola, and as a result the q_m - V plot is not linear and the differential capacitance is not constant and independent of voltage. Deviation from a perfect parabola is greater for some solutions than others, showing a marked sensitivity to the anions present in the electrolyte, especially for potentials more positive that V_{ecm}. This deviation from "Helmoltz" behaviour is due to the contact or specific adsorption of anions which decreases the surface tension, γ, at a given potential. Anions exhibit this effect in the following order

$$I^- > Br^- > Cl^- > OH^-$$

(Bockris and Drazic, 1972). The resultant asymmetry of the electrocapillary curve (figure 4.2) has important implications for the capacitance of the electrode interfaces,

$$C_d = -(\partial^2\gamma / \partial V^2) \text{ const. comp.}$$

which will now vary with potential (figure 4.2).

In order to derive an expression for the differential capacitance one needs a new expression of the Gibbs equation (equation 4.2).

For an ideally polarisable ($R_{CT} = \infty$) electrode

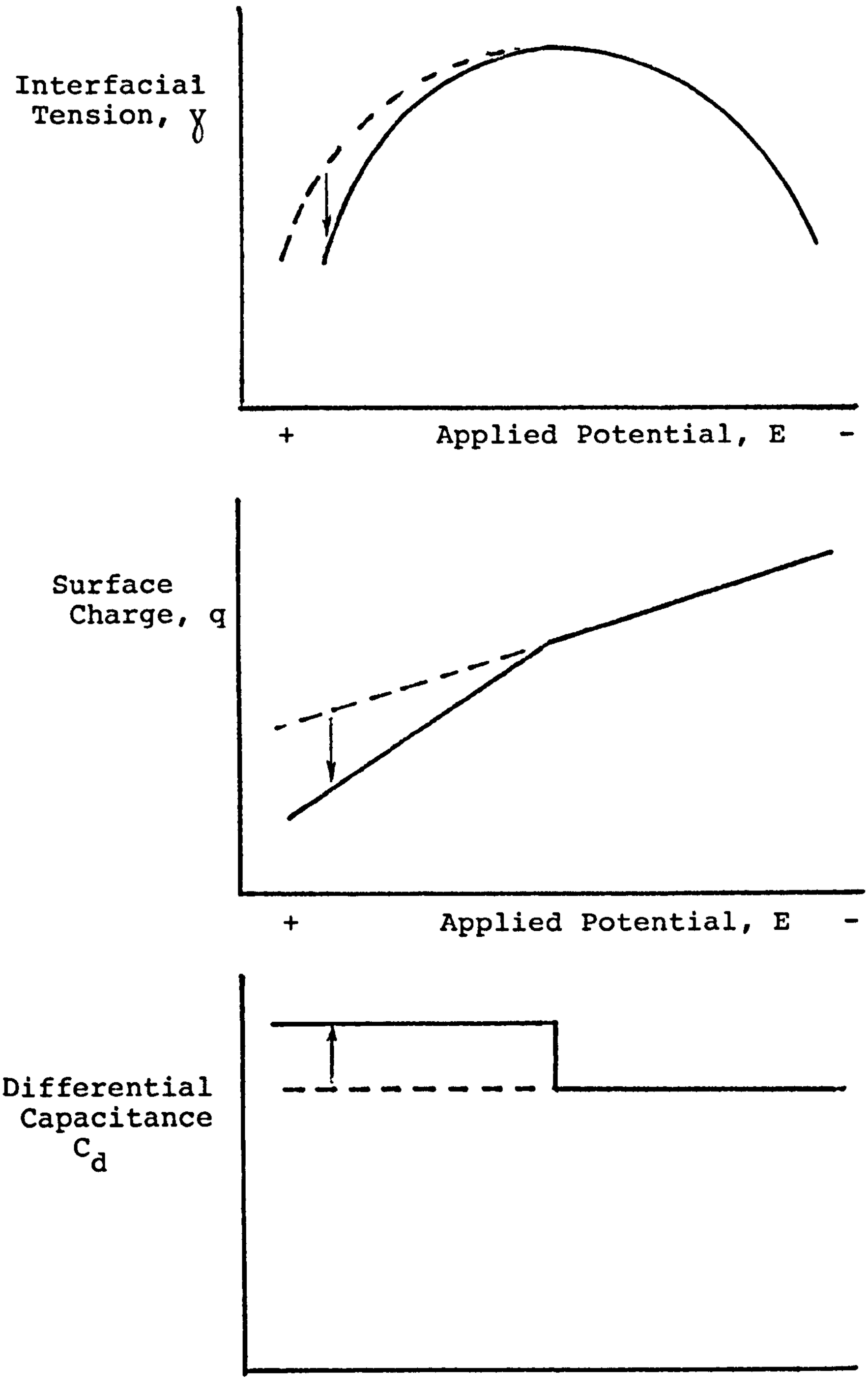

PLOTS OF γ, q AND C_d VS. APPLIED POTENTIAL

IN THE PRESENCE OF SPECIFIC ADSORPTION

Figure 4.2

the Gibbs equation was given by equation 4.2. This equation cannot however be used for a nonideally polarised electrode ($0<R_{CT}<\infty$). For an ideal reversible metal-metal ion electrode, the modified Gibbs equation has been derived as (Sluyters-Rehbach and Sluyters, 1970)

$$-d\gamma = (q_m + nf\Gamma_o)dV + (\Gamma_o + \Gamma_R)d\bar{\mu}_R + \sum_i \Gamma_i \, d\bar{\mu}_i \qquad 4.11$$

For constant composition

$d\bar{\mu}_i = o$ and $d\bar{\mu}_R = o$

hence equation 4.11 becomes

$$-d\gamma = (q_m + nF\Gamma_o)\, dV$$

or

$$-\partial\gamma/\partial V = q_m + nF\Gamma_o \qquad 4.12$$

i.e. a modified Lippman equation (see equation 4.4), giving

$$C_d = -\left(\frac{\partial^2\gamma}{\partial V^2}\right) \text{const comp.} = \frac{\partial(q_m+nF\Gamma)}{\partial V} \text{const comp} \qquad 4.13$$

Hence the differential capacitance can be considered as the sum of two parallel "capacitances"

$$C_d = \partial q_m/\partial V + nF\partial\Gamma_o/\partial V \qquad 4.14$$

ie $C_d = C_{dl} + C_A$

where $C_{dl} = \partial q_m/\partial V$ and $C_A = nF\partial\Gamma_o/\partial V$

The first term of the right hand side of equation 4.14 is the 'double layer' Helmholtz capacitance.

The second term is the adsorption pseudo capacitance, C_A, and is due to changes in surface coverage with voltage. In order to derive the expression for this 'capacitance' one needs to know the

relationship between surface coverage, Γ, and the applied voltage.

In chapter one it was shown that the pseudo capacitance, C_A, could be expressed as (equation 1.30)

$$C_A = \partial q^{SA} / \partial v$$

Where q^{SA} is the charge specifically adsorbed at the inner Helmholtz layer, IHP.

As the degree of coverage of the electrode surface, θ, (where $\theta = \Gamma / \Gamma_S$) is proportional to the faradaic charge passed, i.e.

$$q^{SA} = K\theta \quad (1.32),$$

hence

$$C_A = \frac{dq^{SA}}{dV} = \frac{K d\theta}{dV} = \frac{nFd\Gamma}{dV} \qquad (1.33)$$

(where $K = nf\Gamma_S$)

In order to derive an expression for C_A one needs to know how either q^{SA}, θ or Γ vary with the electrical state of the system.

Adsorption isotherms are just such theoretical relationships, relating the degree of coverage, the activity or concentration of the species in the bulk of the solution and the electrical state of the system. Such isotherms, of necessity, are based on an idealised physical model of the electrode interface. The different isotherms, and other assumptions made have given rise to different expressions for the adsorption pseudo capacitance.

- Isotherms

An isotherm is obtained from the equality of electrochemical potentials for bulk and adsorbed species. The electrochemical potentials, $\bar{\mu}_i$, will be equal when there is equilibrium between species, i, in the adsorbed state and in the bulk of the solution (Bard and Faulkner, 1980). Therefore

$$\bar{\mu}_i^{A} = \bar{\mu}_i^{b}$$

or $$\bar{\mu}_i^{o,A} + RT \ln[f(\Gamma)] = \bar{\mu}^{o,b} + RT \ln a^{b}_i \quad 4.15$$

Where the $\bar{\mu}_i^{o}$ terms are the standard electrochemical potentials.

$f(\Gamma)$ is a function of the surface concentration, Γ, and represents the activity of the adsorbate, a_i^A .

Rearranging the equation one obtains

$$f(\Gamma) = a_i^b \exp(-\overline{\Delta G^o}/RT) \quad 4.16$$

Where $\overline{\Delta G^o} = \bar{\mu}^{o,A} - \bar{\mu}^{o,b}$ is the standard electrochemical free energy change accompanying the migration of a mole of ions from the OHP to the IHP.

[Note: the electrochemical free energy $\bar{G}$ differs from the chemical free energy, G, by inclusion of the effects from the large scale electrical environment i.e. $\overline{\Delta G} = \Delta G + (\Delta G)_e$

Where $(\Delta G)_e$ is the electrical component. The overbar indicates the dependence on interfacial voltage]

Letting $\bar{B} = \exp(-\overline{\Delta G^o}/RT)$ 4.17

($\bar{B}$ is termed the adsorption coefficient) then

$$f(\Gamma) = (a_i^b \ \bar{B}) \qquad 4.18a$$

or alternatively

$$\Gamma = f(a_i^b \ \bar{B}) \qquad 4.18b$$

The surface excess, Γ , (or the degree of coverage, θ) is some function of the activity in the bulk, a_i^b , and the adsorption coefficient, $\bar{B}$, which in turn depends on the electrical state of the electrode. As the adsorption capacitance is proportional to the change of surface coverage with voltage (eqn 1.33), it can be expressed as

$$C_A = K \frac{d \ [f(a_i^b \ \bar{B})]}{dV} \qquad 4.19$$

The best known and most commonly used theoretical isotherm is known as Langmuirs. In Langmuir's rather simple model it is assumed that the rate of adsorption of ions onto the electrode surface is the same as that of desorption of ions at the surface. It is also assumed that the ions adsorbed on the surface do not interact with each other and that there is no heterogenity of the electrode surface.

In order to illustrate the derivation of expressions for the pseudo capacitance, C_A , one will be derived using Langmuir's rather simplistic physical model of the system.

- Adsorption pseudo capacitance under Langmuir's conditions.

In the presence of an applied electrical field, $\overline{\Delta G}^o$ can be separated into a potential independent (chemical) term, ΔG^o , and a potential dependent

(electrochemical) term, $(\Delta G^{o})_{e}$. In this case the standard Gibbs free energies of activation of the forward and reverse processes, $\overline{\Delta G^{o}}_{F}$ and $\overline{\Delta G^{o}}_{R}$ can be expressed as

$$\overline{\Delta G^{o}}_{F} = \Delta G^{o}_{1} + \alpha\, nFE \qquad 4.20\ a$$

$$\overline{\Delta G^{o}}_{R} = \Delta G^{o}_{2} - (1-\alpha)\, nFE \qquad 4.20\ b$$

Where $\overline{\Delta G^{o}}$ is the standard Gibbs energy of activation (kJ/mol),

ΔG^{o}_{1} and ΔG^{o}_{2} represent the chemical part of the activation energy independent of electrical ($E = E^{o}$) and adsorption ($\theta = 0$) work items and

α is the transfer coefficient.

The forward and reverse rate constants for the adsorption / desorption reaction

$$M + A^{-} - \underset{K_R}{\overset{K_F}{\rightleftharpoons}} M\,A_{ads} + e$$

can therefore be written as (Bard and Faulkner, 1980)

$$K_F = \frac{RT}{nF} \exp\left(\frac{-\overline{\Delta G^{o}}_{F}}{RT}\right)$$

$$= K_F^{o} \exp\left(\frac{-\alpha nFE}{RT}\right) \qquad 4.21$$

where $$K_F^{o} = \frac{RT}{nF} \exp\left(\frac{-\Delta G^{o}_{1}}{RT}\right) \qquad 4.22$$

$$K_R = \frac{RT}{nF} \exp\left(\frac{-\overline{\Delta G^{o}}_{R}}{RT}\right)$$

$$= K^{o}_{R} \exp\left[\frac{(1-\alpha)\, nFE}{RT}\right] \qquad 4.23$$

where $$K^{o}_{R} = \frac{RT}{nF} \exp\left(\frac{-\Delta G^{o}_{2}}{RT}\right) \qquad 4.24$$

K_F^o and K_R^o are independent of potential and are equal to the forward and reverse rate constants in the absence of potential. K_F^o and K_R^o are termed "standard rate constants".

The electrochemical rate equations are therefore

$$V_F = (1-\theta)\, a_F\, K_F^o \exp\left(\frac{-\alpha nFE}{RT}\right) \qquad 4.25$$

$$V_R = \theta\, a_R\, K_R^o \exp\left[\frac{(1-\alpha)nFE}{RT}\right] \qquad 4.26$$

At equilibrium, $V_F = V_R$, and it follows that

$$\frac{\theta}{1-\theta} = \frac{a_F\, K_F^o}{a_R\, K_R^o} \exp\left(\frac{nFE}{RT}\right) \qquad 4.27$$

As $\dfrac{K_F^o}{K_R^o} = \exp\left(\dfrac{-\Delta G^o}{RT}\right) = B$ 4.28

[where ΔG^o ($=\Delta G^o_1 - \Delta G^o_2$) is independent of applied potential and equal to nFE^o.

Note: There is no bar above B as it is now independent of potential, see equation 4.17]

$$\text{then } \left(\frac{\theta}{1-\theta}\right) = \left(\frac{a_F}{a_R}\right) B \exp\left(\frac{nFE}{RT}\right) \qquad 4.29$$

Equation 4.29 is known as Langmuir's isotherm and relates the fractional surface coverage, θ, to the activity of the species in the bulk of the solution and to the electrical state of the system.

Rearranging equation 4.29, one has in terms of potential or voltage

$$E \text{ or } V = \frac{RT}{nF} \ln\left[\frac{\theta}{1-\theta}\,\frac{1}{B}\,\frac{a_R}{a_F}\right] \qquad 4.30$$

Differentiating equation 4.30 with respect to θ one obtains

$$\frac{dV}{d\theta} = \frac{RT}{nF}\,\frac{1}{\theta(1-\theta)} \qquad 4.31$$

The adsorption capacitance for Langmuir conditions, C_A^L, is therefore given by (using eqn 1.33)

$$C_A^L = K\,\frac{d\theta}{dV} = \frac{KnF}{RT}\,\theta(1-\theta) \qquad 4.32$$

A plot of C_A^L against surface coverage, θ, is symmetrical about $\theta = 0.5$. Hence the adsorption capacitance increases with surface coverage up to a maximum of KnF/4RT at θ=0.5 and then decreases to zero at $\theta = 1$.

In terms of potential C_A^L can be written as

$$C_A^L = \frac{KnF}{RT}\,\frac{\theta/(1-\theta)}{[1+(\theta/(1-\theta))]^2}$$

$$= \frac{KnF}{RT}\,\frac{(a_F/a_R)\,B\,\exp(nFE/RT)}{[1+(a_F/a_R)\,B\,\exp(nFE/RT)]^2} \qquad 4.33$$

which is also symmetrical with respect to potential at $\theta = 0.5$. Hence the adsorption capacitance, C_A^L, will at first increase exponentially with voltage, reach a maximum when $\theta = 0.5$ and then decrease towards zero.

In Summary - Using the Langmuir isotherm the derived equivalent circuit model of the adsorption pseudo capacitance is a voltage dependent capacitance, C_A^L, which shunts the voltage independent double layer capacitance, C_{dl} (see equation 4.14).

- Short comings of the Langmuir Model

In the Langmuir model the adsorbed ions are assumed not to interact with each other and hence the adsorption coefficient and Gibbs energy of activation

are assumed to be independent of the fraction, θ, of sites occupied by the adsorbed species. The adsorption coefficient has, however, been found to be coverage dependent (Bockris and Drazic, 1972). This is due to interactions between adsorbed species whose interionic forces make further adsorption progressively more difficult. These interactions cause the energy of adsorption to be a function of surface coverage.

A more realistic model will take into account the dependence of the energy of activation on the coverage. In the Temkin isotherm, for example, the Gibbs energy of activation is assumed to vary linearly with coverage.

The use of different isotherms, and the other assumptions and approximations made have resulted in many different expressions for the adsorption pseudo capacitance, C_A. Some of these even account for the frequency as well as potential dependence of the "capacitance".

Perhaps the best expressions so far derived for the impedance/admittance of electrode systems where adsorption of reactants is occuring were derived by Timmer et al in 1966. The work of this group will therefore be briefly reviewed.

-Timmer et al's equivalent circuit model

Using Delahay's (1966) coupling concept (section 1.1.2.3) and a new version of the electrocapillary equation for reversible systems, such that

$$-\left(\frac{\partial \gamma^2}{\partial E^2}\right)_{\bar{\mu}_i} = \left[\frac{\partial(q_m+nF\Gamma_o)}{\partial E}\right] - \frac{n^2F^2}{RT}\,\frac{\sigma_o\sigma_R}{\sigma^2}\,(\Gamma_o\Gamma_R) \qquad 4.34$$

(Where σ_o and σ_R pertain to the Warburg coefficient of the oxidised and reduced component, $\sigma = \sigma_o + \sigma_R$) instead of equation 4.13, Timmer et al derived an equivalent circuit model of the electrode-electrolyte interface impedance (see figure 1.25)

As a consequence of the derivation being based on the coupling concept, the usual double layer capacitance [$(dq_m/dE)_{\bar{\mu}_i}$] is replaced by a high frequency capacitance, C_{HF}, which includes a term due to reactant adsorption

$$C_{HF} = \left[\frac{\partial(q_m + nF\Gamma_o)}{\partial E}\right] \quad (\Gamma_o + \Gamma_R) \qquad 4.35$$

Note that although equation 4.35 appears very similar to equation 4.13, containing the same thermodynamic quantities ($q_m + nF\Gamma_o$), in the latter case it was derived for constant composition, i.e. Γ_o and Γ_R were assumed constant.

The adsorption pseudo capacitive branch is now represented by a pseudo Warburg impedance, Z_{WA}, in series with a capacitance, ΔC, where

$$Z_{WA} = (1-j)\lambda\omega^{-0.5} \qquad 4.36$$

with

$$\lambda = \left[\frac{\partial(\Gamma_o + \Gamma_R)}{\partial \psi}\right]_E \frac{1}{\sqrt{2}(\Delta C)}, \qquad \psi = C_o\sqrt{D_o} + C_R\sqrt{D_R}$$

and $$\Delta C = C_{LF} - C_{HF} \qquad 4.37$$

with $$C_{LF} = \left[\frac{\partial(q_m+nF\Gamma_o)}{\partial E}\right]_\psi - nF\frac{\sigma_R}{\sigma}\left[\frac{\partial(\Gamma_o+\Gamma_R)}{\partial E}\right]_\psi \qquad 4.38$$

Although the Z_{WA} and ΔC have physical significance it has been found that the empirical Z_{CPA} better represents the experimental findings over a wide frequency range. As yet there is no satisfactory physical explanation of the observed fractional power dependence of the interfacial impedance on frequency, though it is known to be caused by adsorption effects (in the absence of surface roughness). Timmer et al's physical and equivalent circuit models come closest to successfully representing the observed behaviour of electrode interfaces.

- Potential dependence of the "differential" Capacitance.

The phenomena associated with specific adsorption of substances onto an electrode's surface can be studied by analysing the "differencial" capacitance as C_d is extremely sensitive to adsorption effects.

A "differential" capacitance-potential plot is obtained by measuring an electrode system's impedance at a given frequency in terms of a parallel capacitance, C_p, and resistance, R_p, using a small amplitude ac signal superimposed on a variable dc bias. The "differential" capacitance can be plotted against the applied dc bias for a given frequency provided the ac voltage, δV used in the measurement does not exceed a few millivolts. In this case the measured values of

"differential" capacitance will be independent of δV.

It will be noted that what is generally termed "differential" capacitance (i.e. the parallel capacitance measured at a certain frequency and dc bias) is not the same as the differential capacitance described by equation 4.14 i.e. $C_d = C_{dl} + C_A$.

The measured parallel capacitance, C_p, is a more complex function of the double layer capacitance and the adsorption pseudocapacitance.

For example, the admittance of Timmer et al's equivalent circuit with a shunting charge transfer resistance, R_{CT}, is given by

$$Z^{-1} = \omega C_{HF} + \left(\frac{1 + (j\omega x)^{1/2}}{j\omega \Delta C} \right)^{-1} + R_{CT}^{-1} \qquad 4.39$$

$$\text{where } x = (\lambda \Delta C^2)$$

Hence the expressions for C_p and R_p of the equivalent parallel model are

$$C_p = \frac{\Delta C \left[1 + (\omega x/2)^{1/2} \right]}{1 + \omega x + (2\omega x)^{1/2}} + C_{HF} \qquad 4.40$$

$$\frac{1}{\omega R_p} = \frac{\Delta C (\omega x/2)^{1/2}}{1 + \omega x + (2\omega x)^{1/2}} + \frac{1}{\omega R_{CT}} \qquad 4.41$$

At high frequencies the parallel capacitance, C_p, tends to that of C_{HF} (where $C_{LF} = C_{HF} + \Delta C$ and is part of the adsorption pseudo capacitive branch).

For a given frequency (especially a low one) C_p will increase as ΔC increases or λ decreases i.e. it is proportional to the admittance of the adsorption branch.

A typical C_p - potential plot for platinum electrodes in a chloride containing electrolyte is

shown schematically on figure 4.3 (Dolin and Ershler 1940, Ohsaka et al 1976, DeRosa and Beard 1977).

The plot can be divided into three important regions as shown.

Region 1 In this potential region, between approximately 0.4 and 0.8 volts RHE (relative to the hydrogen electrode) the plot is the flat bottomed valley of the 'U' shaped curve (Ohsaka et al 1976). The parallel "differential" capacitance is almost constant and independent of voltage and frequency (Ohsaka et al, 1976, Iseki et al 1972). In this region relatively little specific adsorption takes place and the observed capacitive behaviour is largely due to the voltage and frequency independent, Helmholtz double layer capacitance. One can imagine a plate of the capacitor located on the metal surface and the other on the OHP, the IHP being almost free of contact or specifically adsorbed ions.

In this potential range, more negative than V_{ecm}, the electrocapillary curve will approximate fairly well to a parabola in the absence of any significant adsorption effects (figure 4.2).

Minimal frequency dispersion is observed in this region (i.e. $\beta \simeq 1$) and what dispersion there is, will probably be due to surface roughness effects and the specific adsorption of chloride ions present (Breiter, 1963).

As the double layer capacitance dominates the overall nonfaradaic impedance in this potential range, the trough is generally known as the double layer

region (Breiter 1963).

Region 2 (i) For more anodic potentials, i.e. above approximately 0.8 volts RHE, adsorption and the eventual evolution of oxygen takes place (Breiter 1963) Chloride ions adsorbed in the double layer region cause the retardation of the formation of the oxygen layer, causing it to take place at more anodic potentials and thus extending the double layer potential range. Only part of the adsorbed chloride ions are replaced by oxygen and hence both ions are present at the IHP for potentials more anodic than the double layer region. The specifically adsorbed ions populating the IHP give rise to an adsorption pseudo capacitive branch in parallel with the double layer capacitance, C_{dl}. The impedance of this branch decreases rapidly with potential in this region and it soon dominates that of the total nonfaradaic branch. The measured parallel capacitance, C_p increases rapidly in this region (Iseki et al, 1972; De Rosa and Beard, 1977) giving rise to the observed 'U' shaped plot.

As the adsorption "capacitance" is frequency dependent, greater frequency dispersion is noticed in this region (Iseki et al, 1972).

In Timmer et al's model the adsorption pseudo capacitive branch is represented by the series combination of Z_{WA} and ΔC. The observed increase in Cp is therefore interpreted as a decrease in the magnitude of Z_{WA} and an increase in ΔC (Timmer et al, 1968).

The adsorption impedance is however generally

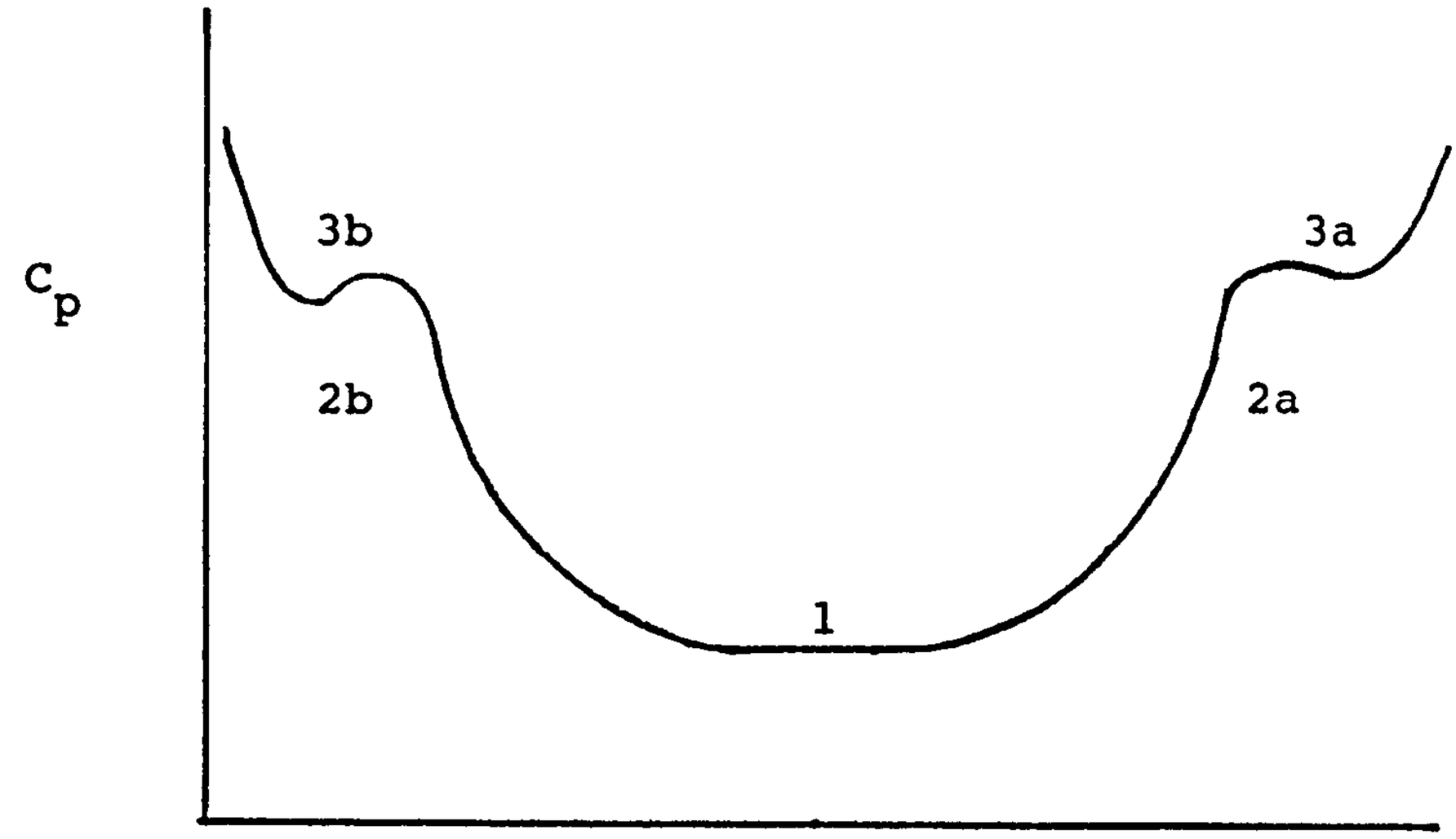

A SCHEMATIC PLOT OF PARALLEL CAPACITANCE VS. APPLIED POTENTIAL AT A GIVEN FREQUENCY FOR PLATINUM ELECTRODES IN A CHLORIDE CONTAINING ELECTROLYTE.

Figure 4.3

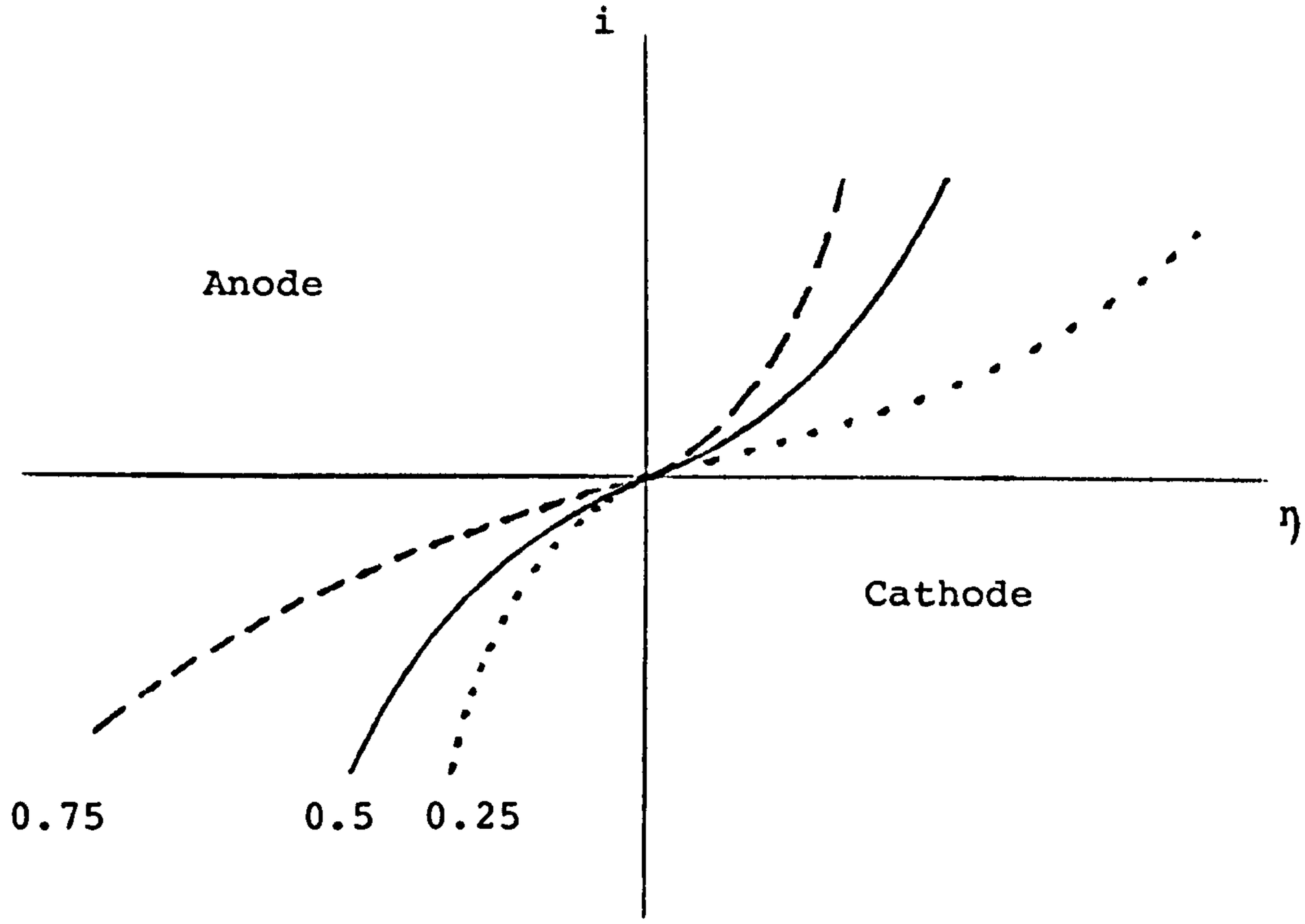

PLOTS OF CURRENT VS. OVERPOTENTIAL FOR VARIOUS VALUES OF TRANSFER COEFFICIENT

Figure 4.4

better approximated by a constant phase angle impedance, Z_{CPA}, over a wide range of frequencies (Iseki et al 1972).

In this case K, which is inversely proportional to the parallel capacitance, should decrease outside the double layer region and β, an inverse measure of frequency dispersion, should decrease from its "double layer" value.

Mund et al (1979) plotted calculated values of K and β against potential for platinum electrodes in 0.15 M NaCl. In the double layer region K and β were found to be almost constant and independent of the applied dc bias. Outside the double layer potential range (0.2 to 0.8 RHE in their case) K and β were observed to decrease as expected, due to the growth of the frequency and potential dependent adsorption pseudo capacitance.

(ii) For potentials more cathodic than the double layer region (i.e. below approximately 0.4 volts RHE) adsorption and eventually evolution of hydrogen takes place (Breiter 1963). Again the adsorption impedance dominates the total nonfaradaic interfacial impedance is observed to increase (Ohsaka et al 1976, De Rosa and Beard 1977) and greater frequency dispersion is observed (i.e. β decreases).

Although Ohsaka et al (1976) used Timmer et al's equivalent circuit model to represent their electrode system in this potential range it would appear that the nonfaradaic impedance is better approximated by a Z_{CPA} (in parallel with R_{CT}) whose values of K and β

decrease as the applied dc potential is altered away from those of the double layer region (Mund et al, 1979).

Region 3 The observed capacitance, C_p, does not continue to increase indefinitely as the voltage leaves the double layer region (i). It is observed to increase up to a maximum and then begins to decrease again - giving rise to a 'hump' in the curve. This hump implies that as the electrode charge, q_m, increases beyond a certain point the rate of growth of the adsorbed layer begins to decrease.

In the Langmuir model this decrease would begin when $\theta = 0.5$ and is due to the rate of adsorption being proportional to the free area, 1-θ. In other models, however, the increasing lateral interaction forces between the adsorbed ions are also taken into account. In such a case the increasing population of specifically adsorbed ions at the IHP establish and gradually accentuate lateral repulsive forces which try to inhibit further increases in surface coverage. The rate of growth of the adsorbed layer will therefore decrease which would result in the observed decrease in the adsorption pseudo capacitance, C_A, as

$$C_A = dq^{SA}/_{dV} = K\, d\theta/dV \qquad \text{(eqn 1.33)}$$

At higher potentials the capactiance, C_p, is observed to increase again due to the evolution of gases, hydrogen at the cathode, oxygen and / or chlorine at the anode.

- Summary and conclusions

The nonfaradaic impedance is well approximated by a constant phase angle impedance, Z_{CPA} (Mund et al 1979). Over a range of potentials, termed the double layer region, the nonfaradaic impedance is relatively constant and K and β have their maximum values. For potentials on either side of the double layer region the adsorption pseudo capacitance increases rapidly in magnitude, dominates that of the double layer and causes the measured values of K and β to decrease.

If it is assumed that the electrode system, in the absence of an applied dc bias, operates close to the centre of the double layer region trough (Simpson et al, 1980) which is approximately 0.4 to 0.6 Volts wide (De Rosa and Beard, 1977; Mund et al 1979), one should be able to apply ac signals of up to 0.2 or 0.3 Volts amplitude before gross nonlinear effects are noticed. The "Voltage limit of linearity", V_L, in such a case would be approximately 250 mV.

4.1.1.2 Non linearity of the faradaic charge transfer resistance, R_{CT}.

The parallel resistance in the proposed equivalent circuit model (figure 2.2a) is, the author believes, the charge transfer resistance and the major source of the observed nonlinearity of the interfacial impedance. R_{CT} will therefore be studied in some length in this section.

In section 1.2.2 the expression for the charge transfer resistance was derived from the Butler-Volmer equation (equation 1.19)

$$i = i_o \left\{ \left(\frac{C_s^o}{C_b^o}\right) \exp\left[\frac{-\alpha nF\eta}{RT}\right] - \left(\frac{C_s^R}{C_b^R}\right) \exp\left[\frac{(1-\alpha)nF\eta}{RT}\right] \right\}$$

As there is no mass transfer involved, $C_s^o = C_b^o$ and $C_s^R = C_b^R$.

Hence the Butler-Volmer equation becomes

$$i = i_o \left\{ \exp\left[\frac{-\alpha nF\eta}{RT}\right] - \exp\left[\frac{(1-\alpha)nF\eta}{RT}\right] \right\} \quad 4.42$$

Letting $f = F/_{RT}$, equation 4.42 becomes

$$i = i_o \left\{ \exp\left[-\alpha nf\eta\right] - \exp\left[(1-\alpha)nf\eta\right] \right\} \quad 4.43$$

$i - \eta$ Plots for various values of α are shown on figure 4.4. As similar plots have been obtained by Shigemitsu et al (1979) for glassy carbon electrodes in 0.9% NaCl, for Pt-Ir electrodes in 0.9% NaCl (Great bach et al, 1969) and for platinum electrodes in 0.01M

(Simpson et al, 1980), the faradaic current flowing through an electrode system is given by equation 4.43 and the faradaic impedance by the charge transfer resistance R_{CT}, which is derived from the above $i-\eta$ relationship - as postulated in chapter two.

In deriving an expression for R_{CT} in chapter one, two approximations were made (i) the i-η characteristic was "linearised" (the exponential expanded and the higher terms neglected) and (ii) it was assumed that the characteristic was symmetrical about the equilibrium potential, E_{rev}, i.e. α is equal to 0.5 (see figure 4.4).

In the above approximate case an ac current signal, when applied to the electrode system, will only result in a sinusoidal voltage of the same frequency as the charge transfer resistance is linear.

However the i - η characteristic is generally not symmetrical about E_{rev} and it only approximates to a linear relationship for very small signal amplitudes (figure 4.4). The charge transfer resistance (= η/i) is therefore generally nonlinear.

The nonlinearity of the charge transfer "resistance" can be subdivided to two categories according to its causes.

(i) Asymmetry of the i - η characteristic. This non-linearily is simply "curvature" of the characteristic about the point i=o, η =o when $\alpha \neq 0.5$. Asymmetry can greatly affect the response of the system to even small amplitude ac signals (see section 4.1.1.2.1)

(ii) Curvature of the i - η characteristic. Even if the characteristic is symmetrical about E_{rev} (ie α = 0.5) there is curvature of the characteristic as the i - η relationship is not a linear one (equation 4.43). This nonlinearity will be most marked for large

amplitude signals (see section 4.1.1.2.2).

4.1.1.2.1 Small signal nonlinearity

If one applies a small amplitude ac current to an asymmetrical system the average voltage of the electrode system is found to differ from that in the absence of the ac perturbation i.e. the voltage response of the system contains a dc component as well as the expected ac component (figure 4.5). This phenomenon is generally referred to as "faradaic rectification".

A similar effect occurs if an ac voltage is applied to the system resulting in a dc component in the current response.

Simpson et al (1980), for example, showed that for applied signals of the form

$$\eta = V_{ac} \operatorname{Sin}\omega t + \eta_{dc} \qquad 4.44$$

the current response is given by

$$i = i_o\left\{\exp[\alpha nf(V_{ac}\operatorname{Sin}\omega t+\eta_{dc})]-\exp[-(1-\alpha)nf(V_{ac}\operatorname{Sin}\omega t + \eta_{dc})]\right\} \qquad 4.45$$

The dc current through the interface, including dc due to rectification, if any, is given by

$$i_{dc} = 1/T\int_o^T i\,(t)dt \quad \text{where } T = 2\pi/\omega \qquad 4.46$$

Equation 4.45 therefore becomes

$$i_{dc}=i_o\left\{\exp[\alpha\, nf\,\eta_{dc}]I_o(\alpha\, nfV_{ac}) -\exp[-(1-\alpha)nf\,\eta_{dc}]I_o\{(1-\alpha)nfV_{ac}\}\right\} \qquad 4.47$$

Where I_o is the Bessel function of order zero. If the dc current is held at zero (i_{dc}=o) and an ac signal applied, the electrodes develop a compensating

steady bias such that

$$\exp(nf\eta_{dc}) = \frac{I_o(\alpha\ nfV_{ac})}{I_o(1-\alpha)nfV_{ac}} \qquad 4.48$$

For small values of nfV_{ac}, i.e. for small signal amplitudes, equation 4.48 can be rewritten as

$$nf\eta_{dc} = (nfV_{ac})^2\ (2\alpha - 1)/4 \qquad 4.49$$

and rearranging

$$\eta_{dc} = nfV_{ac}^2\ (\alpha - 0.5)$$

Hence, for small signals if α = 0.5 (i.e. when the i-η characteristic is symmetrical) there is no resultant dc voltage bias (i.e. η_{dc} = o) and there is therefore no faradaic rectification. If, however, α is not equal to 0.5, η_{dc} will have a finite value proportional to the square of the amplitude of the ac voltage signal, V_{ac}.

The net result of asymmetry is to distort the voltage response and to shift the mean potential, $\bar{E}$, away from E_{rev}, giving rise to a rectification voltage, η_{dc}, where $\eta_{dc} = \bar{E} - E_{rev}$ (figure 4.5)

As a rectification voltage is present, the system cannot be termed linear, even for small signals unless α equals 0.5.

- Small signal value of R_{CT}

In order to derive an expression for R_{CT} the Butler-Volmer equation (4.43) is expanded and, if

$\alpha nf\eta \ll 1$ (i.e. when $\eta \ll RT/\alpha nF = .026/n$ Volts for 25°C and α = 0.5), all resulting terms except the first two are neglected. This results in the approximately linear current - potential relation

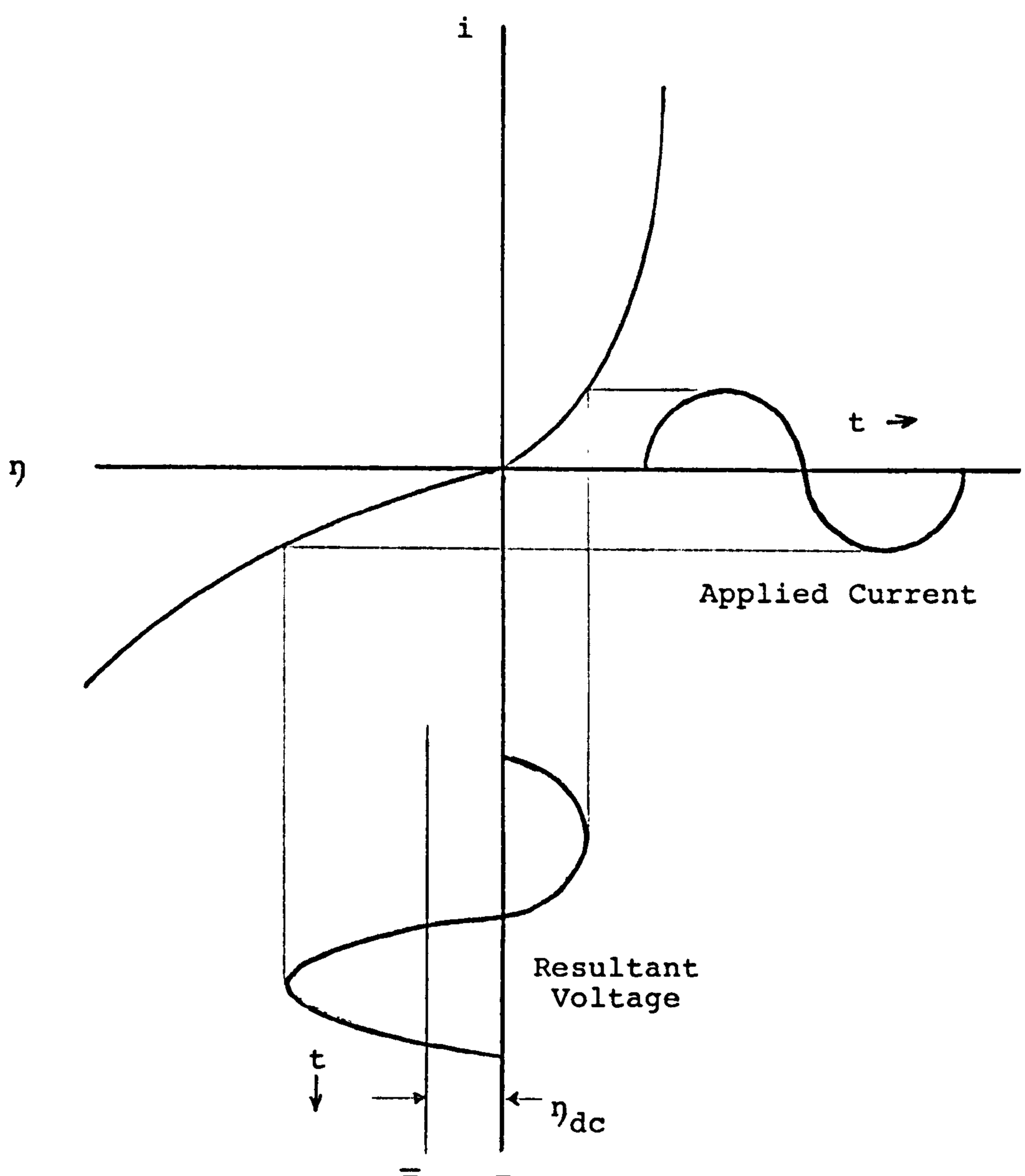

SIGNAL DISTORTION AND FARADAIC RECTIFICATION

Figure 4.5

$$i = -i_o nf\eta \qquad 4.51$$

The ratio - η/i has dimensions of resistance (anodal current being taken as negative in electrochemistry) and is the small signal value of the charge transfer resistance, R_{CT}, where

$$R_{CT} = 1/i_o nf = RT/nFi_o \qquad 4.52$$

As mentioned, if the i-η characteristic is asymmetrical, even this small signal expression for R_{CT} is not strictly linear.

4.1.1.2.2 Large signal nonlinearity

Unfortunately, even if the i-η characteristic is symmetrical about E_{rev}, the characteristic is not a straight line for large signals and hence R_{CT} cannot be a linear resistance at these signal amplitudes.

When the overpotential is large, either the cathodic or anodic current in equation 4.43 is negligible compared with the other, depending on whether the overpotential, η, is positive or negative.

(i) Net cathodic behaviour

If the overpotential is large and negative the second term in the Butler-Volmer equation (equation 4.43) is negligible compared to the first.

Hence $i = i_o \exp[-\alpha nf\eta]$ 4.53

Taking logs

$$\ln i = \ln i_o - \alpha nf\eta \qquad 4.54$$

or $$\eta = \frac{2.303RT}{\alpha nF} \log i_o - \frac{2.303}{\alpha nF} \log i \qquad 4.55$$

Letting

$$a = \frac{2.303RT}{\alpha nF} \log i_o = \frac{.0591}{\alpha n} \log i_o \text{ (at } 25^oC)$$

and $$b = \frac{2.303RT}{\alpha nF} = \frac{.0591}{\alpha n} \text{ (at } 25^oC)$$

it follows that

$$\eta = a - b \log i \qquad 4.56$$

(ii) Net Anodic behaviour

The solution is similar to that of (i) with

$$i = -i_o \exp [(1-\alpha)nf\eta] \qquad 4.57$$

and $$\eta = a' + b' \log i \qquad 4.58$$

(Note that Anodal current is taken as negative)

where $$a' = \frac{-2.303RT}{(1-\alpha)nF} \log i_o = \frac{-.0591}{(1-\alpha)n} \log i_o$$

$$b' = \frac{2.303RT}{(1-\alpha)nF} = \frac{.0591}{(1-\alpha)n} \text{ (at } 25^oC)$$

(Equations 4.56 and 4.58 are known as Tafel equations).

In these Voltage regions the overpotential, η, is proportional to log i - i.e. a linear relationship no longer exists between current and over-Voltage and equation 4.52 for R_{CT} no longer applies.

The non-linear 'log' relationships (equations 4.56 and 4.58) can be expected to hold whenever the back reaction contributes less than 1% of the total current,

$$\frac{\exp [-\alpha nf\eta]}{\exp [(1-\alpha)nf\eta] = \exp [-nf\eta]} \leqslant 0.01$$

In terms of potential, this occurs when

$$\eta \geqslant 4.605\frac{RT}{nF} = \frac{.118}{n} \text{ Volts} \quad (\text{at } 25^oC) \qquad 4.59\ a$$

and in terms of current when

$$i > 10i_o \qquad 4.59\ b$$

The nonlinear, logarithmic relationship applies for over-potentials above $\frac{118}{n}$ mV, where 'n' is the number of electrons taking part in the reaction

$$M^{+n} + ne \rightleftharpoons M$$

The voltage, $118/_n$ mV, can be considered as a "threshold" of non linearity for R_{CT}.

Similarily when the faradaic current is larger than $10i_o$ the charge transfer resistance can be taken as behaving nonlinearly.

In the past the nonlinearity of electrode systems has been investigated using a variety of different waveforms eg

(i) large amplitude ac signals,

(ii) small amplitude ac signals superimposed on a large variable dc bias,

and (iii) large amplitude steps or pulses.

Signals (i) and (ii) will be studied in this chapter which deals with ac nonlinearity, whereas (iii) will be studied in Chapter 5 which investigates nonlinearity effects in the time domain.

As the charge transfer 'resistance' is non linear, its value will very much depend on the amplitude and form of the signal applied. One must therefore be very careful in one's interpretation and definition of measured values of charge transfer 'resistance'.

"R_{CT}" will be, and has been, used to denote the small signal, pseudo linear resistance given by equation 4.52. "$R_{CT(ac)}$", "$R_{CT(dc)}$" and "$R_{CT(ac+dc)}$"

will denote values of charge transfer 'resistance' measured using (i) a large ac signal (ii) a large dc signal and (iii) a large dc signal with a small superimposed ac signal, respectively.

- $R_{CT(ac)}$

Expressions for the charge transfer resistance will be derived in terms of applied current and voltage amplitudes.

- In terms of current (for $i/i_o > 10$)

When applying a large amplitude ac signal, $i_{ac} = I_{ac}\, e^{j\omega t}$ for example, to an electrode system, the value of the charge transfer 'resistance', $R_{CT(ac)}$, is given by

$$R_{CT(ac)} = \left(\frac{\eta ac}{i_{ac}}\right)_{\omega = o} \qquad 4.60$$

From equation 4.57

$$\eta_{ac} = \ln\left[\frac{i_{ac}}{i_o}\right] \frac{1}{(1-\alpha)nf}$$

and hence the quasi dc value of the charge transfer is given by

$$R_{CT(ac)} = \frac{1}{(1-\alpha)nfi_{ac}} \ln\ [\, i_{ac}/i_o\,] \qquad 4.61$$

At $\omega = o$, $i_{ac}=I_{ac}$ and hence

$$R_{CT(ac)} = \frac{1}{(1-\alpha)nfI_{ac}} \ln\ [I_{ac}/i_o] \qquad 4.62$$

As i_o is generally very small, i.e. $I_{ac} >> 30i_o$, the 'ln' term is relatively constant and $R_{CT(ac)}$ is inversely proportional to I_{ac} (see figure 4.6 a)

-In terms of overpotential (above $118/_n$ mV)

Combining equations 4.60 and 4.57 it follows that

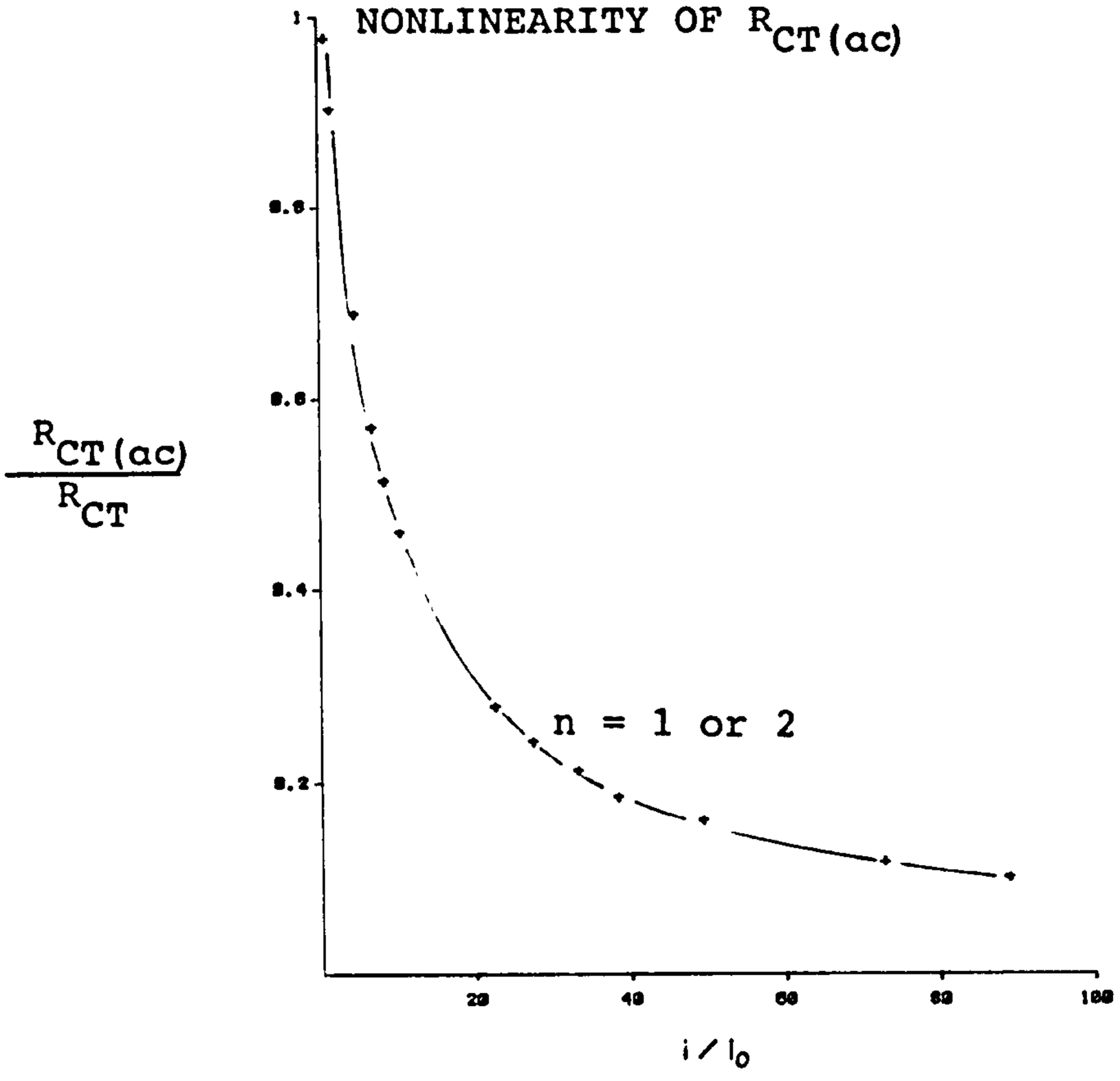

Figure 4.6a

Figure 4.6b

$$R_{CT(ac)} = (\eta_{ac}/i_o) \exp [-(1-\alpha)nf\eta_{ac}] \quad 4.63$$

In equation 4.63 the exponential term dominates and hence $R_{CT(ac)}$ decreases with η_{ac} in a quasi exponential manner (see figure 4.6b)

$-R_{CT(dc+ac)}$

- In terms of current (for $i_{dc}/i_o > 10$)

The value of $R_{CT(dc+ac)}$ measured at a dc voltage other than E_{rev}, i.e. when η_{dc} is not equal to zero, is given by (using equation 4.57)

$$R_{CT(dc+ac)} = \left(\frac{d\eta_{dc}}{di_{dc}}\right)_{\eta dc \neq o} = \frac{d}{di_{dc}}\left(\ln\left[\frac{i_{dc}}{i_o}\right] \frac{1}{(1-\alpha)nf} \right)$$

$$= \frac{RT}{(1-\alpha)nF\ i_{dc}} \quad 4.64$$

Once again the charge transfer 'resistance', in this case $R_{CT(dc+ac)}$, is inversely proportional to the applied current amplitude.

- In terms of voltage (for $\eta_{dc} > 118/n$ mV)

$$R_{CT(dc+ac)} = \frac{RT}{(1-\alpha)nFi_o} \exp [-(1-\alpha)nf\eta_{dc}] \quad 4.65$$

i.e. $R_{CT(dc+ac)}$ decreases exponentially with dc Voltage.

4.1.2 Nonlinearity of the overall electrode-electrolyte interface impedance

In the simplest case the equivalent circuit model of the interfacial impedance consists of (neglecting the relatively small, voltage independent series resistance, R_{TOTAL}) a constant phase angle impedance, Z_{CPA}, in parallel with a charge transfer resistance R_{CT}. The effect of the nonlinearities of Z_{CPA} and R_{CT} on the overall interfacial impedance will be investigated. In section 4.1.2.1 it will be assumed that R_{CT} is linear (which is not very probable) and that Z_{CPA} is the only source of nonlinear behaviour. In section 4.1.2.2 the reverse will be assumed.

4.1.2.1 Overall Nonlinearity due to that of Z_{CPA}

In this section it is assumed that R_{CT} is linear and that Z_{CPA} is the source of all the observed nonlinearity.

The magnitude of the overall interfacial impedance at any frequency is given by

$$Z = \left(\frac{R_{CT}^2}{1+2\omega^{\beta}\cos\phi + \omega^{2\beta}(R_{CT}/K)^2} \right)^{1/2} \qquad 4.66$$

If K decreases from its linear small signal value, K_1, to a new value, K_2, where

$$K_2 = CK_1 \qquad \text{and } 0 < C < 1,$$

then the frequency at which there is a 10% reduction in the magnitude of the interfacial impedance, $\omega_{10\%}$, is derived from the following equality

$$\frac{(0.9)^2 \quad R_{CT}^2}{1+2\cos\phi\,\omega^{\beta}\,\frac{R_{CT}}{K_1}+\omega^{2\beta}\left(\frac{R_{CT}}{K_1}\right)^2} = \frac{R_{CT}^2}{1+2\cos\phi\,\omega^{\beta}\,\frac{R_{CT}}{K_2}+\omega^{2\beta}\left(\frac{R_{CT}}{K_2}\right)^2} \qquad 4.67$$

For very high frequencies this equality is satisfied when

$$\omega_{10\%}^{\beta} = \frac{2K_2}{R_{CT}}\cos\phi\,\frac{[C-(0.9)^2]}{[(0.9)^2-C^2]} \qquad 4.68$$

which applies for $0.9 > C > 0.81$.

From equation 4.68 it is seen that for very small decreases in K [i.e. $K_2 \simeq K_1$, $C \simeq 1$ and $C^2 > (0.9)^2$] no frequency points were affected.

However when C reaches a value of 0.9 (i.e. when $K_2 = 0.9K_1$) extremely high frequencies become affected as their impedances are almost entirely dominated by that of Z_{CPA} - the present source of the nonlinearity. As C is further decreased (i.e. as K_2 is decreased) lower frequencies become affected by the nonlinearity of Z_{CPA} and $\omega_{10\%}$ is given by the expression

$$\omega_{10\%}^{\beta} = \frac{K_2}{2\cos\phi\ R_{CT}}\left(\frac{1-(0.9)^2}{(0.9)^2-C}\right) \qquad 4.69$$

which applies for $C < 0.81$.

At very low frequencies, where the interfacial impedance is dominated by that of R_{CT}, large changes in the magnitude of K have little effect and these points on the impedance locus will remain relatively linear.

Hence, if Z_{CPA} is the source of the observed nonlinear behaviour of the interfacial impedance , nonlinearity will be first noticed at high frequencies as the applied signal amplitude is increased. Larger

signals will affect lower frequencies, and the frequency points on the impedance locus will move anti-clockwise (figure 4.7). For low frequency points, such that $\omega^{\beta} < K_1/R_{CT}$, the reactive component, -Xs, will initially increase as K is decreased, reach a maximum value equal to $R_{CT/2}\ \tan(\phi/_2)$ when $\omega^{\beta} = K_1/R_{CT}$ and will then decrease as K is further decreased.

The real component, R_S, on the other hand, will decrease for all frequencies.

In section 4.1.1 it was shown that Z_{CPA} will become grossly nonlinear for Voltage amplitudes larger than approximately 200 or 300 mV.

Interestingly, Jaron et al (1969) found that Platinum-Iridium, Elgiloy and Stainless Steel electrodes become nonlinear for applied voltage amptitudes in the range of 230 $\pm$50mV to 300 $\pm$ 60 mV (rms) for frequencies between 100Hz and 5 kHz. Although firm conclusions cannot be drawn from their results, it would appear that higher frequency points became nonlinear at slightly lower voltages. These observations would tend to indicate that Z_{CPA} is the major source of the overall interfacial nonlinearity at these relatively high frequencies (above 100 Hz).

At lower frequencies (below 100Hz), however, the limit voltage of linearity, V_L, has been found to be approximately 120 mV (Onaral and Schwan, 1982; Schwan and Onaral, 1985) which does not tally with Z_{CPA} induced nonlinearity. It is very probable that at these lower frequencies the nonlinearity of the charge transfer resistance, R_{CT}, becomes significant. This

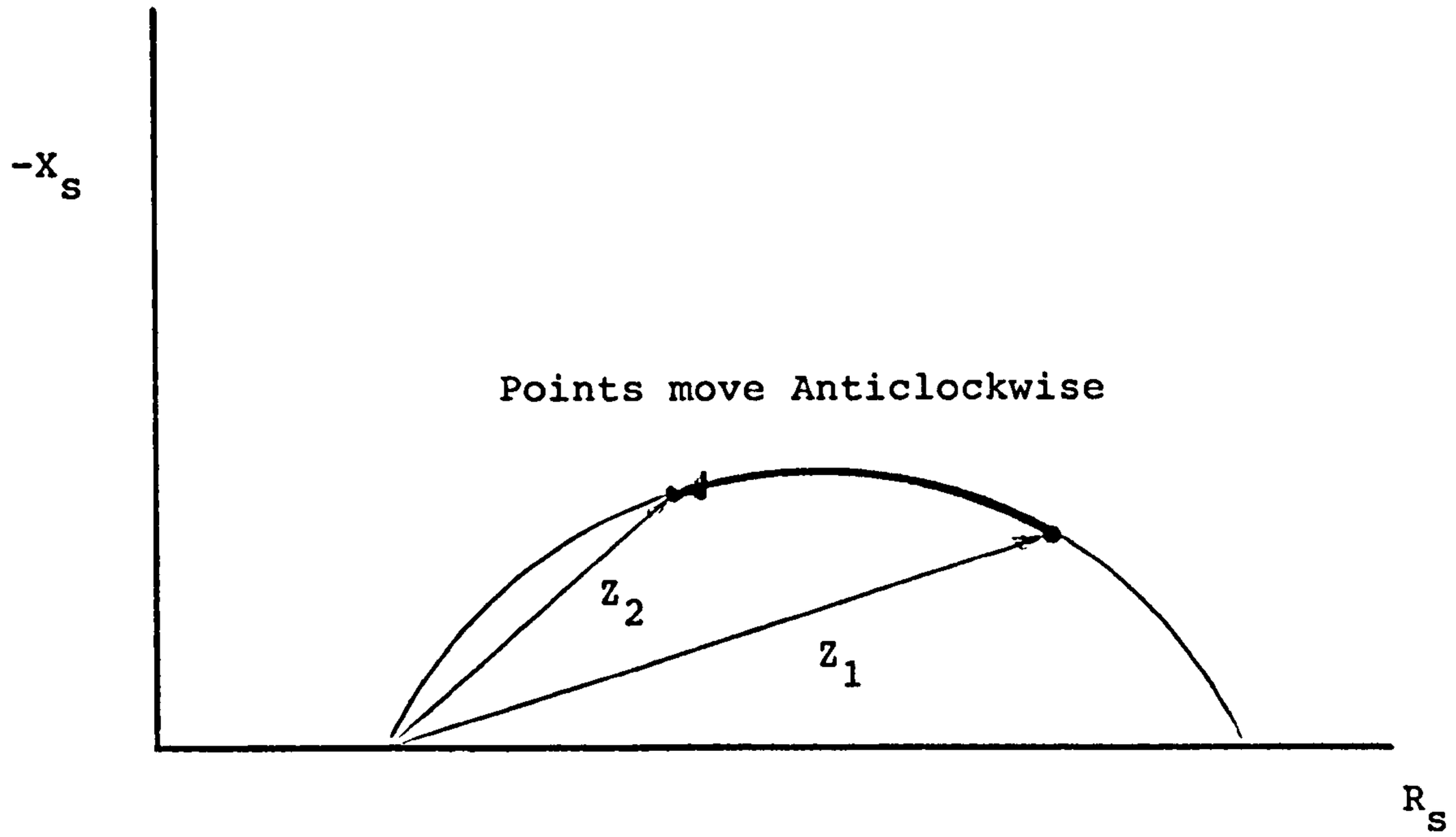

EFFECT OF DECREASING THE MAGNITUDE, K, OF Z_{CPA}.

Figure 4.7

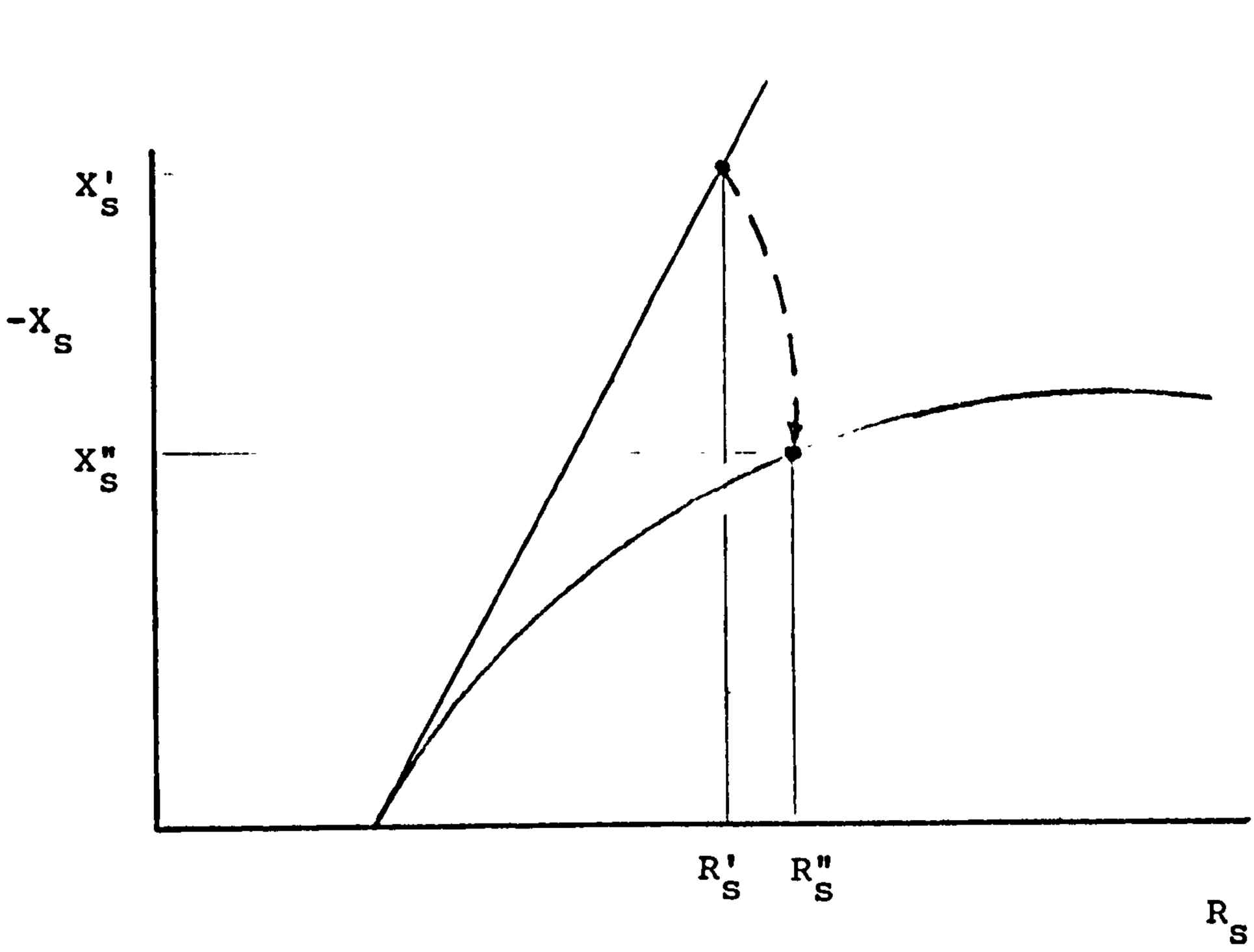

EFFECT OF DECREASING R_{CT}

Figure 4.8

source of nonlinearity will be investigated in the next section.

4.1.2.2 Overall Nonlinearity due to that of R_{CT}

In this section it is assumed that Z_{CPA} is linear and that R_{CT} is the source of all nonlinearity.

As the high frequency end of the Argand locus is dominated by the 'linear' Z_{CPA} impedance the impedances at these frequencies should remain relatively unchanged as the applied current density, for example, is increased. The low frequency end of the arc (figure 4.8), on the other hand, is dominated by the very nonlinear charge transfer resistance and will therefore experience much 'distortion' as the applied signal amplitude is increased. As the value of R_{CT} is approximately inversely proportional to the applied current density (whether I_{ac}, i_{dc} or i_{dc+ac}), when the applied current density is increased, R_{CT}, and hence the arc diameter, will decrease affecting mainly the lower frequency points on the arc.

Many researchers have observed that nonlinearity effects are most dominant at low frequencies. Some (Schwan,1968; Jaron et al,1969) have suggested a limit current of linearity, i_L, which was defined as that current at which C_s and R_s (the series equivalent capacitance and resistance at a given frequency) deviate by a certain percentage (in their case 10%) from their linear values observed at low current densities. A similar 'limit current of linearity' will

be derived from the proposed equivalent circuit model and compared with Schwan's empirical one.

As shown on figure 4.8, points on an impedance locus deviate from their low current density values mainly due to the nonlinearity of the parallel charge transfer resistance. The value of charge transfer resistance needed to deviate a certain high frequency point on the impedance locus, of frequency $f_{10\%}$, by 10% from its linear Z_{CPA} value will be derived. Having established the relationship between R_{CT} and $f_{10\%}$, and knowing that between R_{CT} and the applied current density (equations 4.62 and 4.64), it should then be possible to derive an expression relating the applied current density to the frequency at which there is a 10% change in the magnitude of the impedance. This relation should be of the same form as the empirical nonlinearity rule proposed by Schwan (1968).

In the linear region, R_{CT} is extremely large, and a 'high' frequency point of frequency $f_{10\%}$ has coordinates X_s' and R_s' (see figure 4.8) such that (equation 1.4)

$$R_s' = K\omega^{-\beta}\cos\phi$$

$$X_s' = K\omega^{-\beta}\sin\phi$$

and a magnitude

$$|Z|' = K\omega^{-\beta}$$

As the applied current density is increased the parallel charge transfer resistance will decrease, ω_o [equal to $(K/R_{CT})^{1/\beta}$] will increase and the once straight locus will begin to bend over towards the real axis (figure 4.8). Points of fixed frequency will

follow a semicircular arc given by

$$R_S^2 + \left(X_S - \left(\frac{K}{2\omega^{\beta}\sin\phi}\right)\right)^2 = \left(\frac{K}{2\omega^{\beta}\sin\phi}\right)^2 \qquad 4.70$$

which has intercepts at

$$R_S = o,\ X_S = \frac{K}{\omega^{\beta}\sin\phi}$$

and at $R_S = o,\ X_S = o$

and a radius equal to

$$\frac{K}{2\omega^{\beta}\sin\phi}$$ (see figure 4.9)

When, for a certain frequency, R_S is plotted against R_{CT}^{-1} the resultant curve will have an initial value equal to $K\omega^{-\beta}\cos\phi$ for large values of R_{CT}, i.e. in the linear region. As R_{CT} decreases, R_S initially increases, reaches a maximum value of

$$R_S\ (max) = \frac{K}{2\,\omega^{\beta}\sin\phi} \qquad 4.71$$

at approximately $R_{CT} = K\omega^{-\beta}\sin\phi$ and then decreases towards zero. This 'peak' will be observed for high frequency points such that $\omega^{\beta} > (K/R_{CT})\sin\phi$. For lower frequencies only the decrease in R_S will be observed.

Plots of X_S versus R_{CT}^{-1} will only show a gradual decrease from the linear value,

$$X_S' = K\omega^{-\beta}\sin\phi$$

C_S on the other hand will increase as R_{CT} is decreased from its large, linear value.

At a certain value of current density, and hence of R_{CT}, a point of frequency $f_{10\%}$ will be altered by 10% from its linear value (equation 1.4). It's new coordinates are now X_S'' and R_S'' (figure 4.8) where

$$R_S'' = \frac{R_{CT}[1+\omega^{\beta}(R_{CT}/K)\ \cos\phi]}{1 + 2\omega^{\beta}(R_{CT}/K)\cos\phi + \omega^{2\beta}(R_{CT}/K)^{\beta}} \quad 4.72a$$

$$\text{and} \quad X_S'' = \frac{R_{CT}\ \omega^{\beta}(R_{CT}/K)\ \sin\phi}{1 + 2\omega^{\beta}(R_{CT}/K)\cos\phi + \omega^{2\beta}(R_{CT}/K)^{\beta}} \quad 4.72b$$

$$\text{and} \quad |Z|'' = \left(\frac{R_{CT}^2}{1 + 2\cos\phi\,\omega^{\beta}(R_{CT}/K) + \omega^{2\beta}(R_{CT}/K)^{\beta}}\right)^{1/2} \quad 4.72c$$

The frequency, $f_{10\%}$, at which

(i) $|Z|''$ differs from $|Z|'$ by 10% is given by

$$\omega_{10\%}^{\beta} \simeq 8.53\ \cos\phi\left(\frac{K}{R_{CT}}\right) \quad 4.73$$

(ii) R_S'' differs from R_S' by 10% is

$$\omega_{10\%}^{\beta} \simeq \frac{10}{\cos\phi}\left(\frac{K}{R_{CT}}\right) \quad 4.74$$

(111) X_S'' differs from X_S' by 10% is given by

$$\omega_{10\%}^{\beta} \simeq 18\ \cos\phi\left(\frac{K}{R_{CT}}\right) \quad 4.75$$

and (iv) C_S'' (where $X_S'' = 1/j\omega C_S''$) differs from C_S' by 10% is given by

$$\omega_{10\%}^{\beta} \simeq 20\ \cos\phi\left(\frac{K}{R_{CT}}\right) \quad 4.76$$

For all the coordinates used, the frequency at which there is a 10% change in the impedance, due to the presence of the nonlinear charge transfer resistance, is inversely proportional to $(R_{CT})^{1/\beta}$.

It will be noticed that the frequency at which nonlinearity is taken to commence, $\omega_{10\%}$, depends on

whether one considers the percentage change in $|Z|$, R_S X_S or C_S. Schwan and his colleagues used the real and imaginary axis, R_S and C_S (where $C_S = 1/\omega X_S$), to determine the onset of nonlinearity. Comparing equations 4.74 and 4.76, it is evident that the derived values of $\omega_{10\%}$ differ. If one denotes by $\omega_{R(10\%)}$ that derived from the real axis, and by $\omega_{C(10\%)}$ that from the imaginary axis, one has

$$\frac{\omega_{R(10\%)}}{\omega_{C(10\%)}} = \left(\frac{0.5}{\cos^2\phi}\right)^{1/\beta} \qquad 4.77$$

For example, if $\phi = 80^o$ (ie $\beta = 0.89$), the above ratio equals 23.5 and $\omega_{R(10\%)} > \omega_{C(10\%)}$.

Hence for a given value of R_{CT}, $\omega_{R(10\%)}$ is larger than $\omega_{C(10\%)}$ provided that ϕ is larger than 45^o, which is generally the case.

- Current and voltage limits of linearity, i_L and V_L

Equations 4.62 and 4.64 related the charge transfer resistances, $R_{CT(ac)}$ and $R_{CT(ac + dc)}$, to the applied current density. Substituting these into equations 4.73 to 4.76 will enable the derivation of expressions relating the applied current density, i_{ac} or i_{dc+ac}, to the frequency of the point which is deviated by 10% from its linear value. In other words an expression for the limit current of linearity, i_L, in terms of the applied frequency will be derived.

Expressions for the limit voltage of linearity, V_L, can be derived by combining equations 4.63 and 4.65 with equations 4.73 to 4.76.

As this chapter is concerned with the ac

impedance, the nonlinearity of the electrode system will only be studied when the applied signal is either

(i) a large amplitude ac signal, i_{ac} or V_{ac}

or (ii) a small amplitude ac signal superimposed on a large dc bias, i_{dc+ac} or V_{dc+ac}.

4.1.2.2.1 Large amplitude ac signals

- ac limit current of linearity, $i_{ac.L}$

The limit current of linearity can be derived by substituting equations 4.73 to 4.76, relating $\omega_{10\%}$ to R_{CT}, into equation 4.62 relating R_{CT} to I_{ac} and rearranging. However, it must be remembered that equation 4.62 related the magnitude of R_{CT} to the ac faradaic current flowing through it - not to the total current, i_{TOTAL}, where

$$i_{TOTAL} = i_{R_{CT}} + i_{Z_{CPA}} = i_f + i_{nf}$$

i.e. to the sum of the faradaic and nonfaradaic currents (see figure 1.3)

(i) using $|Z|$

At the onset of nonlinearity

$$Z_{CPA} = K\omega^{-\beta} = \frac{R_{CT}}{8.53\cos\phi} \quad \text{(from equation 4.73)}$$

Therefore

$$i_{TOTAL} = i_f + i_{nf} = i_f[1+8.53\cos\phi] \qquad 4.78$$

As $$i_{f.LIMIT} = \frac{\ln(i_f/i_o)\ \frac{1}{(1-\alpha)nf}}{8.53K\cos\phi}\ \omega_{10\%}^{\beta}$$

(from equations 4.73 and 4.62), then the limit of linearity of total current, $i_{ac.L}$, is

$$i_{acL} = \frac{1+8.53\cos\phi}{8.53\ K\cos\phi} \ln\left[\frac{i_f}{i_o}\right] \frac{\omega_{10\%}^{\beta}}{(1-\alpha)\ nf} \qquad 4.79$$

As $i_f > i_o$, 'ln[i_f/i_o] ' is relatively constant and the limit current of linearity can be taken as being proportional to $\omega_{10\%}^{\beta}$ as found by Schwan (1968).

(ii) using R_s

At the onset of nonlinearity (from equation 4.74)

$$Z_{CPA} = K\omega^{-\beta} \simeq R_{CT}\cos\phi/10$$

Therefore $i_{TOTAL} = i_f\ [1+(10/\cos\phi)]$ 4.80

As $i_{f.LIMIT} = \frac{\cos\phi}{10K} \frac{1}{(1-\alpha)nf} \ln\left[\frac{i_f}{i_o}\right] \omega_{10\%}^{\beta}$

(from equations 4.74 and 4.62)

therefore

$$i_{ac.L} = [1+(10/\cos\phi)] \frac{\cos\phi \ln[i_f/i_o]}{10K} \frac{1}{(1-\alpha)nf} \omega_{10\%}^{\beta} \qquad 4.81$$

(iii) Using C_s

At the onset on nonlearity (from equation 4.76)

$$Z_{CPA} = K\omega^{-\beta} \simeq \frac{R_{CT}}{20\cos\phi}$$

hence $i_{TOTAL} = i_f\ [1+20\cos\phi\ ]$ 4.82

As $i_{f.LIMIT} = \frac{1}{20K\cos\phi} \ln\left[\frac{i_f}{i_o}\right] \frac{1}{(1-\alpha)nf} \omega_{10\%}^{\beta}$

(from equations 4.76 and 4.62), therefore

$$i_{ac.L} = \frac{1+20\cos\phi}{20K\cos\phi} \ln\left[\frac{i_f}{i_o}\right] \frac{1}{(1-\alpha)nf} \omega_{10\%}^{\beta} \qquad 4.83$$

As the total current is increased, $R_{CT(ac)}$ decreases, causing the impedance locus to bend over 'sooner' i.e. at higher frequencies. A larger ac current is therefore required to 'distort' the

magnitude of the interfacial impedance at a high frequency by 10% from its small signal value than at a low frequency. The limit current of linearity, $i_{ac.L}$ is proportional to $\omega^{\beta}_{10\%}$ as observed experimentally by Schwan and his colleagues.

It must of course be remembered that this 'threshold' of nonlinearity is not really a threshold at all, as there is a gradual transition between Z_{CPA} and R_{CT} domination, and hence between linear and nonlinear behaviour. The choice of a 10% deviation 'threshold' is quite arbitrary, and some (eg Geddes et al, 1971) have used a 20% deviation.

It was shown that the equivalent series resistance, R_s, should at first increase, reach a maximum equal to

$$\frac{K}{2\omega^{\beta}\sin\phi}$$ (equation 4.71) and then decrease as R_{CT} is decreased or I_{ac} increased. This peak however will only be observed if the range of applied current amplitudes starts low enough and the range of frequencies high enough. If β is less than or equal to 0.5 (i.e. $\phi = 45^{o}$, see figure 4.9) the peak will not be observed at all.

The series reactive component, X_s should simply decrease, for a given frequency, as the applied current amplitude is increased.

Schwan (1968), Jaron et al (1969) and Geddes et al (1971) observed C_s (equal to $^{1}/\omega X_s$) to increase and R_s to decrease as the applied ac current amplitude was increased. Apparently no 'peak' was observed on their

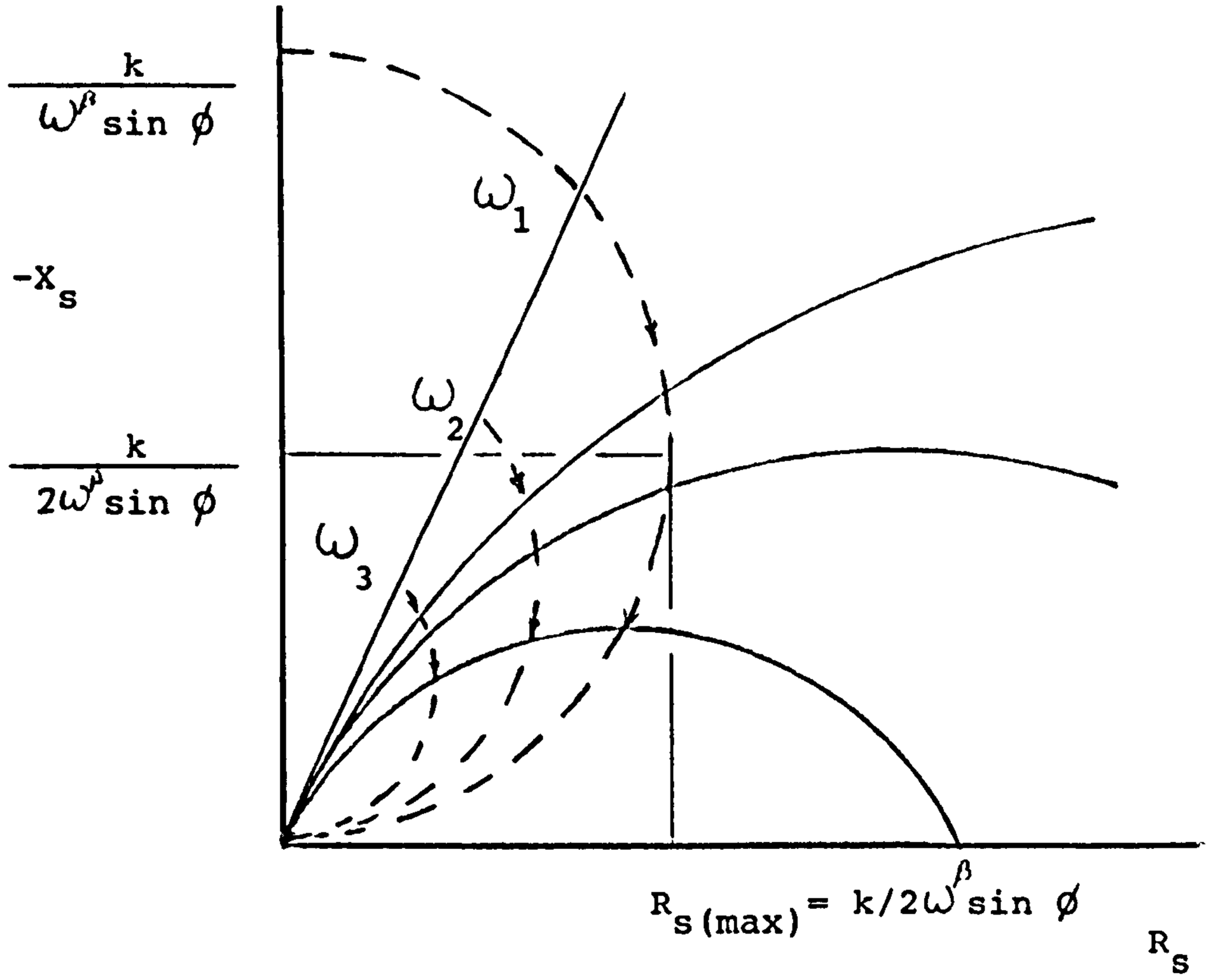

CHANGES IN R_S AND X_S WITH DECREASES IN R_{CT}

Figure 4.9

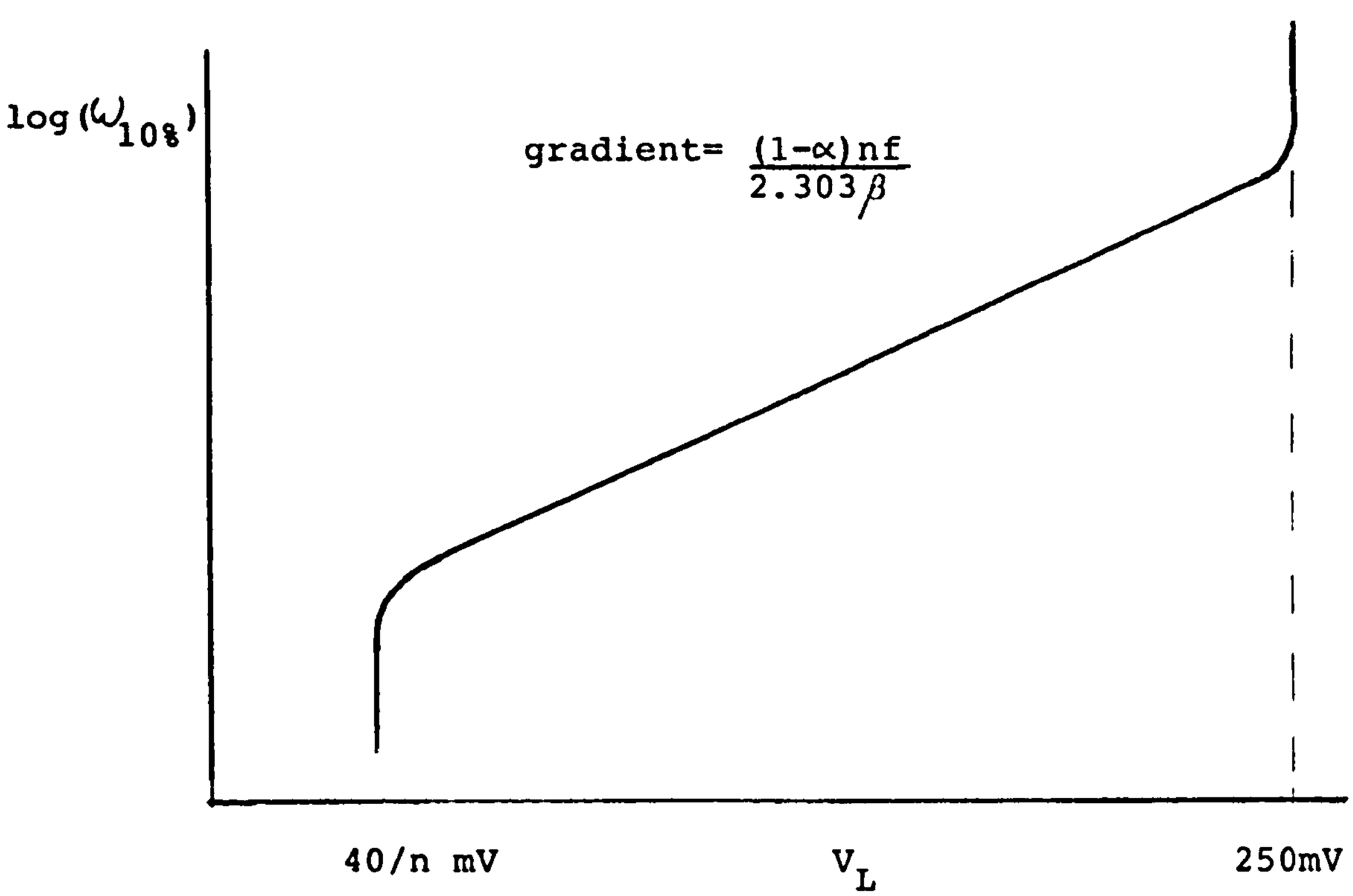

PREDICTED PLOT OF
$LOG(\omega_{10\%})$ VS. THE LIMIT VOLTAGE OF LINEARITY, V_L

Figure 4.10

R_s - log I_{ac} plots. This absence could however be due to one of several factors.

It is possible that the nonlinearity of Z_{CPA}, which results in a decrease in R_s, masks the expected initial increase due to the nonlinearity of R_{CT} - especially at high frequencies. Geddes et al's plot, which has the widest and lowest range of current amplitudes (0.025 to 25 mA(rms) cm^{-2}) is not linear in the small signal region, in contrast to their C_s - log I_{ac} plot. The same applies for the R_s - log I_{ac} plot of Jaron et al (1969).

Most of the plots made (with the exception of that of Geddes et al) were probably not made at frequencies high enough and current amplitudes low enough to witness the peak on the R_s-log I_{ac} plot.

Another problem was that several of the groups plotted curves for electrodes whose values of β were close to 0.5 (Geddes et al 1971, Schwan 1968 and possibly others). Under such circumstances a peak would not be expected and R_s would simply decrease with current amplitude.

R_s and C_s plots against signal amplitude are investigated experimentally as part of this study and the results are described in Section 4.2.3.

From the equivalent circuit model (figure 2.2.a) the derived value of $i_{ac.L}$ using the series resistive component, R_s, generally differs from that derived using C_s as

$$\frac{i_{ac.L} \text{ from } R_s}{i_{ac.L} \text{ from } C_s} = \frac{2\,[\,1 + (10/\cos\phi)\,]\,\cos^2\phi}{[\,1 + 20\cos\phi\,]}$$

(from equations 4.81 and 4.83)

For ϕ >45, as is generally the case, $i_{ac.L}(R_s)$ is smaller than $i_{ac.L}(C_s)$, i.e. the electrode system appears to become nonlinear for smaller current amplitudes if the R_s component is used instead of that due to C_s.

Although Schwan (1968) found $i_{ac.L}(R_s)$ to be smaller than $i_{ac.L}$ (C_s), Jaron et al (1969) and Geddes et al (1971) found the opposite to be true. However Geddes et al's electrodes had a β value of approximately 0.5 and hence no significant difference in the two values of $i_{ac.L}$ is expected. Both Jaron et al and Geddes et al do not appear to have used their lowest current density values of R_s as the linear value and this would result in a larger $i_{ac.L}(R_s)$ threshold than would otherwise have been expected.

- ac limit voltage of linearity, $V_{ac.L}$

For voltages (overpotentials) above 118/n mV the charge transfer resistance is very nonlinear (see figure 4.7) and approximated by equation 4.63, i.e.

$$R_{CT(ac)} = \left(\frac{2}{i_o}\right) \exp\ [-(1-\alpha)nf\eta]$$

At high frequencies the relationship between $R_{CT(ac)}$ and $\omega_{10\%}$ is given by equation 4.73, i.e.

$$R_{CT(ac)} = 8.53\ K \cos\phi\ \omega_{10\%}^{-\beta}$$

Combining these expressions, one has

$$\omega_{10\%}^{\beta} = \frac{8.53K\cos\phi\, i_o}{\eta_L} \exp\ [(1-\alpha)nf\eta_L] \qquad 4.84$$

or rearranging

$$V_{ac.L} = \eta_L = \frac{2.303\beta}{(1-\alpha)nf} \log \omega_{10\%} + \frac{2.303}{(1-\alpha)nf} \log\left(\frac{\eta_L}{8.53K\cos\phi i_o}\right) \qquad 4.85$$

The second term on the right hand side of equation 4.85 is relatively constant and therefore $V_{ac.L}$ can be taken as proportional to $\log \omega_{10\%}$

As the gradient, $\frac{(1-\alpha)nf}{2.303\beta} \cong 20$, of a $V_{ac.L}$ -$\log\omega_{10\%}$ plot is very large, $V_{ac.L}$ will only increase slightly with frequency.

In the past, however, it has been assumed that $V_{ac.L}$ is constant and independent of frequency. Schwan (1968), for example postulated arbitrarily that the voltage across the interface (modelled simply by a Z_{CPA}) could not surpass a certain frequency independent value, $V_{ac.L}$. Schwan admitted that his data did not necessarily indicate that a constant voltage was approached which was entirely frequency independent.

More recently, however, Onaral and Schwan (1982) claimed that the value of the voltage limit of linearity, $V_{ac.L}$, is frequency independent and that it occurs at approximately 100 mV. They obtained average values of 117.3 and 128 mV in 1982 and 125 mV in 1985. Close inspection of their data reveals that $V_{ac.L}$ increases slightly with frequency over the frequency range 0.01Hz to 100Hz. This would agree with equation 4.85.

Schwan's theory neglects the presence of the parallel resistance R_{CT} and hence assumes that ZCPA is

the source of all the observed nonlinear behaviour. At the low frequencies used by Onaral and Schwan(1982), however, the observed nonlinearities are mainly due to those of R_{CT}.

Although Onaral and Schwan have commented on the possibility of modelling the linear interfacial impedance by an equivalent circuit including a parallel dc resistance, they appear to have failed to recognise it as being the major source of the observed nonlinearities. This is most surprising as Schwan and his colleagues (Simpson et al, 1980) had previously pointed out that their dc current-voltage plot obeyed, what they termed, the "Tafel law" (actually the Butler-Volmer equation, see equation 4.43) - from which the expression for the charge transfer resistance is derived! Onaral and Schwan (1982) even noted that at low frequencies "the semi-logarithmic dependence of the interface potential on current right at the exit from linearity is precisely the behaviour described by the empirical relationship formulated for the dc case". In other words, the interfacial impedance becomes nonlinear at low frequencies where the shunting charge transfer resistance begins to dominate. However they concluded that their limit current of linearity expression would no longer be valid at very low frequencies as they expected "strong deviations from the predictions of models neglecting the dc shunt resistance". Hence, instead of perceiving the "dc shunt resistance" as the major source of the observed nonlinear behaviour, they considered it as an

additional, unrelated problem.

Although it is true that Z_{CPA} will "become nonlinear" at a certain voltage (approx 250 mV), R_{CT} "becomes nonlinear" at considerably smaller voltages (at approximately 40/n mV, See fig 4.7) and hence is more important.

As R_{CT} is shunted by a relatively linear Z_{CPA}, all frequency points on the impedance locus do not become nonlinear at the same overpotential. Extremely low frequency points (almost dc)"become nonlinear" when R_{CT} decreases to 90% of its linear value - at approx 40/n mV. Higher frequencies, whose impedances are less dominated by that of R_{CT}, become "nonlinear" at higher voltages - generally over 100 mV. Very high frequency points will however only be distorted when Z_{CPA} becomes nonlinear - at approximately 250 mV (see figure 4.10).

The above probably explains the apparent discrepency between the results of Jaron et al (1969) who obtained values of $V_{ac.L}$ around 250 mV(rms) whereas Onaral and Schwan (1982) obtained values around 120 mV. Jaron et al's measurements were taken at relatively high frequencies (100Hz to 5kHz) whereas those of Onaral and Schwan were taken at low frequencies (10mHz to 100Hz).

The $V_{ac.L}$ - $f_{10\%}$ results of Onaral and Schwan (1982, figure 5) where plotted on a $\log(\omega)_{10\%}$ versus $V_{ac.L}$ graph similar to that of figure 4.10. The resultant gradient was found to have a value of approximately 30,

$$\text{i.e.} \qquad \frac{(1-\alpha)nf}{2.303\beta} = 30$$

As $f = 39$ and $\beta = .8$, it follows that $(1-\alpha)n = 1.4$ and that the most probable values of n and α are $n = 2$ and $\alpha = 0.3$.

The smaller value of α (a value of 0.5 was used in figure 4.10) increases the slope of the $V_{ac.L}$ -log$\omega_{10\%}$ plot and a wider range of frequencies is affected by a given range of applied voltage amplitudes.

Hence Onaral and Schwan observed that $V_{ac.L}$ lay within the small voltage range 106 to 129 mV for frequencies within the wide range of 0.04Hz to 100 Hz.

4.1.2.2.2 Small ac signal superimposed on a large dc bias

- dc + ac current of linearity, $I_{dc+ac.L}$

The frequency at which there is a 10% change in the impedance due to the presence of R_{CT} is given by equations 4.73 to 4.76. By combining these with equation 4.64, expressions for $I_{dc+ac.L}$ can be derived.

(1) Using R_s

As $i_{TOTAL} = i_f + i_{nf} = i_f[1+(10/\cos\phi)]$ (4.80)

it follows that the dc limit of current linearity, $I_{dc+ac.L}$, is given by

$$I_{dc+ac.L} = \left[1 + \frac{10}{\cos\phi}\right] \frac{\cos\phi}{10K} \frac{1}{(1-\alpha)nf} \omega_{10\%}^{\beta} \qquad 4.86$$

and (ii) for C_s (using equation 4.82)

$$I_{dc+ac.L} = \left(\frac{1 + 20\cos\phi}{20K \quad \cos\phi}\right) \frac{1}{(1-\alpha)nf} \omega_{10\%}^{\beta} \qquad 4.87$$

$I_{dc+ac.L}$ is therefore proportional to ω^{β} as in the ac case. Increasing the dc bias decreases the magnitude of $R_{CT(dc+ac)}$, causing progressively higher frequencies to deviate significantly from their linear, small signal values.

Unfortunately the dc+ac nonlinearity of electrode systems does not appear to have been widely investigated and no comparisons were possible.

- dc + ac limit voltage of linearity, $V_{dc+ac.L}$

Combining equations 4.65 and 4.73 one obtains, for high frequencies and voltages above $118/_n$ mV, the expression

$$\omega^{\beta}_{10\%} = 8.53K \cos\phi(1-\alpha)nfi_o \exp[(1-\alpha)nf\eta_L] \qquad 4.88$$

Rearranging equation 4.88 one obtains,

$$V_{dc+ac.L} = \eta_L = \frac{2.303\,\beta}{(1-\alpha)nf} \log\omega_{10\%} + \frac{2.303}{(1-\alpha)nf} \log\left[\frac{1}{8.53K\cos\phi(1-\alpha)nfi_o}\right] \qquad 4.89$$

The second term on the right hand side of equation 4.89 is a constant and therefore $V_{dc+ac.L}$ is proportional to $\log\omega_{10\%}$ as in the ac case (equation 4.85).

Again, it is unfortunate that little, if any, work has been done in this area and no comparisons with experimental data were possible.

4.1.3 Conclusions

The proposed model, comprising a constant phase angle impedance due to adsorption and surface roughness effects and a nonlinear charge transfer resistance, appears to account physically for both the linear and nonlinear behaviour of electrodes in the frequency domain - something which has not hitherto been achieved (Fischler and Schwan, 1981).

Schwan's (1968) empirical "limit current of linearity" relationship (where i_L is proportional to $\omega_{10\%}$) is interpreted as being due to the charge transfer resistance decreasing with applied signal amplitude causing progressively higher frequency points to deviate from their small signal Z_{CPA} behaviour. The voltage limit of linearity is not constant, as postulated by Schwan, but increases for higher frequencies. Again this nonlinear behaviour is due to that of R_{CT}, except at relatively very high frequencies where the interfacial impedance is dominated by that of Z_{CPA}.

In the experimental section, 4.2, the nonlinearities of electrode interface impedances, and the adequacy of the proposed model, will be further-investigated.

4.2 EXPERIMENTAL SECTION

In this section the nonlinear behaviour of various electrode-electrolyte interfaces is investigated experimentally.

The dc current-voltage characteristics are measured and plotted in order to obtain an insight into the current /voltage dependance of $R_{CT(dc+ac)}$ and $R_{CT(ac)}$.

The "dc +ac" impedance is then obtained for various dc bias amplitudes and the dependance of $R_{CT(dc+ac)}$, K and β on applied signal amplitude determined.

The ac impedance is plotted for a range of ac voltage amplitudes to establish the dependance of $R_{CT(ac)}$, K and β on ac voltage amplitude. The limit voltage of linearity, V_L, is calculated for each of the applied frequencies.

Finally the distortion of ac signals at low frequencies is investigated using Lissajous figures.

4.2.1 i -η characteristics

- Experimental set up and technique

Current was applied to the various electrode systems under study (see figure 1.31) using a DC current calibrator (Type 609) and the resultant voltage was recorded using a pen recorder. The current magnitude was progressively increased in small steps and the system was left to settle for only one minute

before the subsequent current increase. The resultant voltage was taken as that reached at the end of each one minute settling period. The use of a relatively short delay enabled rapid measurement of the i-η curve and, although it did not enable accurate quantitative results, it enabled the key characteristics of the curve to be observed. In order to measure a "true" i-η characteristic, a settling time of over half an hour is normally used at each current level. At the higher current amplitudes this would have resulted in gross irreversible changes in the electrode's electrical properties and hence was judged unacceptable as well as time consuming.

The use of a one minute delay is equivalent to measuring the electrode system's impedance at a frequency of 17 mHz, at which frequency the interfacial impedance should be dominated by the parallel, faradaic charge transfer resistance.

4.2.1.1 'Smooth' electrodes

Telectronic 224 (Platinum) Electrode

The i -η curve for the Telectronic 224 electrode is plotted on figure 4.11. Between -1.5 and + 0.7 volts the curve is as expected (see figure 4.4), obeying the Butler-Volmer equation (equation 4.43) and having a reversible potential, E_{rev}, of approximately -450 mV (this parameter however varies greatly with electrode history).

For anodic potentials the i -η characteristic 'levels off' at about 1 Volt, or 10μA, and then rises

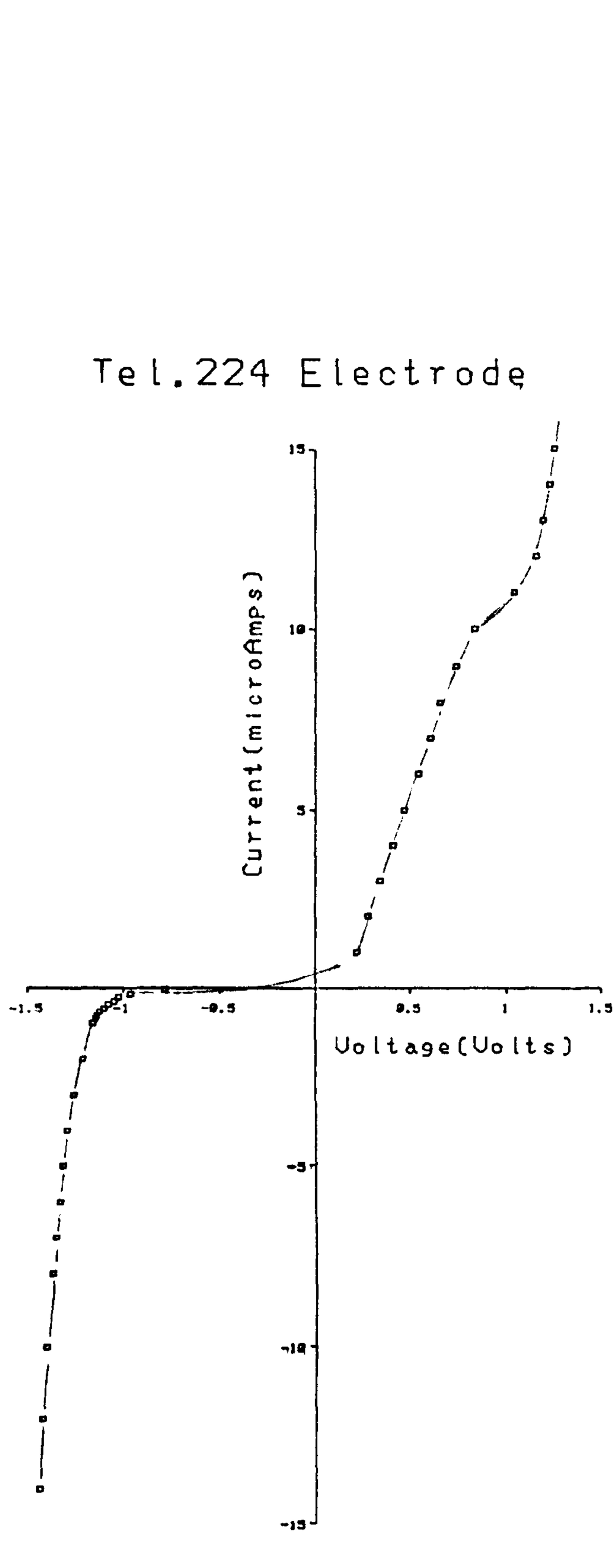

DC CURRENT VS. DC VOLTAGE

Figure 4.11

sharply again (figure 4.11). A Tafel plot (figure 4.12a) shows two "Tafel" regions (ie where η is proportional to log i) separated by a current limiting region.

[As $-i = i_o \exp[(1-\alpha)nf\eta]$ (equation 4.57)

for large anodic potentials, one has

$$\log |i| = \log i_o + \frac{(1-\alpha)nf\eta}{2.303} = c + d\eta$$

i.e. log $|i|$ is proportional to η as found experimentally.]

The gradient, d, which is proportional to $(1-\alpha)$, is smaller and i_o is larger in the second Tafel region. $R_{CT(ac)}$ and $R_{CT(dc+ac)}$ which are both proportional to $(1-\alpha)^{-1}$ (see equations 4.62 and 4.64) will therefore be larger in this region than would be expected from extrapolation of the lower Tafel region results.

Bubbling was observed on the electrode surface for currents above the tempory current limited region i.e. in the second anodic Tafel region.

For cathodic currents only one Tafel region is observed (figure 4.12b), where

$$\log i = \log i_o - \frac{\alpha nf\eta}{2.303} = c^1 - d^1\eta$$

It is possible that the current limitation occurs at very small currents (less that $0.1\mu A$) and thus the first Tafel region is not observable within the applied current range.

For large amplitude signals, bubbles were noticed on the electrode's surface. Estimated values of i_o are less than those found in both anodic Tafel regions.

Tel.224 Electrode

Tafel Plot: log(I) vs Overpotential

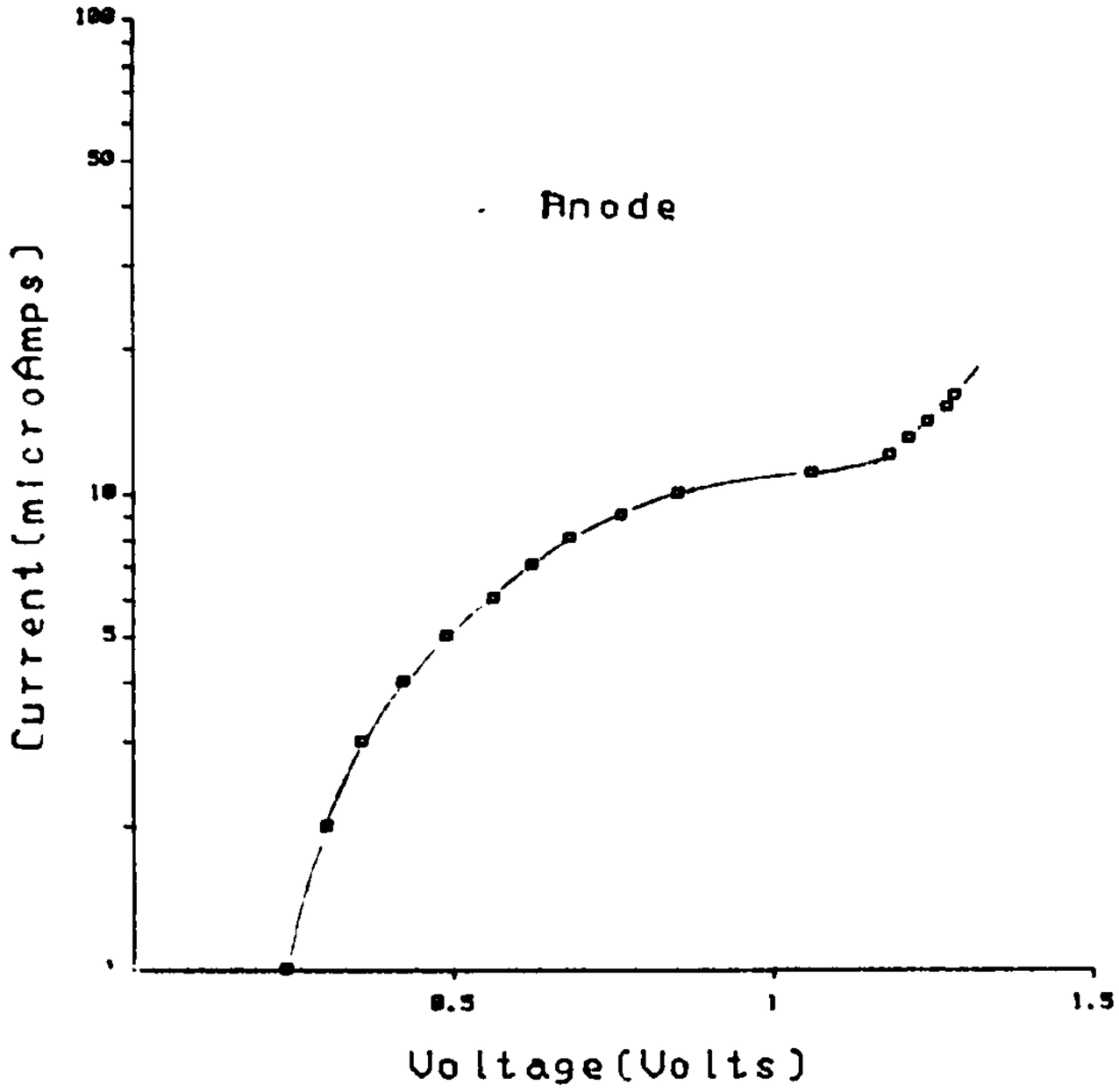

Figure 4.12a

Tel.224 Electrode

Tafel Plot: log(I) vs Overpotential

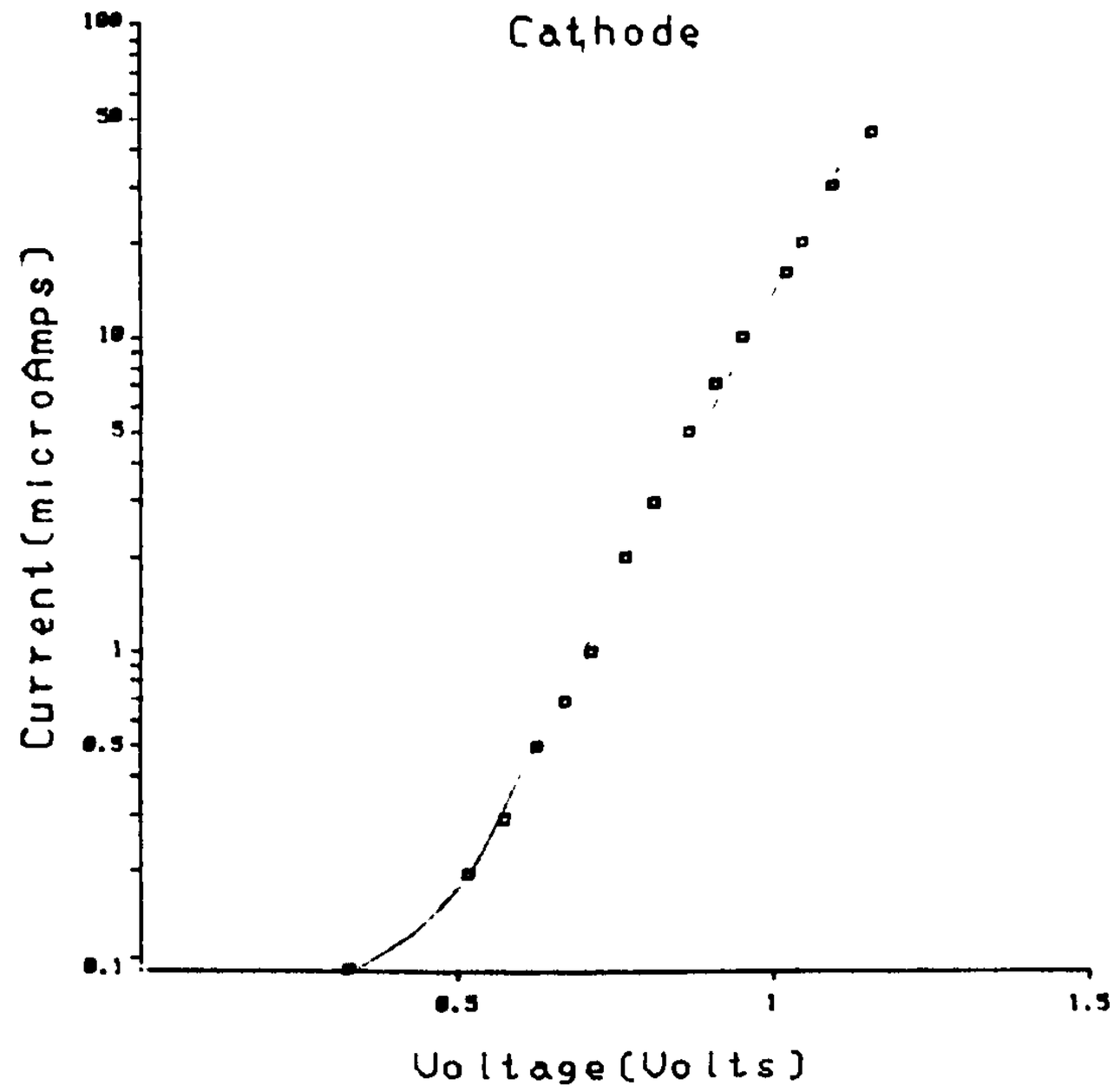

Figure 4.12b

4.2.1.2 Rough electrodes

- Roughened Devices SC Electrode

Using a Devices SC ($21mm^2$, No1) electrode, the effects of surface roughness on the i -η characteristic (and hence on the magnitude of the charge transfer resistances, $R_{CT(ac)}$ and $R_{CT(dc+ac)}$) were investigated.

Initially the measurements were made with a 'smooth' electrode. The electrode was then roughened using P60 Emery paper and the measurements repeated.

(i) Smooth Surface

(a) for positive overpotentials (E_{rev} = - 350mV) there are two Tafel regions (figures 4.13 and 4.14a). Again i_o is larger, and the gradient, d, smaller in the second Tafel region. The 'voltage jump' occurs at approximately 15 to 20μA. Above this region gas bubbles were observed on the electrode surface.

(b) for negative overpotentials two Tafel regions are observed (figures 4.13 and 4.14b) , although on figure 4.13 they are not very cleary distinguishable. The second Tafel region begins at approximately 1μA. In this region i_o is larger and d^1, the gradient, smaller than in the first Tafel region.

It would appear that the electrode interface behaves somewhat as a rectifier with more current flowing for anodal voltages than for cathodal (figure 4.13).

(ii) Rough Surface

(a) For positive overpotentials the Tafel regions are not so clearly separated. The limiting current at

Effect of Surface Roughness

on the dc current-dc voltage plot

Dev. S.C. Electrode

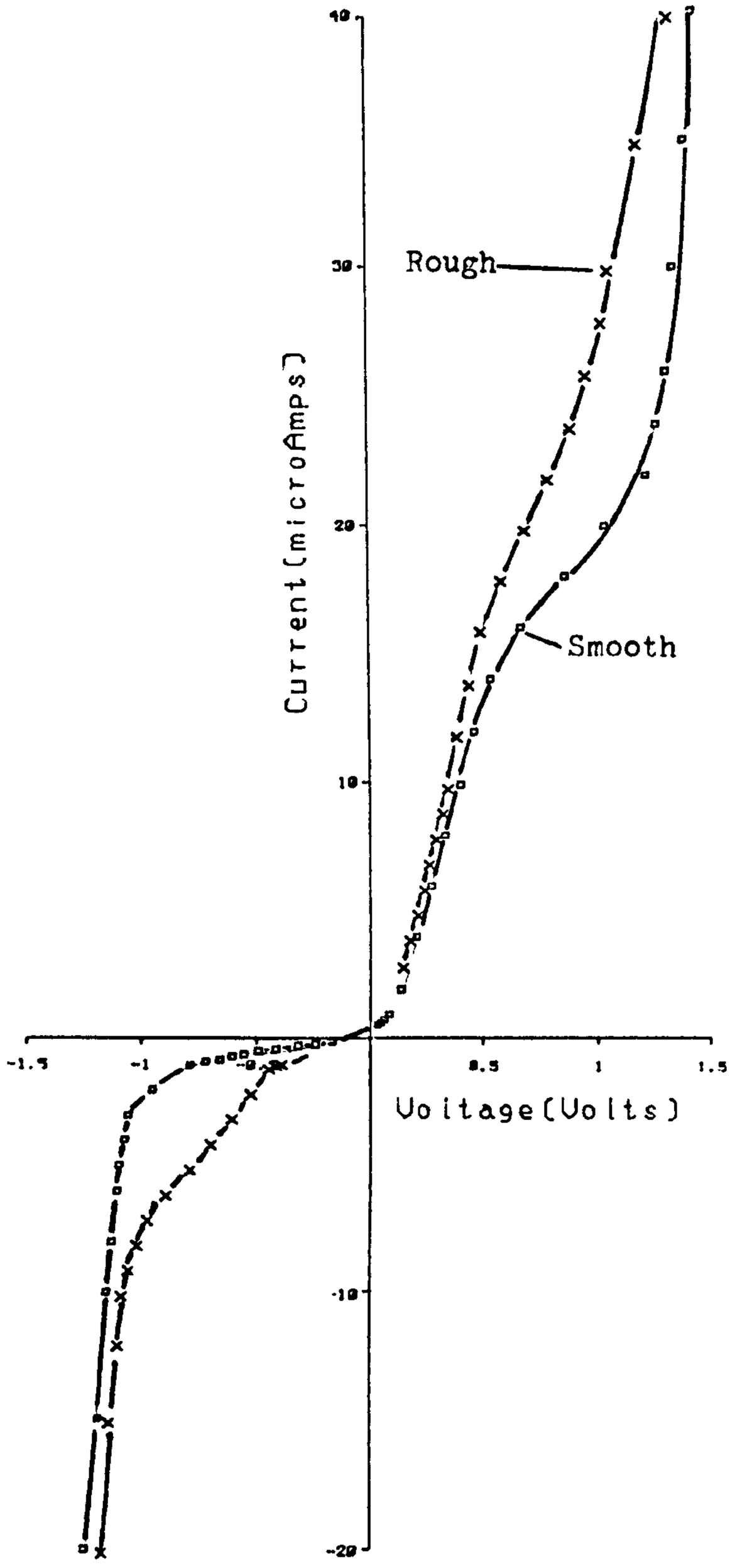

Figure 4.13

Effect of Surface Roughness

Tafel Plot: Log(I) vs Overpotential

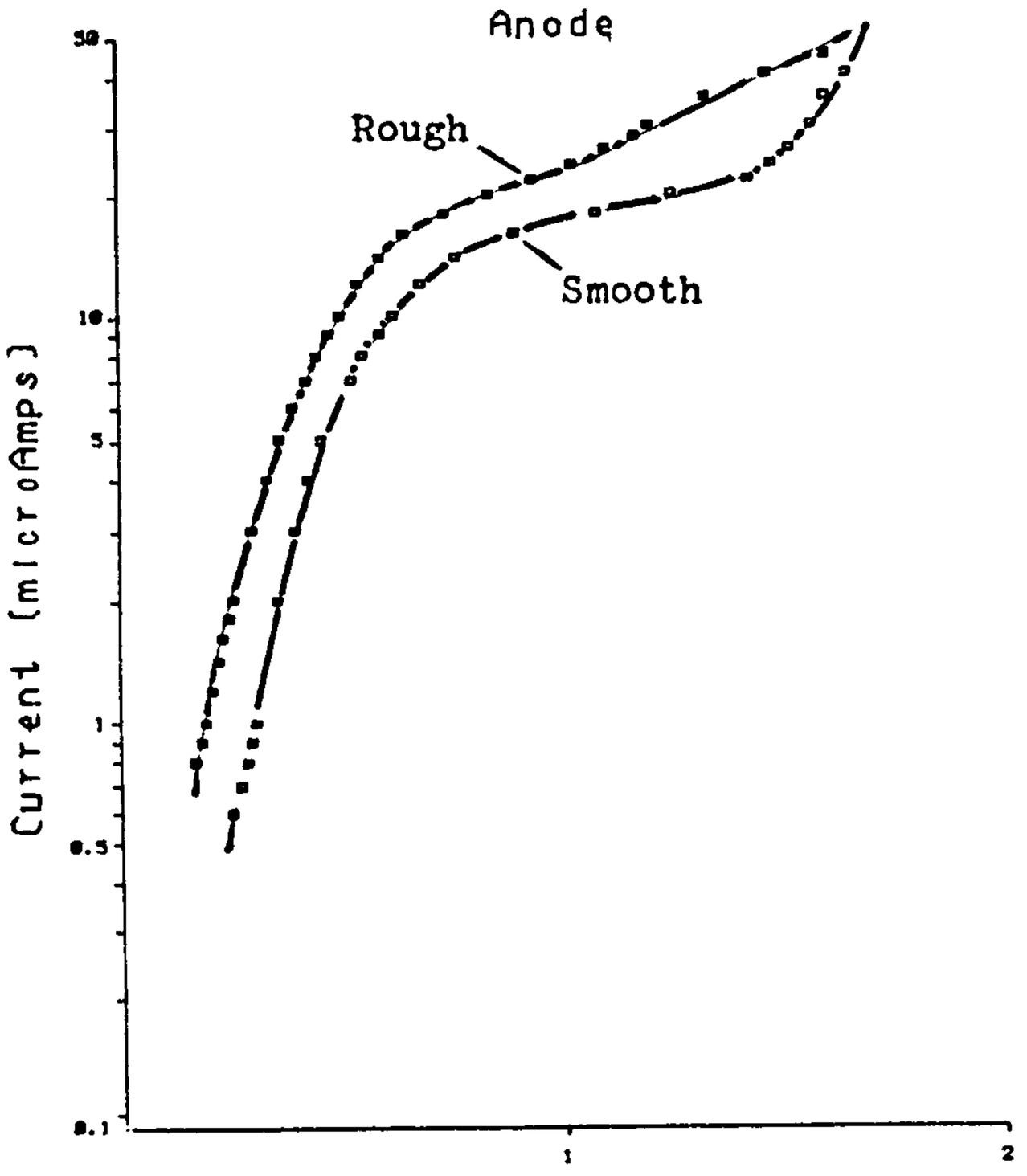

Figure 4.14a

Effect of Surface Roughness

Tafel Plot: Log(I) vs Overpotential

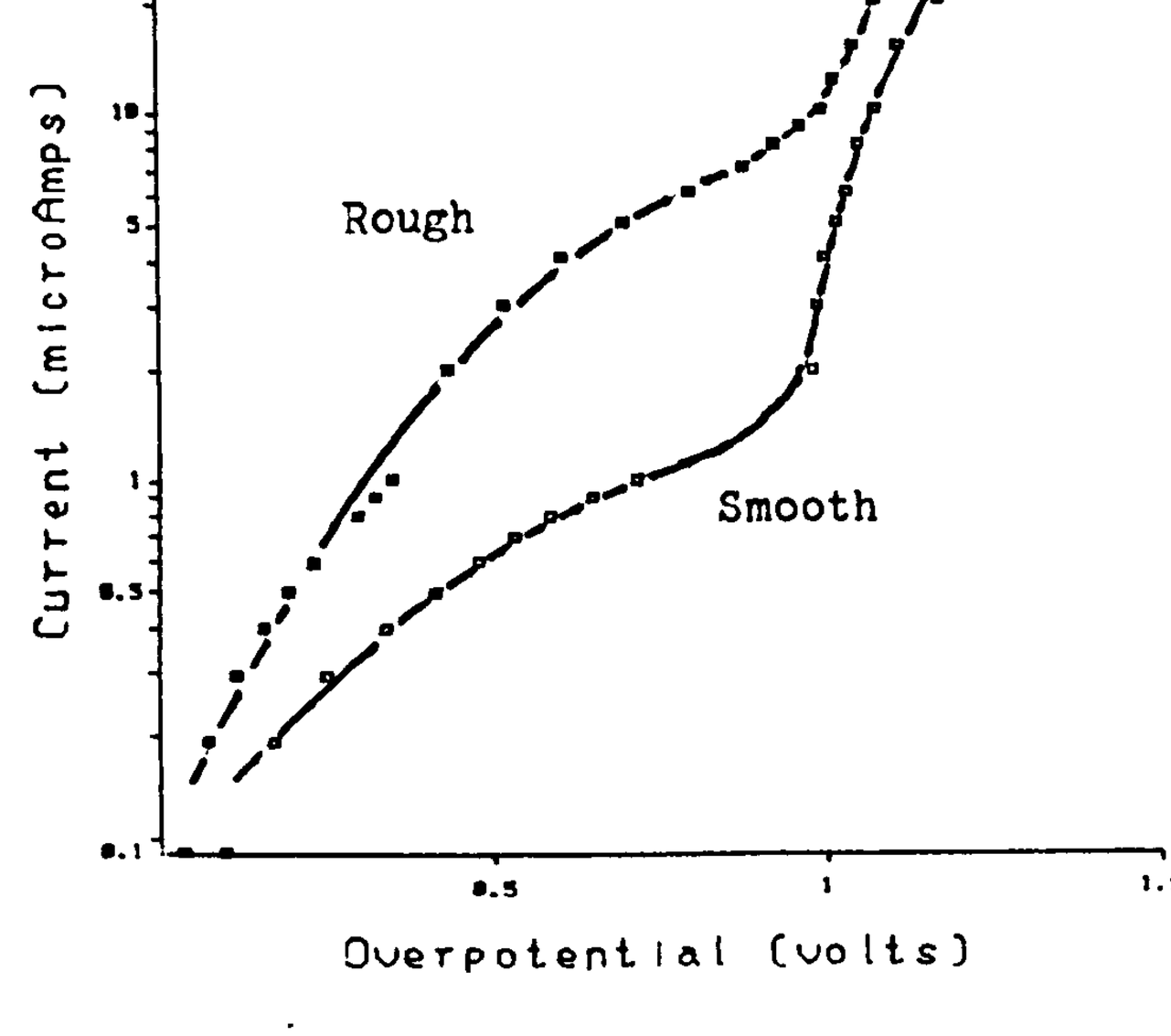

Figure 4.14b

which the "voltage jump" occurs is larger than before - over 20μA (figure 4.14a).

i_o is much larger for the rough surface than for the smooth and hence R_{CT} will be smaller - as observed in chapter 2.

(b) For negative overpotentials two Tafel regions are also observed. Again the "limiting current" is larger than before (approximately 6μA) due to the increased effective area of the electrode surface (figure 4.14b). The value of i_o is smaller for negative overpotentials than for positive and hence R_{CT} will be larger for cathodal overpotentials.

Summary: The main effect of surface roughness is to increase the surface area thus decreasing the interface impedance and increasing the current required to achieve the same voltage. The "limiting current" for a rough electrode is therefore larger than that for a smooth one and hence such an electrode's electrical properties appear more "linear" (Bottelberghs, 1976).

- Porous Sorin S80 Electrode

The i -η characteristic is plotted on figure 4.15 and the Tafel plots on figures 4.16a and b.For anodic overpotentials ($E_{rev} \simeq$ - 250 mV) two Tafel regions are observed (figure 4.16 a) with the current limiting at approximately 12μA. In the second Tafel region i_o is larger than in the first and d is smaller, as noted previously.

For cathodic potentials there are also two Tafel regions (figure 4.16b) and the current limits at

Porous Electrode
dc current - dc voltage plot

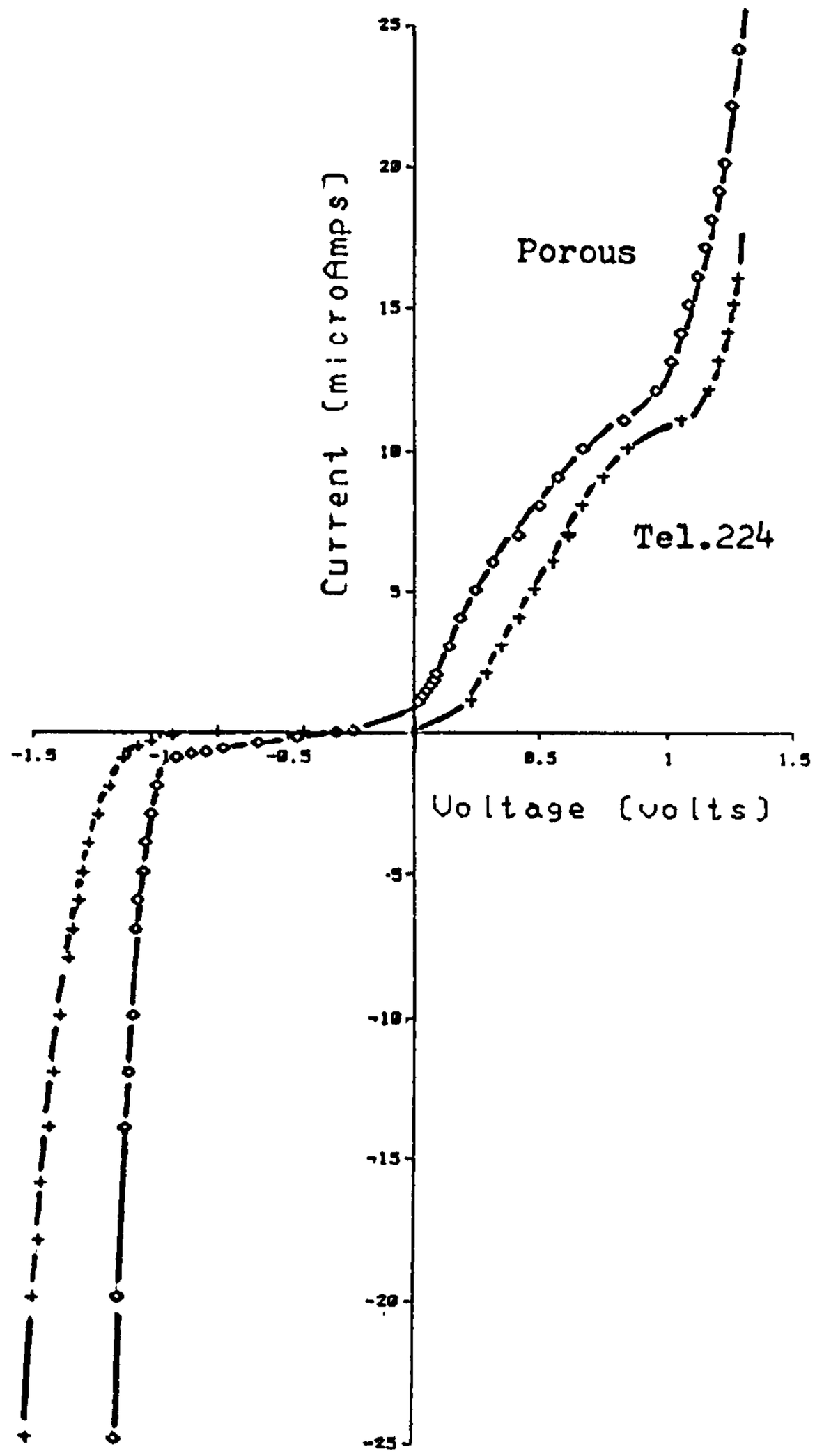

Figure 4.15

Porous Electrode

Tafel Plot: Log(i) vs Overpotential

Anode

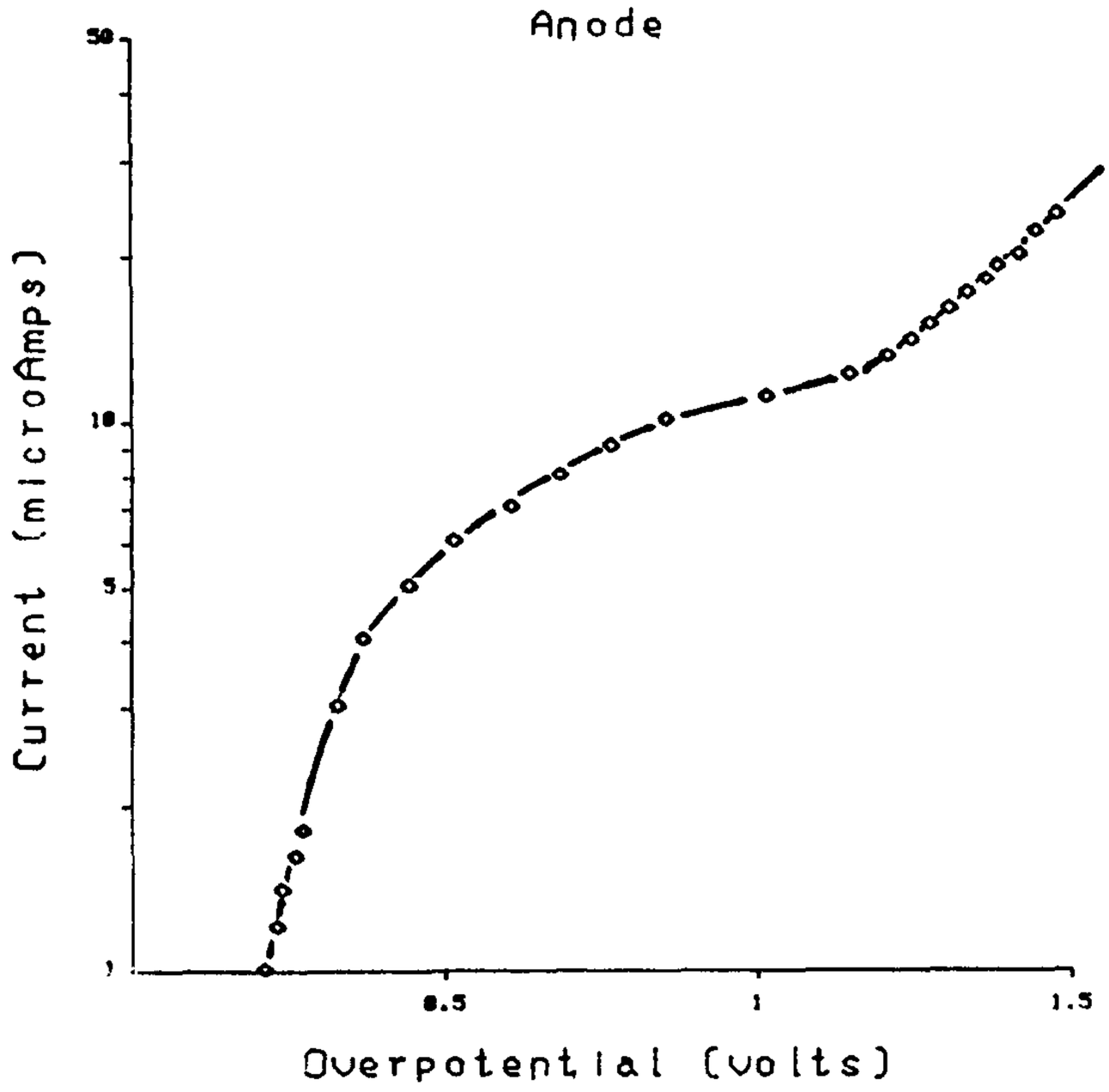

Figure 4.16a

Porous Electrode

Tafel Plot: Log(i) vs Overpotential

Cathode

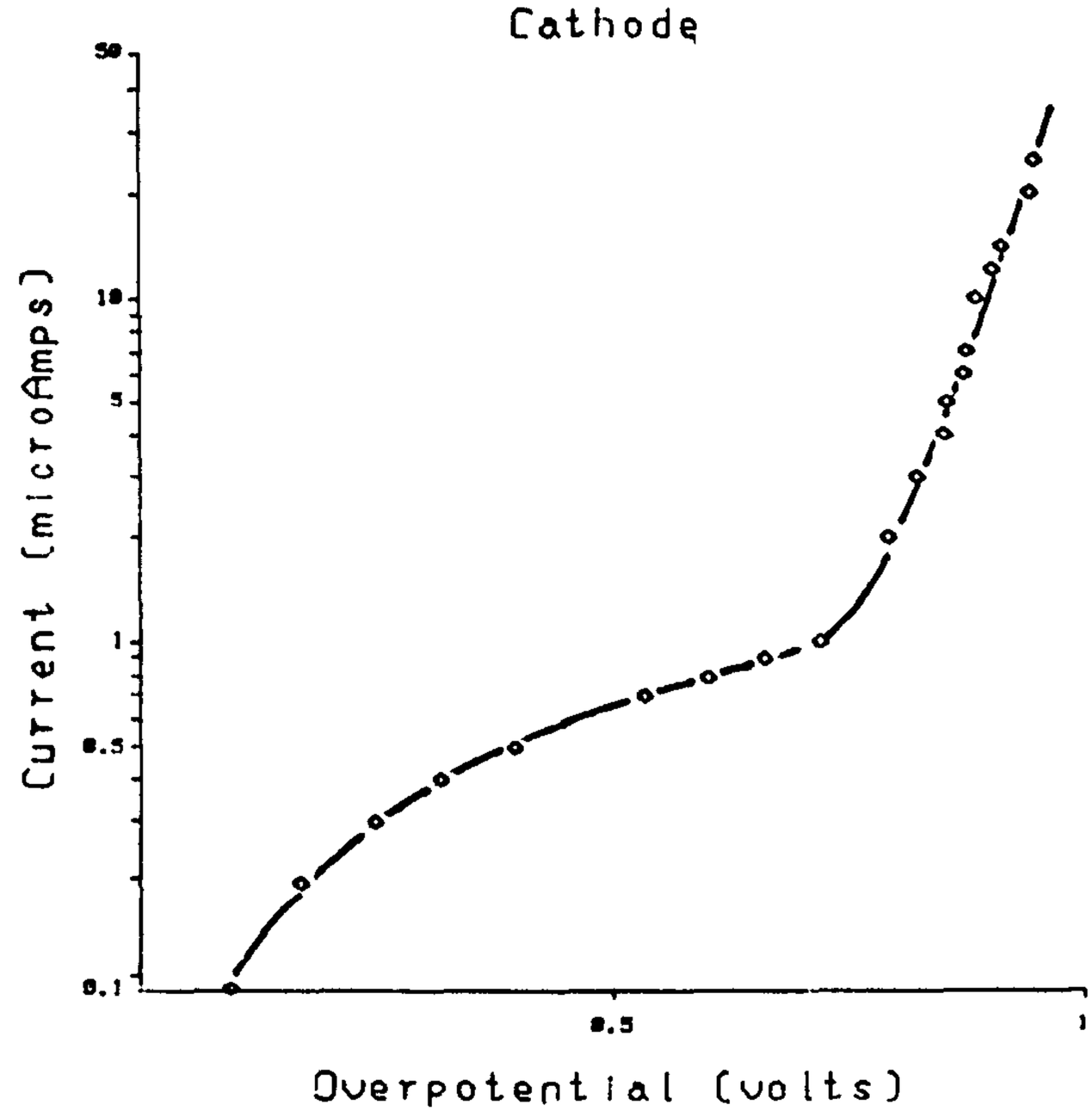

Figure 4.16b

approximately 1μA.

i_o is smaller for cathodic potentials and the gradient, d', is larger.

Comparing the i -η characteristic of the rough surfaced Sorin S80 electrode with the 'smooth' Telectronic 224 (figure 4.15) it is apparent that surface roughness increases the surface area, decreases the interfacial impedance (including the charge transfer resistance) and thus decreases the voltage at any given current.

4.2.1.3 Discussion

For faradaic current to flow through an electrode system, chemical reactions must take place at the electrode surfaces. When such current is passed through an electrode-tissue/saline interface the resultant potential across the interface is determined by whatever reaction mechanism is controlling the transfer of charge. If the current is increased to the limits of the available reacting species, the voltage across the interface will rise very rapidly until sufficient energy is available to initiate a new reaction mechanism capable of meeting the increased demand for current. If the first process takes place at less extreme potentials than the second and the second does not commence until the mass transfer (section 1.1.2.2) limited region has been reached for the first, the i -η characteristic will have the form shown on figure 4.17.

For small current densities up to one half the diffusion limiting current, i_{dL} (where i_{dL} is given by equation 4.90 below), the rate of diffusion of ions to the interface is higher than the rate of the electrochemical reaction: i.e. R_{CT} dominates the faradaic impedance. As the current is increased beyond $^1/_2\ i_{dL}$, the concentration of ions at the surface, C_s, decreases towards zero and the diffusion impedance, Z_W, begins to dominate. When C_s reaches zero, the maximum rate of transport to the interface has been reached

(where $\frac{dQ}{dt} = DC_b/\delta$ and Q is the charge)

as has the maximum current, i_{dL}, where

$$i_{dL} = nFDC_b/\delta \qquad 4.90$$

At this stage a current higher than the diffusion limited current, i_{dL}, cannot be passed across the interface unless another reaction can take place capable of handling such high current.

If any other reactions can occur at higher potentials, eg for other reducible species present in solution, further current "steps" will appear as the potential is raised.

With platinum electrodes in saline a second reaction mechanism was observed to take place (figures 4.12b and 4.16b) for both anodal and cathodal currents, resulting in two Tafel regions for each polarity over the applied current range.

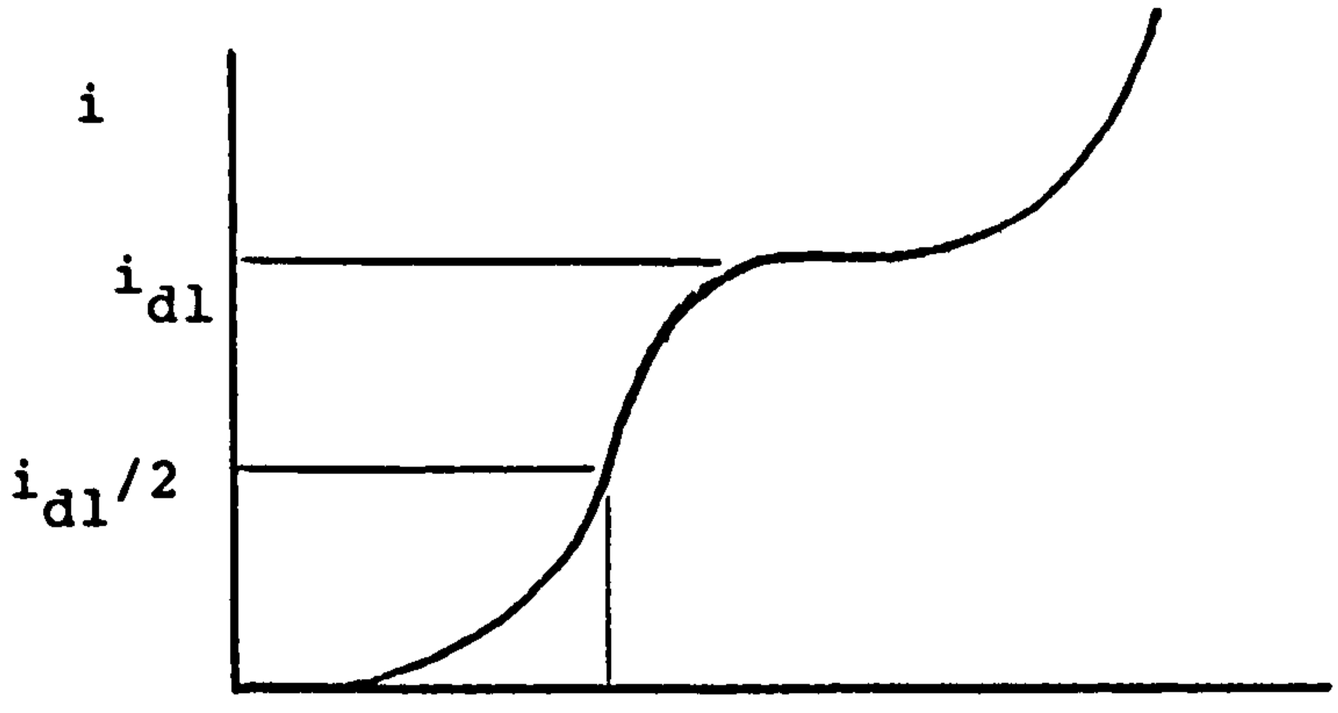

DIFFUSION LIMITING OF THE CURRENT

Figure 4.17

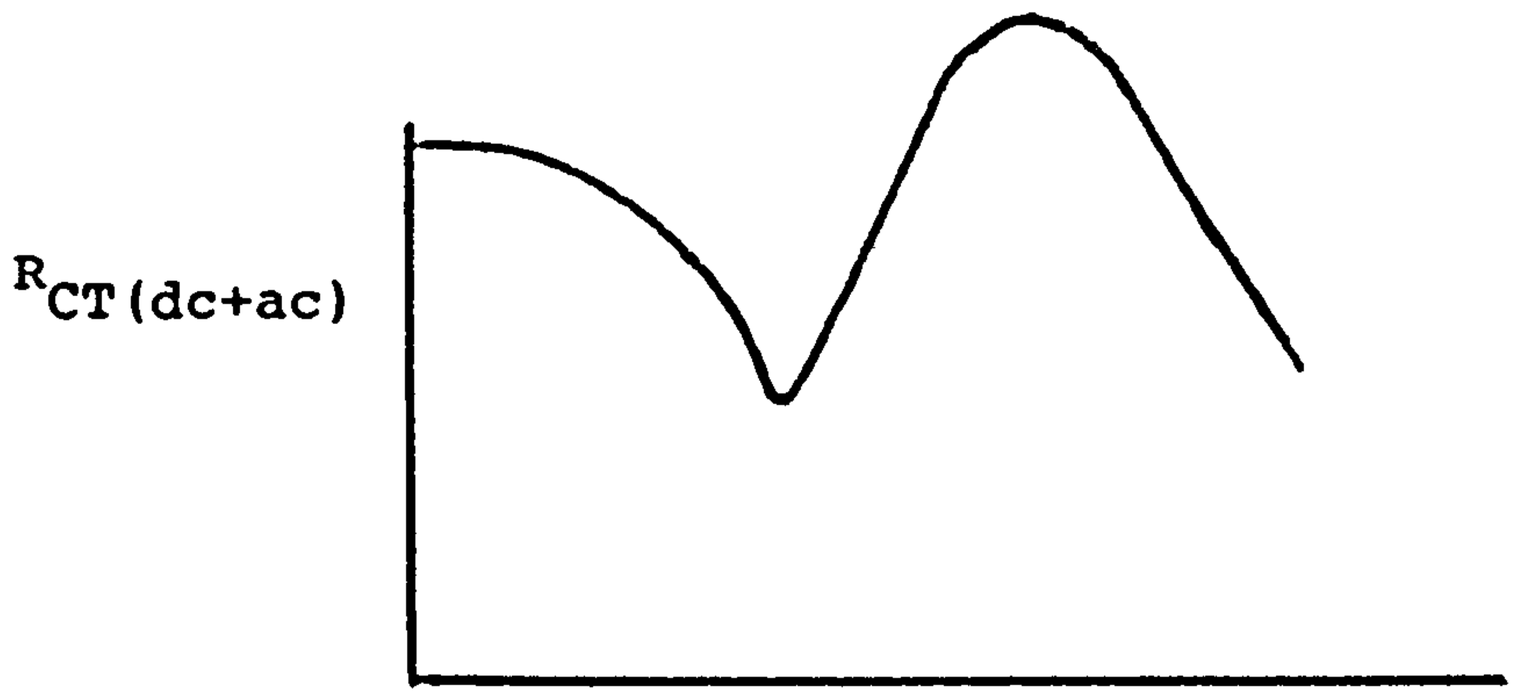

DEPENDENCE OF $R_{CT(dc+ac)}$ ON OVERPOTENTIAL

Figure 4.18

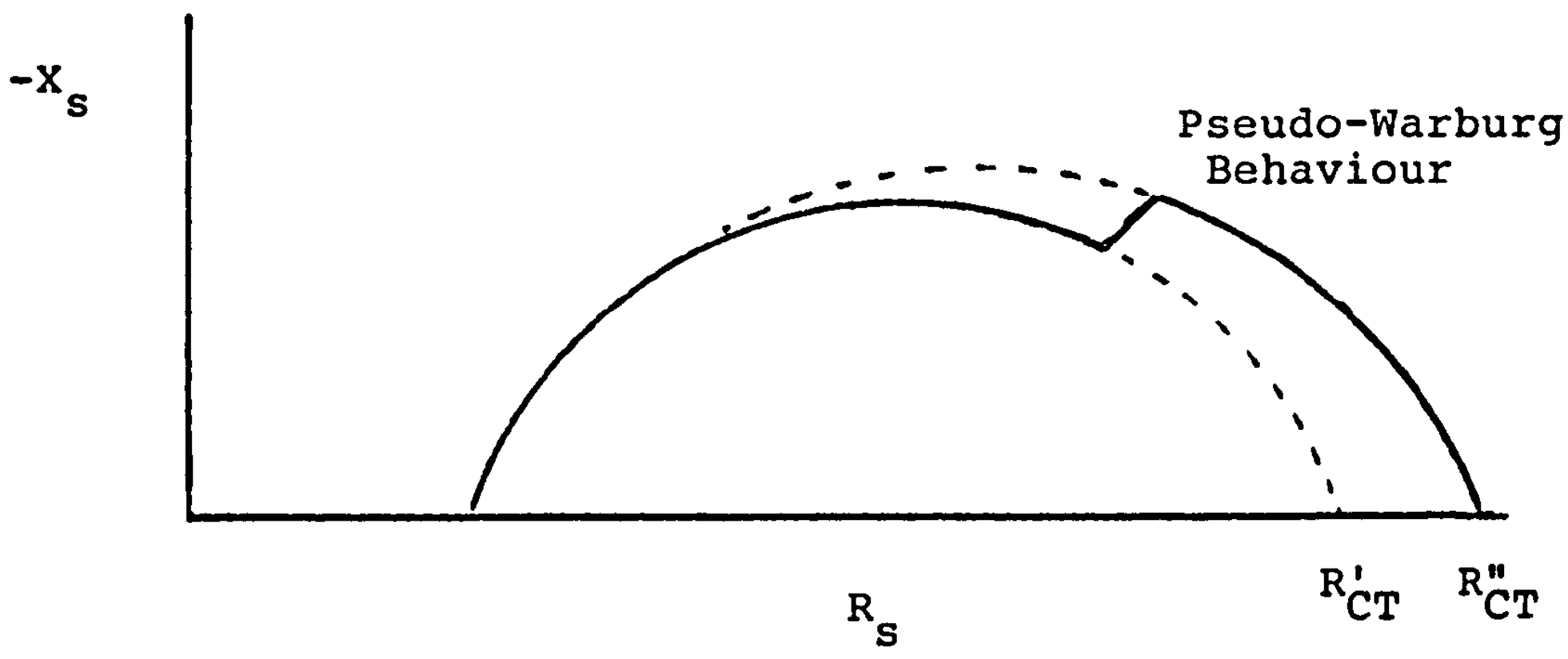

EFFECT OF A SUDDEN INCREASE IN R_{CT} ON THE IMPEDANCE LOCUS

Figure 4.19

- Anodic potentials

For small anodic potentials in electrolytes which do not contain halide ions, the current is attributed to surface oxidation (Hoare 1967; Brummer and Turner 1977) i.e.

$$Pt + H_2O \rightarrow Pt\ OH + H^+ + e^-$$

and

$$Pt\ OH \rightarrow Pt\ O + H^+ + e^-$$

At larger potentials evolution of oxygen occurs for such electrolytes, i.e.

$$2H_2O \rightarrow O_2 + 4H^+ + 4e^-.$$

However in Cl^- containing media, and in physiological saline in particular, the situation is less well understood (Brummer and Turner, 1975) and there is much conflicting data in the published literature (Littauer and Shreir 1966). This is probably due to the many reactions and combinations of reactions possible - eg electrolyis of water, oxidation of saline, oxidation of platinum etc (Brummer and Turner 1977).

It is, however, well established that Cl^- strongly adsorbs onto platinum surfaces and retards the formation of oxygen layers. Zeuthen (1978a) using 120mM NaCl, suggested that Cl_2 was released over the low potential range as the current in this region was found to be dependent on the concentration of Cl^-. Littauer and Schreir (1966), after an extensive literature review and experimenting with 0.5M and 2.0M NaCl, also concluded that, for low anodal voltages, the current was due to the evolution of chlorine on a clean

platinum surface, or one possessing an incomplete chemisorbed* Pt-O or Pt-Cl layer. They observed that for platinum electrodes in an elctrolyte containing Cl^- ions, oxidation of the chloride ion takes place before oxidation of water.

*[Note: Chemisorption is the process of adsorption in which a chemical link is formed between the absorbing and absorbed material].

The temporary limiting of the current between the two observed Tafel regions (figures 4.12, 4.14 and 4.16) could simply be due to diffusion control of the first reaction as described earlier. This would of course assume that the second reaction only begins after the first has been exhausted, and that the "limiting current" is given by equation 4.90 and is hence dependent on the concentration of the current carrying ion - in this case Cl^-. Littauer and Schreir (1966) and Zeuthen (1978a) observed that the limiting current was indeed dependent on the concentration of the chloride ion. However, some researchers (see reviews by Littauer and Schreir 1966; Novak et al, 1982) believe that the observed current limiting and the voltage 'jump' are due to oxide formation (though many other theories have been put forward). It has been pointed out that chloride adsorption onto platinum is competitive with the adsorption of oxygen. At low potentials Cl^- ions block the initial stages of Pt surface oxidation. According to Novak et al (1982) it is the formation of a monolayer of OH on Pt which is blocked whereas the Cl^- ions, for small concentrations,

have little effect on the second stage of the surface oxidation, i.e. the formation of PtO. In any case, it appears that at sufficiently high potentials the inhibition of the formation of an oxygen layer is overcome. The transition from an oxide free surface to an oxide contaminated one is evidenced by a rapid increase in potential, the current density at which this occurs being dependent on the composition of the solution. Although this "limiting current" is proportional to the concentration of the Cl^- ion, Novak (1979) showed that it was not diffusion controlled.

In the higher voltage Tafel region the discharge of chlorine and possibly that of oxygen now occurs on an oxide covered surface with the oxide layer consolidating with the passage of charge. Littauer and Schreir (1966) noted that the charge transfer coefficient, α, increased (as per our notation), as did the exchange current density, i_o, in the second anodic Tafel region, thus indicating a change in the kinetics of the Cl_2 evolution reaction. Such changes were also noticed in our own experiments and would suggest that it is the properties of the surface oxide film on the metal surface that are of greater importance for the Cl_2 evolution reaction than the properties of the bare metal itself (Novak, 1979).

The increases in α and i_o would also indicate that $R_{CT(ac)}$ and $R_{CT(dc+ac)}$, both of which are proportional to $(1-\alpha)^{-1}$, will be larger in this region than expected from extrapoltation of the lower Tafel region results.

In this voltage region gas bubbles were observed on the electrodes' surfaces - due presumably to the evolution of chlorine and possibly that of oxygen (Breiter 1963).

The Cl_2/O_2 evolution Tafel region should be avoided in invivo work. Brummer and Turner (1977) list several potentially harmful reactions which can occur at sufficiently high anodic potentials and these include the evolution of Cl_2 and O_2. Apart from the electrolysis of water (with subsequent evolution of O_2) and oxidation of saline (with subsequent evolution of Cl_2) other harmful reactions listed were the oxidation of platinum and of organic molecules present.

The electrolysis of water results in oxygen evolution which can cause tissue damage due to local pH changes (acidic), which can give rise to irreversible changes in tissue proteins near the electrode, or to the disruptive effects of gross gas bubbles. The local pH changes near the electrode may be tolerated, at least under transient conditions, but gas evolution is very damaging. Additionally, several of the mechanisms proposed to account for adsorbed oxygen and oxide films on platinum surfaces involve peroxides as chemical intermediates, (Hoare, 1967). At any rate studies show that when an electrode which has been used to pass stimuli causing a lesion in one location is implanted elsewhere, further lesions are formed without application of a stimulus (Dymond, 1976). It would therefore appear that the toxic effects of electrode stimulation are due to the chemical reaction and the

resultant changes in the metal surface rather than to thermal effects as has been suggested. It is very probable that the oxide layer formed on the electrode surface is at least partly responsible for the reported toxic effects at platinum electrodes.

The oxidation of saline is likely to produce undesirable species such as ClO^-, $Cl\,O^-_3$ etc (Brummer and Turner, 1977). Oxidation products of chlorine are undesirable as they are strong oxidising agents. A further possibility in Cl^- containing media is the oxidation and dissolution of platinum itself. Platinum dissolution products have been shown to be powerful oxidising agents which can be reduced by organic species present in the medium.

It is therefore concluded that, under invivo conditions, the second, high potential Tafel region should be avoided are far as possible.

Upon decreasing the current density changes were found in the electrode impedance and in E_{rev}, i.e. there was hysteresis. Hysteresis can be defined as the difference at a given potential in the values of current observed on increasing and decreasing the potential.

It has been suggested that the anode has become effectively covered with a stable oxide or chloride film after having passed through the second anodic Tafel region. As the oxide layer is not completely reversible with respect to reduction (Conway and Gothesfeld, 1972), the high potential oxidation of chloride and chlorine evolution on an oxide covered

surface are also irreversible (Mayell and Langer, 1964; Littauer and Shreir 1966). Calculated values of the transfer coefficient, α ,and the exchange current density, i_o, are found to have considerably changed and only one Tafel region is observed were previously there were two.

- Cathodic Overpotentials

This would appear to be a much simpler problem. For small signal amplitudes hydrogen is adsorbed onto the platinum surface, i.e.

$$Pt + H^+ + e^- \rightarrow Pt - H,$$

and the current-voltage relationship is a Tafel one over most of the range.

It has been reported that the potential range of hydrogen adsorption narrows, shifting to more cathodic potentials, with increasing concentration of Cl^- due to the competitive adsorption of hydrogen and halide ions (Breiter, 1963; Novak et al, 1982).

As the cathodic potential is increased the current limits and then rises again as a second reaction, H_2 evolution, occurs:

$$2H^+ + 2e \rightarrow H_2 \uparrow$$

As with anodic potentials, this cathodic, second Tafel region is undesirable due to gas production and local pH changes (alkaline) near the electrode. Spadaro and Becker (1979) carried out a survey of reported undesirable effects at cathodes and concluded that they all occurred when the electrode was operated

in the hydrogen evolution region, ie in the second cathodic Tafel region.

- Nonlinearity of charge transfer resistances, $R_{CT(dc+ac)}$ and $R_{CT(ac)}$

It was observed that the values of i_o and α in second Tafel region differed from those calculated in the first and it was suggested that these differences would affect the values of charge transfer resistances, $R_{CT(dc+ac)}$ and $R_{CT(ac)}$ at large signals.

- $R_{CT(dc+ac)}$

For i-η characteristics of the form shown on figures 4.11,13 and 15, a plot of $R_{CT(dc+ac)}$ (where $R_{CT(dc+ac)}$ is the inverse gradient of the i-η curve) versus η will have the form shown on figure 4.18.

For small overpotentials the value of $R_{CT(dc+ac)}$ is constant and equal to $1/nfi_o$. As i_o is generally very small, $R_{CT(dc+ac)}$ is rather large (Ohsaka et al, 1976).

As the overpotential, η , is increased, Tafel behaviour is observed (η is proportional to log i) and $R_{CT(dc+ac)}$ decreases. In this region $R_{CT(dc+ac)}$ is described by equations 4.64 and 4.65.

When the diffusion of ions to the electrode surface or the formation of an oxide layer becomes significant the current limits resulting in a sharp rise in $R_{CT(dc+ac)}$. If the current is limited due to diffusion effects and the diffusion limiting current, i_{dL} (equation 4.90), is reached, $R_{CT(dc+ac)}$ will tend towards infinity. If, however, the jump in voltage

occurs before the diffusion limiting current is reached, due say to oxide formation, $R_{CT(dc+ac)}$ will reach a large but finite value.

Once the second reaction has taken over from the first, Tafel behaviour is again observed (Littauer and Schreir, 1966) and $R_{CT(dc+ac)}$ will once again decrease, though with a value larger than would be expected from extrapolation of small signal behaviour.

Similar plots to that shown on figure 4.18 have been obtained by Iseki et al (1972) and Conway and Gottesfeld (1972).

- $R_{CT(ac)}$

An $R_{CT(ac)}$ -η plot will be very similar in form to that shown on figure 4.18.

- Total Interfacial Impedance

The changes in the charge transfer resistances upon the formation of an oxide layer on the electrode surface should have a discernable effect on the impedance locus of the electrode system.

The oxide layer will form on the surface at low frequencies and/or high signal amplitudes when sufficient charge crosses the interface. It's formation should be marked by a 'sudden' increase in the parallel charge transfer resistance (and hence in the arc diameter) at low frequencies and the resultant impedance arc should have the form shown schematically on figure 4.19. It is probable that the magnitudes of K and β will also change upon the formation of an oxide layer.

A similar impedance locus would be obtained if the current limiting observed on the 1-η curve were simply due to diffusion effects. At low frequencies the Warburg impedance, Z_W, would become significant and the locus in this region would have a phase angle of 45° (see figure 1.13). At lower frequencies the second charge transfer process would take over with its larger value of charge transfer resistance and the locus would thus form part of a larger arc.

Such loci as described above would be quite similar to those plotted on figures 2.4 and 2.8 for electrode systems with rough surfaced electrodes and where charge transfer is occuring across the interfaces.In both situations there is an increase in the parallel resistance at low frequencies.

It is possible that Onaral and Schwan's impedance plots (1982, figures 1,2 and 3) are due to "two Tafel" behaviour. It is interesting to note that their low frequency arc had a phase angle of approximately 45° whereas one would expect a phase angle of almost 90° for the impedance of a "smooth" surface. Also, Jaron et al (1969) observed that hysteresis generally occured when the voltage across an electrode system was taken beyond V_L, or the applied current beyond i_L (equivalent to decreasing the applied frequency below $f_{10\%}$). Onaral and Schwan (1982) noted a similar effect for their platinum electrodes. The presence of such hysteresis suggests that irreversible electrochemical changes are taking place at the electrode-electrolyte interface (Jaron et al, 1969). Jaron et al noted that

these irreversible impedance changes were in some cases accompanied by evolution of gas and discolouration of the anode surface. All these factors, the low phase angle, the hysteresis and the gas evolution, would tend to indicate the formation of an oxide on the electrode surface. It is the view of this author, however, that the form of Onaral and Schwan's (1982) small signal (65mV) impedance locus is due to surface effects rather than oxide formation for several reasons. No mention was made by Onaral and Schwan of gas evolution at low frequences. Hysteresis was only observed when the applied signal levels were "well in excess of the limit of linearity" and probably occured in the second, large amplitude, Tafel region. Decreasing the frequency below $f_{10\%}$ under small voltage amplitude conditions should only cause the electrode interface impedance to be dominated by the "first Tafel region" charge transfer resistance and not that of the second, large amplitude Tafel region, which occurs at considerably larger voltages than that used by Onaral and Schwan. The small phase angle of their low frequency arc, however, remains unexplained.

In summary, a sudden increase in the magnitude of the charge transfer resistance as the frequency is lowered under small signal conditions is very probably due to surface effects as described in Chapter 2, whereas a similar effect under large amplitude conditions is most probably due to the formation of an oxide layer or diffusion limiting effects as described above.

4.2.2 "Dc + ac" Nonlinearity

Having found two Tafel regions for both anodic and cathodic overpotentials and having postulated their effects on the charge transfer resistance, $R_{CT(dc+ac)}$, the dc voltage dependence of $R_{CT(dc+ac)}$, K and β was investigated experimentally for a Telectronic 224 electrode. It was expected that $R_{CT(dc+ac)}$ would decrease as would K and β (sections 4.1.1.1 and 4.1.1.2.2) with dc voltage magnitude.

-Telectronic 224 Electrode

The experimental results are plotted on figure 4.20 and the calculated values of the equivalent circuit parameters are listed on Table 4.1 and plotted on figure 4.21 for a range of dc voltages. The ac amplitude was 10mV(rms).

TABLE 4.1

dc voltage (mV)	$K(k\Omega s^{-\beta})$	β	$R_{CT(dc+ac)}(M\Omega)$
-100	130	.8	2.27
-50	152	.8	1.85
0	155	.79	1.30
+50	145	.74	0.826
+100	145	.73	0.32

The impedence loci form good arcs except at low frequencies for dc bias of +50 and +100 mv. Under these low frequency, large voltage bias conditions the impedances are observed to be larger than expected. As the distorted points lie on the equi-frequency arcs for constant K (see equation 4.70 and below) it would

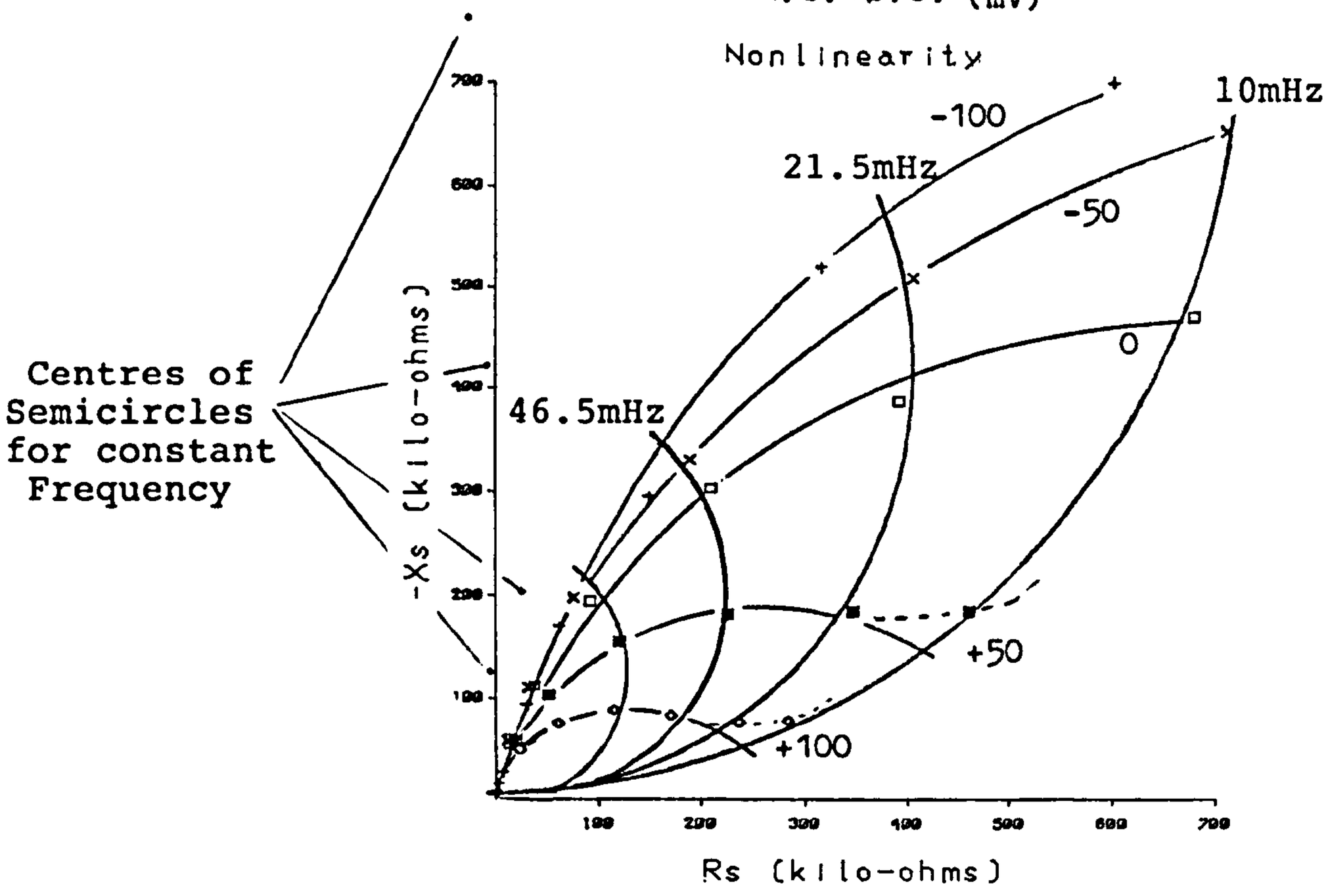

Figure 4.20

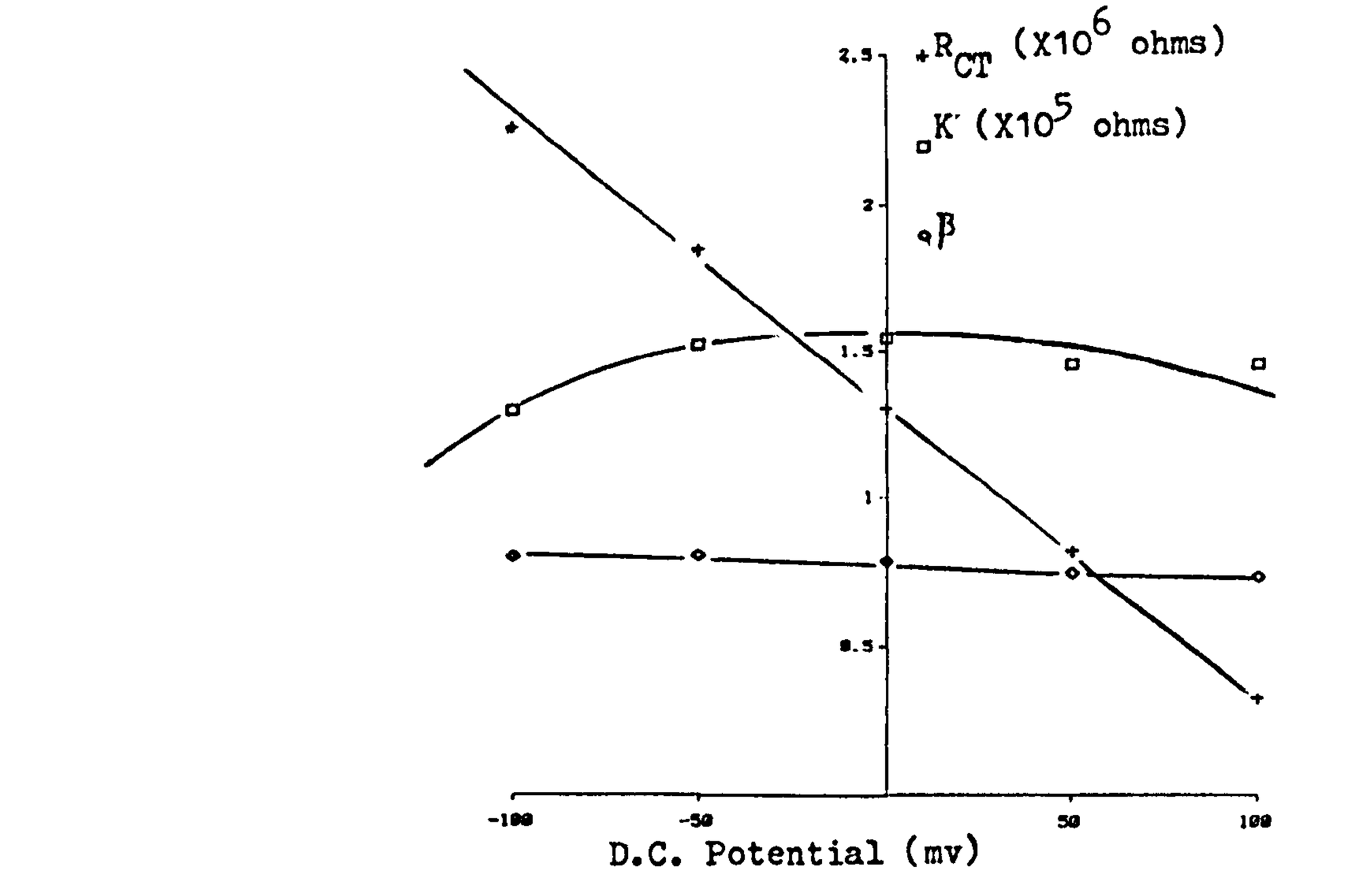

Figure 4.21

appear that this distortion is due to an increase in $R_{CT(dc+ac)}$ and that changes in Z_{CPA} are not involved. This behaviour was anticipated in the last section.

Equi-frequency points are found to lie on semicircular arcs whose centres are close to the imaginary axis, with the exception of points measured at -100mV. This would indicate that $R_{CT(dc+ac)}$ is responsible for the overall nonlinear behaviour of the interfacial impedance, and that K is relatively linear- except at -100mV, where it decreases in magnitude.

These deductions are confirmed on inspection of figure 4.21 and Table 4.1. $R_{CT(dc+ac)}$ decreases linearily as the voltage is made more positive indicating that its linear region, and hence E_{rev}, occurs at cathodic voltages greater than -100 mV. It was shown in section 4.2.1 and figure 4.11 that E_{rev} for this electrode has a value of approximately -450 mV.

K, on the other hand, is very linear and only decreases significantly at -100 mV indicating that the electrode, in the absence of a dc bias, is operating within the double layer region and that the Potential of Zero Charge is close to, or slightly more anodal than, zero mV with respect to the large area, indifferent electrode.

Plots of C_p against dc potential at high frequencies (figure 4.22) are 'U' shaped with the centre of the troughs occuring at approximately +50 mV. The double layer region would appear to be approximately 200 mV wide.

Tel. 224 Electrode

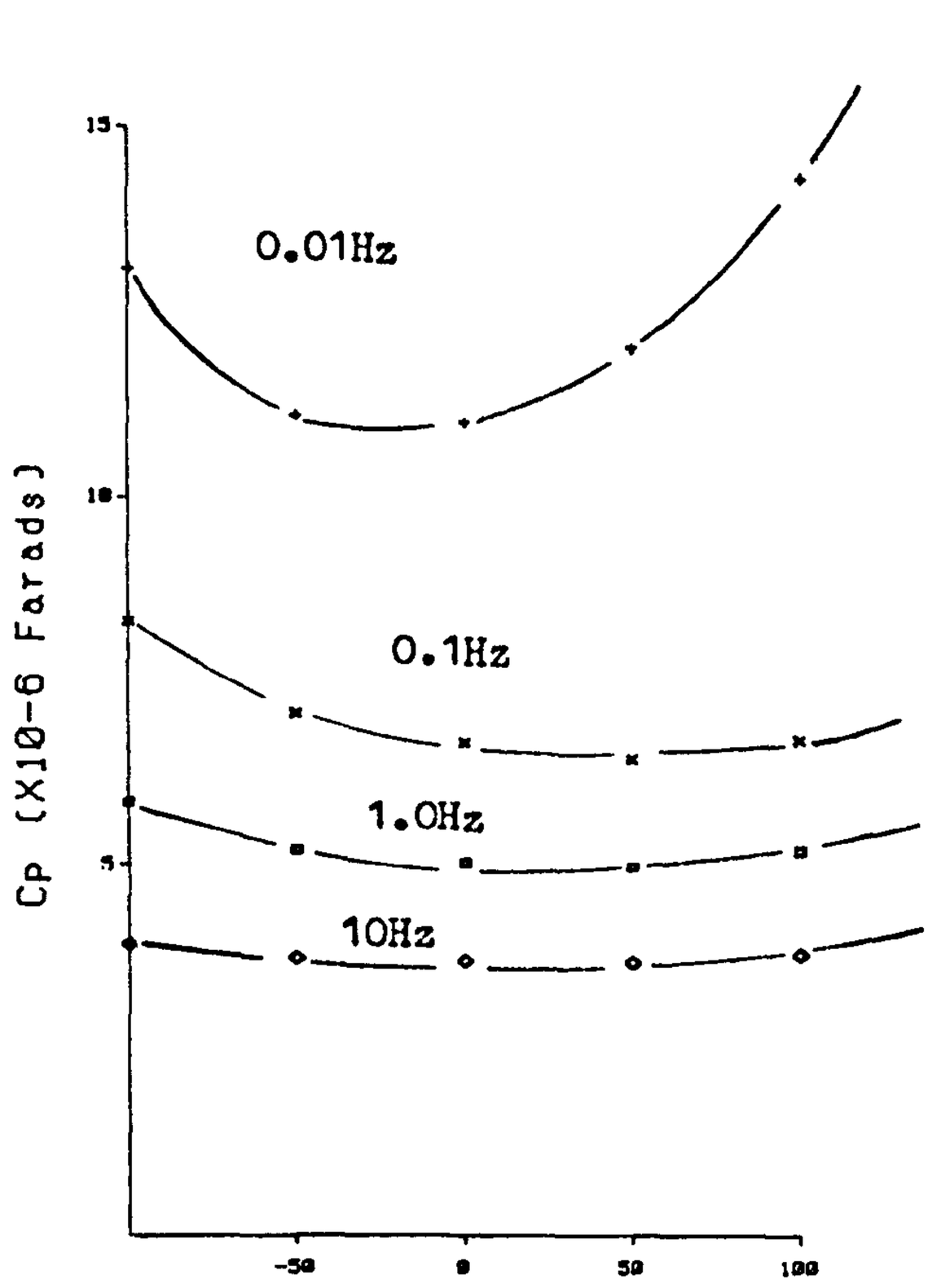

PARALLEL CAPACITANCE AT VARIOUS FREQUENCIES
VS. DC POTENTIAL

Figure 4.22

β is also relatively constant over the applied voltage range with a value of approximately 0.8. β does however decrease slightly for anodic potentials.

4.2.3 A C nonlinearity

Although the 'dc+ac' nonlinearity follows more directly from the i -η and Cp -η plots (figures 4.3 and 4.4), ac nonlinearity has been much more extensively studied in the published literature. This work has largely been carried out by Schwan and his colleagues or has been prompted by their many publications over the past twenty years.

This topic is therefore treated in some detail in this section and the conclusions of Schwan and his colleagues are compared and contrasted with those of this study.

The effect of ac signal amplitude on K, β and $R_{CT(ac)}$ are investigated and the major source of the observed nonlinearities (Z_{CPA} or R_{CT}) is established, and over what frequency range.

The electrode-electrolyte systems' impedances were measured using the Solartron 1250 frequency response analyser with a range of applied ac voltage amplitudes. Ac voltages, rather than currents were chosen as the charge transfer resistance, $R_{CT(ac)}$, will remain constant at a given voltage as the frequency is varied. If current had been used this would not have been the case and distorted loci would have resulted, making interpretation difficult.

Detailed investigation was carried out on three different electrodes

(1) the Telectronic 224 electrode,

(2) the Porous Sorin S80 electrode and

(3) the Activated Vitreous Carbon electrode.

(1) The Telectronic 224 electrode

- AC impedance plots

The impedances for a range of voltage amplitudes are plotted on figure 4.23 and the calculated equivalent circuit model parameter values are tabulated below (Table 4.2) and plotted on figure 4.24.

TABLE 4.2

ac voltage (Vrms)	$K(k\Omega s^{-\beta})$	β	$R_{CT(ac)}(M\Omega)$
10	184	.82	2.06
50	161	.82	1.38
100	144	.73	1.00
150	131	.73	.62
200	65	.67	.197

The experimental results are well fitted by arcs except for voltage amplitudes above 100 mV. These large signal curves deviate at low frequencies from the expected arcs and the reactive components are larger than expected. This behaviour was anticipated in section 4.2.1.3 when an oxide is formed on the electrode surface. As bubbling was noticed on the electrode surface for signal amplitudes above 100 mV, it is very probable that this is the cause of the observed low frequency 'distortion' in this instance.

Close inspection of figure 4.23 would indicate

A.C. Nonlinearity

Tel.224 Electrode

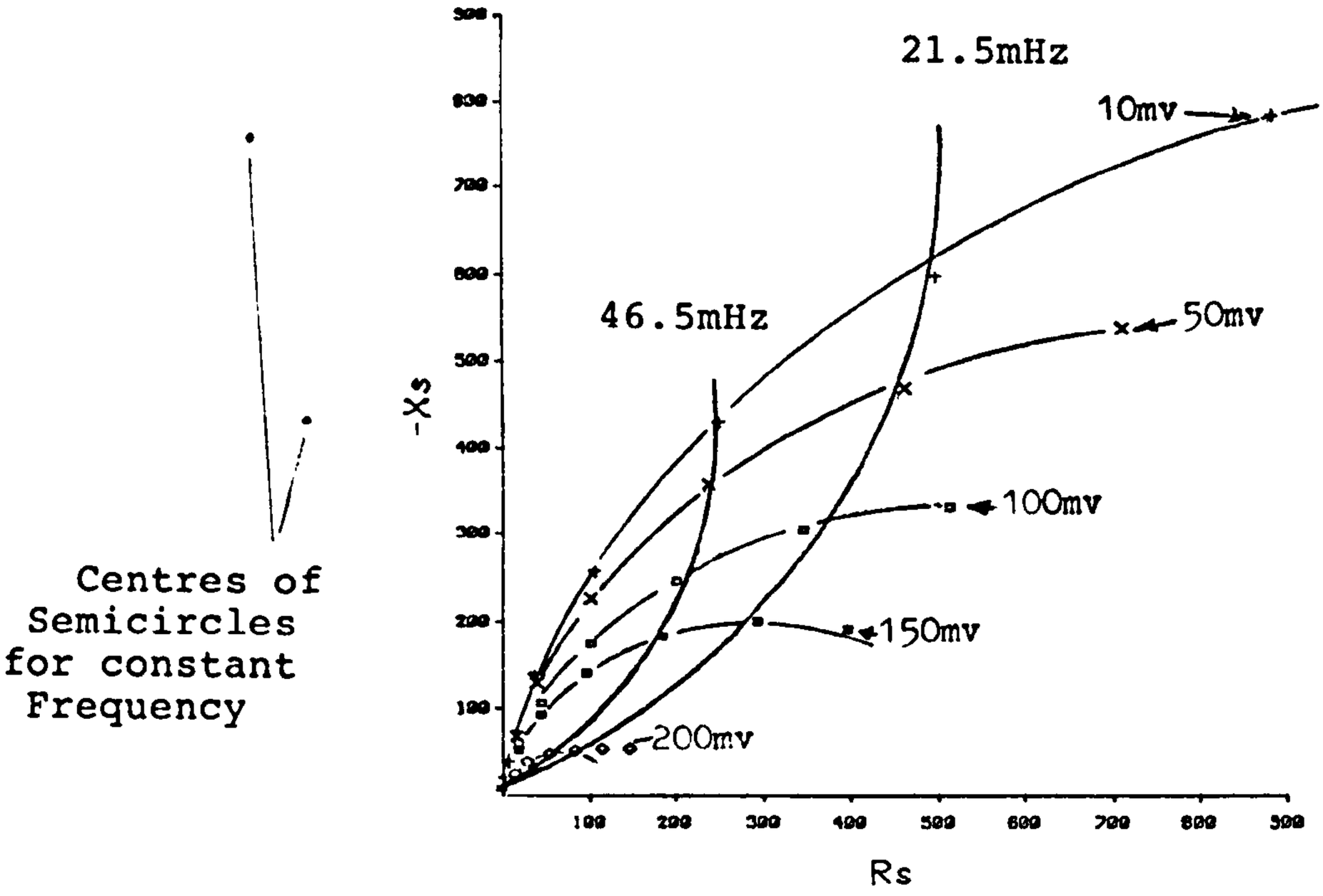

Centres of Semicircles for constant Frequency

Figure 4.23

Tel.224 Electrode

A.C.Nonlinearity

of Equivalent circuit elements

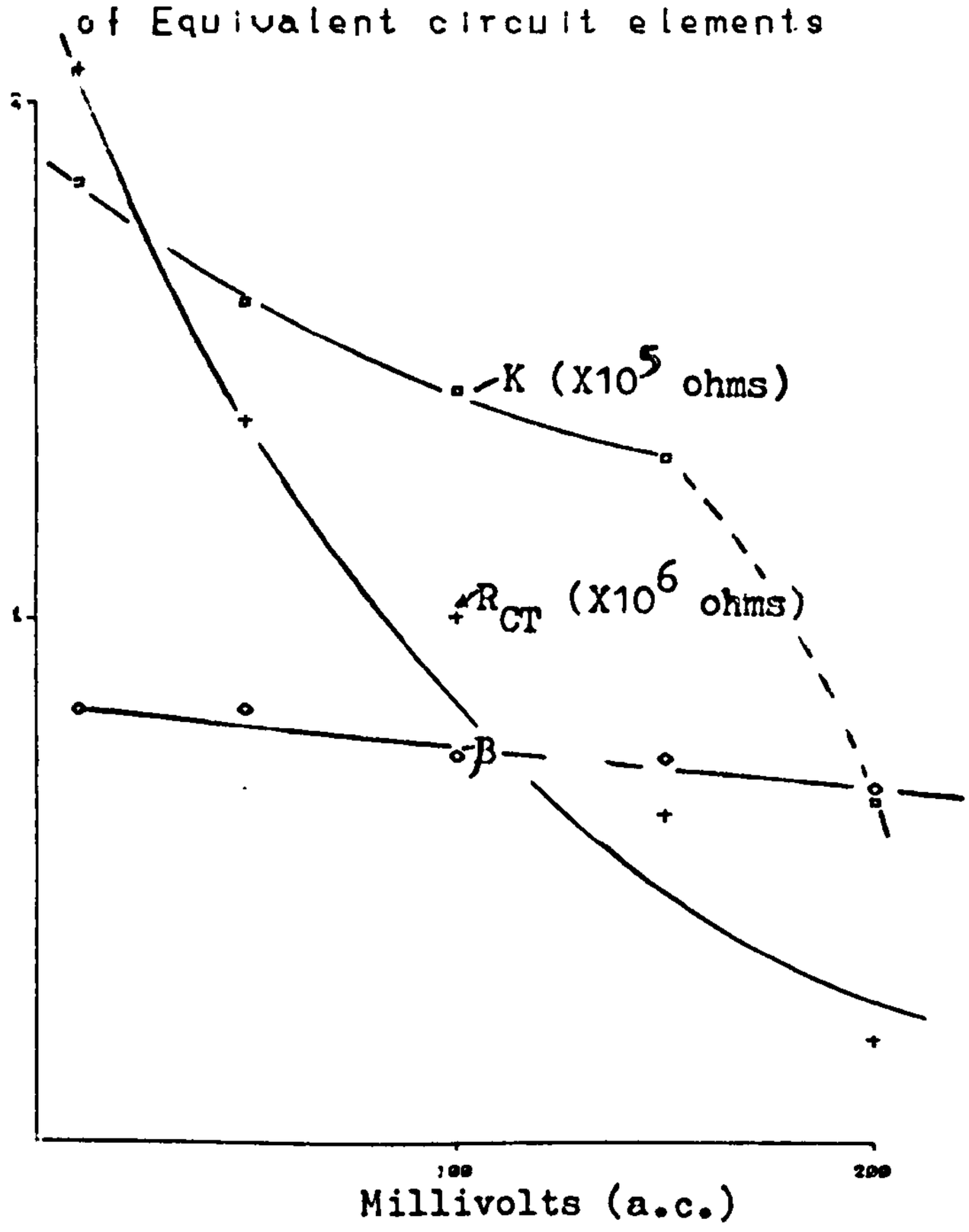

Figure 4.24

that, although points of the same frequency lie on arcs as the applied voltage is varied, the centre of these arcs do not lie on the imaginary axis. This is due to the points on the arcs being rotated anticlockwise along the arcs' circumferences due to the nonlinearity of the constant phase angle impedance, Z_{CPA}. This can be seen more clearly on Table 4.2 and on figure 4.24. K decreases gradually for voltages up to 150mV (rms) and then abruptly drops in value for an applied signal amplitude of 200 mV(rms).

The voltage range over which K is relatively constant (less that 150 mV_{rms}) is the "double layer" region and there is relatively little frequency dispersion (β =.82) in this region. However, even in this "linear" region Z_{CPA} decreases by nearly 30% from its small signal (10 mV_{rms}) value. Very high frequency points, whose impedances are dominated by that of Z_{CPA}, will therefore "become nonlinear" (ie decrease by more than 10%) at voltages around 50 mV. Not so high frequencies will be affected at higher potentials when either the nonlinearity of Z_{CPA}, that of $R_{CT(ac)}$ or a combination of both cause their impedances to deviate by more than 10% from their small signal values.

The frequency dispersion observed in the double layer region is presumably due to the adsorption of chloride ions and surface effects. At 200 mV_{rms} the sudden decrease in K is due to the rapid increase in the adsorption pseudo capacitance.

As the voltage amplitude is increased, the diameter of the impedance loci decrease indicating that

R_{CT} is very nonlinear (figure 4.23). From table 4.2 and figure 2.24 it is seen that $R_{CT(ac)}$ decreases in a roughly exponential manner with V_{ac}. The relationship was calculated as approximately

$$R_{CT(ac)} = 2.6 \times 10^{6} \exp [-11.5\ V_{ac}(rms)]$$

- R_s and X_s

As $R_{CT(ac)}$'s nonlinearity is dominant for most frequencies, an initial increase, for a given frequency, should be observed in R_s, a maximum reached (somewhat less than $K/2\omega^{\beta}\sin\phi$), followed by a gradual decrease as V_{ac} is increased (section 4.1.2.2).

X_s on the other hand should simply decrease as V_{ac} is increased.

Plots of R_s and X_s versus $V_{ac(rms)}$ are shown on figures 4.25a and b for a range of frequencies.

At the very lowest frequency (0.01Hz) the postulated initial rise in R_s is not observed due to the insufficiently low applied voltage range. At higher frequencies more of the 'hump' in the R_s -V_{ac} curve becomes apparent as the peak value of R_s is observed to occur at progressively higher voltages for higher frequencies.

Around 0.46 Hz a well formed 'hump', including much of the initial rise, is observed.

The X_s - V_{ac} plots (figure 4.25b) indicate that the series reactive component decreases with ac voltage amplitude - as was expected for an interface whose nonlinearity is governed for the most part by that of the faradaic charge transfer resistance, $R_{CT(ac)}$.

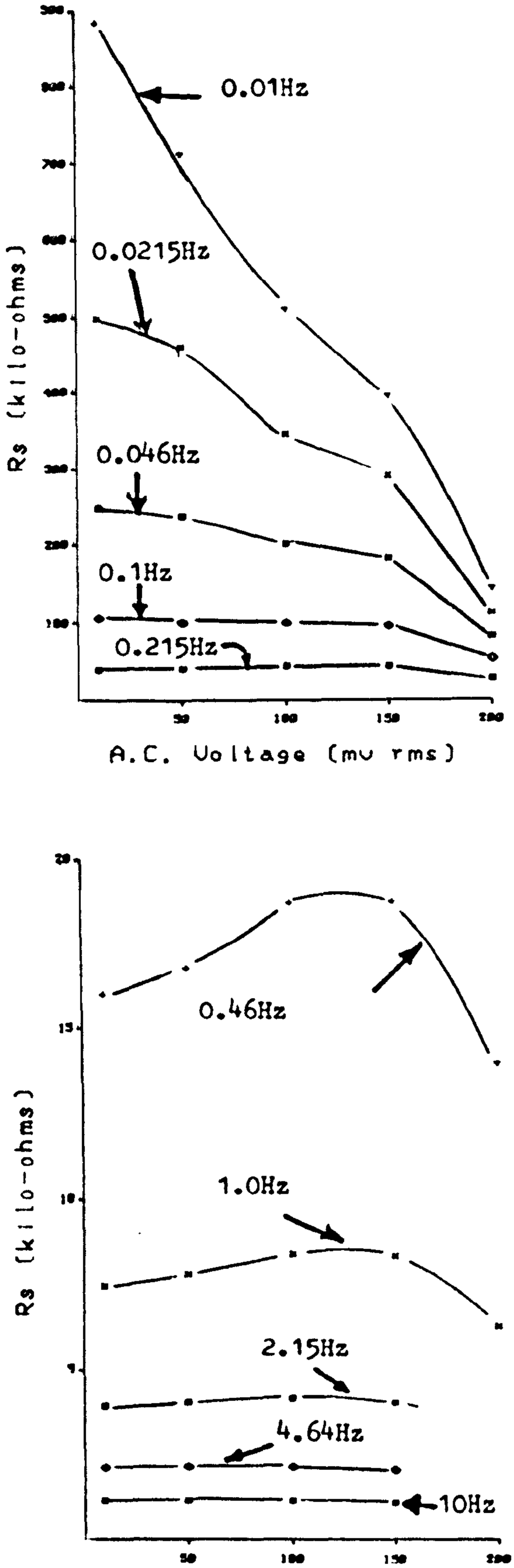

Figure 4.25a

SERIES RESISTANCE VS. APPLIED VOLTAGE FOR VARIOUS FREQUENCIES

Tel. 224 electrode

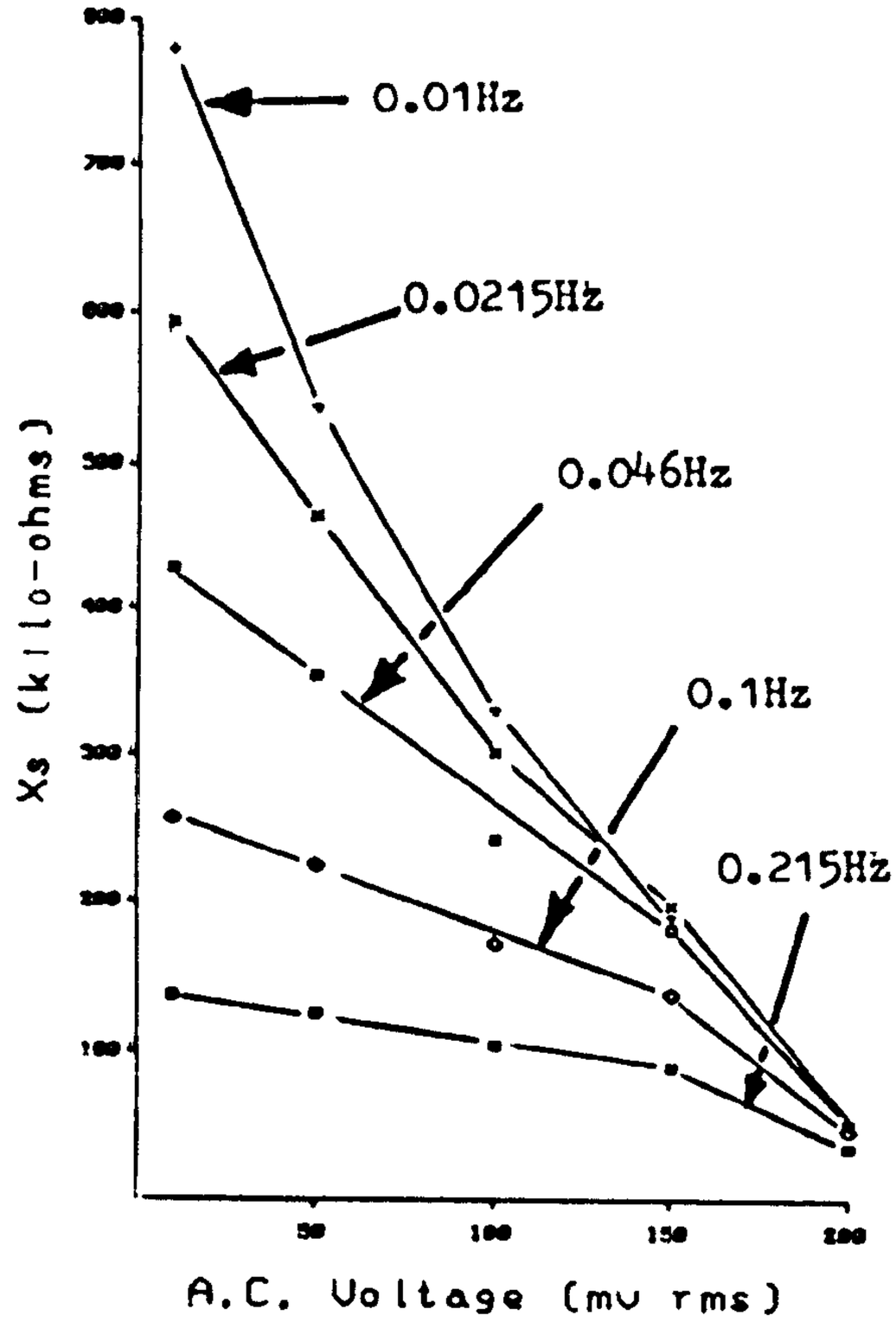

Figure 4.25b

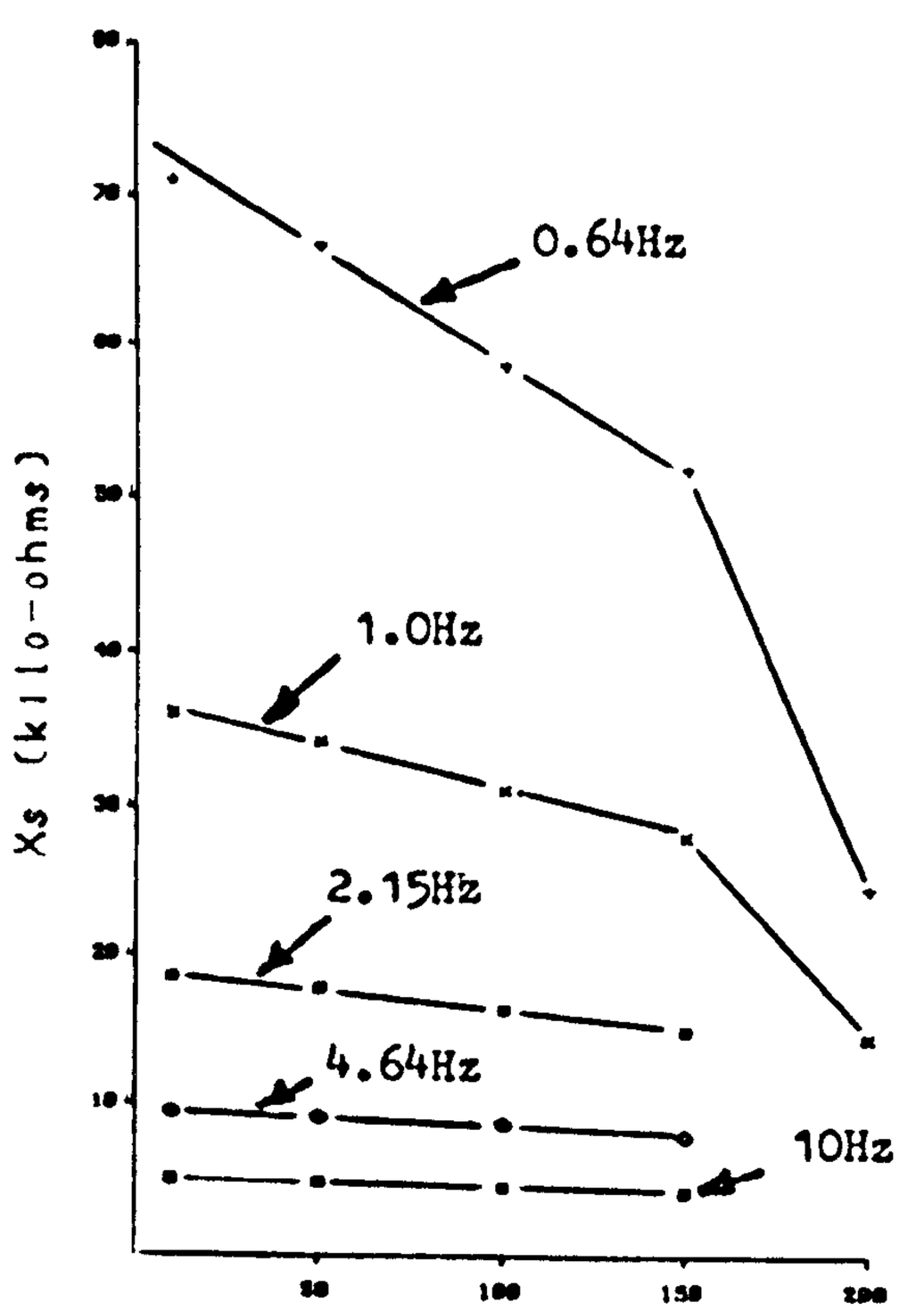

SERIES REACTANCE VS. APPLIED VOLTAGE FOR VARIOUS FREQUENCIES

- Limit voltage of linearity, $V_{ac.L}$

The X_s - V_{ac} plots were used to calculate the limit voltage of linearity as they were not complicated by the presence of a 'hump'. The small signal values of X_s, measured at a voltage amplitude of 10 mV(rms) were taken as the 'linear' values. Inspection of figure 4.25b shows this is to be an approximation as the X_s values at 10 mV do not appear to be constant and independent of voltage. This approximation will lead to calculated values of V_L slightly larger than is truely the case. Similar approximations were made by Schwan and his colleagues.

Calculated values of $V_{ac.L}$ are plotted against log $f_{10\%}$ on figure 4.26 which has the form predicted in figure 4.10. For most of the applied frequency range the plotted points lie on a straight line given by

$$f_{10\%} = 1.03\times10^{-2} \exp\left(7.59\times10^{-2}\ V_{ac.L(mV.rms)}\right)$$

As equation 4.84 can be rewritten as

$$f_{10\%} = \frac{1}{2\pi}\left(\frac{8.53\cos\phi K i_o}{\eta_L}\right)^{1/\beta} \exp\left(\frac{(1-\alpha)\ nf\eta_L}{\beta}\right)$$

then

$$(1-\alpha)nf/\beta = 53.67$$

As β = .82, f = 39 and n = 2 then α = 0.44.

This calculated value of α is larger than the value of 0.3 derived from Onaral and Schwan's results (section 4.1.2.2.2).

At low frequencies $V_{ac.L}$ tends to a constant limiting value. It is at this voltage that $R_{CT(ac)}$ changes by 10% from its small signal value, i.e. at

Tel. 224 Electrode

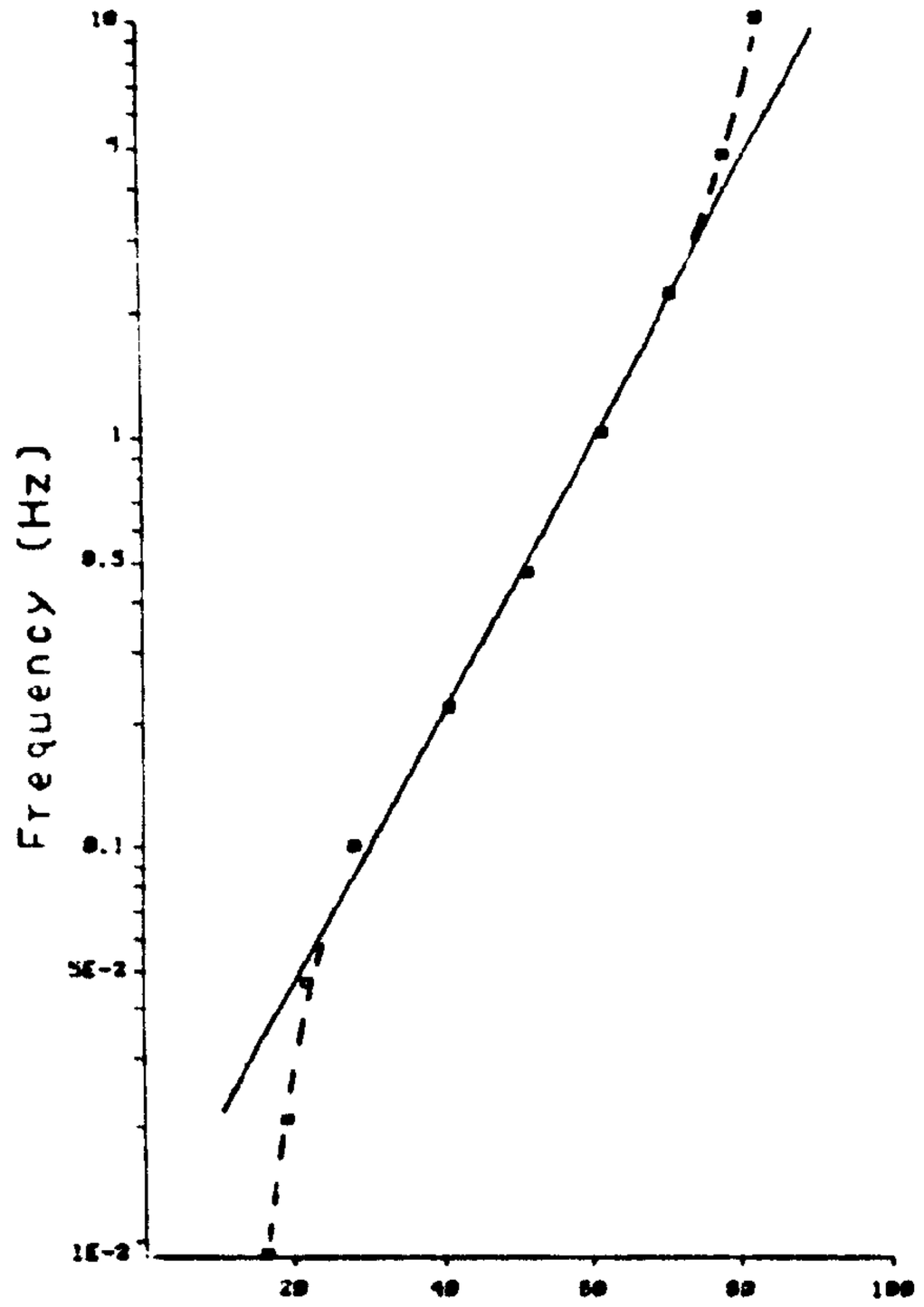

$LOG(f_{10\%})$ VS. $LOG(V_L)$

Figure 4.26

40/n mv. In figure 4.26 the limiting value is approximately 15 mV(rms) or 20 mV amplitude thus infiring that n = 2, the most probable reaction being

$$2\ Cl^- \rightarrow Cl_2 + 2e$$

At high frequencies $V_{ac.L}$ tends to another limiting value due to the nonlinearity of Z_{CPA}. This limiting value is approximately 100 mV(rms) or nearly 300 mV peak to peak.

It was noted above that K became nonlinear (ie decreased by 10%) at approximately 50mV. Very high frequency points should therefore become nonlinear at this voltage. Lower frequencies will become nonlinear at higher voltages due to a combination of the nonlinearities of Z_{CPA} and R_{CT} - at around 100mV(rms) in this case.

- Summary

Although $R_{CT(ac)}$ is the major source of nonlinearity, Z_{CPA} is also very nonlinear, especially for signal amplitudes larger that 150 mV_{rms}.

Distortion of the impedance locus is much as expected for large signal, low frequency conditions due to the formation of an oxide layer and the evolution of gas.

Plots of R_s versus V_{ac} have a peak as anticipated due to the nonlinearity of $R_{CT(ac)}$.

Plots of log $f_{10\%}$ versus $V_{ac.L}$ are also as expected with $V_{ac.L}$ increasing slightly with frequency over the applied range. Two limiting regions are observed, one due to the nonlinearity of $R_{CT(ac)}$ and the other due to a combination of those of Z_{CPA} and of

R_{CT}.

(2) Sorin S80 Electrode

- AC impedance plots

The experimental results are plotted on figure 4.27 and the calculated values of the equivalent circuit parmeters for each of the applied voltages are listed below and plotted on figure 4.28

TABLE 4.3

ac voltage (mVrms)	$K(k\Omega s^{-\beta})$	β	$R_{CT(ac)}(M\Omega)$
10	32.1	0.82	0.81
50	32.1	0.79	0.7
100	30.1	0.77	0.52

Again the experimental data are well fitted by arcs (equations 2.1 and 2.2). As less extreme voltage amplitudes were used for this electrode, no distortion of the arcs was observed at low frequencies.

Points on the loci of the same frequency form arcs whose centres are to the left of the imaginary axis. This would indicate that although $R_{CT(ac)}$ is the major source of the nonlinearity, that of Z_{CPA} makes a significant contribution, more so as the frequency is increased, resulting in the centres of the iso-frequency arcs moving relatively further to the left of the imaginary axis.

The magnitude of the Z_{CPA} impedance, K, is almost contant over the applied voltage range, decreasing slightly at 100 mV(rms). β , an inverse measure of the frequency dispersion, is also almost constant,

Porous Electrode

A.C.Nonlinearity

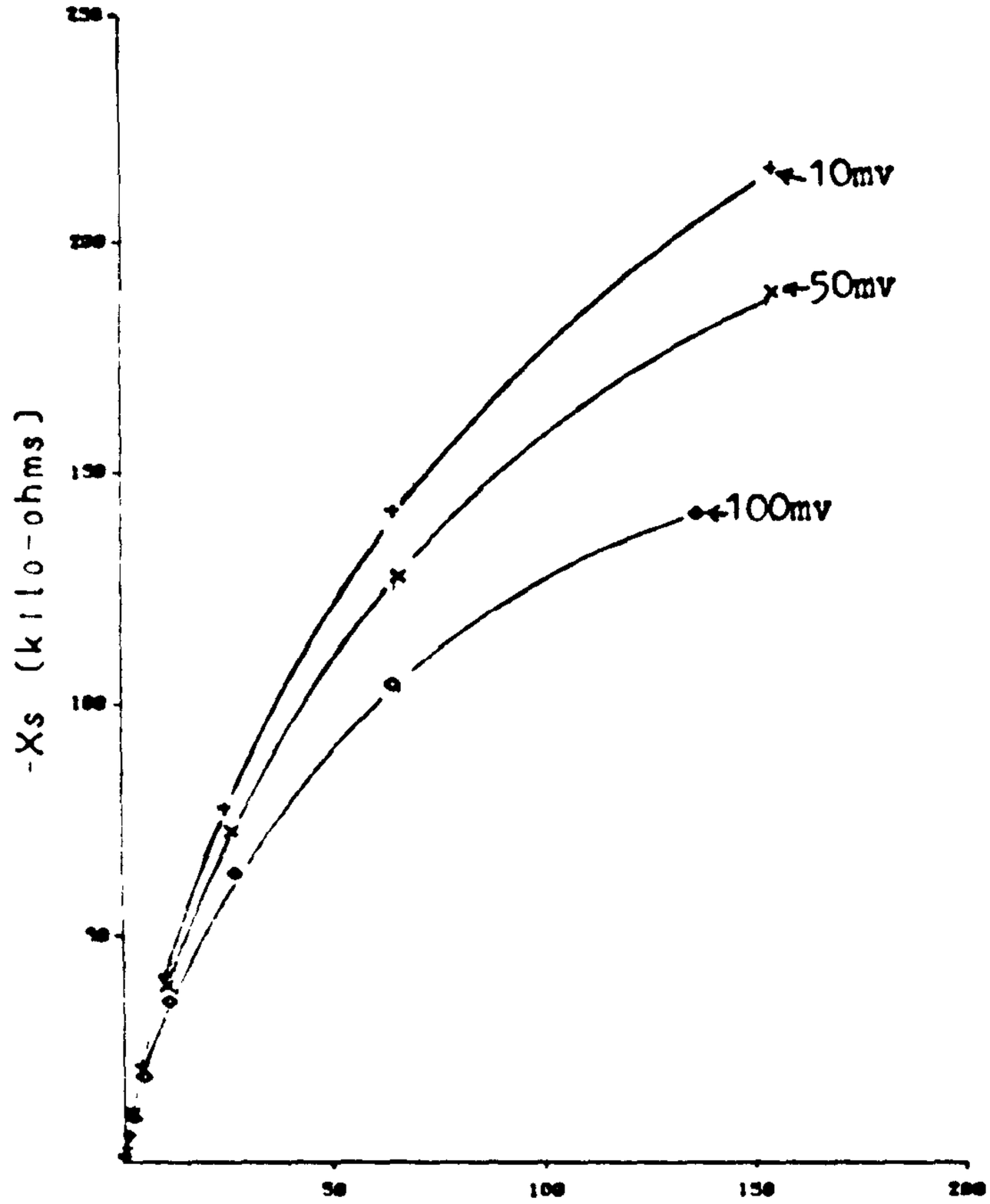

Figure 4.27

Porous Electrode

A.C.Nonlinearity

of Equivalent Circuit Elements

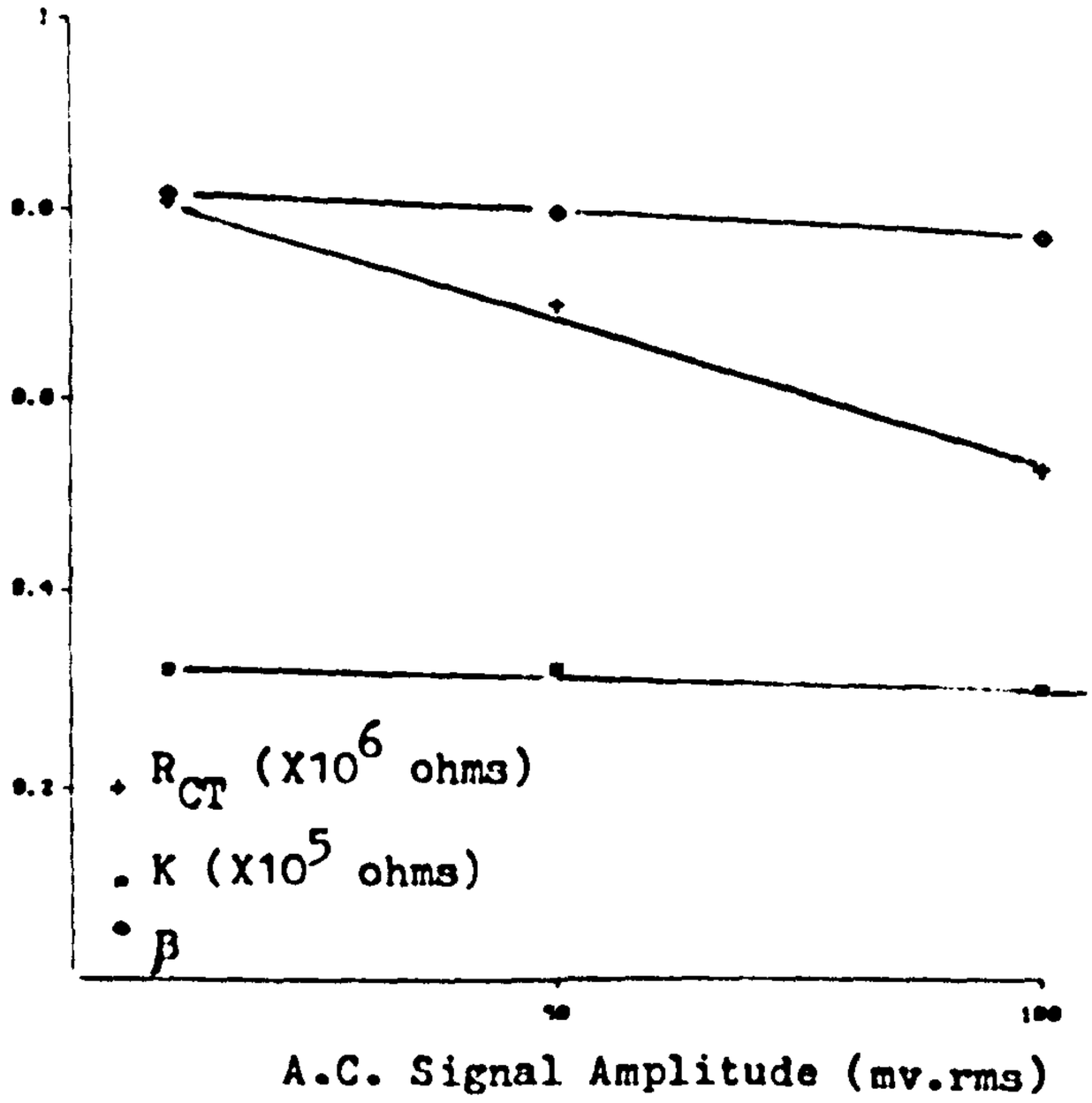

Figure 4.28

decreasing very slightly over the voltage range. It is very probable that the chosen voltage range (10-100 mV(rms)) lies within the double layer region where the capacitance is almost constant and there is relatively little frequency dispersion (i.e. β is a maximum). No dramatic change in the values of K and β were observed. It is very probable that a voltage of at least 150 or 200 mV(rms) would be required to cause the nonfaradaic Z_{CPA} impedance to become grossly nonlinear.

Over the rather limited voltage range (10-100 mVrms) $R_{CT(ac)}$ decreases linearly with voltage. Fitting the results to an exponential relationship gave

$$R_{CT(ac)} = 8.6 \times 10^5 \exp(-4.9\ V_{ac(rms)})$$

$-R_s$ and X_s

Plots of R_s and X_s versus the applied voltage amplitude (rms) are shown on figures 4.29a and b.

At the relatively high frequency of 21.5 mHz the 'hump' is discernable on the R_s - V_{ac} plot as R_s initially increases, reaches a maximum, and then decreases. The peak of the hump occurs at higher voltages for higher frequencies and hence, for most of the applied frequencies, only the initial rise in R_s is observed, the peak occuring beyond the applied voltage range.

X_s decreases almost linearly with the voltage amplitude (figure 4.29b)

- $V_{ac.L}$

The limit voltage of linearity was calculated using the X_s values. Again it was assumed that values obtained at 10 mV(rms) were the linear values (which is

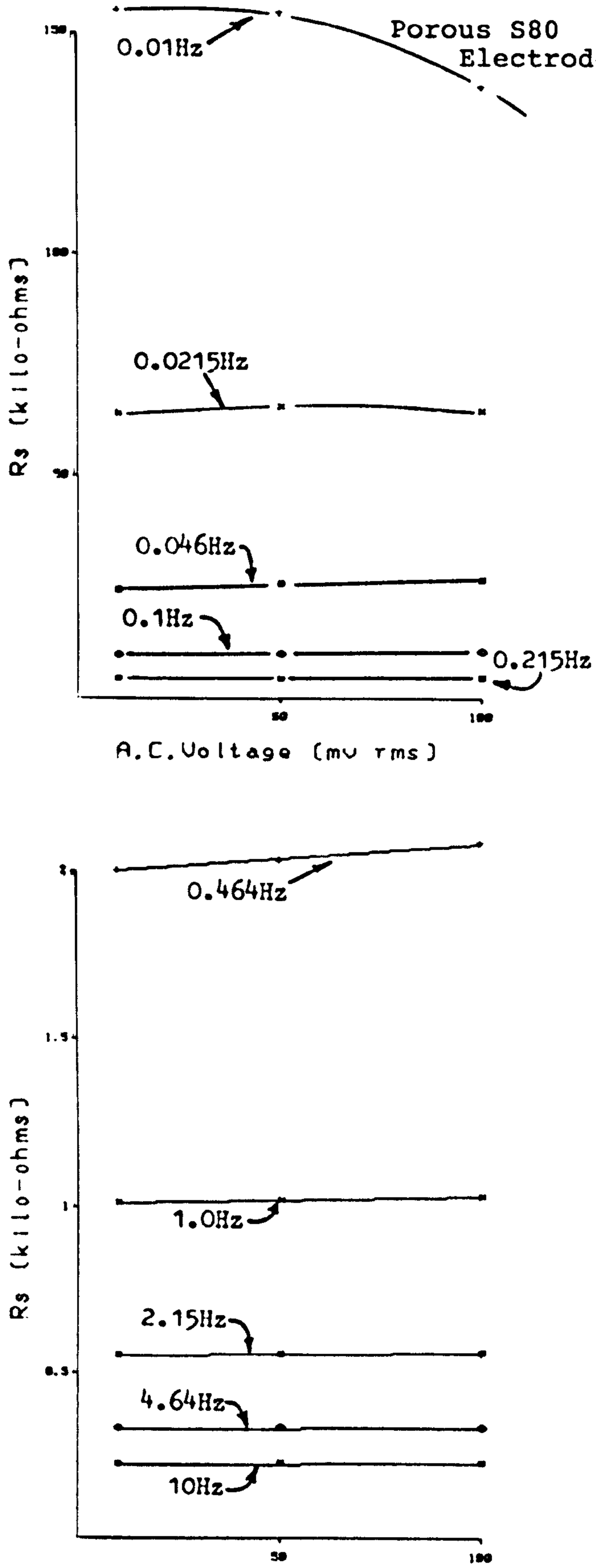

Figure 4.29a

SERIES RESISTANCE VS. APPLIED VOLTAGE FOR VARIOUS FREQUENCI

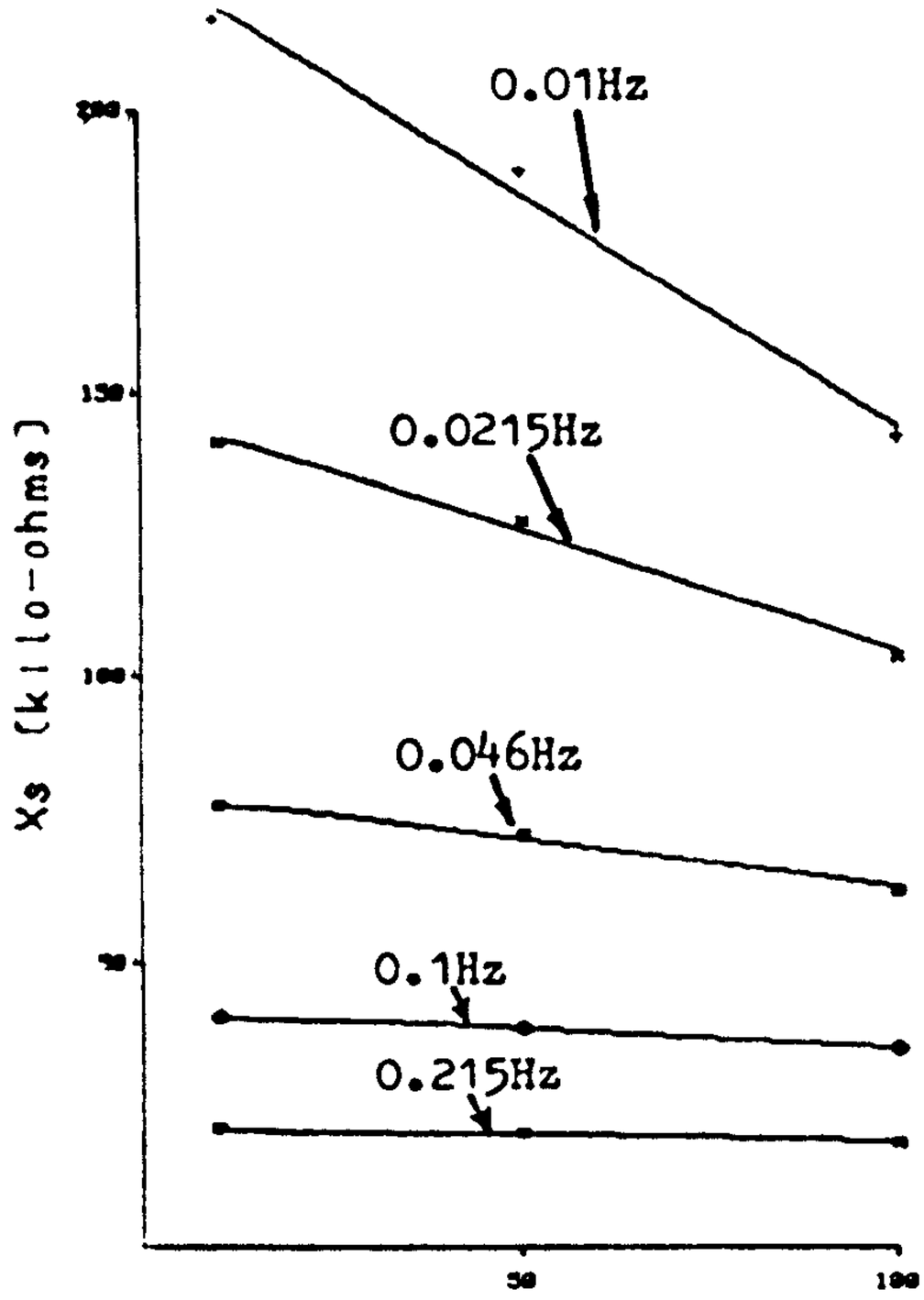

Figure 4.29b

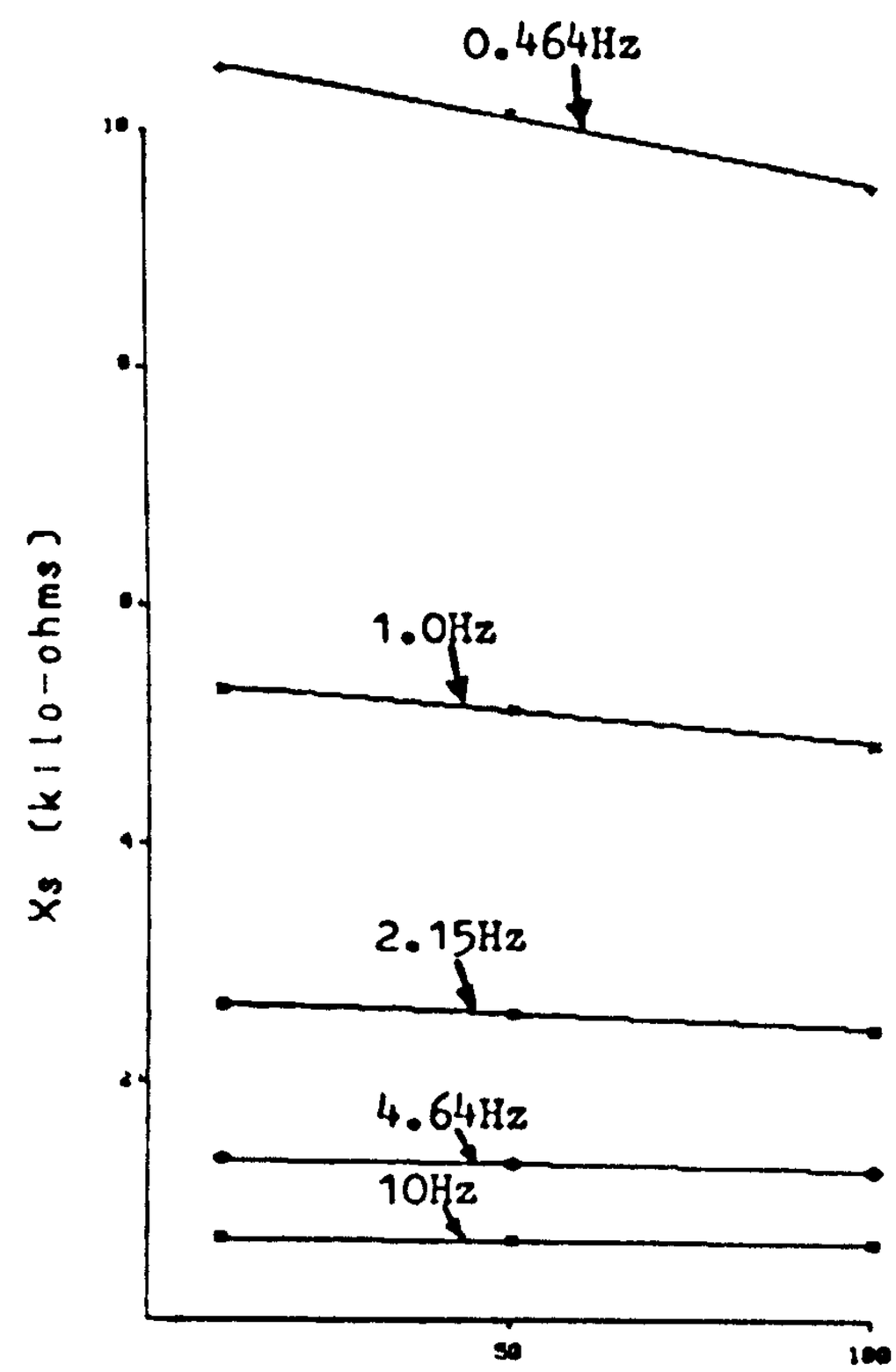

SERIES REACTANCE VS. APPLIED VOLTAGE FOR VARIOUS FREQUENCIES

not strictly the case).

Calculated values of $V_{ac.L}$ are plotted against log $f_{10\%}$ (figure 4.30). The plot is approximately linear and was represented by the equation.

$$f_{10\%} = 1.85 \times 10^{-3} \exp [(6.37 \times 10^{-2} V_{ac.L(mV\ rms)}]$$

At low frequencies $V_{ac.L}$ approaches a limiting value (approx 15 or 20 mV(rms)) similar to that found for the Telectronic electrode (figure 4.26).

At high frequencies there are signs of $V_{ac.L}$ tending towards another limiting value beyond the applied voltage range, due to the nonlinearity of Z_{CPA}. It was shown on figure 4.28 and Table 4.3 that K was fairly linear within the applied voltage range. The results would tend to indicate that $V_{ac.L}$ limits at high frequencies at approximately 130 or 140 mV(rms), at which stage Z_{CPA} becomes grossly nonlinear. If this is the case, the double layer region is approximately 350 to 400 mV wide.

(3) The Activated vitreous Carbon Electrode

- Ac impedance

The experimental results are plotted on figure 4.31 and the calculated values of the equivalent circuit parameters are plotted on figure 4.32 and listed on Table 4.4.

TABLE 4.4

ac Voltage mV(rms)	$K(k\Omega s^{-\beta})$	β	R_{CT} (kΩ)
10	13.9	.66	181
50	13.8	.67	171
100	12.8	.66	165

Porous S80 Electrode

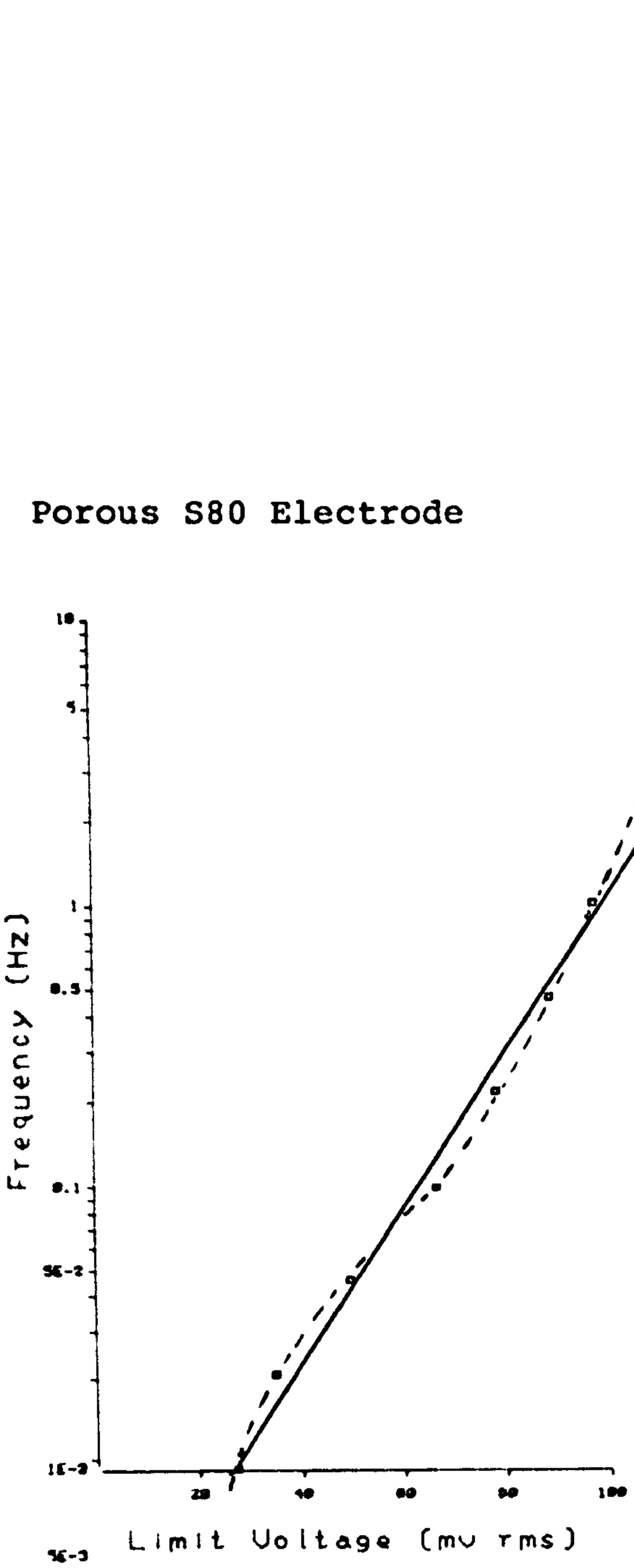

$LOG(f_{108})$ VS. $LOG(V_L)$

Figure 4.30

Vitreous Carbon Electrode

A.C.Nonlinearity

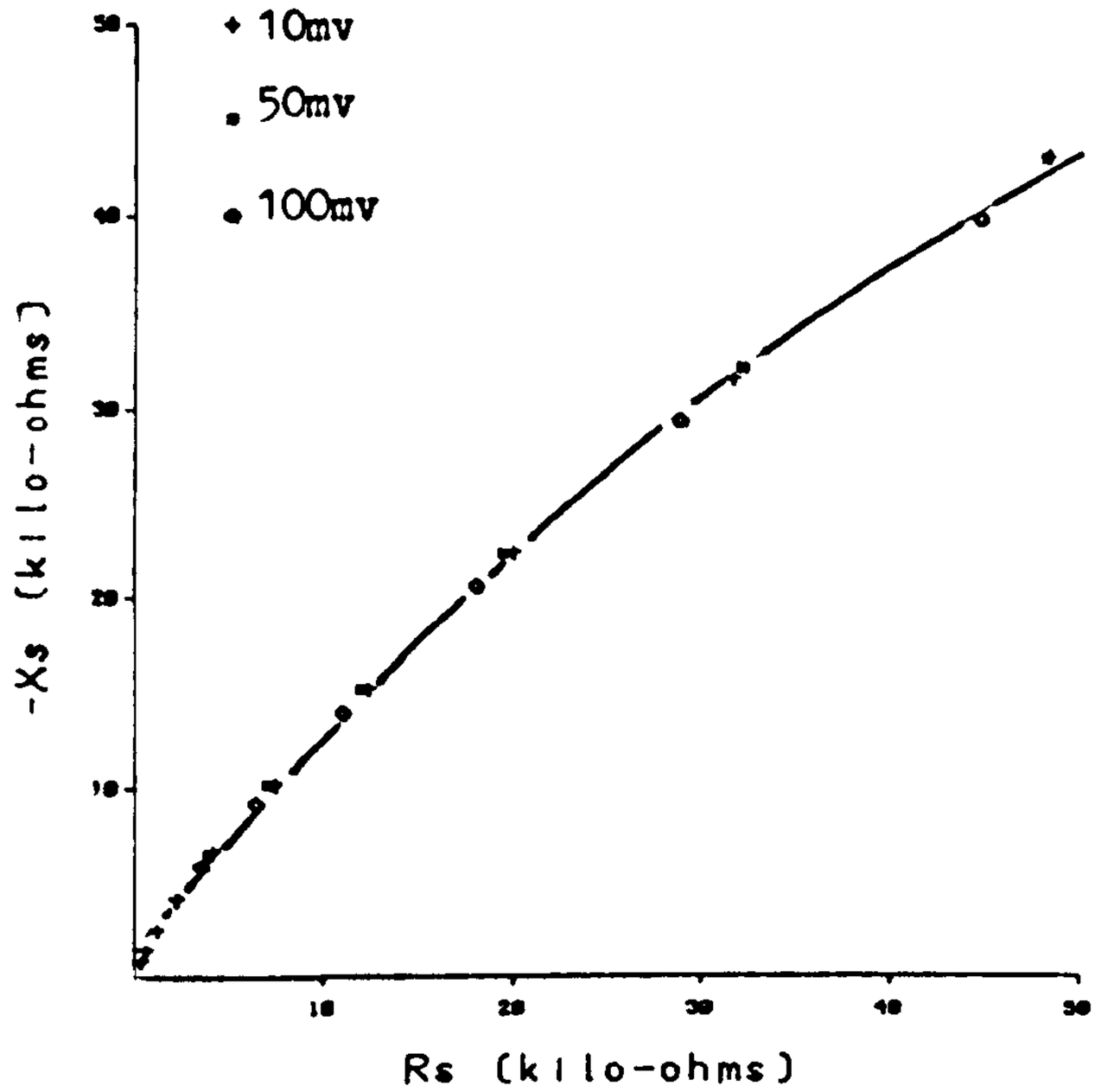

Figure 4.3

Vitreous Carbon Electrode

A.C.Nonlinearity

of Equivalent Circuit Elements

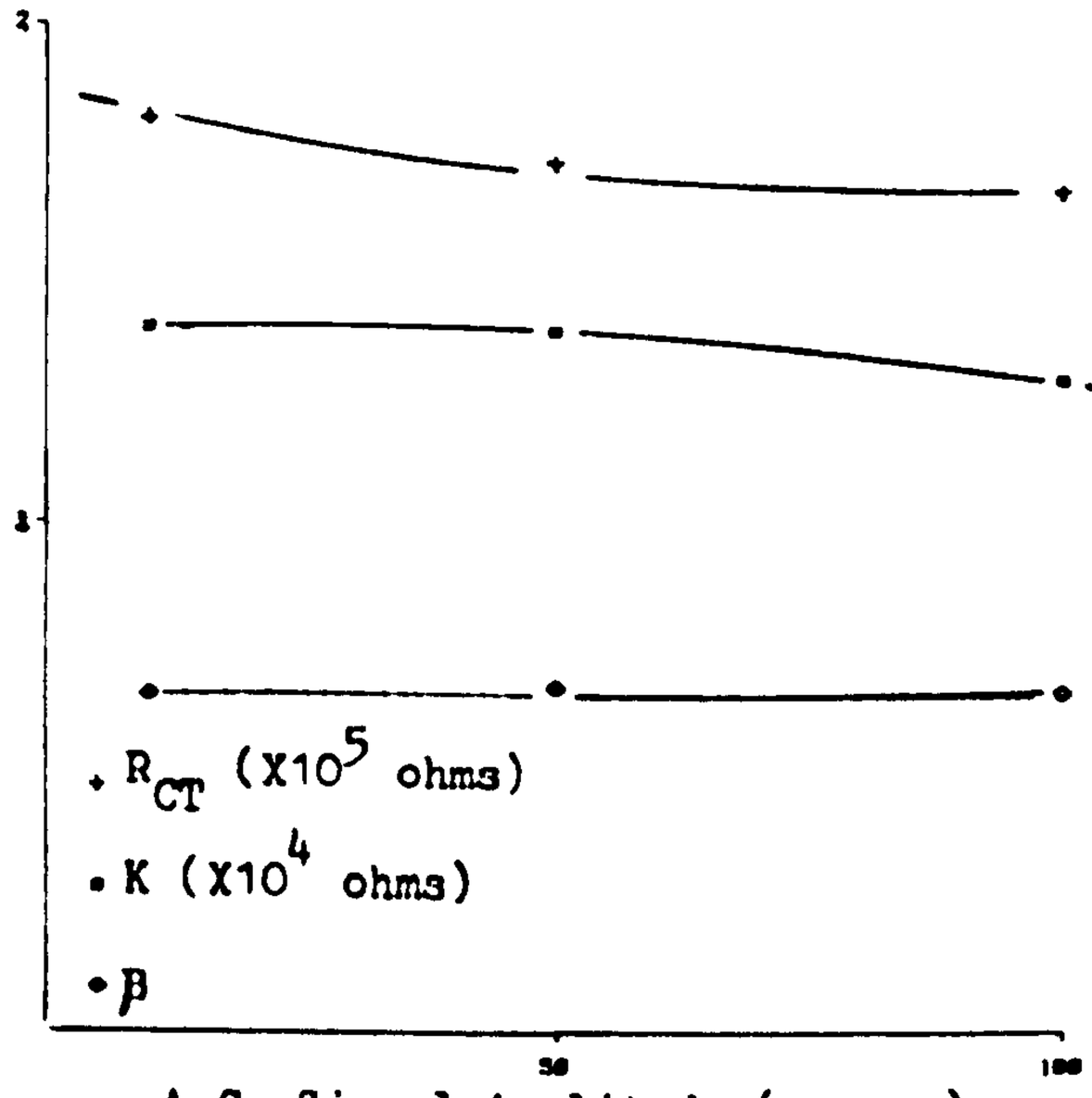

Figure 4.3

The activated vitreous carbon electrode is relatively linear. Very little change is observed in the parameter values and hence in the impedance loci.

R_{CT} decreases slightly with applied voltage and the decrease was fitted by the equation

$$R_{CT(ac)} = 1.8 \times 10^5 \exp(-1.01\ V_{ac(rms)})$$

K is almost constant over the whole of the applied voltage range, as is β .

It would appear that the electrode system is operating well within the double layer voltage region. A plot of the ac impedance of the A.V. Carbon electrode measured at 300 mV is shown on figure 1.42. The values of K and β appear to have changed relatively little whereas R_{CT} has decreased to approximately 50kΩ .

- R_s and X_s

The R_s and X_s versus V_{ac} plots are shown on figures 4.33a and b.

R_s decreases with voltage amplitude and no 'hump' is observed as $R_{CT(ac)}$ is not significantly more nonlinear than K.

X_s also decreases with voltage amplitude except at 21.5 mHz where a 'hump' is observed in the plot.

- $V_{ac.L}$

The limit voltage of linearity was calculated using both the R_s and X_s results. Values of $V_{ac.L}$ calculated using the X_s data are generally larger than those derived from R_s data. Plots of $V_{ac.L}$,as calculated from R_s and X_s values ,versus log $f_{10\%}$ are shown on figure 4.34. Once again values of R_s and X_s measured at 10 mV(rms) were taken as linear values.

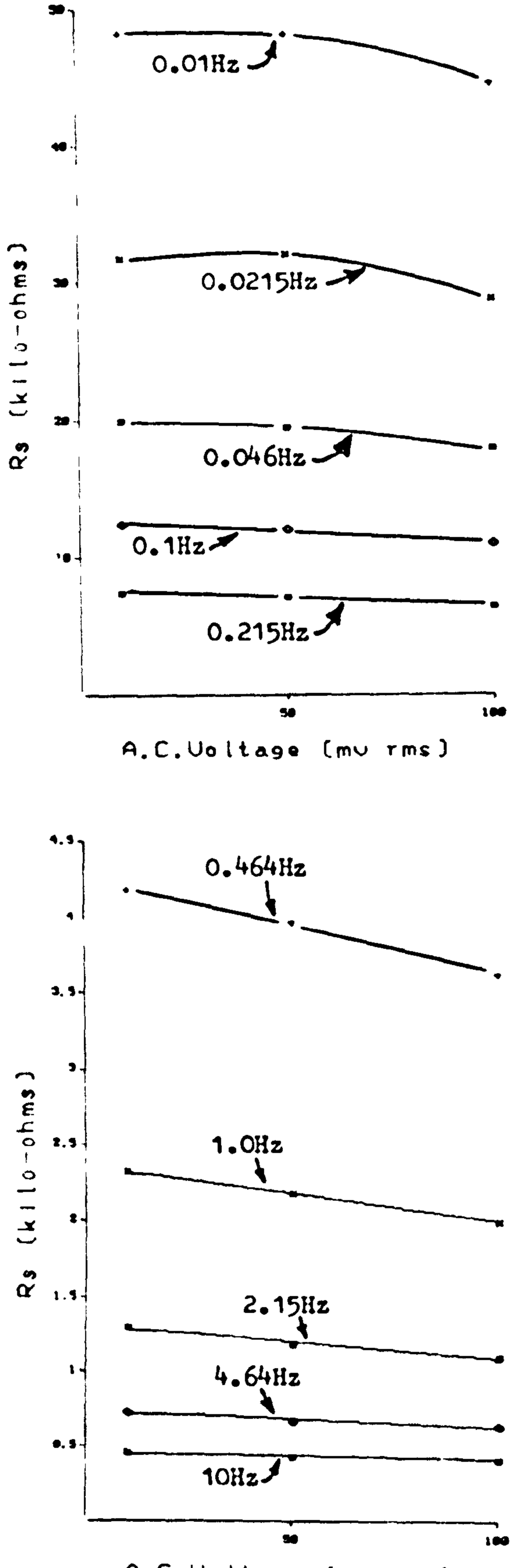

Figure 4.33a

SERIES RESISTANCE VS. APPLIED VOLTAGE FOR VARIOUS FREQUENCIES

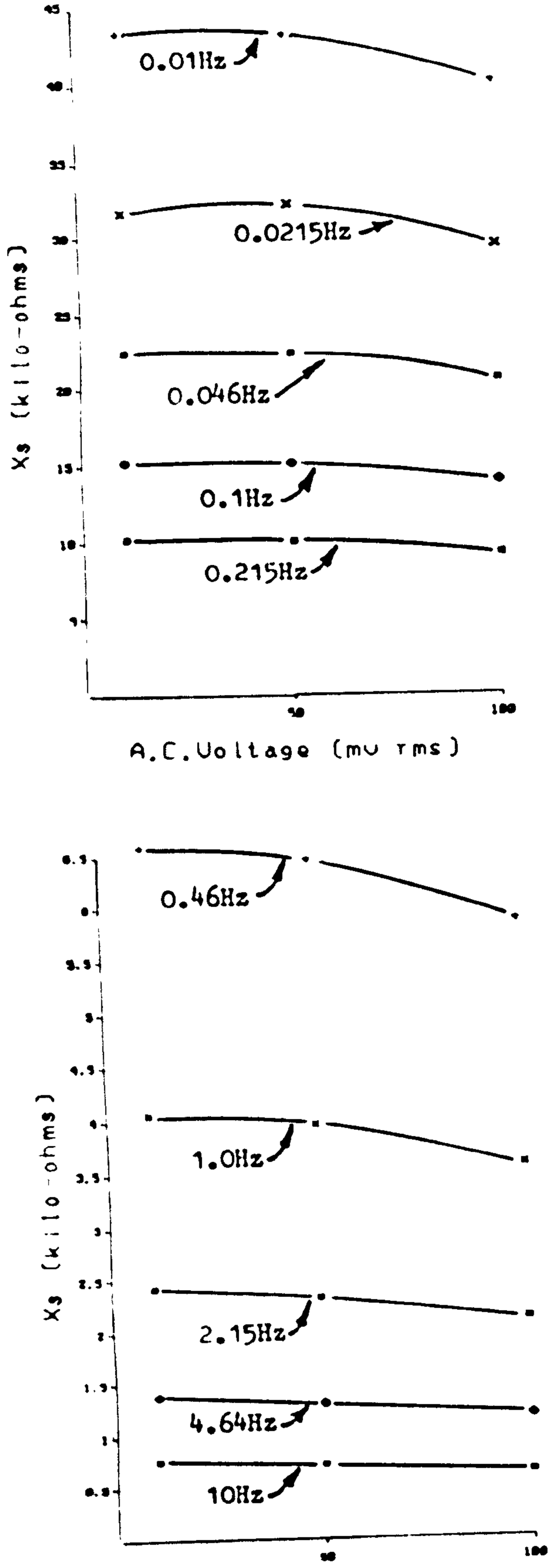

Figure 4.33b

SERIES REACTANCE VS. APPLIED VOLTAGE FOR VARIOUS FREQUENCIES

The $V_{ac.L}$ - log $f_{10\%}$ plot for the activated vitreous carbon electrode differs from those for the Telectronic 224 and Sorin S80 electrodes (figures 4.26 and 4.30). As neither $R_{CT(ac)}$ nor K decrease significantly within the applied voltage range, overall nonlinearity is due to a combination of both their nonlinearities. It would appear that mid frequencies become nonlinear at approximately 60 mV, before either the high or low frequencies, due to this combination effect. High and low frequency points only become nonlinear at larger voltage amplitudes. For low frequencies, $V_{ac.L}$ tends towards a limiting value of 120 mV(rms) - outside the applied voltage range.

- Discussion

As expected the overall impedance loci are arcs whose diameters decrease with applied signal amplitude. As an arc's diameter decreases, progressively higher frequency points are observed to become nonlinear.

Contrary to Schwan's statements $V_{ac.L}$ generally varies between two limiting values, increasing as the frequency is increased.

As postulated there is an initial rise in the R_s - V_{ac} plot which has, apparantly, not been previously noticed.

At low frequencies and larger amplitude signals the impedance locus deviates from a simple arc due to the 'sudden' increase in $R_{CT(ac)}$ upon the formation of an oxide layer.

Of the electrodes tested the activated vitreous

Activated Vitreous Carbon Electrode

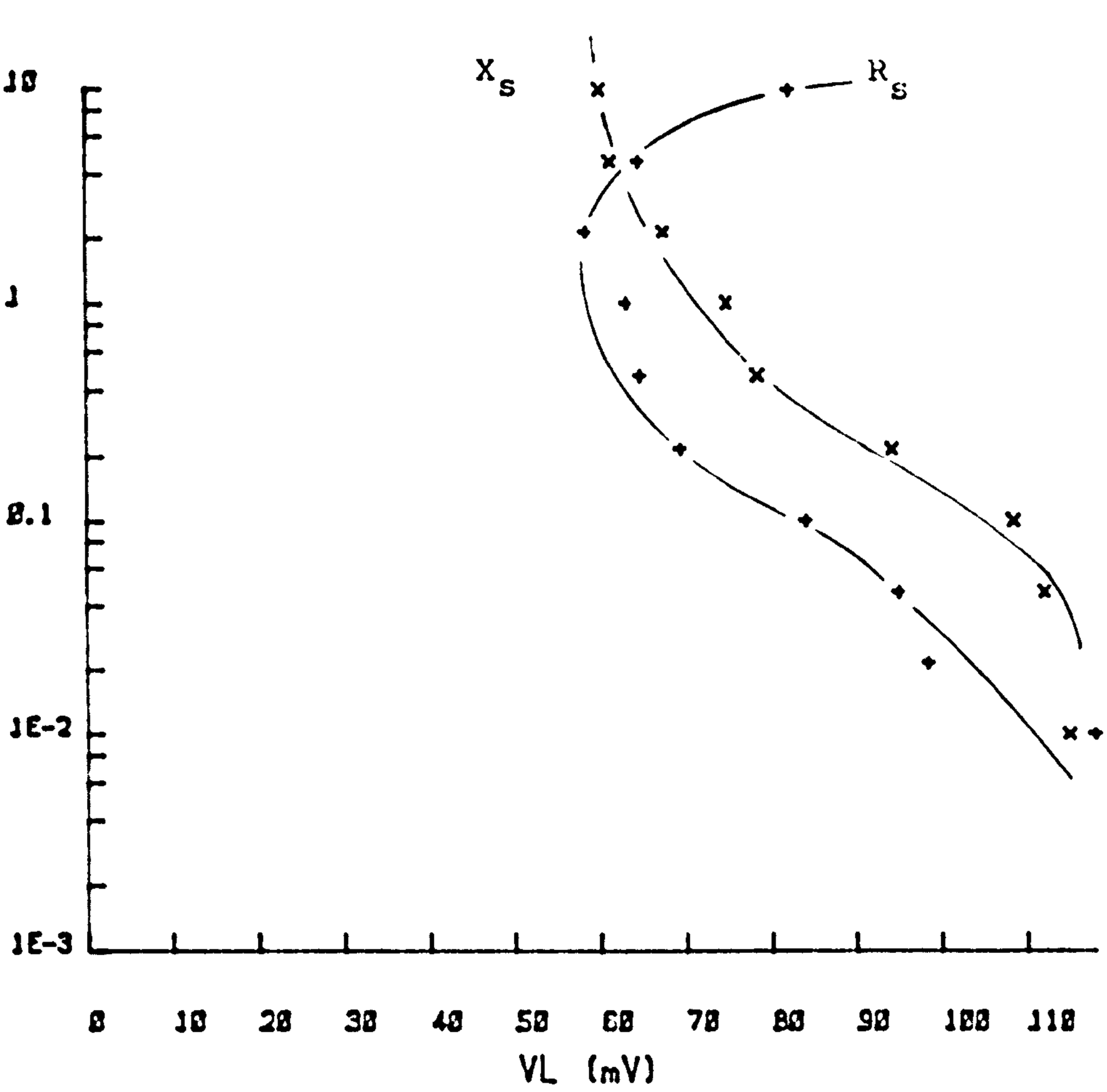

$\text{LOG}(f_{10\%})$ VS. $\text{LOG}(V_L)$

Figure 4.34

carbon electrode is the most linear with very little decrease in $R_{CT(ac)}$, K or β.

The decrease in $R_{CT(ac)}$ with applied voltage amplitude was fitted to the exponential

$$R_{CT(ac)} = a \exp(-b V_{ac.\,rms})$$

for each of the electrodes tested. 'a' is inversely related to i_o, the exchange current density, which is a measure of the electrode reaction and an indication of the liability of the electrode system to polarisation. 'b' is a measure of the linearity of $R_{CT(ac)}$ - the smaller value, the more linear the electrode impedance

Table 4.5

Electrode	a($x10^6$)	b
Tel. 224	2.6	11.2
Porous S80	0.86	4.9
A.V. Carbon	0.18	1.0

As the activated vitreous carbon electrode has the smallest value of 'a', it has the largest value of exchange current density and hence the smallest charge transfer resistance. It will therefore be the least easily polarised and hence the 'best' of the three electrodes investigated.

The activated vitreous carbon electrode also has the smallest value of 'b' and hence is the most linear electrode. This is to be expected as it has the roughest surface.

The activated vitreous carbon electrode also has the smallest, most linear values of K.

The "smooth" electrodes have large values of K and R_{CT} and are the most nonlinear.

It is concluded, based on these large ac signal experiments, that the a.v. carbon electrode is the 'best', being the most linear and the least prone to polarisation.

The 'worst' electrode is the 'smooth' surfaced Pt-Ir electrode which is the most polarisable and the most nonlinear. The porous Pt-Ir electrode is a great improvement as its rougher surface decreases the value of $R_{CT(ac)}$ thus making the electrode less prone to polarisation. It also makes the electrode more linear.

4.2.4 Signal Distortion

- Introduction

At low frequencies and high signal amplitudes signal distortion was observed in some of our early experiments.

At low frequencies the interfacial impedance is governed by the charge transfer resistance which is derived from the i -η curve. As the i -η curves are nonlinear, one can expect the low frequency waveforms to be distorted.

When a low frequency sinusoidal voltage, for example, is applied to such a nonlinear system, the resultant current waveform should be as shown on figure 4.35.

During the first quarter cycle the current response will have a form similar to that of the i-η characteristic and hence, for a time, the current will

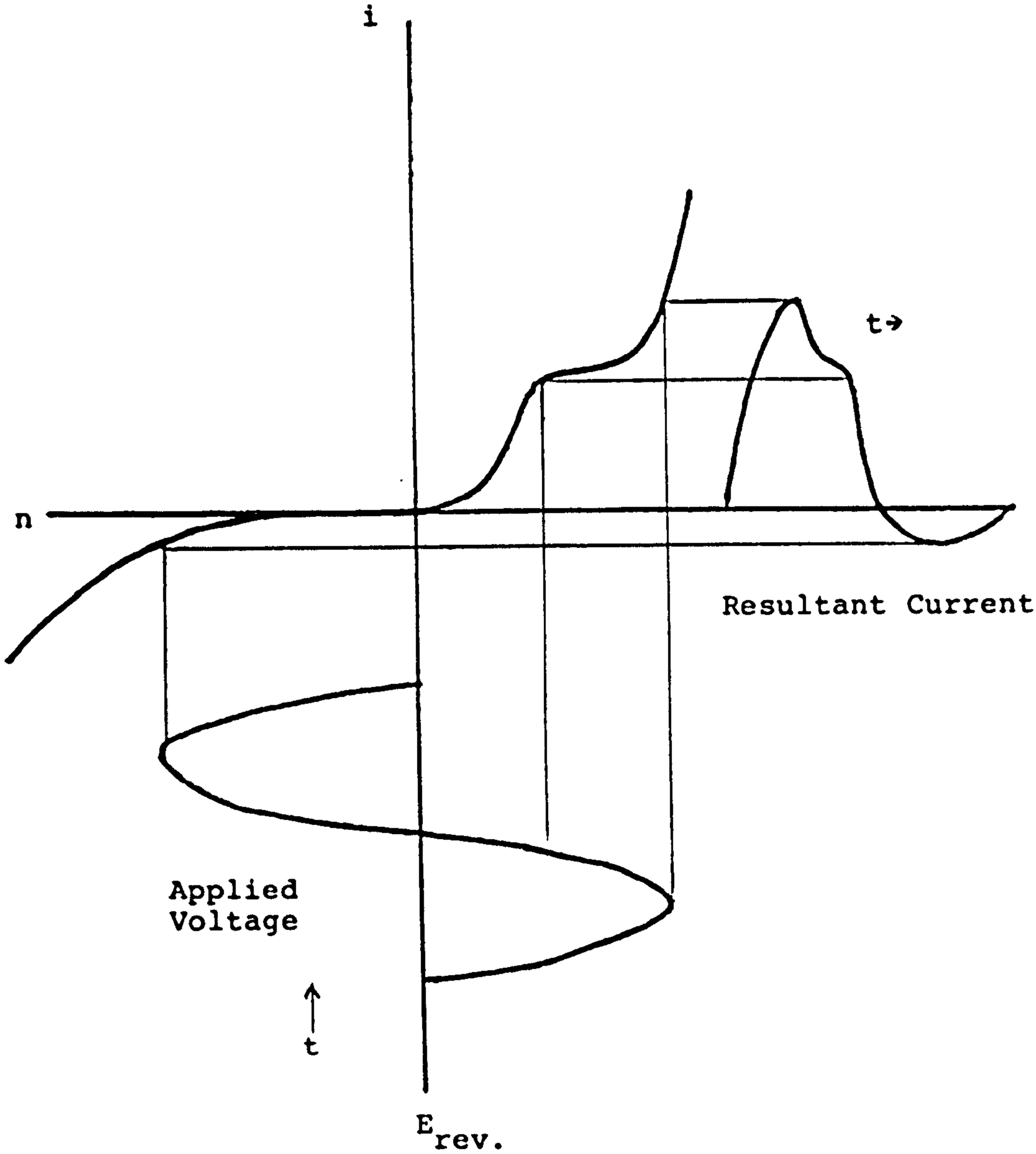

SIGNAL DISTORTION

Figure 4.35

limit due to the "voltage jump". It will then continue to increase during the rest of the first quarter cycle.

The second half of the current waveform would simply be the reverse of the first, were it not for the fact that the cathodal

than that of the anode. This can be deduced from the i-η characteristics shown on figure 4.13. Very little cathodal current will flow, the waveform will be 'clipped' and there will be a net positive shift of the average current i.e. there is a rectification current.

Guld (1963) obtained similar current waveforms using large amplitude voltage signals applied to platinum micro-electrodes in NaCl. Brownstein (1982), although using large amplitude Cyclic Voltammetry (a periodic triangular voltage, 1200 mV peak to peak), also observed such signal distortion for Pt electrodes in NaCl, KBr and KI.

- Experimental set up and results

A 200 mV peak to peak signal was applied across a Telectronic 224 electrode and the large area indifferent in saline. The frequency was incrementally decreased from 2Hz to 0.01Hz and the resultant current waveforms observed (figure 4.36).

At 2Hz the waveform appears to be a perfect sinusoid. However at 1Hz the beginning of some anodal distortion is noted at approximately 10 μA due to the abrupt change in the i-η characteristic. As the frequencey is further decreased, the 'second Tafel' region is evidenced by a rapid increase in current (eg at 0.1Hz). The waveforms are very much as predicted on

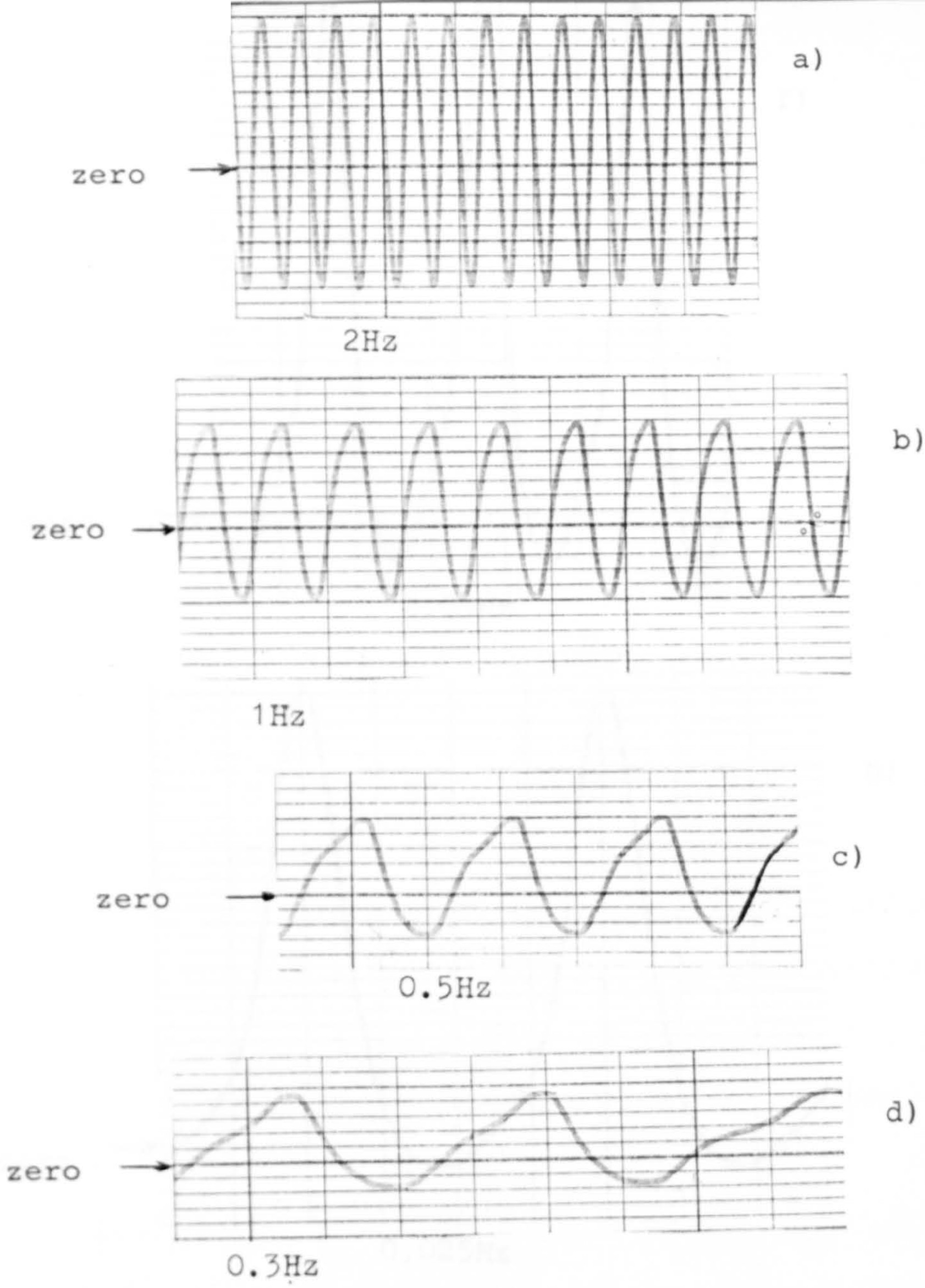

Vertical scale 10^{-5} Amp/cm

SIGNAL DISTORTION

Figure 4.36 A

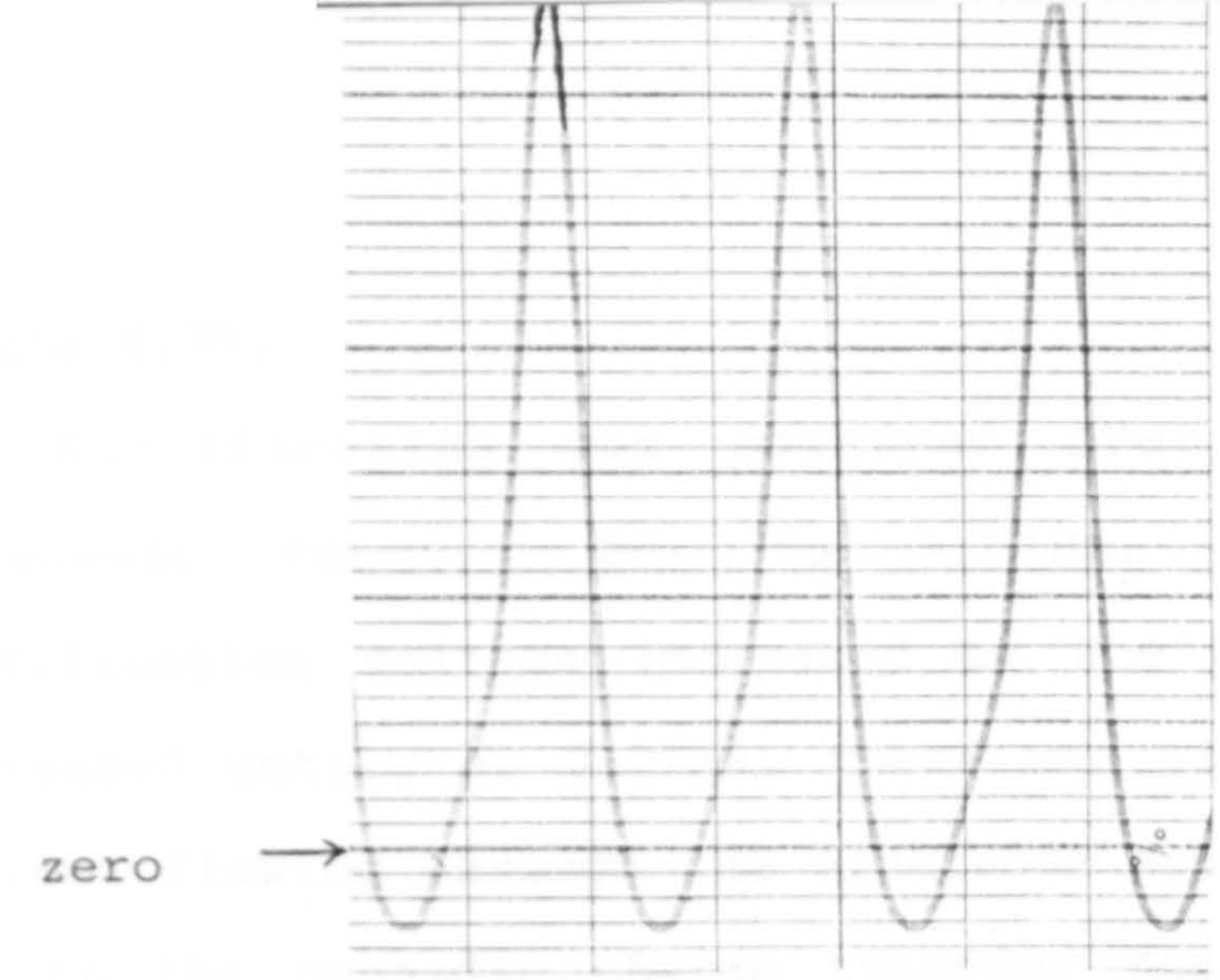

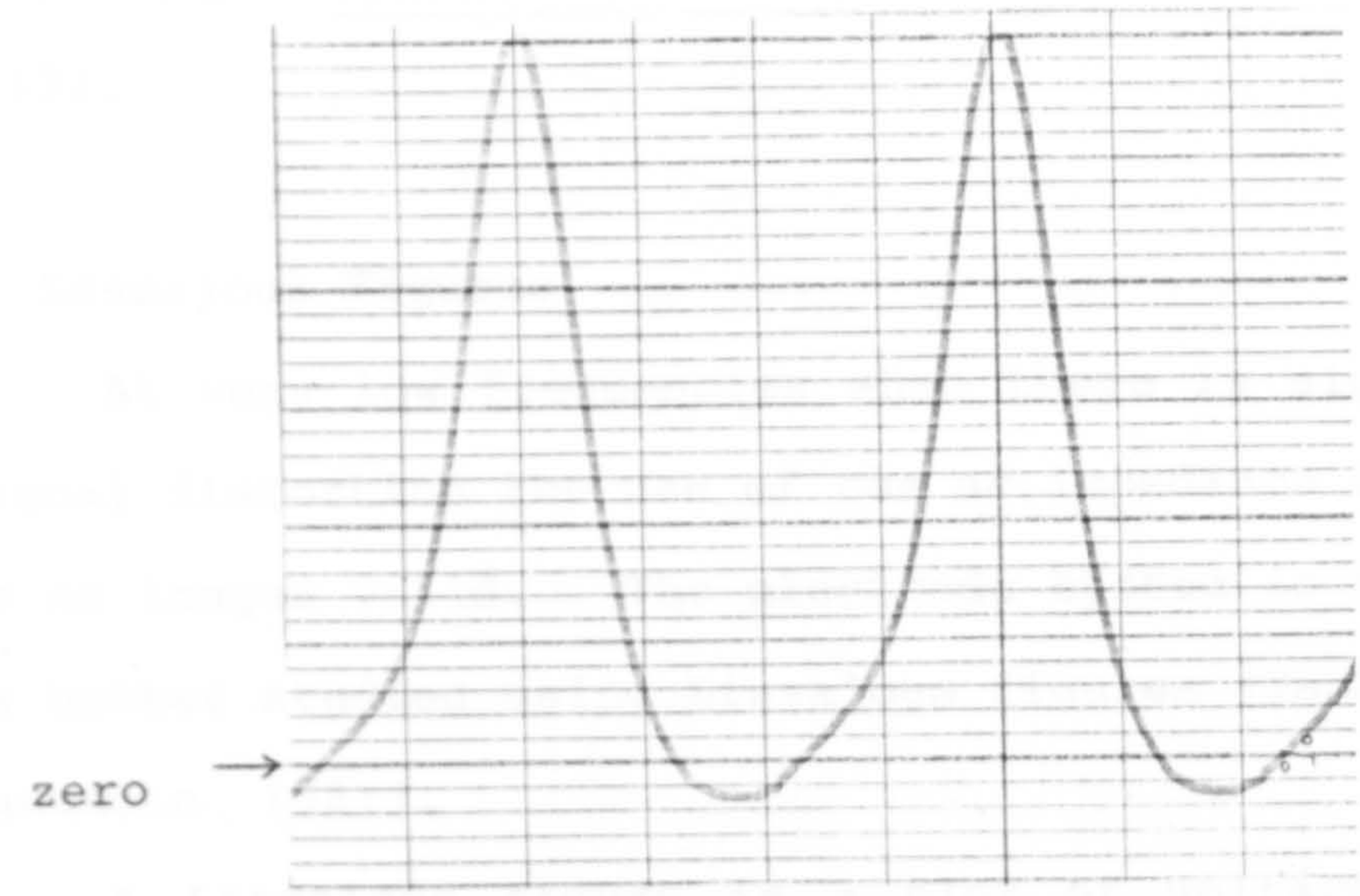

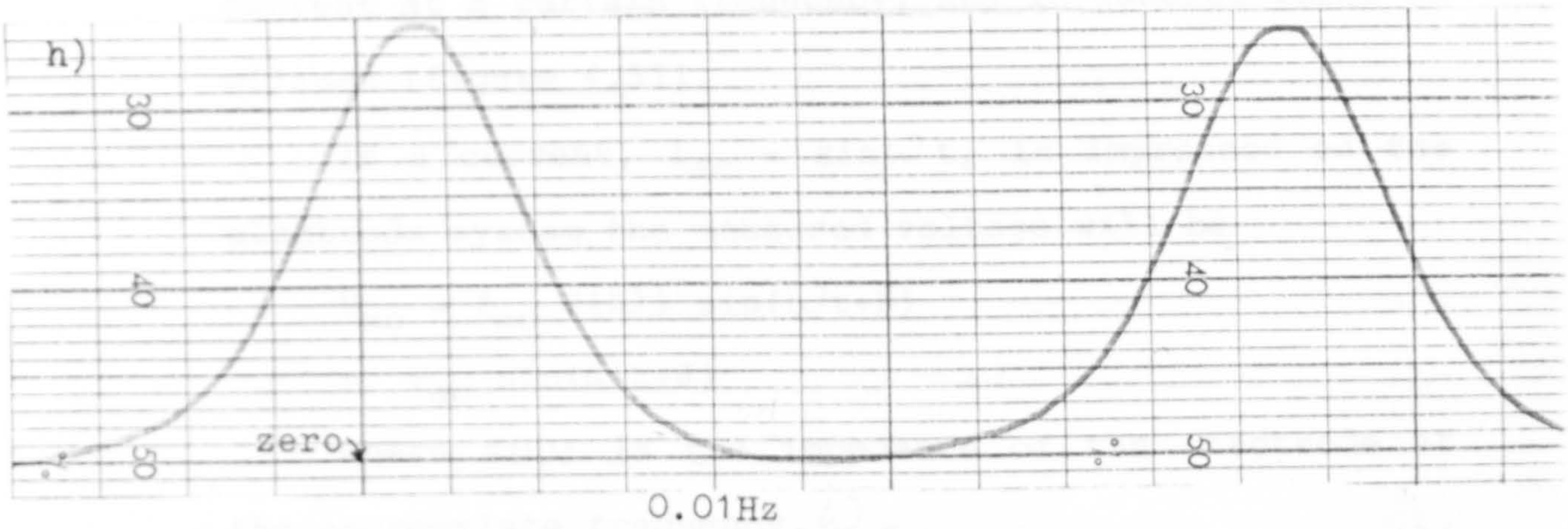

Vertical scale 10^{-6}Amp/cm

SIGNAL DISTORTION

Figure 4.36 B

figure 4.35.

Rectification was observed over the entire frequency range, 2Hz to 0.01Hz. The anodic rectification voltage increased as the frequency was decreased until, at 0.01Hz, there was little cathodic current flowing through the electrode system. This is due to the cathodic charge transfer resistance being very large relative to that of the anode (see figure 4.13).

- Lissajous Figures

At very low frequencies when there is significant signal distortion the use of the ac impedance technique is no longer valid. The electrode system in this case is better studied using Lissajous figures (Yamamoto and Yamamoto 1981).

A Lissajous figure is a plot of voltage against current at a certain frequency, and in general forms an ellipse (figure 4.37).

If a current, $i_{ac} = \sin\omega t$, is impressed on the electrode system the measured voltage will be

$$V_{ac} = I_{ac}\, Z(\omega)\, \sin(\omega t+\phi)$$

$$= V_{ac}\, \sin(\omega t+\phi)$$

Where $Z(\omega)$ is the impedance of the electrode at the appropriate frequency, ω.

The impedance can be found from the resultant ellipse as follows,

$$/Z/ = \frac{V_{ac}}{I_{ac}} = \frac{Y_{max}}{X_{max}} \quad \text{and} \quad \phi = \sin^{-1}\left(\frac{x}{X_{max}}\right)$$

At high frequencies and low current densities the

Lissajous figure of an electrode system will be an ellipse similar to that shown on figure 4.37, as the interfacial impedance is dominated by that of the relatively linear Z_{CPA}.

As the applied frequency decreases, the reactive component, X_S, and the phase angle, $\emptyset$, decrease and R_{CT} begins to dominate the form of the interfacial impedance. Lissajous figures in this region will become narrower, as 'x' is proportional to sin $\emptyset$. If 'x' were to reach zero the interfacial impedance would be purely resistive and equal to the charge transfer resistance.

As R_{CT} is not a linear resistance, one can expect that Lissajous figures made at very low frequencies and / or high current densities will deviate from the simple ellipses observed for linear impedances.

Low frequency Lissajous figures are very similar to Cyclic Voltammograms (eg Zeuthen, 1978 figure 2) which are obtained using triangular waves as opposed to sinusoids. The use of Cyclic Voltammograms is very common in electrochemistry and much work has been done on their interpretation. As a Lissajous figure and a Cyclic Voltammogram of an electrode system share the same key features, reference will be made to results obtained using Cyclic Voltammograms to aid understanding of our own Lissajous figures.

The importance of Cyclic Voltammetry and Lissajous figures lies in the fact that generally each distinct peak observed on the i-V curves corresponds to a separate electrode process. However, although low

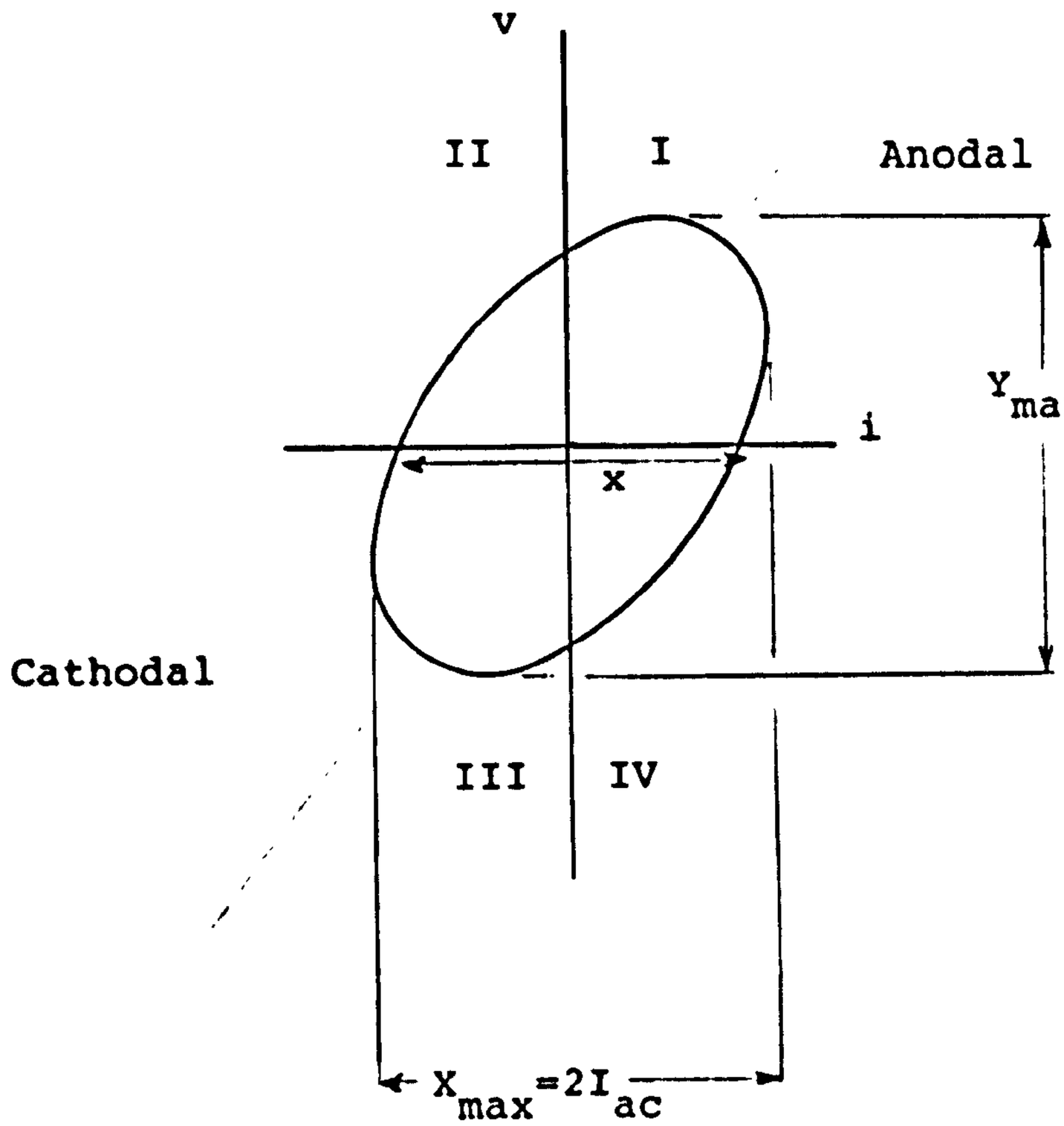

LISSAJOUS FIGURE

Figure 4.37

frequencies are used (in the present case 1 or 2 Hz), steady state conditions are never reached and hence nonfaradaic processes will also be present (Hoare, 1967). Caution must therefore be used when interpreting these curves as the method cannot distinguish between the faradaic and nonfaradaic processes present, since both produce current which is recorded.

-Telectronic 224 Electrode

The Lissajous figure for a simple Pt-Ir electrode (Telectronic 224) is shown on figure 4.38. The applied frequency was 1Hz and the applied voltage was approximately 4 Volts peak to peak. A series resistance of 900Ω was used to measure the current. Figure 4.39 is the Lissajous figure of a small spherical platinum electrode (not a pacing electrode) with an approximate area of 5 mm^2 subjected to a large amplitude (almost 8 volts peak to peak) 4Hz signal.

Note that the Lissajous figures have been centered and hence scales are relative to the centre of the figures.

The Lissajous figures (figures 4.38 and 39) have been divided into several regions according to the dominant reaction(s) believed to be taking place. Again it must be emphasised that interpretation of results obtained for electrode systems which involve electrolytes containing halides is very difficult and there have been many contradictory publications.

Region 1: This is the double layer region where

Tel.224 Electrode

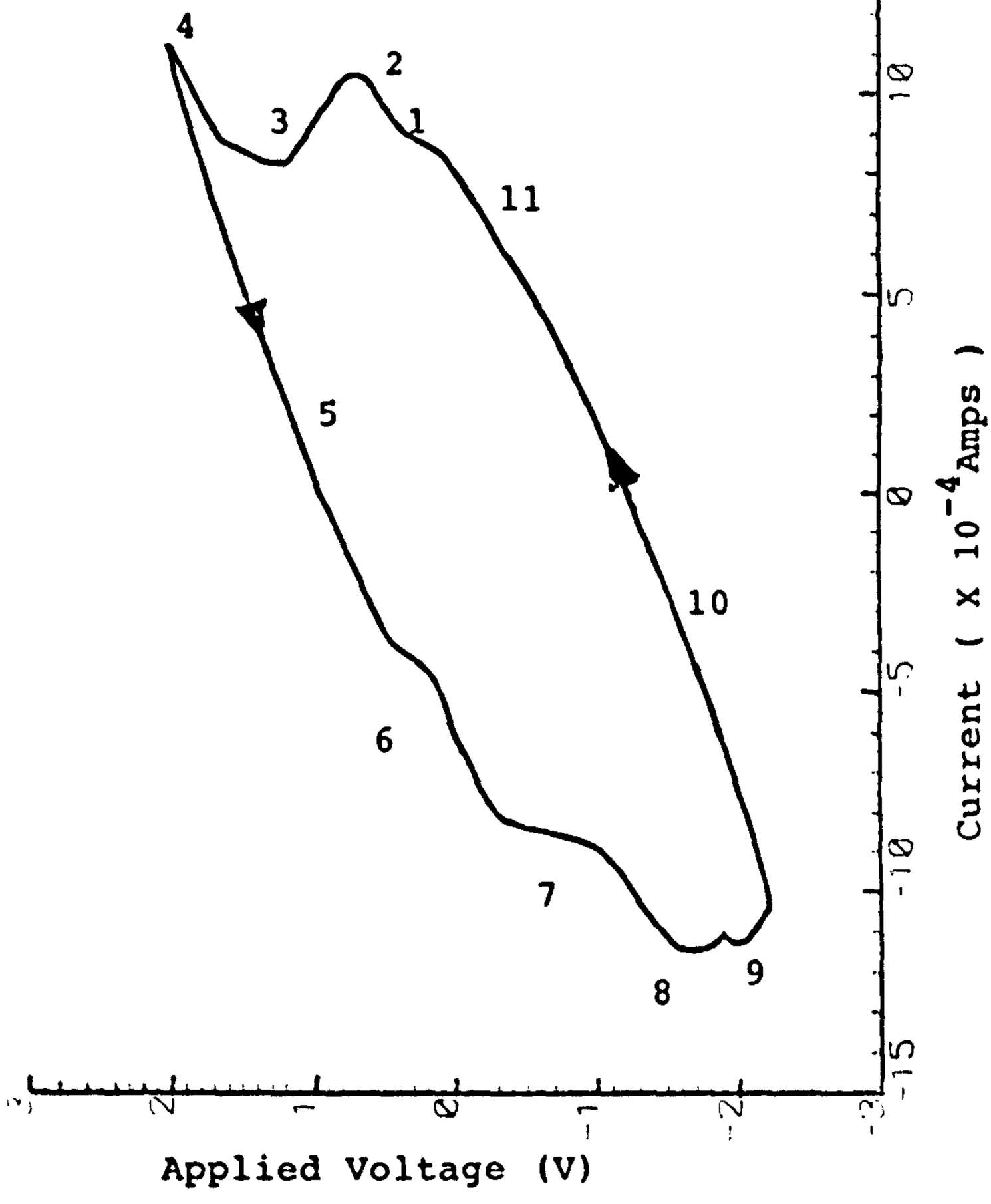

LISSAJOUS FIGURE

Figure 4.38

little current flows as the charge transfer resistance is very large. Over this potential range Cl^- ions adsorb onto the platinum surface. Cl^- has a maximal coverage of 0.45 (De Rosa and Beard, 1977) and these occupied sites are not available for adsorption of oxygen. The double layer region of the anodic sweep broadens with increasing halide ion concentration as the formation of the oxygen layer must start at more anodic potentials (Breiter, 1963).

Region 2: In this region the current rises with applied voltage, forming presumably the first Tafel region. In electrolytes which do not contain halide ions, the current is attributed to the adsorption of an oxygen layer (Breiter, 1963; Hoare, 1967). In the presence of chloride ions the problem is less simple, the system's response being governed by the adsorption of Cl^- and/or OH^- ions and there may be an overlap of several possible reactions.

Zeuthen (1978a) suggested that Cl_2 was released over this voltage range. This would agree with Littauer and Shreir's (1966) conclusion that, for low anodal voltages, the current is due to the evolution of chlorine on a clean platinum surface.

Region 3: In this region the current limits, in fact decreases, over a range of voltages. This of course could simply be due to the first reaction becoming exhausted and the current limiting due to a finite rate of mass transport to the electrode surface. On the other hand it could be due to the 'sudden' formation of an oxide layer on the electrode surface

Lissajous Figure of small area Platinum Electrode (4 Hz)

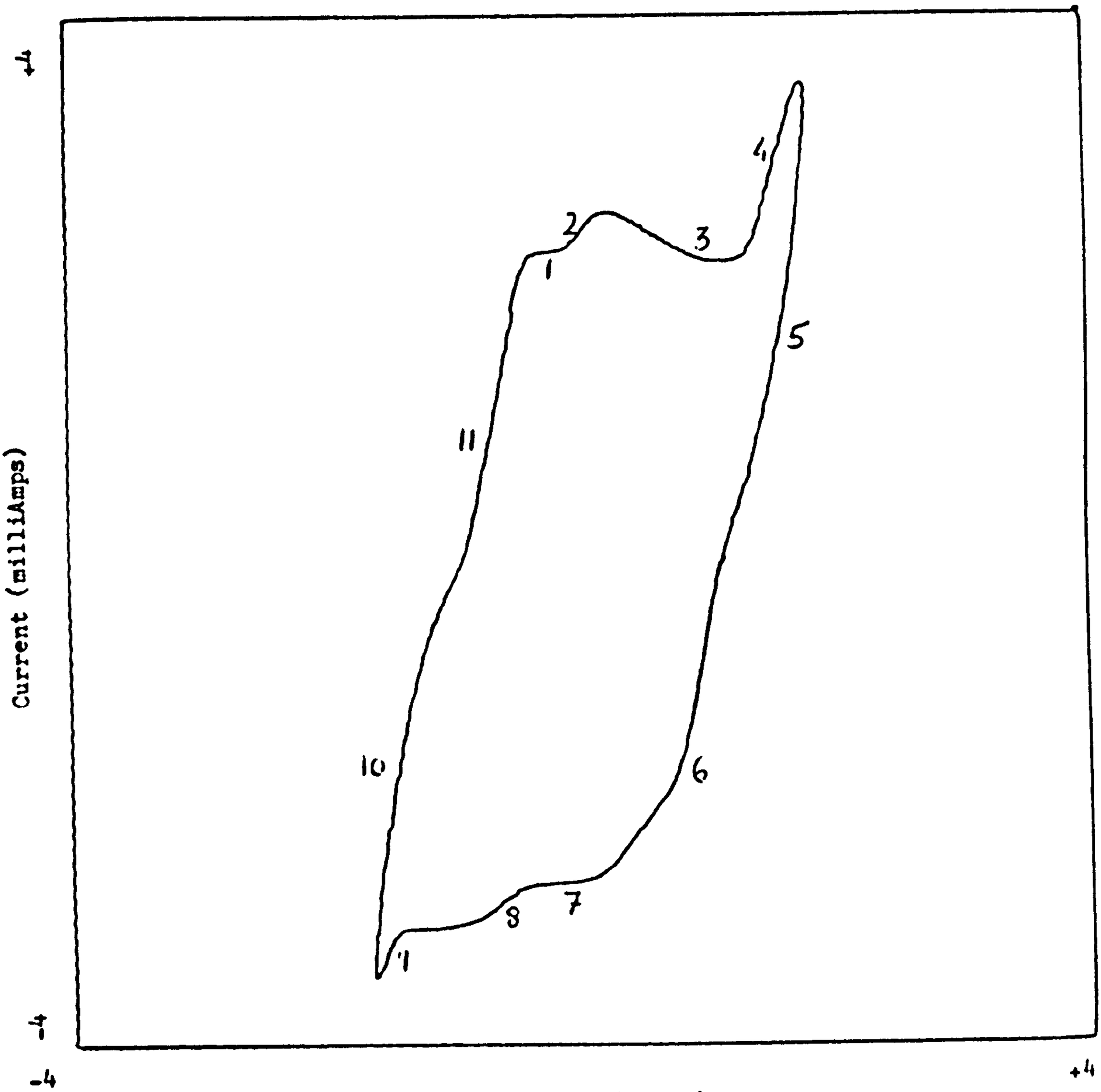

Figure 4.39

(Littauer and Schreir, 1966; Novak et al, 1982).

Region 4: In this higher voltage region the current increases once again. It is believed that Cl_2 evolution now proceeds on the oxidised surface of the anode metal surface (Littauer and Schreir, 1966). The current is observed to increase with the concentration of chloride (Breiter, 1963; Novak et al 1982).

It is very probable that O_2 is also evolved in this region (Breiter, 1963; Zeuthen, 1978a).

It is in this region that toxic effects have been observed and hence this region should be avoided in invivo situations.

Region 5: Upon decreasing the current density considerable hysteresis is observed. It has been suggested that the anode becomes effectively covered with a stable oxide layer after passing through region 3. This layer is not completely reversible with respect to reduction (Conway and Gottesfeld, 1972). Hence the high potential oxidation of chloride on the oxide covered surface tends to be also irreversible (Littauer and Schreir, 1966).

Region 6: This 'bump' is very probably due to the reduction of the oxygen layer. In Cyclic Voltammograms this peak is reduced in size as the concentration of chloride ions is increased (Breiter, 1963; Novak et al, 1982). This would indicate that this region is due to an oxygen reduction current which decreases if there has been previous anodic blocking of the initial stages of platinum surface oxidation by the chloride ions present.

As the potential is made increasingly more cathodic, reduction of Cl_2 occurs on a now oxide-free surface.

Region 7: In this voltage range the current limits and it is identified with the double layer region (see region 1).

Region 8: After the double layer region there is a rise in the current due to hydrogen adsorption.

Region 9: At more cathodic voltages the current limits and then increases as hydrogen is evolved.

According to Brummer and Turner (1977) and Bergveld (1976) the generation of hydrogen is potentially toxic due to tissue pH shifts (alkaline) and the disruptive effects of gross gas bubbles. Spadaro and Becker (1979) carried out a survey of reported undesirable effects at cathodes and concluded that they all occured when the electrode was operated in the hydrogen evolution region. This region should therefore be avoided in invivo work.

Regions 10 and 11: Upon decreasing the voltage, the current also decreases and two regions are faintly observed due to the oxidation of hydrogen. These regions are more discernable on figure 4.39 for the small area platinum electrode subjected to the large amplitude 4Hz signal.

- Porous S80 Electrode (Pt - Ir)

The Lissajous figure of the Porous S80 electrode is shown on figure 4.40. A sinusoidal voltage of approximately 4 volts peak to peak at a frequency of

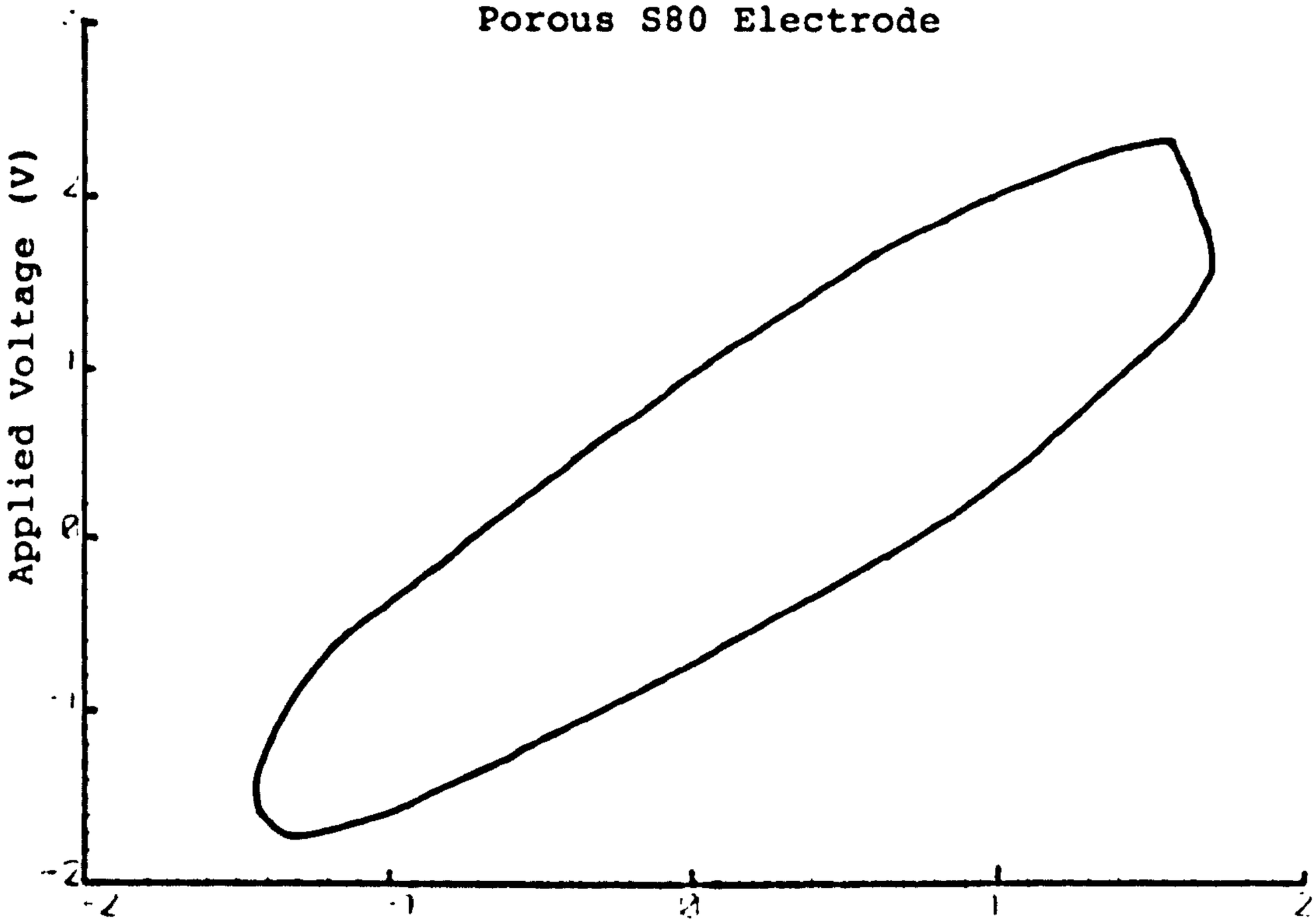

Figure 4.40

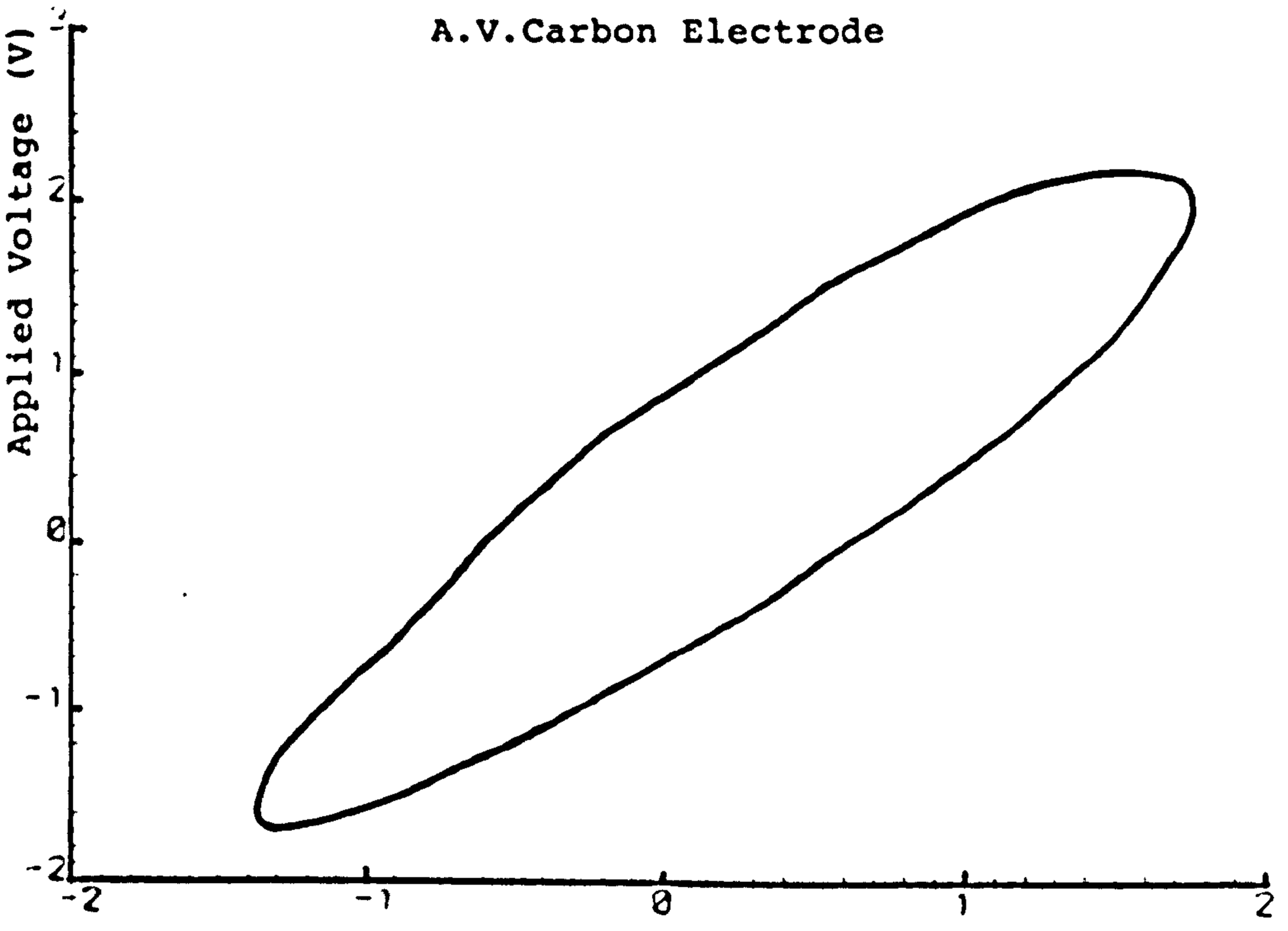

Figure 4.41

1Hz was applied across the electrode system.

In contrast to the 'smooth' Pt-Ir electrode, there is a marked absence of any great distortion under the above conditions for the porous Pt-Ir electrode. There is however a pseudo "current limiting" region for high anodic voltages (above 1.4 volts on the figure), with the suggestion of the double layer and first Tafel regions (regions 1 and 2) at lower anodic voltages.

- Activated vitreous carbon electrode

The Lissajous figure for the very rough surfaced A.V.C. electrode is shown on figure 4.41 and was obtained using a 4 volt peak to peak 1Hz signal.

Again, in contrast to the 'smooth' Telectronic electrode, there is an absence of any great distortion - more so even than with the porous S80 electrode. Although not a perfect ellipse, the Lissajous figure is free of any prominant 'bumps'. The narrowness of the ellipse for cathodic potentials would indicate that the impedance is less reactive in this region.

- Conclusions

Rough surfaced electrodes have a lower interfacial impedance than similar 'smooth' surfaced ones as the electrodes effective area is considerably larger. This increase in area decreases the current density and the impedance. The impedances of electrodes with rough surfaces are more linear as the second Tafel region is less readily attained.

The magnitude and phase angle of the impedances of

the electrodes were calculated including the series 900Ω resistor and their values are listed on table 4.6

TABLE 4.6

Electrode	/Z/ (Ω)	ϕ(degrees)
Tel. 224	9,300	35
S80	1,300	28
AVC	1,300	24

For a large amplitude ac signal of 4 volts peak to peak the interfacial impedances have decreased considerably from their small signal values (section 1.2.3.2).

Electrodes which have relatively low, small signal impedances are not necessarily as "good", comparitively speaking, under large signal conditions.

Although the Telectronic 224 electrode still has a relatively large impedance, that of the Porous S80 is now comparable with that of the activated vitreous carbon electrode. This would indicate that firm conclusions cannot be drawn on the relative performance of pacing electrodes based on the comparison of their small signal impedances.

It was noticed in section 4.2.3 that electrodes with the lowest small signal impedances are also the most linear, ie their impedances do not decrease greatly with applied signal amplitude. Electrodes with large impedances in the small signal region on the other hand, are the most nonlinear and their impedances decrease rapidly with applied signal amplitude. It is therefore to be expected that at high enough signal amplitudes, what appeared to be "poor" electrodes in

the linear region will have characteristics which match those of "good" electrodes, as observed above.

4.2.5 Discussion and Conclusions on ac nonlinearity

Both elements of the equivalent circuit model, Z_{CPA} and R_{CT}, are found to be nonlinear with applied signal amplitude. This is especially true for R_{CT}.

R_{CT} is derived from the i - η curve. As such curves contain two Tafel regions separated by a current limiting region, R_{CT} is a rather complex function of current or voltage. For relatively small signal amplitudes, R_{CT} decreases with signal amplitude according to equations 4.62, 4.63, 4.64 and 4.65. At large signals an oxide layer is formed on the electrode surface thus changing its electrical proporties - including the value of R_{CT}.

Z_{CPA} is due to adsorption effects on the electrode surface (neglecting surface effects). In the double layer region little adsorption occurs and K and β are relatively large and constant. It would appear that in the absence of an applied dc bias the electrode system operates within the double layer region, close to the potential of zero charge, P.Z.C. At the onset of gross adsorption effects the magnitudes of K and β rapidly decrease indicating a sharp increase in the adsorption pseudo capacitance and in frequency dispersion.

The overall impedance locus is an arc whose diameter decreases with applied signal amplitude. As

the arc diameter decreases, progressively higher frequency points are observed to "become nonlinear". The relationship between the applied current amplitude and the frequency at which nonlinearity occurs is given by equations 4.79, 4.81, 4.83, 4.86 and 4.87, which are very similar in form to the empirical expression derived by Schwan (1968). This is the first time such a relationship has been explained physically.

Contrary to Schwan's statements, though agreeing with his results (Onaral and Schwan, 1982), higher frequency points have been shown to become nonlinear at progressively larger voltage amplitudes (equations 4.84 and 4.88) over a wide range of frequencies. It has also been shown that there are two limiting values of $V_{ac.L}$ at very high and low frequencies due to the nonlinearities of Z_{CPA} and R_{CT} respectively. For the first time apparent contradictions between various publications have been explained and 'harmonised'.

Of the electrodes compared in this chapter, the very rough surfaced, activated vitreous carbon electrode appears to be the 'best' with the smallest and most linear interfacial impedance which shows a lack of "second Tafel" behaviour over the applied voltage range.

The point was made, however, that electrodes with the smallest interfacial impedances under small signal conditions may not perform relatively as well under large signal conditions. This is an important point when comparing pacing electrodes using the linear ac impedance technique and does not appear to be widely

appreciated.

In the next chapter the nonlinearity of the interfacial impedance under transient conditions will be discussed.

CHAPTER 5

The nonlinearity of the electrode-electrolyte Interface impedance under transient conditions

5.1 THEORETICAL SECTION

This chapter is concerned with the response of the electrode system to a voltage or current step or pulse of large amplitude.

5.1.1 Nonlinearity of the "3-component" model

Although it has been shown that the electrode-saline (or tissue) interface is better modelled by the parallel combination of a constant phase angle impedance, Z_{CPA}, and a non-linear charge transfer resistance, R_{CT}, many researchers have opted for a simple capacitor instead of "Z_{CPA}". Although this model is an oversimplification, it is qualitively useful in giving an understanding of the response of the system to a pulse or step.

- Inaccuracies involved using the "3-component" model

The series resistance, R_{TOT}, due to the sum of the lead and tissue (or saline) resistances, may be estimated by dividing the height of the applied voltage pulse by the initial or peak current response. If, for a certain pulse duration and voltage amplitude, the current decays to a steady value before the end of the pulse, the sum of R_{CT} and R_{TOT} can be calculated by dividing the applied voltage amplitude by the limiting value of the current. The value of C_{dl} is calculated from the time constant which is considered to best fit the current decay. When the parallel combination of

C_{dl} and R_{CT} is fitted to the observed current response, discrepancies will be involved due to approximating Z_{CPA} by C_{dl}. The problem can best be demonstrated if one considers for a moment the ac impedance locus of the actual impedance and compares it with that of the three component model (figure 5.1)

If one endeavours to fit the system's impedance to that of a 3 component model over the entire frequency range, $\omega = 0$ to $\omega = \infty$ (or in the time domain, $t = \infty$ to $t = 0$) the calculated value of R_{TOT} will be too large, that of R_{CT} too small and that of τ ($= 1/\omega_o$) will also be too small (Chabli et al, 1982). These errors are all due to setting $\beta = 1$ (for a capacitor) whereas generally $0.5 < \beta < 1$.

The problem is further complicated if one endeavours to fit the model over a limited frequency range (ie over a short period of time, hence not allowing the decaying current to reach equilibrium). This is important as the pulse widths used in pacing are in general a lot shorter than the time needed for the voltage or current responses to reach their constant limiting values. This is underlined in the work of Weinman et al (1964) where C_{dl} and R_{CT} were found to depend on pulse duration. If, for example, R_{CT} is calculated from the height of the current response at the end of a pulse of width, t_p, (see figure 5.2) its calculated value will be smaller than its true value. De Boer et al (1978) showed that the calculated value of R_{CT} greatly increased as the pulse width increased. ω_o decreased as did Cdl. Hence calculating

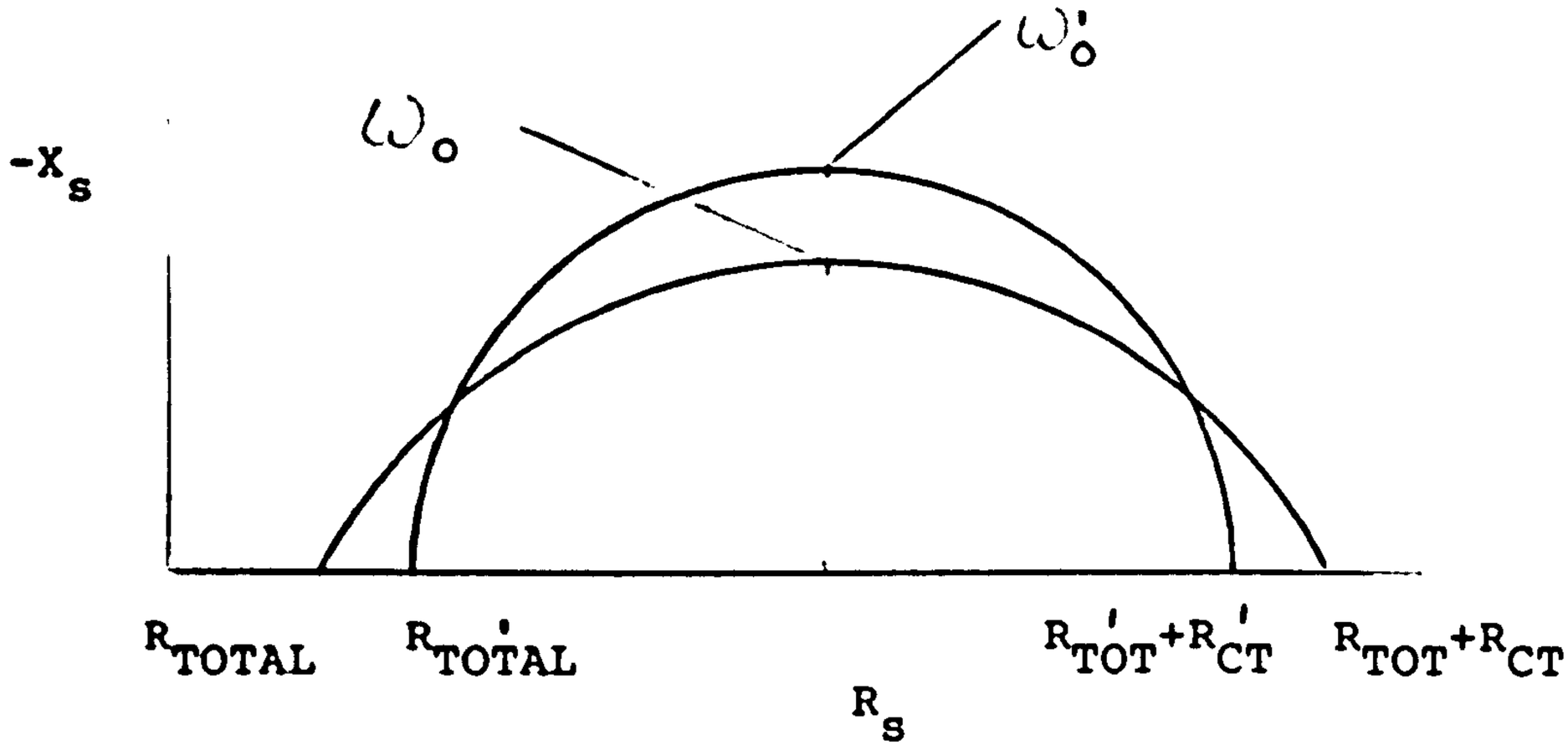

ERRORS INCURRED WITH THE USE OF THE
'THREE COMPONENT'MODEL

Figure 5.1

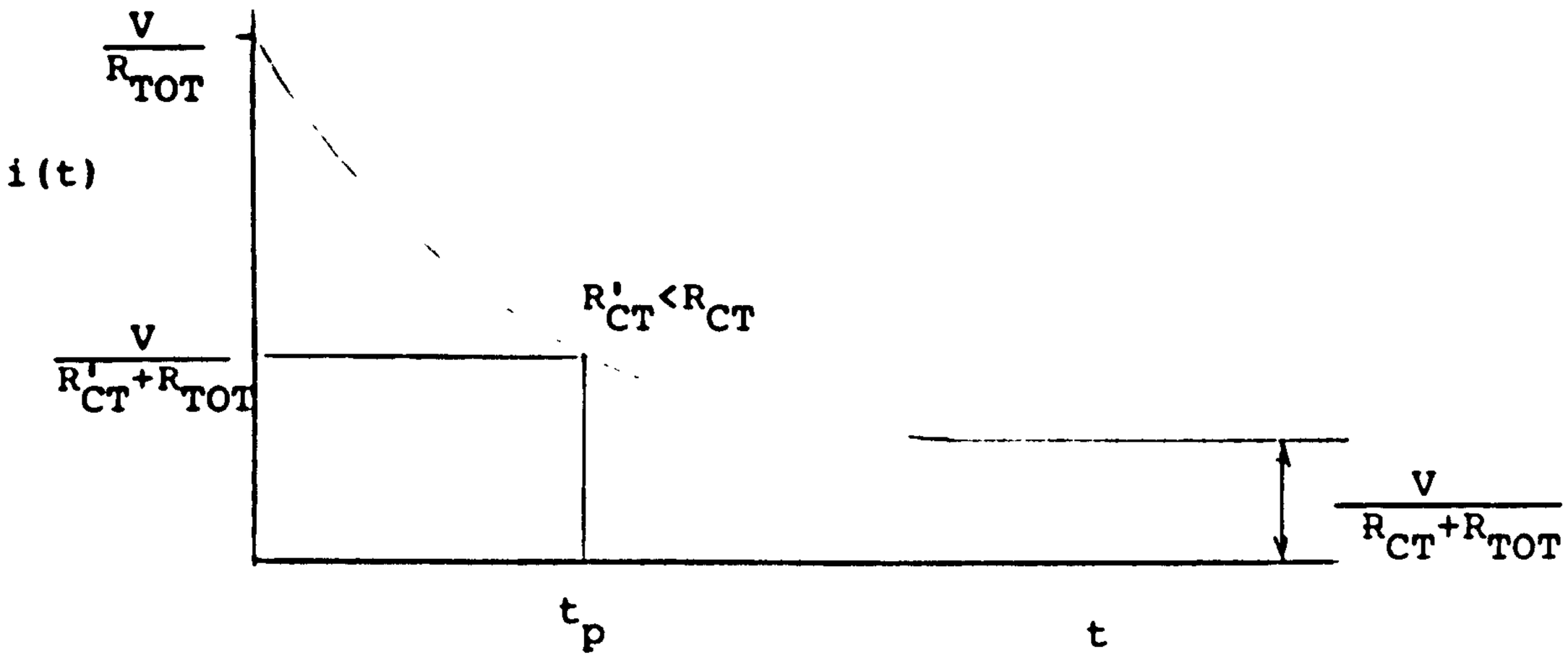

POSSIBLE ERRORS IN THE CALCULATION OF R_{CT}.

Figure 5.2

C_{dl} and R_{CT} using a 1 or 2 millisecond pulse results in an underestimation of R_{CT} and an overestimation of C_{dl}. The observed dependence of the elements of the "three component" circuit on the pulse width is simply due to the wrong choice of equivalent circuit model.

Having shown that this method of analysis will render inaccurate values of C_{dl} and R_{CT}, the observed qualitative effects of nonlinearity on these elements will however be reviewed as they will give some insight into the phenomena. It is expected that 'C_{dl}', which is inversely proportional to Z_{CPA}, will increase and that 'R_{CT}' will decrease with pulse height.

- Effect of current pulse amplitude

Weinman et al (1964) considered the nonlinearity of the "3 component" model and found that as the current density increased, R_{CT} decreased markedly, C_{dl} increased less dramatically and that τ, where $\tau = R_{CT} C_{dl}$, decreased.

The decrease in R_{CT} with current pulse height, I_{dc}, was expected from equation 4.62, ie (rewriting in terms of I_{dc})

$$R_{CT(dc)} = \frac{1}{(1-\alpha)nfI_{dc}} \ln\left[\frac{I_{dc}}{i_o}\right] \qquad 5.1$$

Similar changes in circuit parameters were observed by Meldrum (in a private communication) under in-vivo conditions.

- Effect of voltage pulse amplitude

Fischler (1979, 1981) and Morkrid et al (1980) studied the nonlinearity of the electrode system using

very large voltage amplitudes. They also found that C_{dl} increased, though not dramatically, whereas the decrease in R_{CT} was very marked. R_{CT} appeared to decrease in an exponential manner as predicted by Pollak (1974) and expected from equation 4.63. ie, (rewriting equation 4.63 in terms of η_{dc})

$$R_{CT(dc)} = (\eta dc/i_o) \exp [-(1-\alpha)nf\eta_{dc}] \qquad 5.2$$

For large values of η_{dc} (ie when $\alpha nf\eta_{dc} > 1$) the exponential term dominates the response of $R_{CT(dc)}$ to an increasing voltage. Hence when $\eta_{dc} > 1/\alpha nf = 50mV$ (if $\alpha = 0.5$ and $n = 2$), $R_{CT(dc)}$ is proportional to $\exp [-\eta_{dc}]$ as observed experimentally by the above researchers.

- Summary

The results found using a model comprising frequency independent components, although less accurate, compare well with the predictions made based on our theoretical model.

"C_{dl}", which is inversely proportional to Z_{CPA}, was found to be relatively linear though it does increase with current or voltage amplitude. R_{CT} was found to be very non-linear and decreases in a pseudo exponential manner with the applied voltage. The relationship between R_{CT} and current density however does not appear to have been investigated by the above researchers, but R_{CT} is expected to decrease linearly with the applied current amplitude. R_{TOT}, as expected, was found to be independent of the height of the applied current or voltage pulses.

5.1.2 Nonlinearity of the Z_{CPA} - R_{CT} model

Onaral and Schwan (1983) investigated the transient nonlinearity of electrode-electrolyte interfaces and obtained some empirical expressions describing the relationships between V(t), I_{dc} and time, t.

Using the proposed, parallel Z_{CPA} - R_{CT} model of the interface impedance, similar theoretical relationships will be derived and compared with those empirically derived.

In the linear region, when $R_{CT(dc)}$ is very large, the voltage response to a current step, I_{dc}, is given by equation 3.22 for a large range of t, ie

$$V(t) = \frac{I_{dc}\ K\ t^{\beta}}{\Gamma(1+\beta)}$$

the response being governed by the Z_{CPA} impedance.

A log V(t) - log t plot will be a straight line of gradient β (see figure 5.3).

As the pulse height increases, $R_{CT(dc)}$ decreases and the transient response deviates from simple Z_{CPA} behaviour at progressively shorter times.

The transient response is now given by equation 3.33, ie

$$V(t) = I_{dc}\ R_{CT}\ \{1-f(\bar{t})\}$$

A log V(t) - log (t) plot of this expression is as shown schematically on figure 5.3. At short times equation 3.33 approximates to equation 3.22, ie Z_{CPA} dominates the response. However at longer times $R_{CT(dc)}$ begins to dominate and the plot levels off,

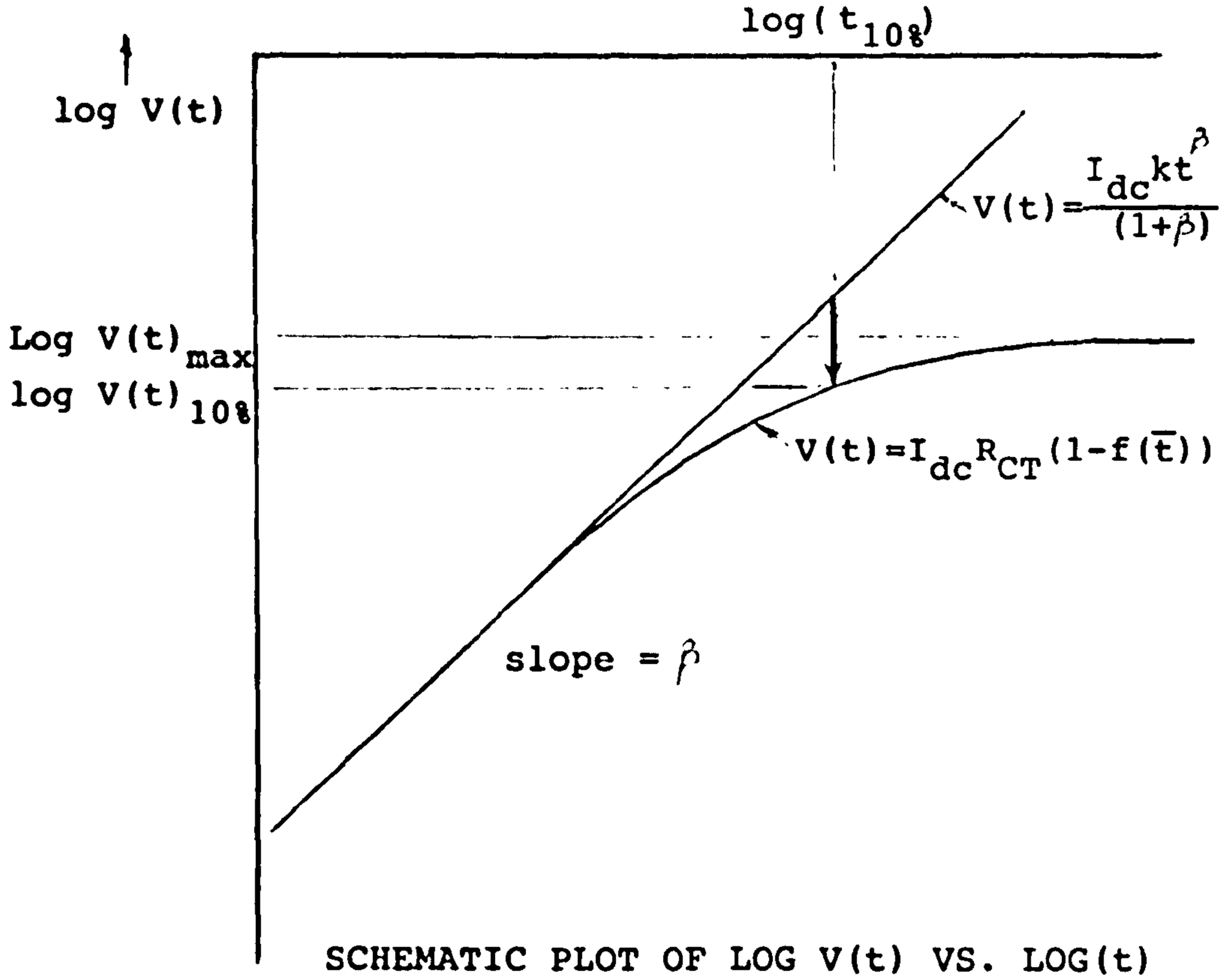

SCHEMATIC PLOT OF LOG V(t) VS. LOG(t) SHOWING THE EFFECTS OF DECREASING R_{CT}.

Figure 5.3

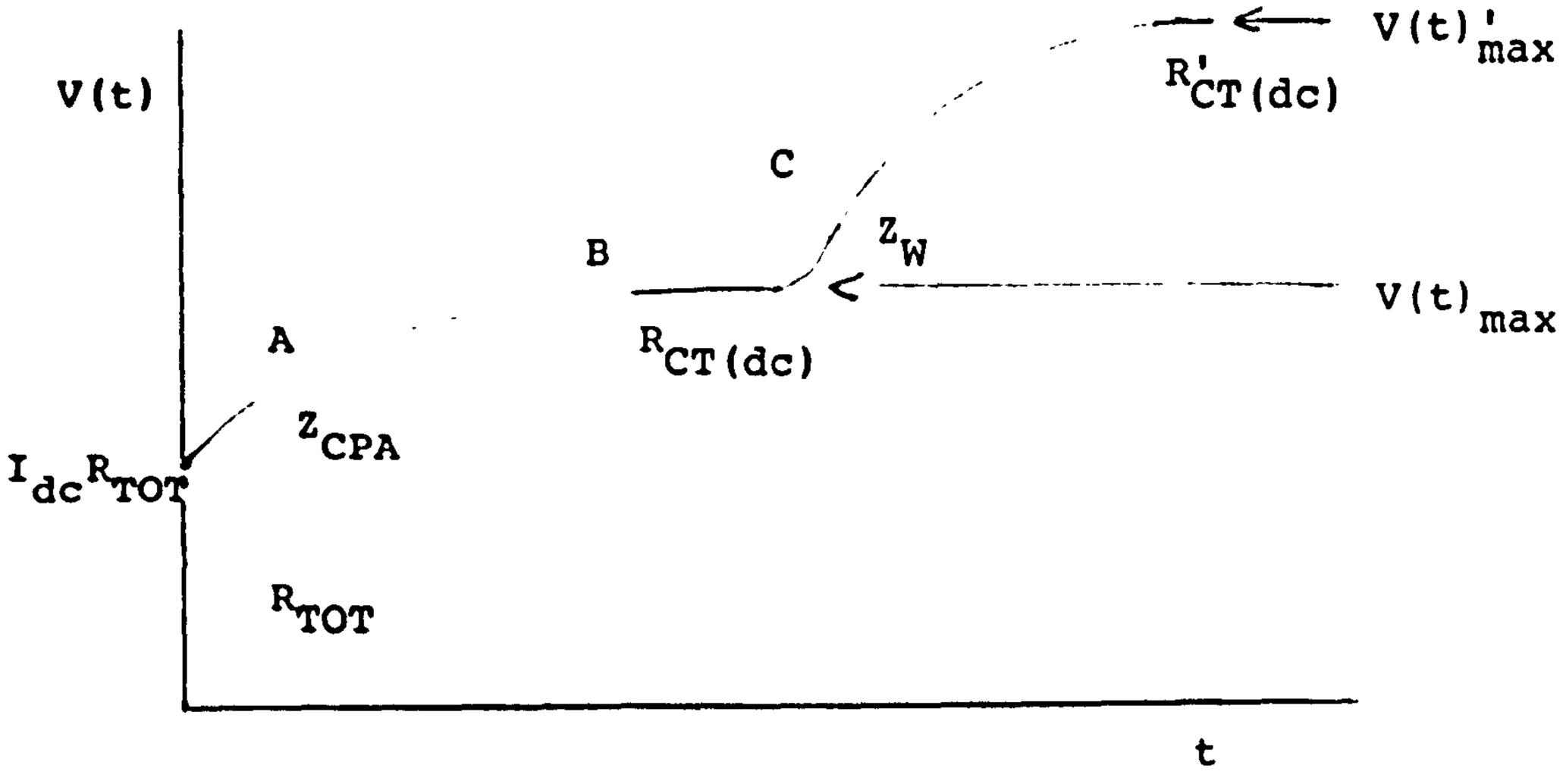

VOLTAGE RESPONSE WITH "SECOND EXPONENTIAL"

Figure 5.4

approaching the limit, V(t) max = $I_{dc}\ R_{CT(dc)}$.

Although Onaral and Schwan (1983, figure 3) and Schwan and Onaral (1985, figure 2) obtained similar plots to that shown on figure 5.3 they apparently did not consider the possibility that the limiting of the voltage response, and hence the nonlinearity, was due to the presence of the parallel resistance, $R_{CT(dc)}$, whose value decreases with the applied current pulse amplitude.

They observed that the limiting value, V(t)max, remained approximately constant as the current pulse amplitude, I_{dc}, was varied (Onaral and Schwan 1983, figure 5). This is to be expected as

$$V(t)max = I_{dc}R_{CT(dc)}$$

and hence (using equation 5.1)

$$V(t)max = \frac{1}{(1-\alpha)nf}\ In\left[\frac{I_{dc}}{i_o}\right] \qquad 5.3$$

which is practically constant (V(t)max will however increase slightly with I_{dc} as is evidenced in figure 5, 1983).

They also plotted log $[V(t)/I_{dc}]$ against log (t) for increasing values of I_{dc}. The limiting value, $V(t)max/I_{dc}$, was found to decrease as I_{dc} was increased. This also is as expected from the proposed model as

$$V(t)\ max/I_{dc} = R_{CT(dc)}$$

and $R_{CT(dc)}$ decreases as I_{dc} is increased (see equation 5.1).

Their plots and observations are therefore compatible with the proposed model which includes a

non-linear, parallel, charge transfer resistance.

One of the most important observations made by Onaral and Schwan (1983) was that the dc current limit of linearity, $I_{dc}(10\%)$, is proportional to $t^{-\beta}$.

They demonstrated this by plotting (1983, figure 8) log $[I_{dc}(10\%)]$ against log t and obtained a straight line of slope $-\beta$.

A relationship will now be derived based on the proposed theoretical and equivalent circuit model and compared with the above.

Considering figure 5.3, it becomes apparent that at a certain time, $t_{10\%}$, the magnitude of the voltage response, will have decreased by 10% from its linear, Z_{CPA} dominated value due to the decrease in the value of the parallel charge transfer resistance, $R_{CT(dc)}$. This will occur when (using equations 3.22 and 3.33)

$$0.9 \frac{Kt_{10\%}}{\Gamma(1+\beta)} = R_{CT}\{1- f(\bar{t})_{10\%}\} \qquad 5.4$$

In order to proceed with the derivation of the relationship between $t_{10\%}$ and $R_{CT(dc)}$, and eventually that between $t_{10\%}$ and I_{dc}, one must first take a closer look at the function $f(\bar{t}_{10\%})$. For short times $f(\bar{t})$ can be written, (equation 3.14)

$$f(\bar{t}) = \sum_{n=0}^{\infty} \frac{(-1)^n}{\Gamma(1+n\beta)} \bar{t}^{\beta n}$$

Considering only the first 3 terms one has,

$$f(\bar{t}) = 1 - \frac{\bar{t}^{\beta}}{\Gamma(1+\beta)} + \frac{\bar{t}^{2\beta}}{\Gamma(1+2\beta)} \qquad 5.5$$

In terms of un-normalised time, t

$$f(t) = 1 - \frac{t^{\beta}(K/R_{CT})}{\Gamma(1+\beta)} + \frac{t^{2\beta}(K/R_{CT})^2}{\Gamma(1+2\beta)} \qquad 5.6$$

and hence equation 5.4 can be written as

$$0.9\ \frac{t^{\beta}_{10\%}}{\Gamma(1+\beta)} = \frac{t^{\beta}_{10\%}}{\Gamma(1+\beta)} - \frac{t^{2\beta}_{10\%}\ (K/R_{CT})}{\Gamma(1+2\beta)} \qquad 5.7$$

It therefore follows that

$$t^{\beta}_{10\%} = 0.1\ \frac{R_{CT}}{K}\ \frac{\Gamma(1+2\beta)}{\Gamma(1+\beta)} \qquad 5.8$$

i.e. $t^{\beta}_{10\%}$ is proportional to R_{CT}.

The time at which the voltage response deviates from the linear, Z_{CPA} value, $t_{10\%}$, is proportional to $R_{CT(dc)}^{1/\beta}$. The smaller the value of $R_{CT(dc)}$, the shorter the length of time Z_{CPA} dominates the response.

As $t_{10\%} = \bar{t}_{10\%}\ (R_{CT/K})^{1/\beta}$, then from equation 5.8 it follows that

$$\bar{t}_{10\%} = 0.1\ \frac{\Gamma(1+2\beta)}{\Gamma(1+\beta)} \qquad 5.9$$

The ratio of Gamma functions is approximately 2, depending on the value of β, and hence $\bar{t}_{10\%}$ is a constant with a value between approximately 0.1 and 0.3. For a given value of β, an electrode system will become nonlinear at the same value of normalised time, $\bar{t}$.

Equation 5.8 therefore approximates to

$$t^{\beta}_{10\%} \cong 0.2\ (R_{CT/K}) \qquad 5.10$$

Transforming equation 5.10 into the frequency domain one obtains

$$\omega^{\beta}_{10\%} = x\ K/R_{CT} \qquad 5.11$$

Where x lies between approximately 3 and 10. Comparing equation 5.11 with that derived in Chapter 4

under ac conditions (equations 4.73 and 4.76)

$$\omega^{\beta}_{10\%} = y\ (K/R_{CT}) \qquad 5.12$$

Where y lies between 8.53cosØ and 20cosØ.

As Ø is generally around 70°, y lies approximately between 3 and 7. On comparison the two expressions (equations 5.11 and 5.12) for $\omega^{\beta}_{10\%}$ are very similar - as would be expected.

So far a relationship between $t_{10\%}$ and $R_{CT(dc)}$ has been derived. In order to obtain an expression relating $t_{10\%}$ and the applied current amplitude, I_{dc}, one needs to know the relationship between $R_{CT(dc)}$ and I_{dc}.

Equation 5.1 relates $R_{CT(dc)}$ to the faradaic current flowing through $R_{CT(dc)}$, $I_{f.dc}$,

$$\text{i.e.}\quad R_{CT(dc)} = \frac{1}{(1-\alpha)nfI_{f.dc}}\ \text{In}\left[\frac{I_{f.dc}}{i_o}\right]$$

Hence in terms of $I_{f.dc}$

$$t_{10\%} = 0.1\ \frac{\Gamma(1+2\beta)}{\Gamma(1+\beta)}\ \frac{1}{K}\ \frac{1}{(1-\alpha)nfI_{f.dc}}\ \text{In}\left[\frac{I_{f.dc}}{i_o}\right] \qquad 5.13$$

At the onset of nonlinearity, $t = t_{10\%}$, which is expressed by equation 5.8. At this time the voltage across Z_{CPA} is, (using equation 3.22)

$$V(t) = 0.1\ I_{nf.dc}\left(\frac{\Gamma(1+2\beta)}{(\Gamma(1+\beta))^2}\right)\ R_{CT(dc)} \qquad 5.14$$

Where $I_{nf.dc}$ is the transient nonfaradaic current flowing through Z_{CPA} - obviously true 'dc' current cannot flow through the nonfaradaic branch.

As the voltage across $R_{CT(dc)}$ (= $I_{f.dc}\ R_{CT(dc)}$) is the same as that across Z_{CPA}, it follows that at $t_{10\%}$

$$I_{f.dc} = 0.1 \; I_{nf.dc} \left(\frac{\Gamma(1+2\beta)}{(\Gamma(1+\beta))^2} \right) \qquad 5.15$$

The applied dc current, I_{dc}, is the sum at any time of $I_{f.dc} + I_{nf.dc}$. therefore

$$I_{dc} = I_{f.dc} \left[1 + \left(\frac{10[\Gamma(1+\beta)]^2}{\Gamma(1+2\beta)} \right) \right] \qquad 5.16$$

letting $\Gamma(1+\beta) = A$; $\Gamma(1+2\beta) = B$

$$t_{10\%}^{\beta} = 0.1 \left(\frac{B}{A} \; \frac{1}{K} \; \frac{(1+(10A^2/B))}{(1-\alpha)nfI_{dc}} \; In \left[\frac{I_{dc}}{i_o(1+(10A^2/B))} \right] \right) \qquad 5.17$$

As the 'In' term is relatively constant, $t_{10\%}^{\beta}$ is proportional to I_{dc}^{-1}.

Or, the limit current of linearity, $I_{dc}(10\%)$, is proportional to $t^{-\beta}$.

This relationship, derived from the proposed equivalent circuit model, has the same form as that empirically derived by Onaral and Schwan (1983) and Schwan and Onaral (1985). This is the first time the empirical relationship has been physically explained.

Now to derive an expression for the limit voltage of linearity.

The potential at which the electrode system becomes nonlinear for a given current pulse amplitude, $V(t)_{10\%}$, is given by the product of $I_{f.dc}$ and $R_{CT(dc)}$. Using equations 5.1 and 5.16 , it follows that

$$V(t)_{10\%} = \frac{1}{(1-\alpha)nf} \; In \left[\frac{I_{dc}}{i_o(1+(10A^2/B))} \right] \qquad 5.18$$

Where A and B are as defined for equation 5.17.

It will be noted that equation 5.18 for $V(t)_{10\%}$ is very similar to that for $V(t)_{max}$ (equation 5.3). The

value of $V(t)_{10\%}$ is obviously smaller than that of $V(t)_{max}$ and their ratio is given by

$$\frac{V(t)_{10\%}}{V(t)_{max}} = 1 - \frac{\text{In } [1+(10A^2/B)]}{\text{In } [I_{dc}/i_o]} \qquad 5.19$$

which has a value approximately between 0.5 and 0.8 depending on the values of I_{dc}, i_o and β (the latter affecting the values of A and B). The larger the applied current pulse amplitude, the closer $V(t)_{10\%}$ is to $V(t)_{max}$.

From equation 5.18 it can be seen that $V(t)_{10\%}$ should be almost constant, increasing slightly with the applied current amplitude - as was the case with $V(t)_{max}$ (equation 5.3).

Onaral and Schwan (1983) and Onaral et al (1984) have stated that $V(t)_{10\%}$ is a constant and independent of time or applied current amplitude and has a value of approximately 120 mv for a range of current density amplitudes between 0.14mA/cm^2 to 40 mA/cm^2. They did however concede that there were some deviations to this rule.

Close examination of their log $[V(t)/I_{dc}]$ - log $[I_{dc}]$ plot (Onaral and Schwan, 1983 figure 6) indicates that $V(t)_{10\%}$ appears to increase with $t_{10\%}$ - or decrease with I_{dc}.

These deviations are in the opposite direction to that expected from equation 5.18. This is most surprising as $V(t)_{max}$, which is proportional to $V(t)_{10\%}$, was observed to increase with I_{dc} and similar behaviour would be expected for $V(t)_{10\%}$.

This deviation at large current amplitudes and

short pulse lengths is probably due to the nonlinearity of Z_{CPA} whose impedance dominates in these regions. The decrease in 'K' which occurs when Z_{CPA} becomes nonlinear would result in a decrease in $V(t)_{10\%}$ as observed.

- Summary

It would appear that the proposed model agrees with the available reported data on the transient nonlinearity of biomedical electrode-electrolyte systems.

5.1.3 Gross nonlinearity and Waveform distortion

The voltage response of an electrode system to a current step can be divided into several regions under different control ie Z_{CPA}, R_{CT} and pseudo Warburg control (see figure 5.4).

a) for small current amplitudes and over short periods of time the voltage response of the electrode system rises with time according to t^{β} (Weinman and Mahler 1959 and de Boer et al , 1978), ie there is Z_{CPA} control.

Greatbatch et al (1969) noticed that the anodal and cathodal voltage responses to short, low amplitude current pulses, were very similar in both magnitude and shape for platinum electrodes, thus suggesting that the coupling mechanism was purely capacitive and involving no irreversible faradaic reactions. This led Greatbatch et al (1969) to propose that with platinum

electrodes in this region the adsorption pseudo capacitance dominated the electrode impedance. They believed that monatomic oxygen was absorbed and desorbed from the surface in a very reversible manner. With platinum electrodes, therefore, according to Greatbatch et al, "electricity couples into the body by a modulation of the level of catalytically absorbed oxygen on the surface of each electrode".

b) At longer times, R_{CT} dominates the impedance and the voltage response levels off. One cannot expect faradaic anodal behaviour to mimic cathodal behaviour in this region as each may involve a different chemical reaction (Clynes and Milsum, 1970). Asymmetry of the voltage waveforms in the two directions for platinum electrodes has been noted by Greatbatch et al (1969) amongst others. The difference between the two polarities grows as the current amplitude is increased (Weinman and Mahler, 1964).

For small pulse amplitudes the faradaic processes involved give rise to, what Brummer and Robblee (1983) term, "reversible" charge injection. They define a "reversible" charge injection process as one that introduces no new species into solution. This of course is possible by a capacitive process such as double-layer charging, but also by "surface faradaic" reactions involving species that remain bound to the electrode surface. Charge injected by other faradaic reactions, eg the electrolysis of water to H_2 or O_2, will at least be partially "irreversible" as some of the products will escape from the surface and possibly

give rise to toxic effects. Examples of "reversible" faradaic reactions are, according to Brummer and Robblee (1983), surface oxidation and "H-atom plating" which occur at low potentials.

It would appear that the faradaic reactions which occur at small signal amplitudes are "reversible" and can be defined as 'safe'with little or no toxic effects.

c) Weinman and Mahler (1964) noted that stainless steel electrodes became "unstable" for long duration anodic current pulses. They found that other electrodes demonstrated a similar effect but under different quantitative conditions. They described the voltage response waveform as having a "wavy" appearance when the instability was present. There appeared to be an unexpected rise in the voltage response to a current step after a certain period of time. This would point to a sudden increase in the value of $R_{CT(dc)}$.

This "wavy" voltage response can be understood if one considers the i -η characteristics shown on figures 4.11, 13 and 15 for multiple step charge transfer reactions. If the impressed current step is too large for the first reaction mechanism, after a certain time (or charge) the voltage response will show diffusion limited behaviour, ie the voltage will be a function of $\sqrt{t}$. A large 'jump' in the voltage response will occur until a voltage is reached where a second reaction eg chlorine, oxygen or hydrogen evolution, is possible. Alternately the 'jump' could be due to the sudden formation of an oxide layer, as noted

previously. In either case the voltage response will have the form shown schematically on figure 5.4.

$V(t)_{max}$ is the maximum value of voltage the system would have achieved in absence of the 'jump', ie

$$V(t)_{max} = I_{dc} R_{CT(dc)}.$$

After a certain time the first reaction breaks down and eventually a second takes over. The charge transfer resistance, $R'_{CT(dc)}$, is now larger than before, as is $V(t)_{max}$, where

$$V(t)_{max} = I_{dc} R'_{CT(dc)}.$$

Weinman and Mahler (1959 and 1964) obtained a voltage response very similar to that schematically drawn on figure 5.4 for a stainless steel electrode when subjected to current pulses of either polarity.

Kingma (1977) observed the same phenomenon with vitreous carbon electrodes for current pulses of either polarity.

Bergveld (1976) noted the effect with platinum electrodes. He considered the 'jump' to be due to diffusion control, ie that V(t) in this region is proportional to $\sqrt{t}$, and that this was followed by gas evolution. Kingma made similar conclusions.

Fischler and Schwan (1981) obtained similar voltage-time curves for negative current pulses applied to platinum electrodes.

Unfortunately, even if the current amplitude is kept small, problems can arise. Dymond (1976) pointed out that practical stimulation requires pulse rates with interpulse intervals too short to allow the potential from the preceding pulse to completely decay.

This is especially true when R_{CT} is large. If the voltage does not have time to completely recover before the next pulse, the potential will be gradually driven from equilibrium. Thus even if the pulse amplitude and height are not such as to drive the system into distortion, ie gas evolution, a similar effect will arise if the pulse repetition is too fast (Bergveld, 1976). A gradual drift in the voltage will be noticed (Greatbatch et al, 1968, 1969; Bergveld, 1976; Fischler and Schwan, 1981) and if this is allowed to continue for some time the system will be pushed into its nonlinear region, irreversible changes will occur and there will be a residual 'rectification' voltage (Weinman and Mahler, 1959; Clynes and Milsam, 1970). Fischler and Schwan (1981) found that the response eventually stabilised after a minute or so. The sudden rise in the voltage response, or "second exponential", appeared earlier with each consecutive pulse supporting the observation that the response had insufficient time to recover in between pulses and was hence being pushed further into non-linearity with each pulse. This is further underlined by the observation that for short pulse widths or low pulse repetition rates the distortion or breakdown does not occur (Bergveld, 1976; Weinman and Mahler, 1964).

The distortion of the response waveform and the insueing rectification is generally larger for one polarity of current pulse. As already noted the value of $R_{CT(dc)}$ depends on the polarity of the current. The larger the value of $R_{CT(dc)}$ the longer the voltage

response will take to decay and hence will be more prone to the above 'rectification' effect. This observation is supported by the work of many researchers, eg Weinman and Mahler (1964) and Greatbatch et al (1969).

5.1.4 Tissue Damage

It has been observed that total control of the voltage response by the faradaic charge transfer resistance is accompanied by a levelling off of the voltage response ie it becomes independent of charge. Bergveld (1976) therefore suggested that the undesirable accumulation of reaction products occurs in this "ohmic" region and that the appearance of this region could be used as an invivo criterion of "irreversible" charge injection and hence should be avoided. However faradaic current flows through $R_{CT(dc)}$ before the response is dominated by $R_{CT(dc)}$, causing it to level off. Hence, the absence of an "ohmic" region in the potential transient is not sufficient to ensure 'reversible' charge injection. For example, oxygen evolution commences well before the anodic transient levels off and other undesirable reactions (eg metal dissolution) may occur without any discernable effect on the response (Brummer and Robblee, 1983). Bergveld's criterion is therefore likely to overestimate the limits of safe 'reversible' charge injection.

In the past, the applied waveforms found experimentally to minimise electrode and tissue damage are consistent with the basic goal of minimising the flow of faradaic current across the electrode interface (Dymond, 1976) and thus ensuring little, if any, net transfer of charge. Decreasing the duration, amplitude and rate of current pulses have all been suggested as each of these ensures Z_{CPA} control of the transients and thus avoids, to some extent at least, the undesirable faradaic processes.

An alternative method proposed by Lilly (1955) is to reverse the faradaic reactions before any damage occurs. In this procedure a pulse of one polarity is quickly followed by another pulse, equal in amplitude and duration of opposite polarity. These balanced biphasic pulses theoretically recover any electrochemical species released by the first pulse before they diffuse away from the electrode surface. Although this method does indeed reduce the extent of lesion formation, the theory involved is not totally correct. Weinman (1965) pointed out that stimulation with a symmetrical biphasic waveform does not necessarily lead to symmetrical electrochemical reactions at the electrode surface. Toxic products formed in one direction are not necessarily recovered on reversing the polarity. Even in the case where the net current flowing through the electrode is zero, some rectification will occur and the mean dc voltage of the electrode will be displaced from it's reversible potential (equation 4.50 and figure 4.5).

To conclude, it would appear that the solution to the toxicity problem is to inject charge via non-faradaic or "surface faradaic" processes as far as possible and thus avoid the injection of any possibly-toxic materials into the body (Brummer and Turner, 1975).

5.1.5 Conclusions

The Z_{CPA} - R_{CT} equivalent circuit model more accurately represents the electrode system under transient conditions than the ever popular '3-component model'.

The magnitude of Z_{CPA} is relatively constant, decreasing with applied signal amplitude. R_{CT}, on the other hand, is very nonlinear and decreases rapidly with signal amplitude.

The limit current of linearity, $I_{dc}(10\%)$, was found to be proportional to $t^{-\beta}$ as found empirically by Onaral and Schwan (1983). The voltage limit of linearity, $V(t)_{10\%}$, was found to be almost constant, increasing slightly with the applied current amplitude.

'Safe' charge injection is achieved via the non faradaic, Z_{CPA} impedance. $R_{CT(dc)}$ control of a transient response should, were possible, be avoided in order to avoid tissue and electrode damage.

5.2 EXPERIMENTAL SECTION

In this section the interfacial impedance's nonlinearity is investigated experimentally using large pacing voltage pulses.

Of interest is the form of the impedance under large signal conditions and the nonlinearity of the individual equivalent circuit parameters.

Several pacing electrodes are tested and compared.

Various means of analysing transient data are also considered and evaluated. These include

(a) the transformation of the transient data into the frequency domain prior to analysis and

(b) the direct inspection of the transient waveforms.

In section 5.2.1 the use of Fourier transforms is reviewed. Section 5.2.2 deals with the experimental setup and in 5.2.3 the electrode setup is described. In section 5.2.4 the experimental results are presented and these are discussed in section 5.2.5.

5.2.1 Use of Fourier Transforms

As pointed out in the introduction to chapter 3, the advantage of using the transient analysis technique in the investigation of the inter-electrode impedance is in the relatively short period of time required to record the electrode system's response to a given input. The applied waveform (a step or pulse in this case) can be considered as being composed of a wide

range of sine waves of different frequencies which are related one to another in a specific manner describable by a Fourier series. The response waveform is therefore the collective response of the electrode system to the individual sine waves present in the applied waveform. Each of these sine waves will experience an amplitude and phase change. By close analysis of the input and output waveforms one can deduce the impedance of the system at each of the component frequencies and eventually plot an impedance locus diagram. This is similar to what was done in chapters one and two using the varying frequency ac method, with the important difference that all the component frequencies are applied "simultaneously" over a relatively short period of time. Rapid measurement of the system's impedance is thus possible.

In order to obtain the impedance function from the observed time domain behaviour, it is necessary to decompose or separate the applied and resultant waveforms in to their component sine waves of different frequencies. This is achieved by use of the Laplace transform which transforms a time function f(t) into a complex frequency function F(s) according to equation 3.2, ie

$$F(s) = \int_0^\infty f(t) \exp(-st)\, dt$$

where s is the Laplace transform variable. s is a complex number given by $s = a+j\omega$.

The impedance of an electrode system can be found by using the transformed voltage and current waveforms such that

$$Z_{(s)} = \frac{V(s)}{i(s)} = \frac{\int_o^\infty V(t)\ \exp\ (-st)\ dt}{\int_o^\infty I(t)\ \exp\ (-st)\ dt}$$

(Z (s) is sometimes known as the "operational impedance").

It is possible to perform the integration (equation 3.2) along either or both the real, a, and imaginary, $j\omega$, axis of the complex frequency plane. Conversion into the frequency domain by imaginary axis transformation ($s=j\omega$) causes equation 3.2 to become

$$F(\omega) = \frac{1}{2\pi}\int_{-\infty}^{\infty} f(t)\ \exp\ (-j\omega t)\ dt \qquad 5.23$$

The Laplace transform restricted in this way to the imaginary axis of the complex frequency plane is known as the Fourier transform.

- Aperiodic functions

The Fourier transform enables an aperiodic function, f(t), to be represented as an integral sum of sinusoids over a continuous range of frequencies.

In order to illustrate this point let us take the Fourier transform, $F(\omega)$, of a function f(t) and then take the inverse transform of the derived function $F(\omega)$. This should result in the original function f(t). Writing these two successive transforms as a repeated integral, one obtains the usual statement of Fourier's integral theory,

$$f(t) = \int_{-\infty}^{\infty} \left[\int_{-\infty}^{\infty} f(t)\ e^{-j\omega t}\ dt \right] e^{j\omega t}\ d\omega$$

$$= \qquad A(\omega)\ \cos\omega t \quad + B(\omega)\ \sin\omega t \quad d\omega$$

5.24

where $A(\omega) = 1/\pi \int_{-\infty}^{\infty} f(t) \cos\omega t \, dt$

$B(\omega) = 1/\pi \int_{-\infty}^{\infty} f(t) \sin\omega t \, dt$

In Equation 5.24 the function f(t) is expressed as an integral sum of sinusoids over a continuous range of frequencies. The determination of the functions $A(\omega)$ and $B(\omega)$ represent the central goal of Fourier analysis.

- Periodic functions

Although a periodic waveform or function f(t) cannot be represented by a Fourier integral, it can, however, be represented by the infinite Fourier series,

$$f(t) = a_o + \sum_{n=1}^{\infty} a_n \cos n\omega_o t + \sum_{n=1}^{\infty} b_n \sin n\omega_o t \qquad 5.25$$

where $\omega_o = 2 \quad f_o$

f_o is the fundamental frequency

$T = 1/f_o$ is the repetition period of the periodic waveform

$a_o = 1/T \int_o^T f(t) \, dt$

$a_n = 2/T \int_o^T f(t) \cos (n\omega_o t) \, dt$

and $b_n = 2/T \int_o^T f(t) \sin (n\omega_o t) \, dt$

The Fourier series allows a periodic function to be represented by an infinite sum of sinusoids at definite frequencies which are multiples of the fundamental frequency, f_o - all other frequencies are missing.

Note the similarity between equations 5.24 and 5.25. The Fourier integral is equivalent to the

Fourier series representation as the repetition period, T, of the periodic waveform tends to infinity. In this case, f_o tends to zero and one has an integral, as opposed to a series, with all frequencies present.

Treating a signal as periodic, ie deciding on a repetition period T by which the signal has reached equilibrium, proves a useful approximation to the aperiodic case where the Fourier transform is a continuous function of frequency (see equation 5.24).

From equation 5.25 the amplitude of the nth sinusoid component of a given waveform can be calculated as follows,

Amplitude of nth sinusoid = $(a_n + b_n)^{0.5}$

and the corresponding phase angle by

$\phi_n = \tan^{-1} (b_n/a_n)$.

The determination of these coefficients is the aim of Fourier analysis.

- Need for a digital computer

Separating equation 5.23 into its real and imaginary parts one has

$$F(\omega) = \int_o^\infty f(t) \cos\omega t dt - j \int_o^\infty f(t) \sin\omega t \, dt \qquad 5.26$$

It can be seen that in both cases the original time function, f(t), is multiplied by a trignometric function between t=o and the time at which the waveform reaches equilibrium. The area under the resulting curve is equal to the integral defined in equation 5.23. The above operation is performed, for both the real and imaginary parts of $F(\omega)$, for as many ω values

as desired (Pilla, 1970). The resulting complex function $F(\omega)$ is then the frequency domain representation of the time domain function, f(t). Such a series of operations must be performed on both the applied and resultant waveforms in order to derive the impedance, $Z(\omega)$.

To carry out manually the above calculations would prove long and extremely tiresome. Such integral transforms are more realistically implemented with the aid of a digital computer and the Fourier transform ($s=j\omega$) is made particularly appealing by the existence of the so-called Fast Fourier Transform (FFT) algorithm (Creason et al, 1973). The FFT is an algorithm for computing the Fourier Transform of a function with minimum computational effort.

- Sampling and Truncation

Implementation of a Fourier transform with a digital computer necessarily involves a discrete, digital approximation to the continuous analog signal. The signal must be sampled and the sampling rate $1/t_s$, must be decided. It will also be necessary to truncate the sampled waveform after a certain period ,T, as only a finite number of points, N, (where $N = T/t_s$) can be considered.

A waveform observed over period, T, can be fully specified over the period t = o to t = T by the Fourier transform as if the waveform repeated with a repetition frequency $f_o = 1/T$. The observation time T should of course be longer than the duration of the

waveform. Otherwise any value of T can be chosed arbitrarily. Setting the value of the observation period, T, also sets that of the fundamental frequency, $f_o = 1/T$, and the spacing between higher ac components. Too short a value of T and the frequency points on the derived impedance locus will be spaced too far apart making accurate interpretation difficult.

The sampling rate, $1/t_s$, determines the highest frequency, f_h. However, due to aliasing effects (see later) the high frequency component completely characterisable (free from distortion) is only one half this value. As each frequency component is a multiple of the fundamental, f_o, setting the sampling rate also determines the number of points, N, in the frequency and time domain arrays, ie

$$N = f_h/f_o = T/t_s \qquad 5.27$$

- Errors which arise from incorrectly Sampling and Truncating a waveform

"Aliasing" occurs when the time function is not sampled at a sufficiently high rate,ie t_s is too large. In this case the analog signal contains frequency components higher than those measurable (ie higher than one half of the data sampling rate, $1/t_s$). The net result is that these high frequency components contribute to component magnitudes below the high frequency cut off ($f_h/2$) and therefore distort these lower frequency components. Such "aliasing" can be avoided by either increasing the sample rate until the sample interval, t_s, is smaller than one half the

reciprocal of the highest frequency component, and/or by low pass filtering the analog signal before Analogue to Digital conversion thus removing the unwanted high frequencies.

Incorrect truncation also introduces errors. If a periodic waveform has not reached equilibrium within the observation time, T, the amplitudes at the start and finish of the sampling range will not be equal. Sub harmonic components ($f < f_o$) are therefore present in the signal to be sampled. Such truncation results in a frequency transform which has a "noisy" ripple. To reduce this effect the length of the truncation should be as long as possible.

- Fast Fourier Transform

In the case of the Fast Fourier Transform (FFT) algorithm, the data record to be transformed must contain $N = 2^x$ sampled points, where x is any integer. This requirement is accommodated by appropriate adjustment of the time interval at which the waveform is sampled, t_s, and/or the total time used to acquire the data, T.

If f(t) is negligible outside the region t=o to t=T and the waveform is divided into N equal intervals, the Fourier Integral Transform (equation 5.23) becomes (Brigham, 1974)

$$F_n = F(n/T) = T/N \sum_{K=O}^{N-1} f(KT/N) \exp(-j2\pi nK/N)$$

for $n = 0,1...N-1$ 5.28

The above "discrete" Fourier transform serves as an approximation to the Fourier integral transform

(equation 5.23) in the region f=0 to f = N/T = f_h and the expression relates N samples of the waveform in the time domain to N samples in the frequency domain. Any differences between the integral and discrete transforms will arise through incorrect sampling and/or truncation of the waveform to be transformed.

5.2.2 Experimental Set up

Two methods of recording and digitising the signal waveforms were used and these are reviewed in the next two sections.

5.2.2.1 Initial Experimental set up

The voltage pulse was applied to the electrode system (section 1.2.1, figure 1.31) and, along with the resultant current, was displayed on an oscilloscope screen and photographed. The photographs were enlarged and the waveforms sampled, plotted, smoothed and resampled. The data was then fed by hand into the University Computer for discrete Fourier Transformation.

The finite Fourier Transform routine (C06 ECF) from the University of Leeds computer library was used to transform the voltage and current signals. The transformed data was presented in real and imaginary series components. The impedance at a given frequency F(I) was calculated by dividing the voltage data, C(I)+jD(I), by the current data, G(I)+jE(I), as follows

$$Z(I) = \frac{C(I)E(I)+G(I)D(I)}{E(I)^2+G(I)^2} + j\,\frac{D(I)E(I)-G(I)C(I)}{E(I)^2+G(I)^2}$$

For a listing of the computer program, see figure 5.5.

- Sources of error

The computer program used requires that a sample point must be located at the midpoint of any abrupt change in the sampled waveform's amplitude. For a voltage step of 4 Volts, for example, the sample point on the step must be located at 2 Volts and not at either 4 or 0 Volts. Problems were encountered in locating the initial point of the current response due to the finite rise times of the oscilloscope and the pulse generator and to the distortion of the waveform incurred by photographing it from the oscilloscope screen. The initial current peak was calculated by extrapolating the waveform back to t = 0. As the current initially decays rapidly with time, there was some uncertainty as to the exact value of the peak current. Half the extrapolated value was used as the first point of the current transient data. A similar procedure was used in locating points on the sharp changes in the voltage and current waveforms at the end of the applied pulse.

Additional sources of inaccuracy were "barrel" distortion of the oscilloscope screen and distortions to the waveform due to photographing and enlarging it.

LISTING OF THE FOURIER TRANSFORM PROGRAM

Figure 5.5

```
      IMPLICIT REAL *8 (A-H, O-Z)
C************************************ LOCAL SCALARS
      INTEGER NIN, NOUT, I, N, IFAIL
C************************************ LOCAL ARRAYS
      REAL *8 TITLE(7), X1, X2, X(4100), Y(4100), C(170), D(170),
     * T, E(4100), F(170), G(170), H(170), O(170), CB, VB,
     * Q(170), R(170), P(170), CG, VG, RS
      DATA NIN /5/, NOUT/6/
C************************************ READ IN TITLE
      READ (NIN,99999)TITLE
99999 FORMAT (7A4)
      WRITE (NOUT,99998) (TITLE(I),I=1,7)
99998 FORMAT (////1H , 7A4, 7HRESULTS/)
C************************************ READ IN NO OF POINTS, TOTAL PERIOD
C************************** BIAS AND GAINS,VB,CB,VG,CG, RS IS SERIES
      READ (NIN,*) N, T, VG, CG, VB, CB, RS                RESISTANCE
      WRITE (NOUT,99995)
99995 FORMAT (1H , 4HFREQ, 14X, 7HVOLTAGE, 15X, 7HCURRENT, 12X,
     * 9HIMPEDANCE,/13X, 4HREAL, 4X, 4HIMAG, 10X, 4HREAL,
     * 7X, 4HIMAG, 7X, 4HREAL, 7X, 4HIMAG)
C******************** READ IN DATA FROM FILE
C******************** X1 IS VOLTAGE, X2 IS CURRENT
      DO 20 I= 1,N
         READ (NIN,*) X1, X2
         X(I)=X1
         E(I)=X2
   20 CONTINUE
C******************** VOLTAGE AND CURRENT POINTS
C******************** SUBTRACTING DC BIAS, VB AND CB
      DO 30 I=1,N
         E(I)=E(I)-CB
         X(I)=X(I)-VB
   30 CONTINUE
C******************** DIVIDING BY GAIN, VG AND CG
      DO 40 I=1,N
         X(I)=X(I)/VG
         E(I)=E(I)/CG
   40 CONTINUE
C************************** FIXING IMAGINARY VALUES =0
      DO 180 I=1,N
         Y(I)=0.0
  180 CONTINUE
      IFAIL = 0
      CALL C06ECF(X, Y, N, IFAIL)   ********FOURIER TRANSPORM OF
      DO 190 I = 1,165                              VOLTAGE
         C(I) = X(I)
         D(I) = Y(I)  ****************** STORE RESULTS IN C(I)AND
         F(I) =(I-1)/T ********FREQUENCY  D(I) FOR FIRST 165 POINTS
  190 CONTINUE
C************************ CHANGE X AND Y TO CURRENT DATA
      DO 200 I=1,N
         X(I)=E(I)
         Y(I)=0.0
  200 CONTINUE
      CALL C06ECF(X, Y, N, IFAIL)
      DO 210 I =1,165
         E(I) = X(I)
         G(I) = Y(I)  ************** STORE RESULTS IN E(I)
  210 CONTINUE                                    AND G(I)
C************************** CALCULATE Z=V/I
C************************** Q IS REAL PART, R IS IMAGINARY
      DO 220 I=1,160
         H(I) = (C(I)*E(I))+(G(I)*D(I))
         O(I) = (D(I)*E(I))-(G(I)*C(I))
         P(I) = (E(I)**2)+(G(I)**2)
         Q(I) = H(I)/P(I)
         R(I) = O(I)/P(I)
  220 CONTINUE
      DO 230 I=1,160   ******************** SUBTRACT SERIES
         P(I)= Q(I)-RS                              RESISTANCE
         H(I)= (P(I)**2)+(R(I)**2) ********* CALCULATE TOTAL
         O(I)= H(I)**0.5                          IMPEDANCE
  230 CONTINUE
      DO 240 I= 1,160
C************************** WRITE ANSWERS
      WRITE (NOUT,99994) F(I), C(I), D(I), E(I), G(I), Q(I), R(I:
     * P(I), O(I)
99994 FORMAT (F8.1, 2X, E9.3, 2X, E9.3, 2X, E9.3, 2X, E9.3, 2X, E9.3, 2X, E
     * 2X, E9.3, 2X, E9.3, 2X, E9.3)
  240 CONTINUE
      STOP
      END
```

- Testing the accuracy of Fourier Transform method of analysis

The current response to a voltage square wave (5 volts, 1.28 ms pulse width, t_p) of a "three component" circuit was calculated using the equations

(I) for $t \leq t_p$,

$$i(t) = V/(R_{TOT}+R_{CT}) + V(1/R_{TOT} - 1/(R_{TOT}+R_{CT}))\exp(-t/A)$$

and (II) for $t > t_p$

$$i(t) = \exp(-t/A)\ V(1/R_{TOT} - 1/(R_{TOT}+R_{CT})(1-\exp[-T_p/A])$$

5.29

where $A = \dfrac{R_{TOT}\ R_{CT}\ C_{dl}}{R_{TOT} + R_{CT}}$

The circuit component values used in the calculation were

$R_{TOT} = 500\Omega$ $C_{dl} = 6.25\times10^{-7}F$ and $R_{CT} = 2k\Omega$

Hence for

$t \leq t_p$, $i(t) = 2\times10^{-3} + 8\times10^{-3} \exp[-4000t]$

and $t > t_p$, $i(t) = 7.95\times10^{-3} \exp[-4000t]$

The value of the current transient was calculated every 1×10^{-5} seconds and the "observation" period, Tp, was 5.12 msec, ie N, the number of sample points, $= 512 = 2^9$.

The calculated sample values were fed into the computer, transformed and the impedance calculated and plotted (see figure 5.6).

The points lay on a semicircle as expected and the calculated parameter values were identical to those used to calculate the current response. R_{TOT} was calculated from the high frequency intercept (500Ω),

and R_{CT} from the low (2.5kΩ- 500Ω = 2kΩ). C_{dl} was calculated using the equation

$$C_{dl} = (1/R_{CT}\omega)\ [(1-\cos\alpha/1+\cos\alpha)]^{1/2}$$

$$= 6.25 \times 10^{-7}F$$

Where α is the angle of the line joining the centre of the semicircle to a point on the arc of frequency $f = \omega/2\pi$ (Laxminarayan et al, 1979).

Interestingly, at frequencies higher than approximately 25kHz the calculated values of $-X_s$ begin to increase again, forming a "semicircle" for frequencies up to $f_h/2$ (ie 50 kHz). This high frequency distortion is presumably due to aliasing of the voltage and current transforms due to an insuffiently highly sampling rate, $1/t_s$. Such high frequency distortion does not however appear to affect the "low frequency" semicircle as evidenced by the form of the latter and the accuracy with which the parameter values were calculated.

The effect sampling accuracy has on the resultant impedance locus and on the derived circuit parameter values was investigated. Sampling of the waveforms was initially carried out to 5 significant figures and then to 2 significant figures and the resultant impedances compared. The maximum error involved in sampling to 2 significant places was less than 0.15%! Such "inaccuracies" in sampling have therefore little effect on the accuracy of the derived circuit parameter values and they appear to only give rise to high frequency components beyond the range of interest.

- Accuracy of the initial experimental set up

The accuracy of the total set up was tested using an actual 3 component electrical circuit with measured values of

$R_{TOT} = 500\Omega$ $R_{CT} = 2k\Omega$ and $C_{dl} = 7.2x10^{-7}F$

A 6 volt pulse was applied to the circuit and the voltage and resultant current waveforms were photographed and sampled as previously described. The final sampling period, t_s, was 7.95×10^{-6} sec and the total period T, was 8.14×10^{-3} sec. These parameters enabled the calculation of the impedance over a frequency range of 122.8Hz to 63kHz

The resultant impedance (Exp T1A) locus is plotted on figure 5.7 and forms a good semicircle. The parameter values were calculated as

$R_{TOT} = 0.48k\Omega$ (4% error);

$R_{CT} = 1.9k\Omega$ (5% error) and

$C_{dl} = 7.57x10^{-7}F$ (5.1% error).

These errors are largely due to the difficulty in locating the first point on each waveform, to the barrel effect of the oscilloscope screen and to the waveforms.

The above errors were however decreased to around 1% by very carefully compensating for some of the distortions incurred in the recording of the transient data (see below). One could not be sure, however, that such 'compensation' was entirely objective. It was therefore decided that an accuracy of 5% was

acceptable, though some alterations were made to scaling factors as described below.

The effect of using fewer samples of the waveforms was investigated. The results are tabulated below.

No of Samples	Sample length($x10^{-6}$s)	R_{TOT} (Ω)	R_{CT} (kΩ)	C_{dl} ($x10^{-7}$F)
1024	7.94	500	1.98	7.19
512	15.8	500	1.98	7.17
256	31.7	500	1.96	7.17
128	63.5	480	2.01	7.13
measured values		500	2	7.2

Note the above values were calculated after the distortions due to photographing and enlarging the waveforms were taken into account. There is significant improvement in the calculated values of C_{dl}. This is largely due to compensating for the 'shrinkage'(2.5%) of the waveforms relative to the oscilloscope grid on the photographs. Increasing the horizontal (time) axis caused the frequency of derived impedance points to decrease and thus gave rise to a decrease in C_{dl}, as observed above.

From the above table it can be concluded that the use of fewer points does not incur a great lose in accuracy, although high frequency points will suffer aliasing effects.

5.2.2.2 Final Experimental Set up

The initial experimental set up, as described in the last section, suffered a serious drawback as the enlargement of the photographic record of the waveforms and their digitisation by hand proved very time consuming. We were therefore very grateful when offered the use of an analog to digital converter build by G. Tomlinson of the Department of Medical Physics, Leeds General Infirmary.

The voltage pulses (of 1msec. duration) were applied to the electrode systems by a Devices Pacemaker E4161 (figure 5.8). The voltage and current signals were then fed through an isolator (used for invivo work) which had variable filtering and amplification control. The amplified signals were then digitised (the digitiser having two channels) and displayed on the oscilloscope screen to enable inspection. The digitised points were read off the digitiser and fed into the computer by hand for processing as already described.

The digitiser had 256 vertical units and could sample 4,000 points horizontally. The vertical scale was 200 units = 2.5 volts and hence one could sample signals with amplitudes of up to 3.2 volts.

As the applied pacing pulses for our experiments were generally of 4 volts amplitude, a pre-amplifier with a nominal gain of 0.702 was built (figure 5.9), limiting the maximum voltage supplied to the digitiser to 2.8 volts.

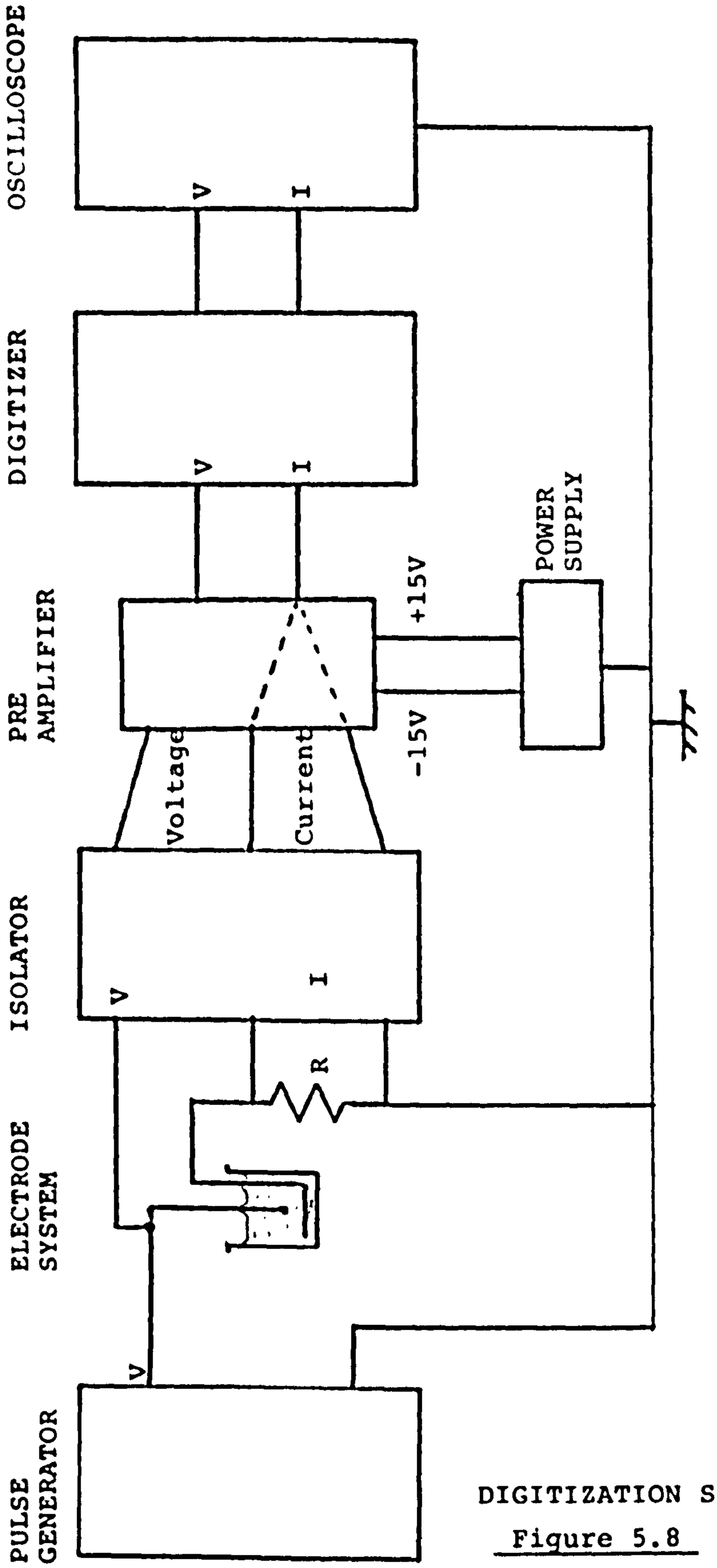

DIGITIZATION SYSTEM

Figure 5.8

After the pulse of duration, t_p, the voltage waveform falls below the origin for a period of time. A biasing circuit was therefore built (figure 5.9) as the digitiser could only accept monophasic signals. The biasing circuit provided a variable offset between $\pm$ 0.9V and the level of the bias could be altered as required by simply varying the 10kΩ potentiometer.

The maximum current response to an applied pacing pulse was generally of the order of 20 to 30 mA. As this was measured across a variable resistance of approximately 10Ω, the maximum signal was approximately 0.2 to 0.3 Volts. Obviously pre-amplification was required before the signal could be fed to the digitiser. A pre-amplifier of nominal gain 5.5 was built which, coupled with a gain of 2 on the isolator, gave a total gain of 10 x 5.5 x 2 = 110, ie the amplified signal supplied to the digitiser was 2 to 3 Volts. The variable resistance "box", whose resistance value could be varied in steps between 7Ω and 14Ω, enabled further "fine tuning" of the amplified current signal to ensure it was as large as possible, without passing the maximum permissable voltage of 3.2 volts.

A biasing circuit was built (figure 5.9) to ensure that the current signal was monophasic when supplied to the digitiser. The level of bias could be varied between $\pm$ 1.82 Volts as required by varying the 10kΩ potentiometer.

Once built, the pre-amplifiers' gains were measured and these values were used in the calculation of the inter-electrode impedances.

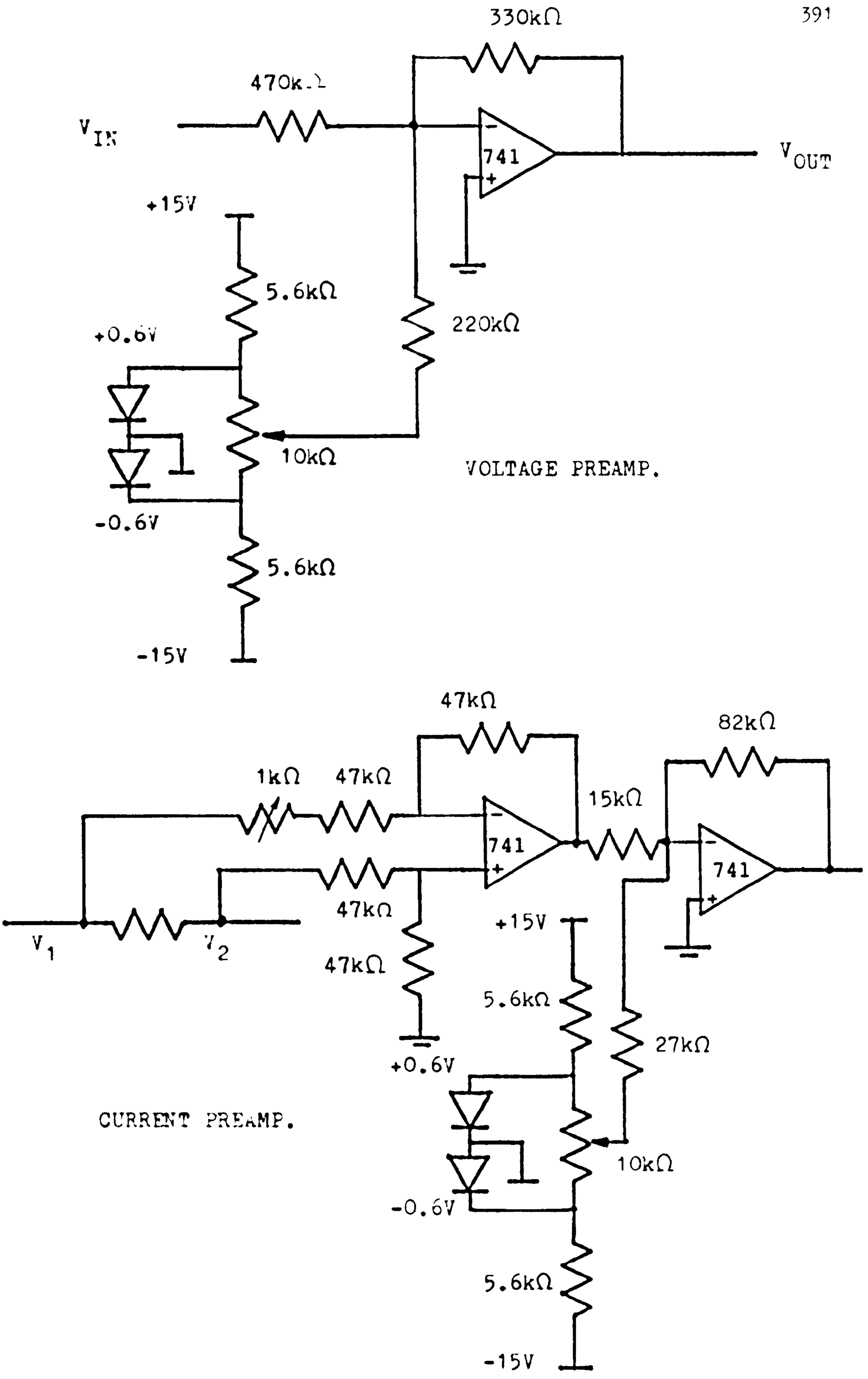

VOLTAGE PREAMP.

CURRENT PREAMP.

PREAMPLIFIER CIRCUITS

Figure 5.9

The digitiser offered a choice of two total sampling time periods - 0.2 or 2 seconds. The total sampling period of 0.2 seconds was chosen as it enabled the digitisation of the signal waveforms into 4,000 samples at intervals of 50×10^{-6} sec. The lowest observable frequency possible was therefore 5Hz and the highest was 10kHz. The 2 second total sampling period was routinely checked to ensure that the waveforms had reached equilibrium before the end of the 0.2 sampling period. If this was found not to be the case for a certain waveform, the extra points were obtained from the 2 second sampling period.

For most of the experiments carried out the signals were filtered at 10kHz to minimise aliasing effects.

- Accuracy of the final experimental set up

In an effort to test the accuracy of the experimental set up, a three component electrical circuit was built with the following measured component values, $R_{TOT} = 810\Omega$ $R_{CT} = 507\Omega$ $C_{dl} = 1.09\mu F$

This circuit was then connected to the experimental set up and its impedance calculated (Exp.T4E) using an applied Voltage pulse of 4 Volts. The number of points used was 1024, ie $N = 2^{10}$, giving a fundamental frequency of almost 20Hz. The circuit parameter values were calculated as,

$R_{TOT} = 806\Omega$ (error 0.5%)

$R_{CT} = 501\Omega$ (error 1.25%)

$C_{dl} = 1.15 \times 10^{-6}F$ (error 5.1%)

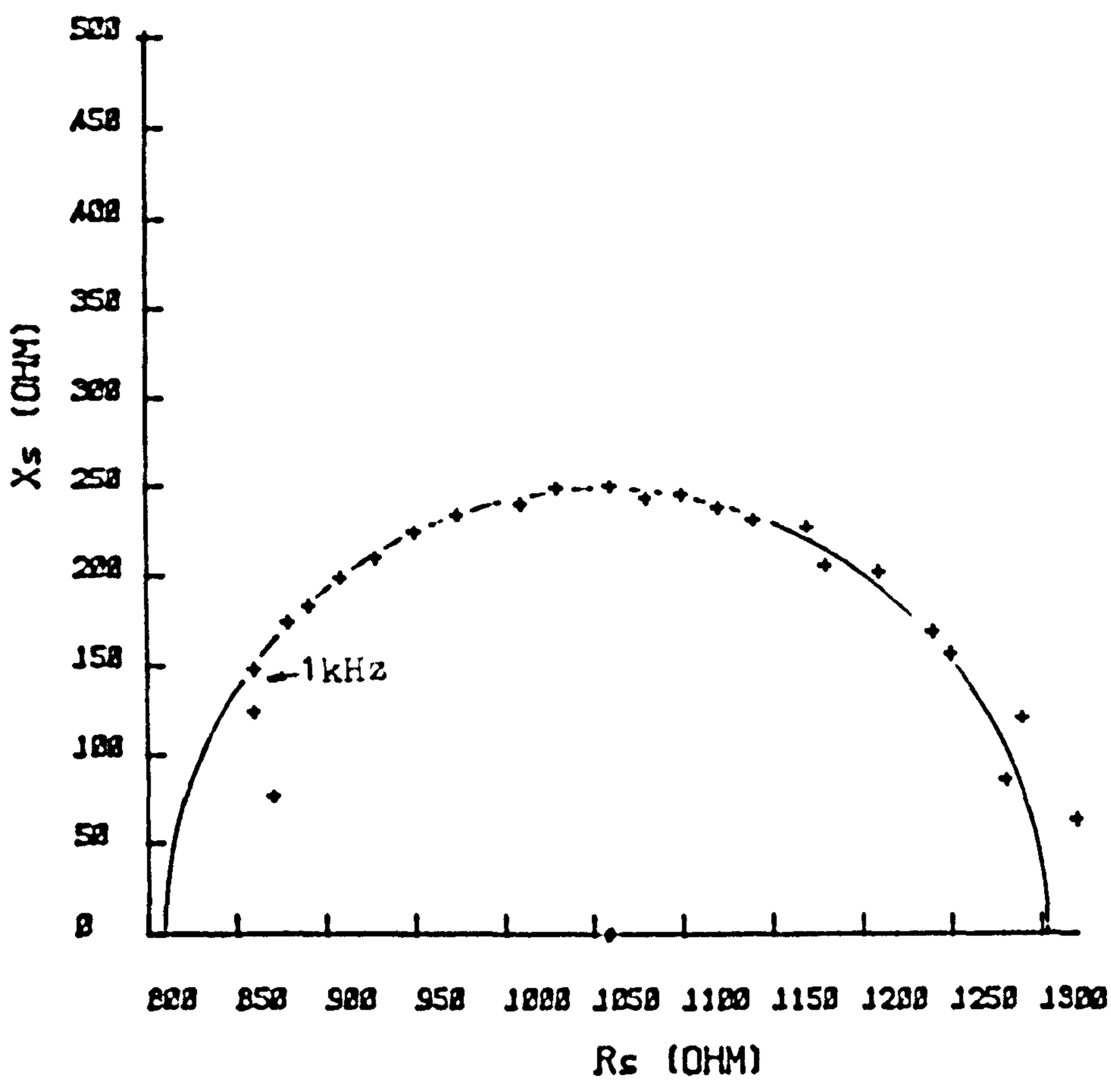

TEST OF ACCURACY OF EXPERIMENTAL SETUP

Figure 5.10

The experimental error using this set up was judged to be acceptable.

The semicircular impedance locus was however observed to be distorted at frequencies above approximately 1kHz (figure 5.10). This was due to 'aliasing' caused by frequencies above $f_h/2$. As the waveforms were sampled every $50x10^{-6}$ sec, the highest meaningful frequency was

$$f_h/2 = 1/2t_s = 10kHz$$

In subsequent experiments the waveforms were filtered at 10kHz to remove this problem.

5.2.3 Electrode Set up

According to Greatbatch et al (1969) the load impedance of electrodes in vivo is "identical" to that seen when the same electrodes are inserted into a physiological saline bath, except that a small resistor (approx 185Ω) must be added in series with the saline bath to compensate for the body's lower electrical conductivity. The above infers that the interfacial impedance, Z_i, of metal electrodes is the same in vivo as invitro; which, as shall be shown, is not the case. In the first few experiments, a 200Ω resistor was connected in series with the bath and used to measure the resultant current waveforms. Later a variable resistance box was constructed with resistance values around 10Ω.

5.2.4 Experimental results

The results section is in two parts. In section 5.2.4.1 the results are obtained by first transforming the transient results into the frequency domain. In section 5.2.4.2 the transient data is analysed directly without recourse to the use of transforms.

Fourier Transformers are generally used in the study of linear systems. As electrode systems are nonlinear, the interpretation of impedance loci obtained by Fourier analysis of current and voltage waveforms must take account of the following:

(i) The derived 'impedance' is only applicable for the input signal applied.

(ii) As the system is nonlinear, the derived impedance loci will suffer harmonic distortion.

It was found, however, that the derived impedance loci formed arcs similar to those found under linear, small signal conditions. The distortion was therefore considered sufficiently negligable to allow the study of qualitative changes in equivalent circuit parameters with applied signal amplitude.

5.2.4.1 Transform Analysis

The nonlinearity of the interfacial impedance under transient conditions was investigated using a range of different electrodes.

- Devices LC Electrode

  Electrode no 1

Using the initial experimental set up enabled the system's impedance to be investigated to relatively low frequencies.

A 5.2 Volt pulse of 1msec duration was applied across the electrodes in the saline bath. In this experiment a 200 Ω resistance was connected in series with the electrodes as suggested by Greatbatch and Chardack (1968). This was however discarded in later experiments.

The waveforms were sampled (after smoothing) every 5.36×10^{-5} sec over a total sampling period of 0.887 second. This gave 2^{14} points, a maximum frequency of 9.3 kHz and a minimum frequency 1.13 Hz.

The derived impedance plot (Exp T3) is shown on figure 5.11b.

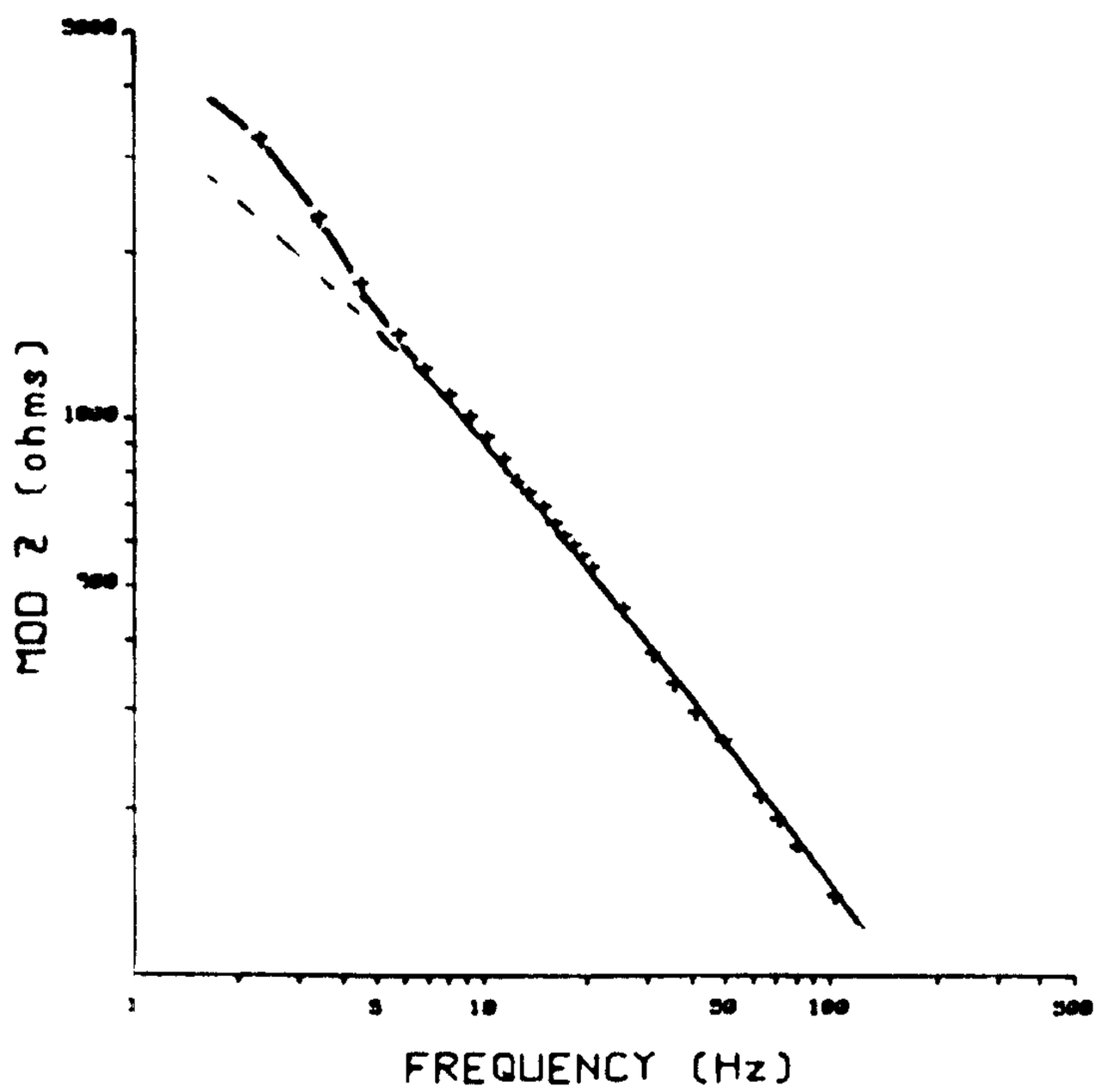

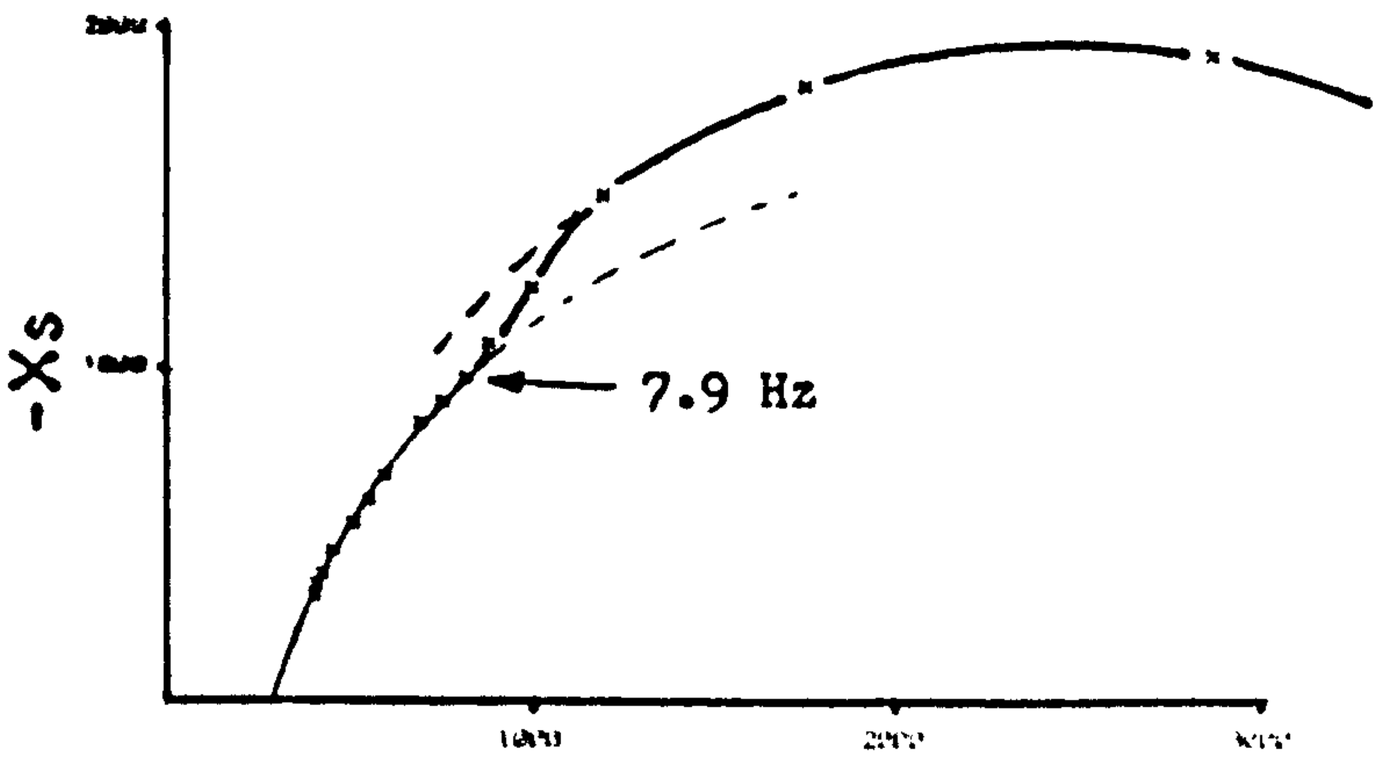

IMPEDANCE OF DEVICES LC ELECTRODE

Figure 5.11 a&b

At high frequencies (f > 30 Hz) the locus is a straight line indicating Z_{CPA} behaviour, where

$$R_{TOTAL}' = R_{TOTAL} + 200\Omega = 307.6\Omega$$

R_{TOTAL} = 107.6Ω, ϕ = 71° (β =0.79),

K = 25k$\Omega s^{-\beta}$, β= 0.8

At lower frequencies (30 > f > 10 Hz) the locus bends over forming part of a high frequency arc which has an approximate diameter of 3kΩ.

Below 10 Hz, the locus rises again to join a low frequency 'smooth surface' arc which has equivalent circuit element values in the region of

K = 45 k$\Omega s^{-\beta}$ β = 0.93

R_{CT} = 4.5 kΩ

The values of β, K and R_{CT} are larger for the low frequency arc as anticipated in chapter two.

Comparing the above results with those obtained for the Devices LC electrode (no.1) in the linear, high frequency region using the ac technique (Exp. 52), where

R_{TOTAL} = 108Ω ϕ = 74° (β = 0.82)

K = 102k$\Omega s^{-\beta}$ β = 0.8

and with those for a Devices SC electrode (no.3) in the low frequency region, where (figure 2.10)

R_{TOTAL} = 131Ω K = 62k$\Omega s^{-\beta}$ β= 0.85

R_{CT} = 4.4 MΩ

(Note the SC electrode has a different surface area and lead resistance to the LC electrode) it is observed that the values of K and R_{CT} for the low frequency arc have dramatically decreased due to the nonlinearity of the electrode system. K has decreased

by approximately 50% whereas R_{CT} has decreased to 0.1% of its original value.

A 'kink' similar to that shown on figure 5.11 was found in the linear, small signal impedance plot (figure 2.10). Nonlinearity of the charge transfer resistance causes the low frequency arc diameter to decrease. As the diameter of the high frequency, "rough surface" arc is in extreme cases proportional to the square root of that of the low frequency, "smooth surface" arc, it also decreases with applied voltage. In the linear region the high frequency arc (figure 2.10) had an approximate diameter of 500kΩ and that of the low frequency arc was 4.4MΩ, ie approximately 9 times larger. Under the present nonlinear conditions (5.2 Volt pulse) the high frequency arc diameter is approximately 3kΩ and that of the low frequency arc is 4.5kΩ, ie only 1.5 times larger.

- Final Experimental Set up

Further experiments were carried out on the Devices LC (no.1) electrode using the A to D converter. The lowest observable frequency was 5Hz and the highest was 10kHz.

The transformed data is plotted on figure 5.12 for a range of voltage amplitudes and the calculated parameter values are listed on table 5.1 below

DEVICES LC ELECTRODE

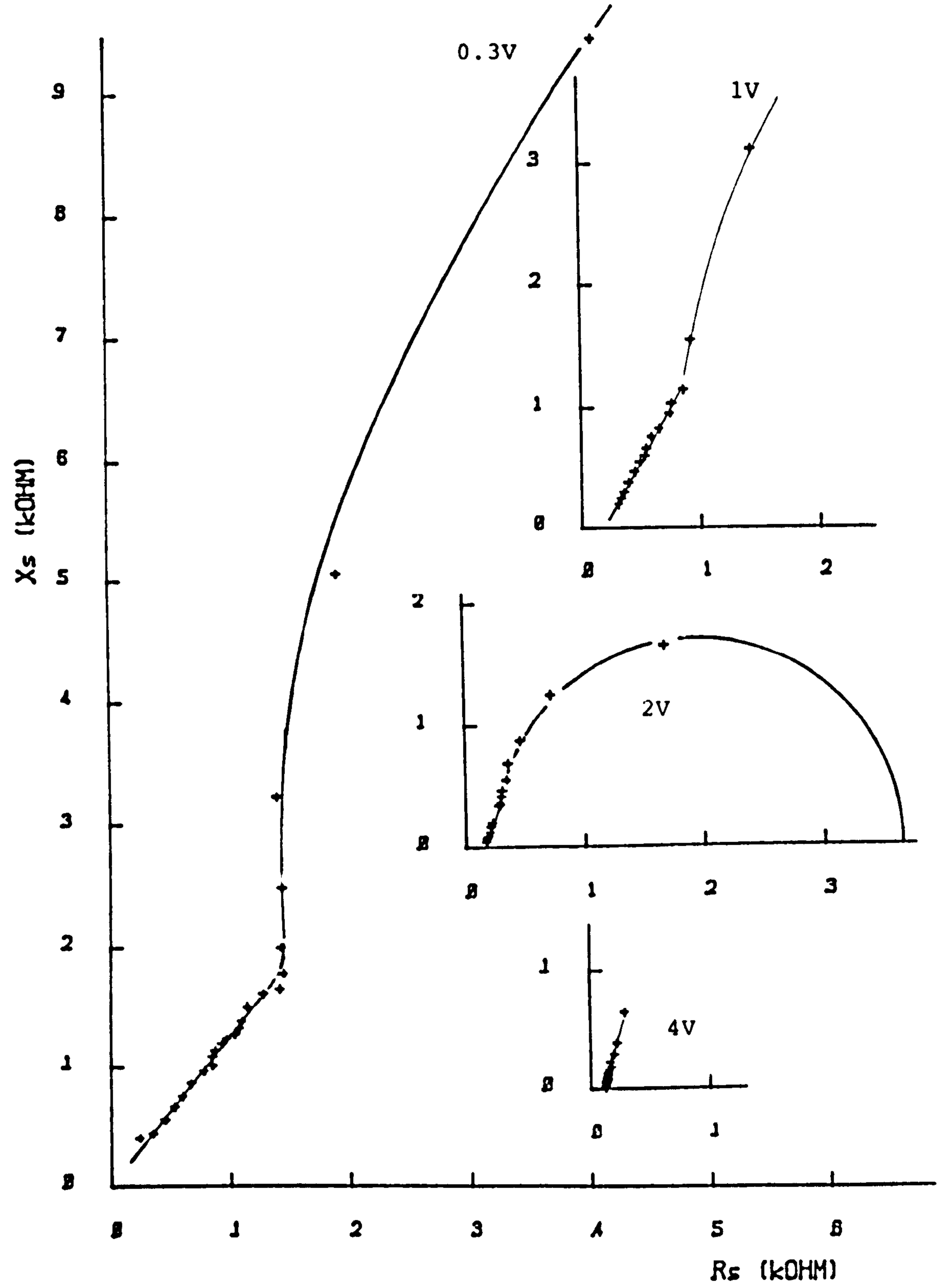

Figure 5.12

TABLE 5.1

Voltage Amplitude (V)	Experiment no	β_1	β_2	K ($k\Omega s^{-\beta}$)	R_{CT} ($k\Omega$)
4	T6	.83	.86	23.9	-
2	T8	.79	.81	34	3.7
1	T9	.7	.73	62.1	15
0.32	T7	.71	.67	112.2	30

At high frequencies the loci form straight lines indicative of Z_{CPA} behaviour. In this region the value of K decreases pseudo exponentially with applied voltage amplitude (figure 5.13). At 4 volts K has decreased to $1/5^{th}$ of its linear value.

The decrease in K is due to the electrode operating in the adsorption region (figure 4.3) where the adsorption pseudo capacitance increases dramatically with applied voltage and dominates the voltage independent, double layer capacitance.

Surprisingly, β was observed to increase steadily with voltage amplitude over the applied range. The measured values of β for a voltage amplitude of 0.32V were however considerably smaller than the linear values (0.67 and 0.71 compared to 0.8). It would appear that for small voltage amplitudes β decreases, due presumably to adsorption effects. As the voltage amplitude is increased further, β increases again indicating, possibly, that surface roughness has less effect in this region. This is supported by the observation that the 'kink' (see later) in the curves becomes less pronounced with voltage amplitude.

Since the penetration depth, p^{-1}, is equal to the

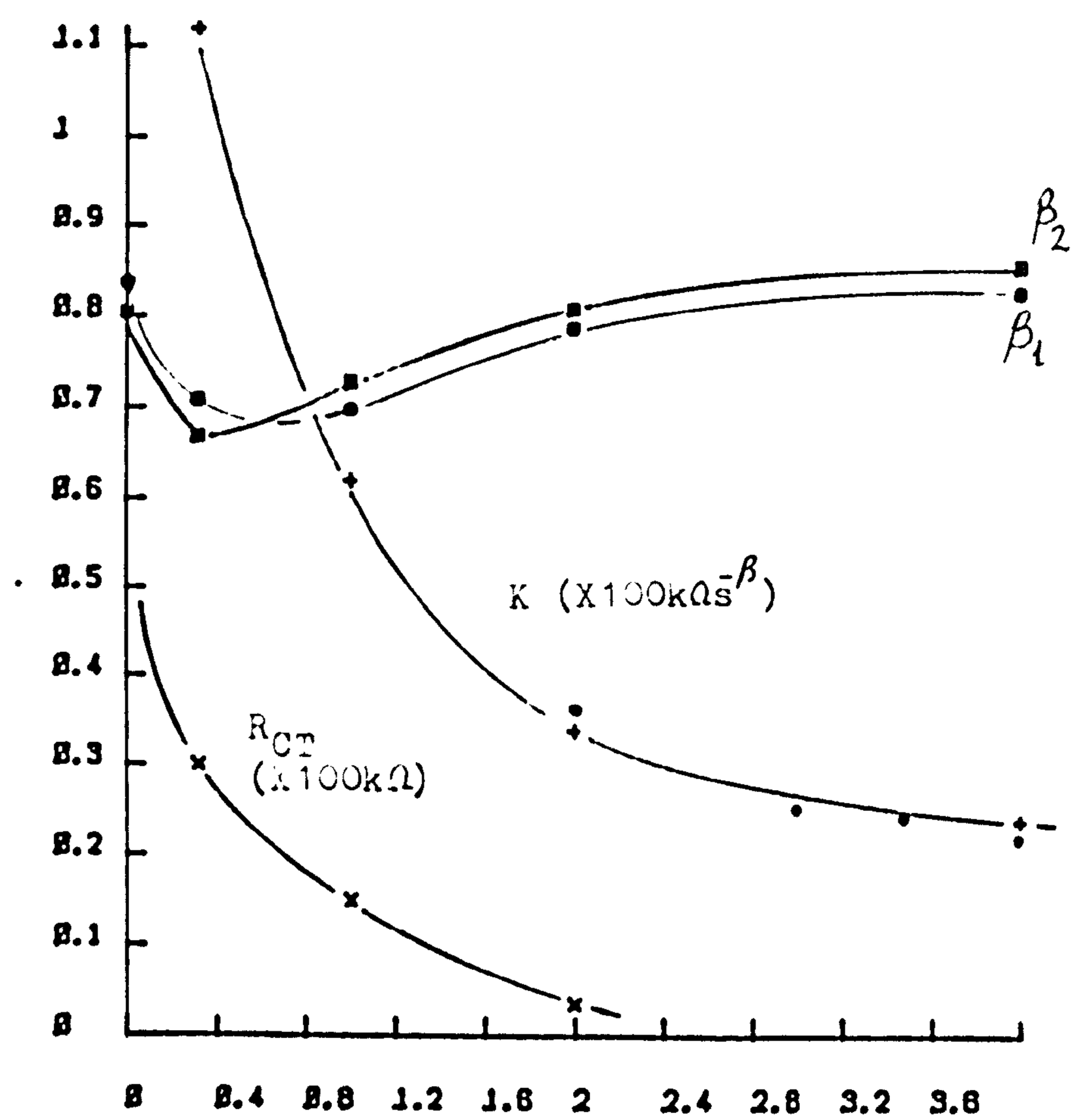

NONLINEARITY OF EQUIVALENT CIRCUIT PARAMETERS

Figure 5.13

ratio, $(Z_i/R_e)^{1/2}$, then as K decreases, the penetration decreases and surface effects should become more pronounced. One would therefore have expected β to decrease as the voltage amplitude was increased.

It is possible, however, that the adsorbant decreases the nonuniformity of the surface (Ramaley and Enke, 1965) and thus decreases the frequency dispersion, ie β increases as observed.

It was noticed for this and the other electrodes tested, that the values of β derived from R_s - X_s and from log Z - log f plots generally differed. This, of course, is most probably due to the limited accuracy of the measurement system. β_1, from the R_s - X_s plot, determines how far the centre of the arc is depressed below the real axis and hence determines the phase angle of Z_{CPA}. β_2, derived from the log Z - log f plot, determines the frequency dependence of the impedance. In the linear region $\beta_1 = \beta_2 = \beta$ and Z_{CPA} is given by equation 1.3, ie $Z_{CPA} = Kj^{-\beta}\omega^{-\beta}$

However when Z_{CPA} becomes nonlinear there is no physical reason why β_1 should equal β_2 as this is a condition of linearity. The more general expression for Z_{CPA} is therefore

$$Z_{CPA} = kj^{-\beta_1}\omega^{-\beta_2} \quad \text{where } \beta_1 \neq \beta_2 \qquad 5.30$$

and the overall impedance is (Yamamoto and Yamamoto, 1981)

$$Z_{TOTAL} = R_{TOTAL} + \frac{R_{CT}}{1 + j^{\beta_1}\omega^{\beta_2}(R_{CT}/K)} \qquad 5.31$$

β_2 is generally found to be larger than β_1 under nonlinear conditions. The limited accuracy of the

experimental set up, however, precludes any firm conclusions.

At lower frequencies the loci become much steeper in gradient, forming the high frequency end of large, low frequency arcs. These low frequency arcs are almost semicircular and hence β in this region approaches unity. These arcs, the author believes, are the characteristic impedances of the electrodes in the absence of surface effects.

The transistion between "smooth" and "rough" surface behaviour appears to occur at progressively lower frequencies for higher voltage amplitudes. At very low signal amplitudes, ie in the linear region, the transistion should therefore occur at relatively high frequencies. Similar increases in phase angle were indeed observed in our high frequency, linear results (100Hz to 10kHz). Using Delevie's equation (eqn 1.38) and equation 1.39, the nonlinear impedance loci can be approximated at high frequencies by an equivalent circuit model comprising a Warburg type impedance, Z_W, in series with a capacitance, C_{LF}, where

$$Z_W = (1-j)\ (R_e/2\omega C_{LF}).$$

As the frequency is reduced, the impedance loci bend over towards the real axis indicating the presence of R_{CT} shunting the low frequency capacitance (or $Z_{CPA(LF)}$).

Due to the lowest observable frequency being relatively high (5Hz), estimated values of R_{CT} were very approximate. It can be seen, however, that the low frequency arc diameter decreases pseudo

exponentially as the applied voltage amplitude is increased (figure 5.13 and Table 5.1).

From figure 5.12, it would appear that surface effects have diminished before the presence of R_{CT} has any significant effect on the impedance loci at lower frequencies and hence a concave portion, rather than a lemniscate or arc, was observed at the high frequency end of the low frequency arc.

- Electrode No 2

The calculated parameter values are listed on Table 5.2 for this electrode

TABLE 5.2

Voltage amplitude (V)	Experiment number	β_1	β_2	K($k\Omega s^{-\beta}$)
4	T45	.86	.93	21.4
3.5	T46	.91	.93	23.9
3	T47	.88	.92	24.7
2	T48	.89	.925	35.8

The values of K are plotted against voltage amplitude on figure 5.13. They too form part of a pseudo exponential curve similar to that obtained for electrode no 1.

Once again β_2 is found to be larger than β_1, both values remaining fairly constant and independent of applied voltage amplitude.

There was no sign of the loci bending over at low frequencies towards the real axis and hence R_{CT} could not be estimated.

- Telectronic 224 (no.1) electrode

Only two experiments were carried out on this electrode and the calculated parameter values are listed below on Table 5.3.

TABLE 5.3

Voltage Amplitude (V)	Experiment no	β_1	β_2	K($k\Omega s^{-\beta}$)
4	T86	.84	.89	26.2
3	T87	.87	.88	29.3

The linear, small signal impedance parameters of this electrode were calculated as (Exp 50, electrode No. 2)

$K = 121.6 k\Omega s^{-\beta}$ $\beta_1 = .88$ $\beta_2 = .84$

K has decreased to approximately one fifth of its 'linear' value.

- Sorin S80 Electrode

Electrode No 1

Only one experiment, at 4 Volts, was carried out on this electrode and the calculated parameter values were (Exp T11, see figure 5.14)

$K = 11.9 k\Omega s^{-\beta}$ $\beta_1 = .84$ $\beta_2 = .79$

For this porous S80 electrode K has only decreased to 91% of its linear value.

As the impedance locus did not bend over towards the real axis within the applied frequency range, the value of R_{CT} could not be estimated.

Electrode No 2

Two experiments were performed on this electrode and the calculated parameter values are listed in Table 5.4.

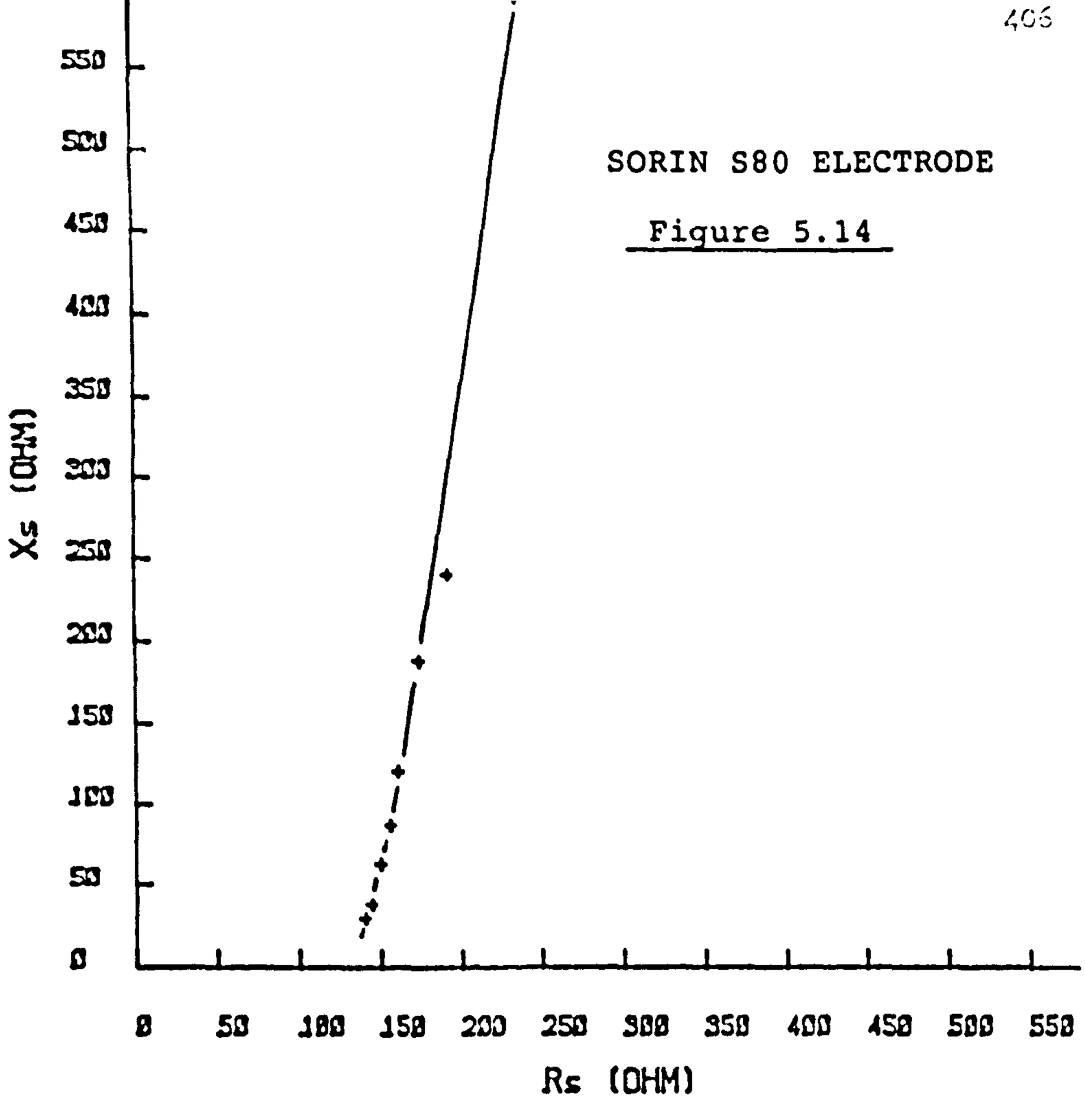

SORIN S80 ELECTRODE

Figure 5.14

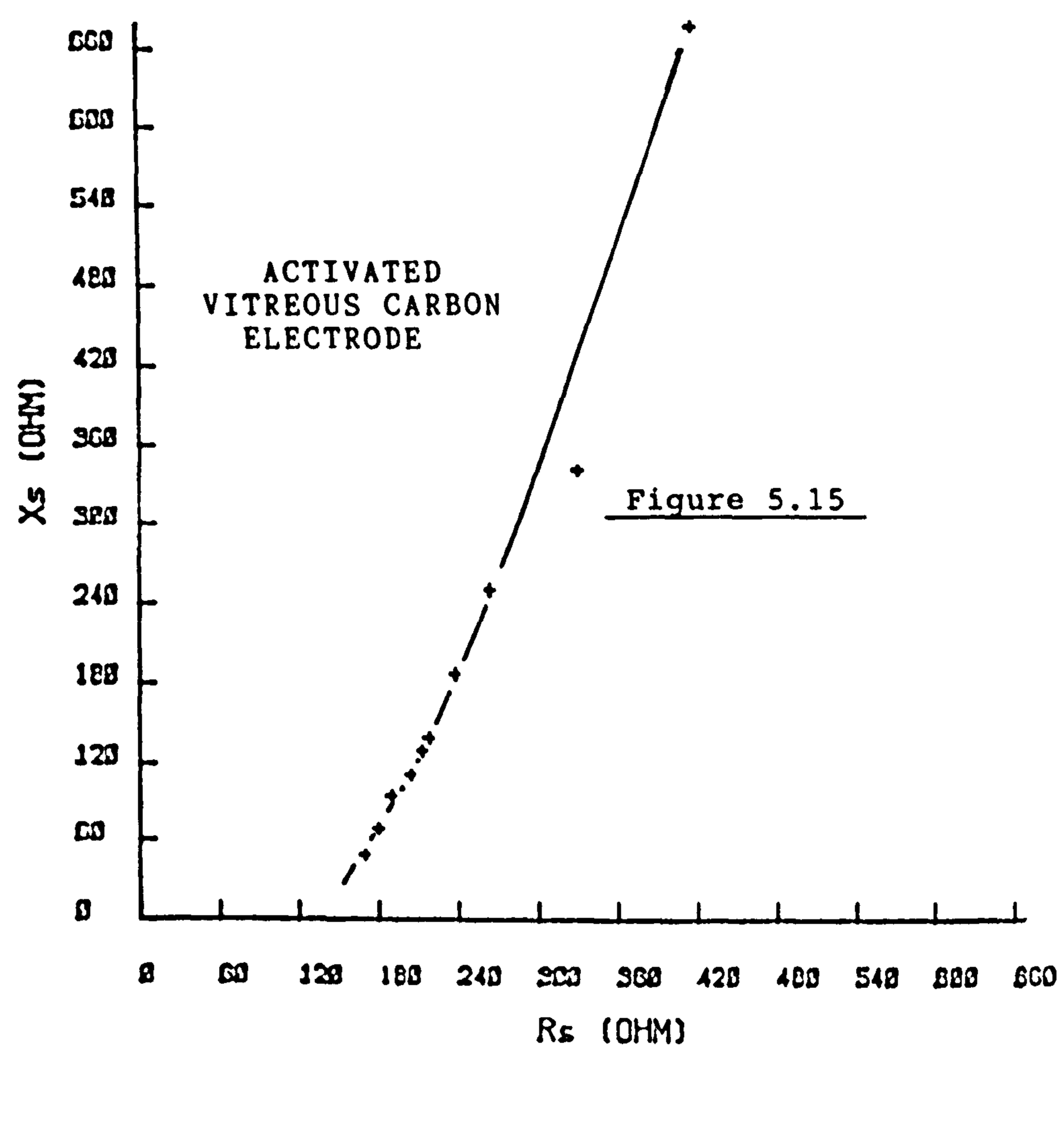

ACTIVATED
VITREOUS CARBON
ELECTRODE

Figure 5.15

TABLE 5.4

Voltage Amplitude (V)	Experiment No	β_1	β_2	K($k\Omega s^{-\beta}$)
4	T81	.87	.93	22.7
3	T84	.83	.90	23.9

The small signal impedance parameters of this electrode were

$$K = 35.2k\Omega s^{-\beta} \quad \beta_1 = .79 \quad \beta_2 = .84$$

The value of K has decreased relatively little indicating that the porous electrode is very linear. At 4 Volts for example, K has only decreased to 64% of its linear value.

The values of β are surprisingly high for a rough surfaced electrode, possibly indicating that surface effects are not as dominant in this region. This could be due to adsorbant decreasing the nonuniformity of the electrode surface (Ramaley and Enke, 1965).

- Activated Vitreous Carbon electrode

  Electrode No 1

  Only one experiment, at 4 Volts, was carried out on this electrode and the experimental results are listed below (Exp T12, figure 5.15)

$$K = 7.51k\Omega s^{-\beta} \quad \beta_1 = .74 \quad \beta_2 = .71$$

Once again the value of R_{CT} could not be established.

No small signal impedance measurements were carried out on electrode No 1 using the Solatron 1250 FRA. However its linear impedance had been measured using the Wien Kerr bridge, where

$K = 11.3k\Omega s^{-\beta}$ $\beta_1 = .59$ $\beta_2 = .59$

K has only decreased to 66% of its linear value and hence the activated A.V.C. electrode is relatively very linear.

The values of β appear to have increased with voltage amplitude though firm conclusions cannot be made based on the early Wien Kerr measurement.

- Summary on Nonlinearity of the electrode interface impedance under transient conditions

The derived impedance loci are similar to those obtained in the linear small signal region.

For a typical locus, the phase angle increases as the frequency is decreased thus forming a concave locus. This, it is believed, is due to surface effects. At lower frequencies the locus bends over to the real axis forming an arc or semicircle due to the impedance of a 'smooth' surface. In some cases, where surface effects dominate to low enough frequencies, part of a high frequency arc or lemniscate is also observed.

Due to the limited accuracy ($\pm$ 5%) of the experimental set up, the small number of experiments carried out and the problems encountered in reproducing results due to the change in electrode impedance with electrode history, great care must be taken in the interpretation of observed variations in equivalent circuit parameter values.

In an effort to minimise changes in the impedances

due to electrode history the electrodes were periodically ulstrasonically cleaned. Such cleaning was found to reverse these changes to a significant degree. More research is however required in this area in order to establish a reliable surface cleaning procedure which does not alter the surface topography-which may be the case with the use of ultrasound.

Comparative experiments were also carried out consecutively in as short a time period as possible, thereby minimising changes in the impedance with time of immersion in the electrolyte and avoiding changes due to intervening experiments.

Nonlinearity of individual components

R_{CT}/ Where measureable (figures 5.11, 5.12 and 5.13), R_{CT} was observed to decrease in a pseudo exponential manner. At voltage pulse amplitudes of 4 Volts, R_{CT} had decreased to less than 0.1% of its liner value.

K/ Where sufficient experiments were carried out, K was observed to decrease in a pseudo exponential manner with voltage beyond approximately 300 mV. Those electrodes which had the highest values of K in the linear region proved to be the most nonlinear, with dramatic decreases in K with applied voltage amplitude.

A similar observation was made concerning $R_{CT(ac)}$ in Chapter 4. Electrodes which were "poor" in the linear region improve in the nonlinear region relative to "good" electrodes. This is due to the latter being more linear and undergoing relatively little change in their values of K. The porous, Sorin S80 and the

activated vitreous carbon electrodes do however remain the 'best' at 3 or 4 volts with smaller values of 'K' than the 'smooth' surfaced electrodes.

The calculated values of K and β for each electrode at an applied voltage amplitude of 4 Volts are tabulated below to facilitate comparison.

TABLE 5.5

Equivalent Circuit Parameter	Electrodes					
	Tel 224 No 1	Dev LC No 1	Dev LC No 2	S80 No 1	S80 No 2	AVC No 1
K ($k\Omega s^{-\beta}$)	26.2	23	21.4	11.9	22.7	7.5
β_1	.85	.84	.86	.89	.87	.74
β_2	.89	.87	.93	.84	.93	.72

β/ For the Devices LC (no1) electrode, whose impedance was measured for a wide range of voltage amplitudes, the calculated values of β_1 and β_2 were observed to increase with voltage over the range 0.32 to 4 Volts. The initial, low voltage (0.32V) values of β were however found to be less than those observed in the linear, high frequency region (see figure 5.13). With the other electrodes tested, although fewer experiments were carried out at different amplitude levels, the increase in β was also generally observed. This behaviour is surprising as β was expected to decrease in the adsorption potential region.

It was postulated that the values of β decrease for relatively small signal amplitudes (300 mv) due to adsorption effects. As the applied voltage amplitude is further increased the adsorbant decreases the nonuniformity of the electrode surface and hence gives

rise to the observed increase in β.

It was generally observed that β_2 was larger than β_1 (equation 5.30) and a possible explanation is the nonlinearity of Z_{CPA}. However these differences were generally not significant (Table 5.5) and firm conclusions cannot therefore be drawn.

5.2.4.2 Direct analysis of Transients

So far information on the electrical properties of the electrode-electrolyte interface has been sought from impedance plots obtained by transforming the transient data into the frequency domain. In this section information on the electrode interface will be obtained directly from the untransformed response waveforms.

Close study of current (or voltage) response waveforms enables qualitative deductions to be made concerning an electrode's impedance. The key points to note are summarised on figures 5.16a and b.

- Voltage response

Fitzhugh and Cole (1973) showed that the voltage response of the proposed equivalent circuit model was given by equation 3.33

$$V(t) = I_{dc} R_{CT} (1-f(\bar{t})) + I_{dc} R_{TOT}$$

where $\bar{t} = t/T$ and $T = (R_{CT}/K)^{1/\beta}$

for short times this simplifies to (equation 3.35)

$$V(t) = I_{dc} [R_{TOT} + \{Kt^{\beta} / \Gamma(1+\beta)\}]$$

After an initial jump, $I_{dc} R_{TOT}$, the voltage response increases and is proportional to Kt^{β}. The larger the values of K and β, the steeper the initial slope.

The voltage response eventually reaches a limiting value, $V(t)_{max} = I_{dc} (R_{CT}+R_{TOT})$. As the "time constant" of the system, T, is equal to $(R_{CT}/K)^{1/\beta}$, $V(t)_{max}$ will be reached sooner if R_{CT} is small and/or K and β are large.

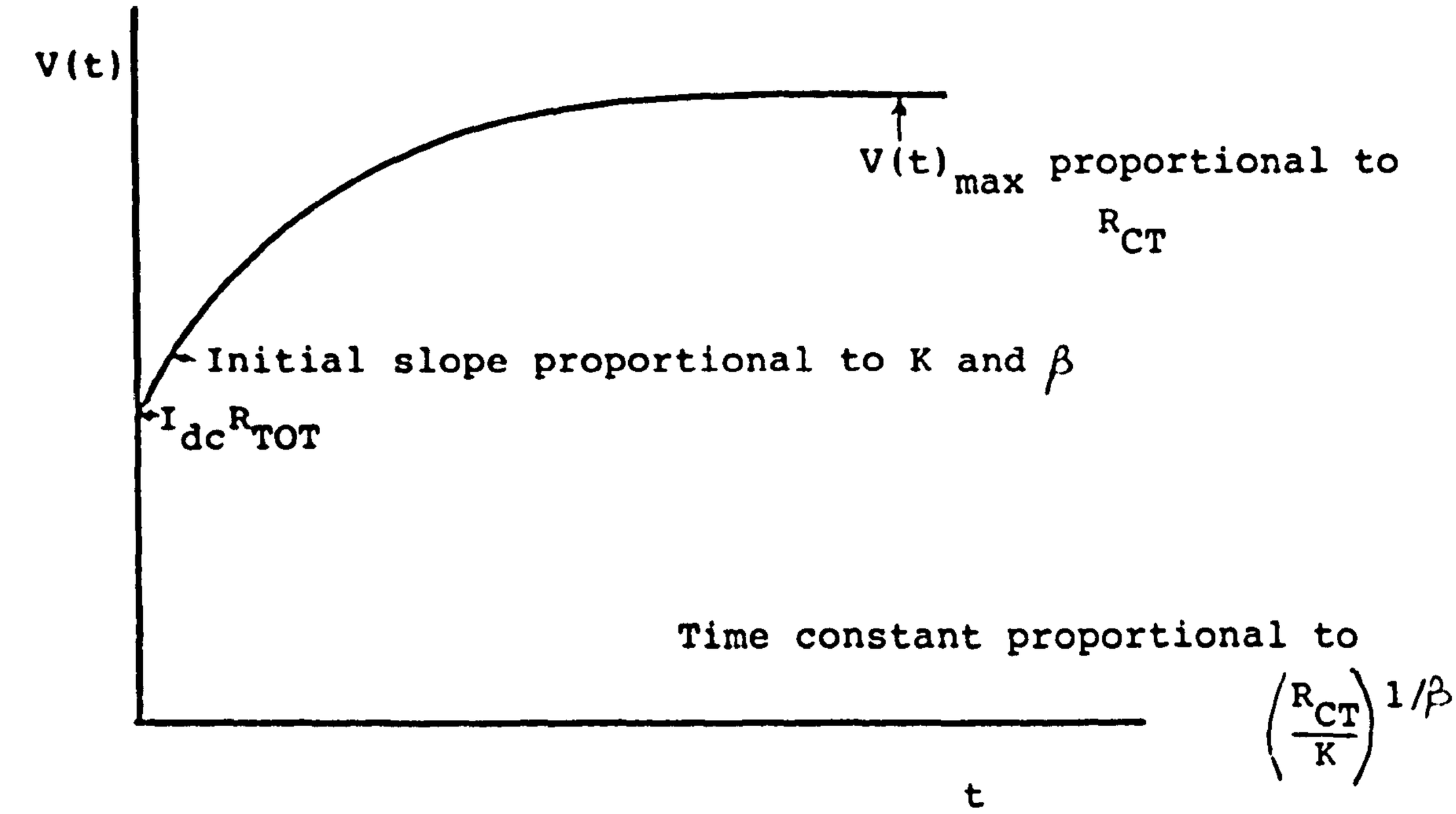

KEY CHARACTERISTICS OF VOLTAGE RESPONSE

Figure 5.16a

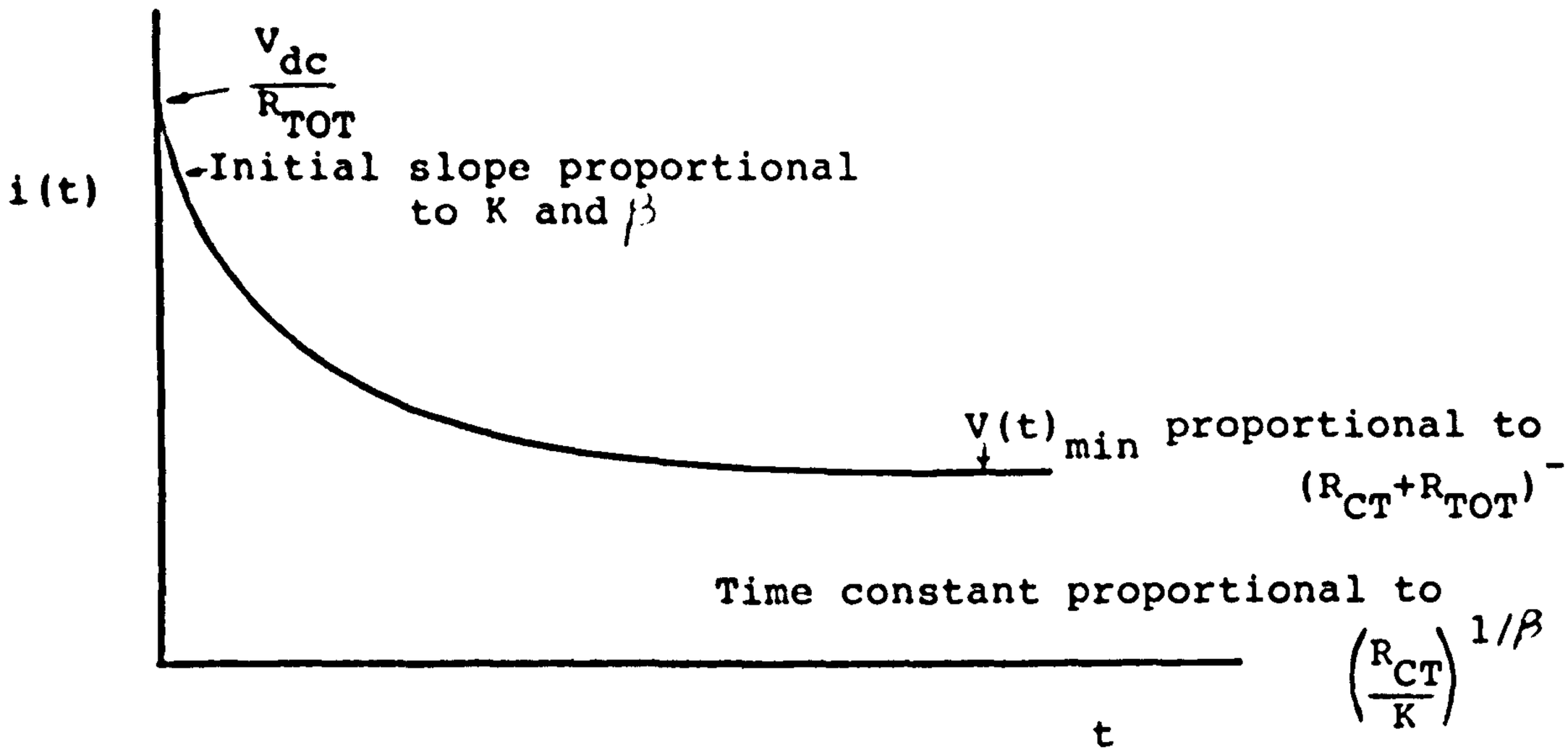

KEY CHARACTERISTICS OF CURRENT RESPONSE

Figure 5.16b

- Current response

Fitzhugh and Cole also showed that the current response was given by equation 3.38, ie

$$i(t) = V_{dc}\,[1/(R_{CT} + R_{TOT}) + g\ f\ (\bar{t}_1)]$$

where $g = \dfrac{R_{CT}}{[R_{TOT}\ (R_{TOT} + R_{CT})]}$

$$\bar{t}_1 = t/T_1$$

and $$T_1 = \left[\frac{R_{CT}\ R_{TOT}}{(R_{CT}+R_{TOT})K}\right]^{1/\beta}$$

After an initial jump, V_{dc}/R_{TOT}, the current decays and is proportional to $t^{-\beta}/K$ (eqn 3.40). The current will eventually reach a limit of $V_{dc}/(R_{TOT}+R_{CT})$. As the "time constant", T_1, is proportional to R_{TOT} and R_{CT} and inversely proportional to K and β, the limiting value will be reached sooner if K and β are large and if R_{CT} and R_{TOT} are small.

- Visual Inspection of response waveforms

The current responses are plotted against time on figures 5.17 a,c and e for a range of electrodes. The pulse amplitude was 4 Volts in each case and the pulse duration was 1 millisecond.

From these plots it is observed that the porous S80 electrode (no 2), which has the smallest value of R_{TOT}, has the largest value of $i(t)_{max}$. The Telectronic 224 electrode (no 1) has the largest value of R_{TOT} and hence the smallest value of $i(t)_{max}$.

The initial slope of the current decay is largest for the porous S80 and the A.V. Carbon electrodes. The slope is small, on the other hand for the Devices LC

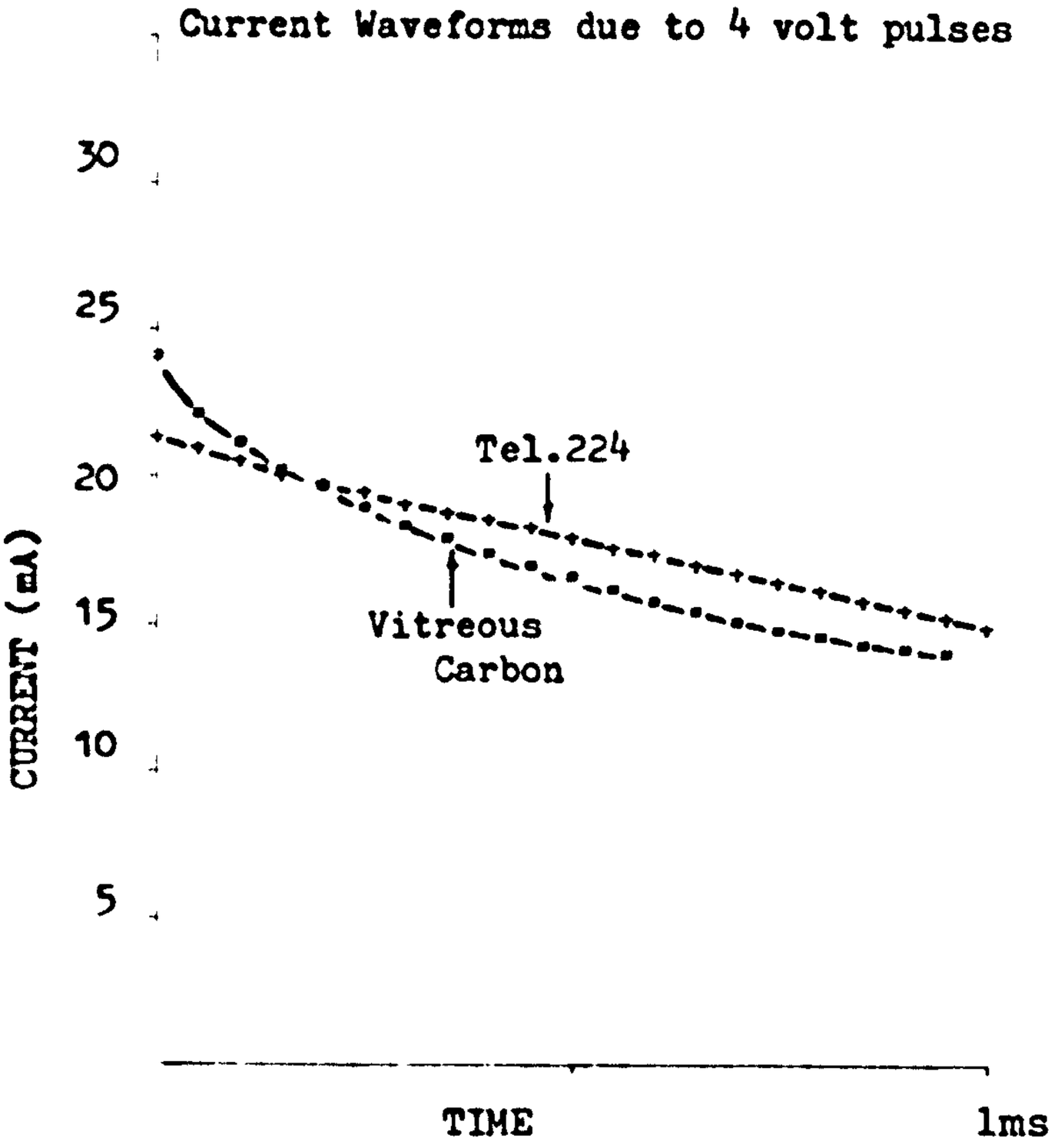

Figure 5.17a

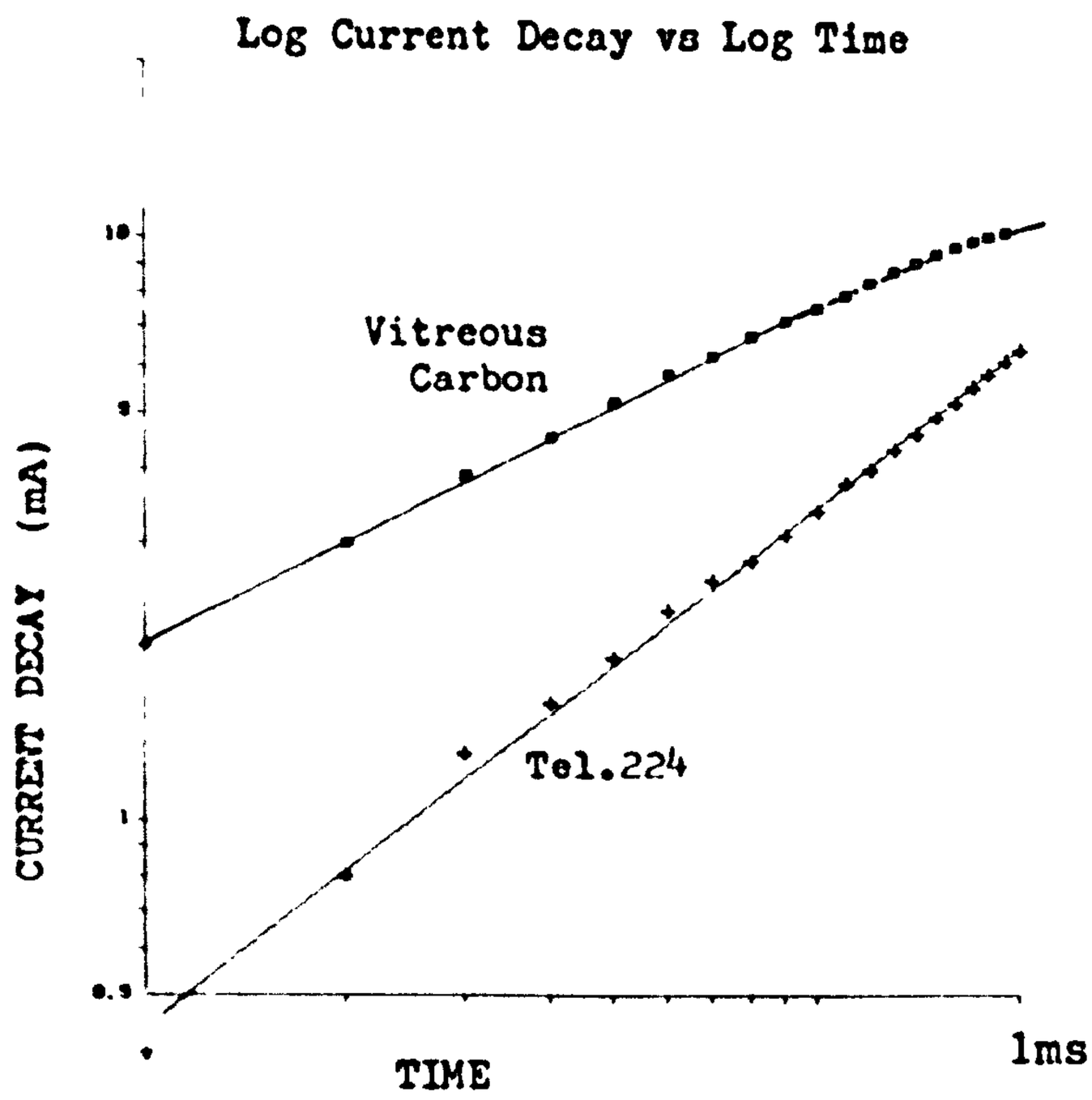

Figure 5.17b

Current Waveforms due to 4 volt pulses

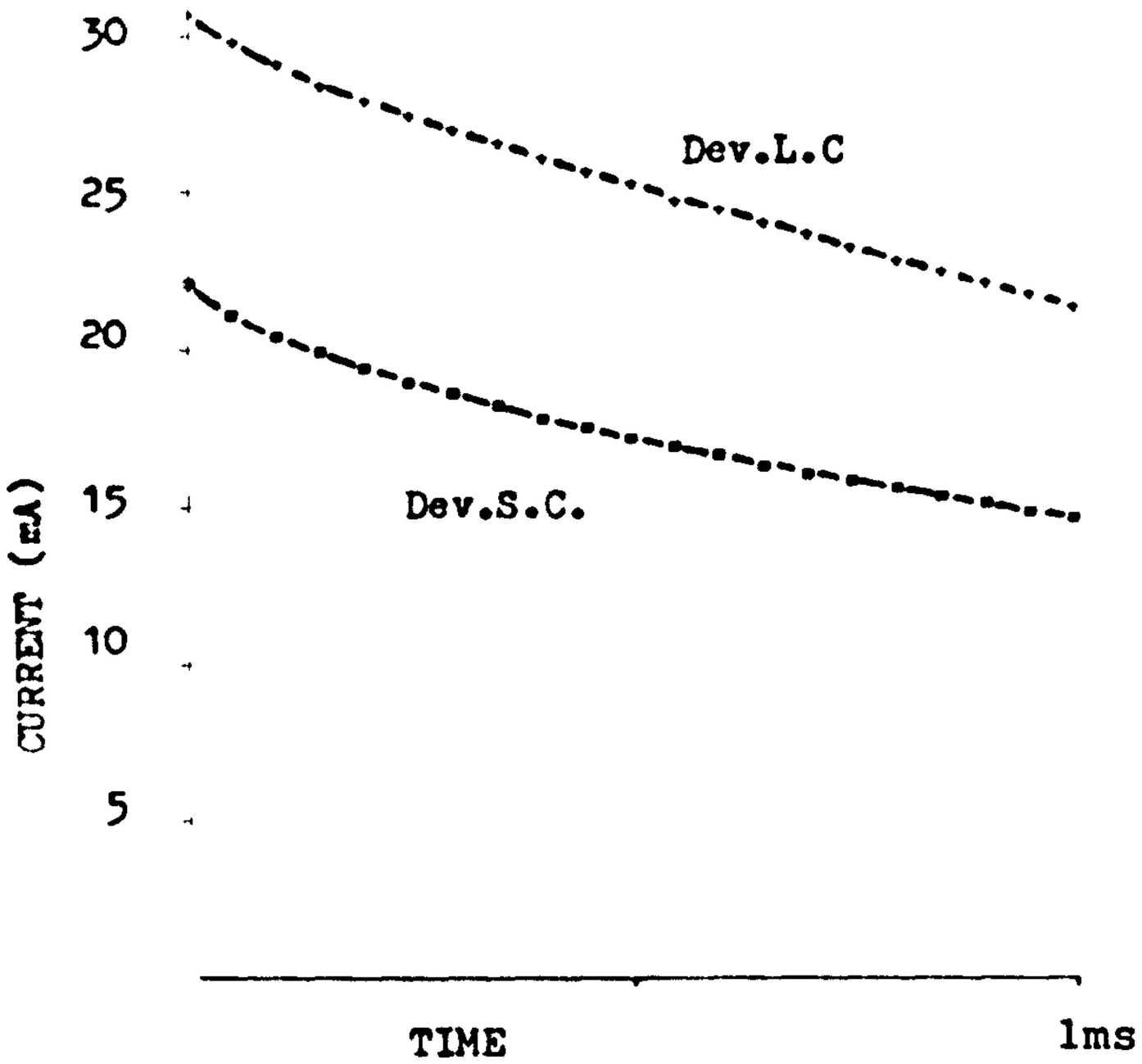

Figure 5.17c

Log Current Decay vs Log Time

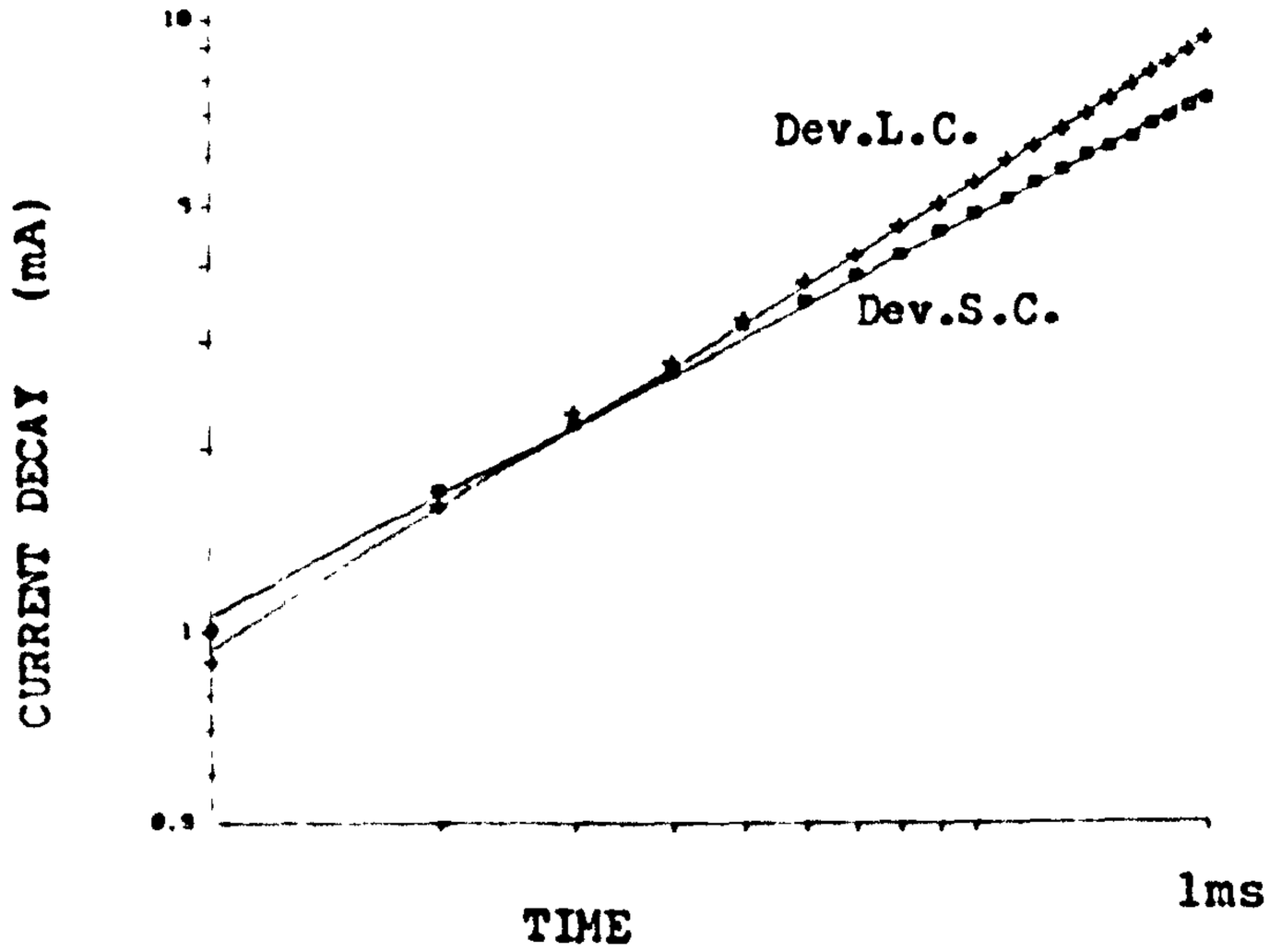

Figure 5.17d

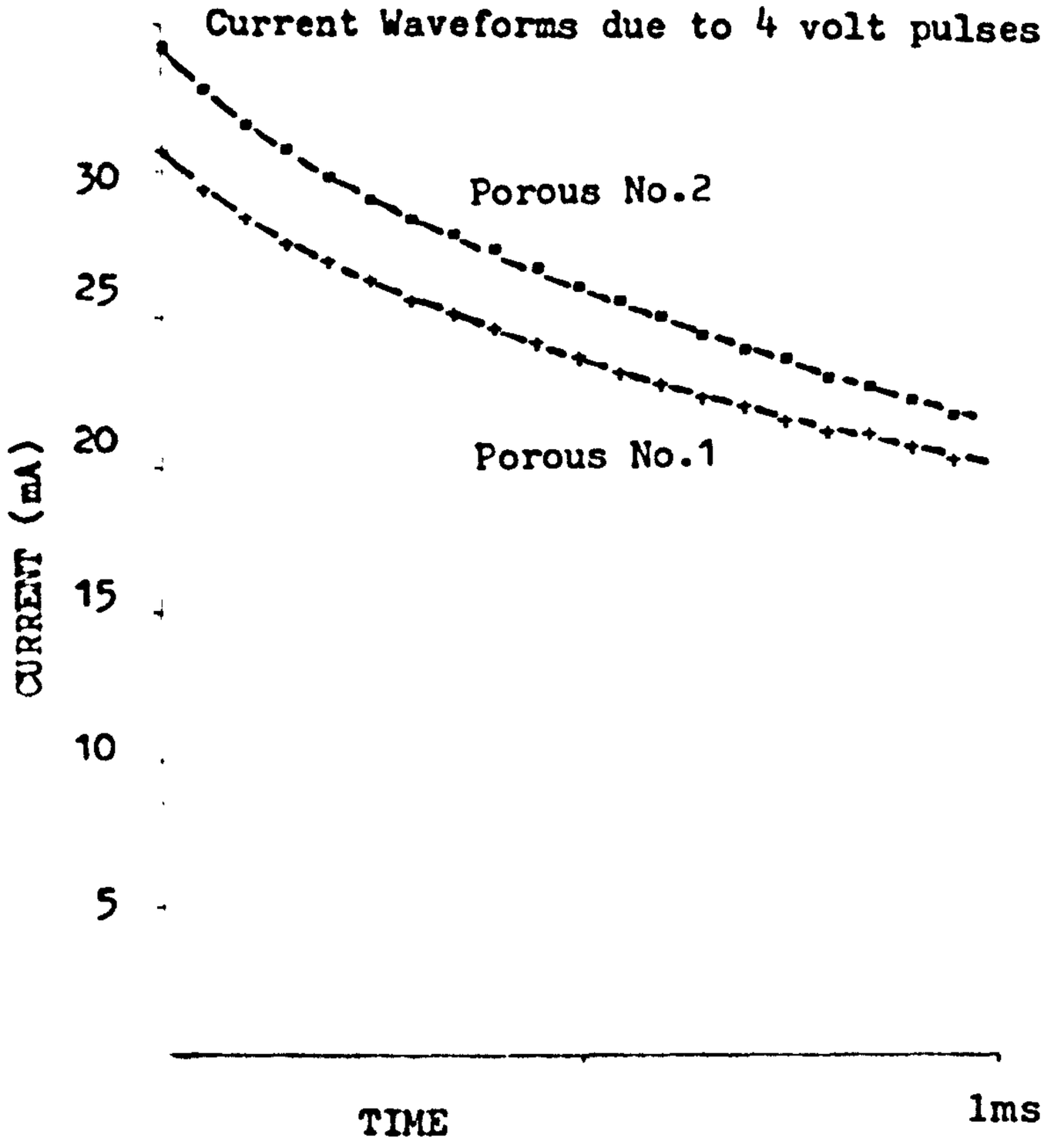

Figure 5.17e

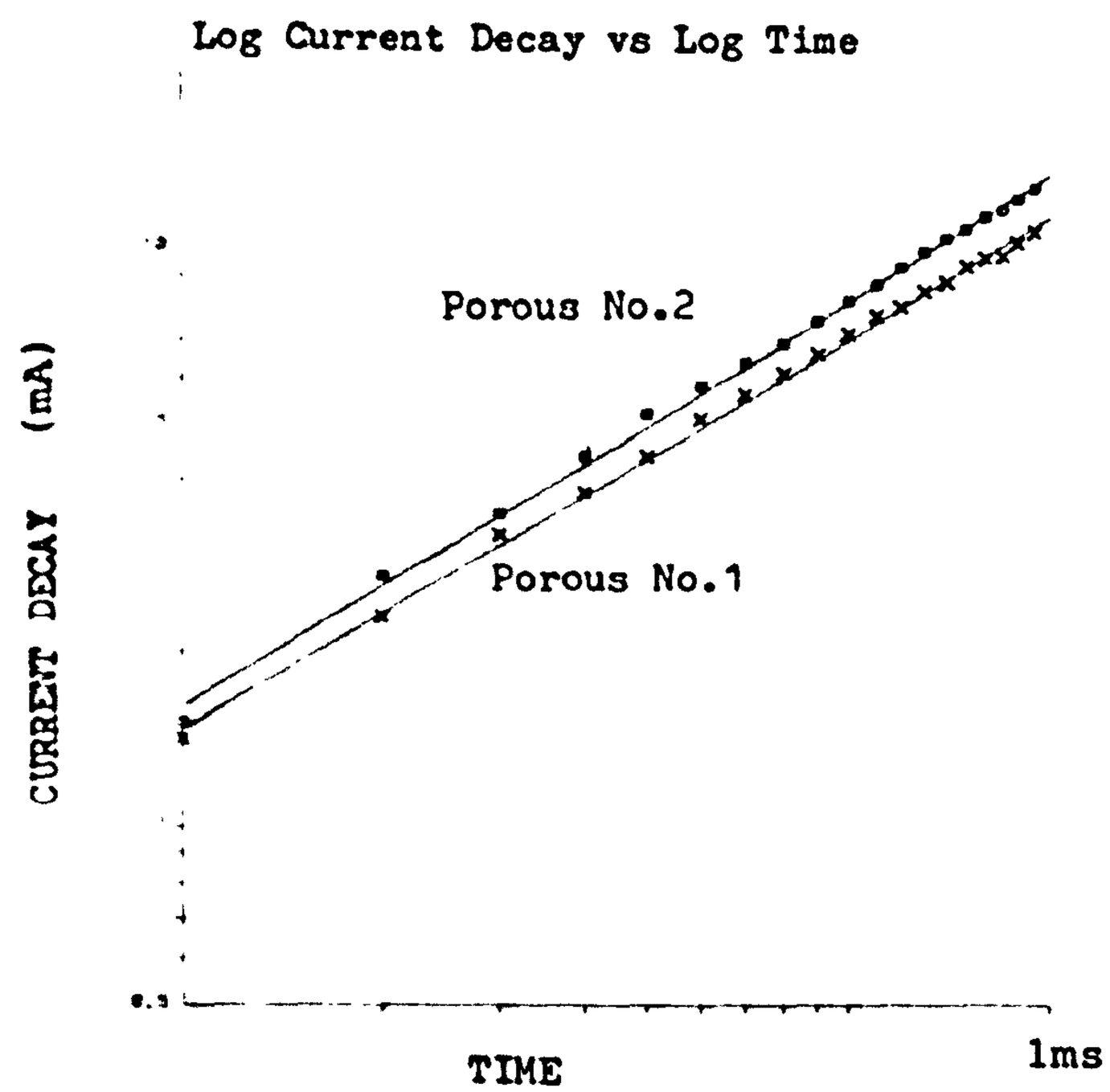

Figure 5.17f

and the Telectronic 224 electrodes. It can therefore be deduced that the S80 and A.V.C. electrodes have smaller values of 'K' and/or β than have the Devices LC and Telectronic electrodes.

It was observed that the current response of the A.V.Carbon electrode had almost decayed to its final value during the pulse duration (1msec). It can therefore be concluded that this electrode's response waveform has a very short "time constant", T_1, compared to the other electrodes. As the initial slope was found to be small, it was concluded earlier that the values of K and β are small. R_{CT} must therefore be relatively very small to give rise to a short time constant.

Similar comparative plots of current response waveforms for various electrodes have been carried out by Ripart and Mugica (1983) amongst others. Voltage response waveforms have been compared by Greatbatch and Chardach (1968) and Ripart and Mugica (1983).

As the parallel resistance, R_{CT}, and hence the time constant, T_1, is relatively very small for the A.V.Carbon electrode, the voltage response is often observed to reach its final value well before the end of the applied pulse duration. The Z_{CPA} controlled voltage rise may even be so short that the response appears to be a perfect square wave, ie that due to a purely resistive load, R_{TOT} (Richter et al, 1979; Mund et al, 1979).

This has lead several researchers to conclude that the activated vitreous carbon electrode is a

"nonpolarisable" one (ie $R_{CT} = 0$), which is not strictly correct as R_{CT}, although small, has a finite value.

- Decay Ratio

A possibly more objective method of comparing waveforms is to use the "Decay Ratio". The Decay Ratio, DR, has been defined as the ratio of the current amplitude after 0.5 msec to the peak amplitude, $i(t)_{max}$, (Sowton, 1967), where

$$i(t)_{max} = V_{dc}/R_{TOT}.$$

For a short pulse of duration, tp, the decay ratio is given by (using equation 3.17)

$$DR = \frac{V_{dc}\left[1 - \frac{K\ (0.5\times10^{-3})^{\beta}}{R_{TOT}\ \Gamma(1+\beta)}\right]}{V_{dc}/R_{TOT}}$$

$$= 1 - \frac{K\ (0.5\times10^{-3})^{\beta}}{R_{TOT}\ \Gamma(1+\beta)} \qquad 5.32$$

Hence, in most cases where the contribution of R_{CT} can be ignored over the limited time period of 0.5msec, DR increases when K and/or β increase. The DR is therefore a measure of the magnitude of K and β.

In table 5.6 the calculated values of Decay Ratio for each electrode are compared with their values of K and β. β in this case is the average of β_1 and β_2.

TABLE 5.6

Parameter	Electrode					
	Tel 224 no 1	Dev LC no 1	Dev LC no 2	S80 no 1	S80 no 2	AVC no 1
DR	0.86	0.8	0.86	0.79	0.79	0.71
K($k\Omega s^{-\beta}$)	26.2	23	21.4	11.9	22.7	7.5
β average	0.87	0.86	0.9	0.87	0.9	0.73

In general, electrodes with large values of K and β have current responses with large Decay Ratios. "Smooth" electrodes have therefore large DR's (.8-.86), with the porous S80 electrodes having smaller values (.79) and the very rough surfaced, AV Carbon electrode having the smallest value (.71). Hence the DR is a measure of the magnitude of the high frequency (short time) impedance of the interface and can be used as a measure of surface roughness effects. The technique would of course be more accurate if the applied voltage pulse had been a better square wave.

- Log [i_{decay}] - log (t) plots

After subtraction of the current due to R_{TOT}, V_{dc}/R_{TOT}, the log of the current decay was plotted against log of time for the above electrodes (figures 5.17 b, d and f).

A plot of log (i_{decay}) versus log t should have a slope of β for short times and should limit at

$$\frac{V_{dc}\ R_{CT}}{R_{TOT}\ (R_{CT}+R_{TOT})}$$

for long pulse durations (see figure 5.3). As the curve is dominated by Z_{CPA} at short times, the intercept on the y axis should be

inversely proportional to K, the magnitude of Z_{CPA}, as (using equation 3.40)

$$\log[i(t)-V_{dc}/R_{TOT}] = \log[AK/\Gamma(1+\beta)] + \log(t) \quad 5.33$$

where A is a constant.

As the applied voltage pulse is not a perfect square wave this method will only give qualitative results.

In table 5.7 values of β calculated from the slope are listed and the electrodes are numbered in order of increasing magnitude of "K" as estimated from the intercept.

TABLE 5.7

	Tel 224	Dev LC	Dev LC	Porous		V.C.
	No 1	No 2	No 1	No 1	No 2	No 1
β	.89	.77	.66	.68	.7	.58
"K"	6	5	4	3	2	1

As noted previously the A.V. Carbon is the 'best' electrode with the smallest impedance and phase angle. The impedance and phase angle increase for the Porous, Devices and Telectronic electrodes in that order.

The above results are in qualitative agreement with those obtained from the impedance plots.

It was noted that the A.V.Carbon electrode's log-log plot (figure 5.9b) showed signs of limiting towards the end of the pulse duration. This indicated that the A.V. Carbon electrode's time constant is relatively very short and, as the limiting value of current is quite large (figure 5.9a), R_{CT} must be very small.

5.2.4.3 Conclusions

- Technique accuracy

Transforming the transient data into the frequency domain enables more accurate analysis of the experimental results. The accuracy of direct methods would be improved considerably if the applied voltage pulse were a good square wave. This was not the case, and, as the waveform is load dependent, it therefore varied from one electrode system to another. The transform technique did not suffer from this problem as no assumptions were made concerning the applied voltage waveform - it was transformed along with that of the current response.

- Electrode nonlinearity

At large Voltage pulse amplitudes (4 Volts) the charge transfer resistance, $R_{CT(dc)}$, was found, as expected, to have decreased dramatically - to less than one percent of its linear small signal value.

K, although less nonlinear, decreased in a pseudo exponential manner with Voltage. Electrodes with the highest linear values of K were found to be the most nonlinear. In general, however, rough surfaced electrodes still had lower values of K than 'smooth' ones and hence K can be used as a measure of surface roughness, even under large signal conditions.

β was observed to increase with applied voltage amplitude.

- Electrode comparisons

Of the electrodes tested the activated vitreous carbon electrode remained the 'best' at high voltage amplitudes, having the smallest values of K and β . "Smooth" surfaced electrodes generally have larger values of K and β than rough surfaced ones, though the differences are less pronounced than in the linear region.

5.2.5 Discussion

In pacing one requires an electrode with an impedance which is as small as possible throughout the stimulus duration, which can be up to 1 ms (ie for frequencies above 1kHz). In this high frequency, large signal region the interfacial impedance is indeed generally very small (about 10 or 20 Ω) compared to that of the series resistance, R_{TOT}. Hence, surprisingly, the most important parameter to be minimised is R_{TOT} and not Z_{CPA} or R_{CT} whose contributions in this region are almost negligible. The electrodes tested can therefore be assessed in these terms.

R_{TOT} is the series combination of R_{LEAD} and R_{SALINE} (or R_{TISSUE}). R_{LEAD} depends on the wire material and its length whereas R_{SALINE} (or R_{TISSUE}) depends on the resistivity of the electrolyte and on the radius of the electrode, ie

$$R_{SALINE} = \rho/4\pi r \qquad 5.34$$

where ρ is the electrolyte resistivity and r is the

electrode radius.

The values of R_{TOT}, R_{LEAD} and R_{SALINE} measured for the electrodes throughout this work are listed on table 5.8.

From figure 5.17 one can see that the electrodes with the smallest values of R_{TOT} allow the largest currents to flow through the electrode-tissue system and would hence appear to stand most chance of effectively stimulating the heart. Using only this criteria one would have to conclude that the vitreous carbon electrode (Siemens-Elema 4115) is a rather poor one.

However, one also requires that as little energy as possible be wasted in the lead resistance, R_{LEAD}, and as much energy (i^2R) as possible be dissipated across R_{SALINE}.

For a constant current generator it is therefore desirable that the ratio R_{SALINE}/R_{LEAD} be as large as possible. This can be achieved by either increasing R_{SALINE} or decreasing R_{LEAD}.

Unfortunately increasing R_{SALINE} also increases R_{TOT} and hence decreases the current flowing through the electrode system when a constant voltage source is used. The maximum energy delivered to R_{SALINE} in this case is found by differentiating the equation

$$E = V^2x/(1+x)^2R_L$$

where E = Energy $R_L = R_{LEAD}$ $x = R_{SALINE}/R_{LEAD}$ 5.35

The maximum occurs when $x = 1$ ie when $R_L = R_{SALINE}$ (or R_{TISSUE}) and $Energy_{max} = V^2/4R_L$ 5.36

TABLE 5.8

Electrode	$R_L(\Omega)$	$R_{SALINE}(\Omega)$	$R_{TOT}(\Omega)$	$E_{SALINE}(J)$
-Devices				
LC($12mn^2$)No1	39.3	69	108	0.094
long lead No 2	55	61	116	0.072
-Devices				
SC($21mm^2$)No1	139	39	178	0.02
No2	140	43	183	0.021
Short lead No3	95	36	131	0.033
Tel. 224				
($10\ mm^2$) No1	86	86	172	0.046
No2	87	77	165	0.046
-Medtronic				
6917A($6.6mm^2$)	9	50	59	0.228
-Vitatron				
Helifix($23mm^2$)	125	39	164	0.023
-Sorin S80				
($8mm^2$) No1	53	87	140	0.071
No3	52	79	131	0.074
-A.V. Carbon				
($12mm^2$)	135	35	170	0.019

Hence it is desirable that R_{SALINE} and R_{LEAD} be equal and as small as possible. If R_{SALINE} is fixed by other influences, R_L should be as small as possible.

Using equation 5.35, the energy (neglecting the interfacial impedance) delivered to R_{SALINE} was calculated for each of the electrodes with V = 4 Volts. The results are listed on Table 5.8 under the heading E_{SALINE}. The 'best' electrode in this case is the Medtronic 6917A electrode due to its very small value of R_{TOT}. The 'worst' electrode is the vitreous carbon electrode as it has a very large value of R_L and only a very small (the smallest) value of R_{SALINE}.

The above results were calculated based on in vitro resistance values and are not necessarily representative of in vivo conditions. According to Geddes and Baker (1967) the resistivity of cardiac muscle is approximately twice that of 0.9% saline whereas Fischler and Schwan (1981) set the ratio at approx 10. Hence the value of R_{TISSUE} can be between two and ten times that of R_{SALINE}. The amount of energy which would be delivered to R_{TISSUE} (neglecting the interfacial impedance) was calculated for the vitreous carbon electrode assuming $R_{TISSUE} = 5xR_{SALINE}$. It was found that .029 Joules were now delivered to R_{TISSUE} - an increase of 153%. However, inspite of this improvement, the V. Carbon electrode was still one of the "worst".

The increase in R_{TISSUE} to a value more comparable with that of R_{LEAD} increased the energy delivered to R_{TISSUE} for the V.C. Electrode. If one also decreases

the lead resistance, R_L, to 60Ω for example, the energy will be further increased to .051 J A decrease in R_L to 20Ω will cause the energy to increase to .082 Joules, making the vitreous carbon electrode one of the 'best' electrodes.

Hence to improve the performance of this electrode, the value of R_L should be decreased as much as possible.

When R_L and R_{SALINE} (or R_{TISSUE}) are very small the energy 'wasted' by the interfacial impedance may become significant. This 'waste' can be minimized by making the interfacial impedance as small as possible. Of the electrodes tested the vitreous carbon electrode is the 'best' in this respect with the smallest values of R_{CT} and K. If $\beta = 1$, the energy delivered to Z_{CPA} is recovered during the pulse-free phase and hence prolongs the life of the generator (Mund et al, 1977). However, at present the most important consideration is to maximise the energy delivered to R_{TISSUE} which requires K to be as small as possible, the value of β being relatively unimportant. Also, any effort to decrease K (such as surface roughening) will also decrease β.

It is interesting to note that Mund et al (1976, 1977, 1979) compared the "mean power consumption" of the interface impedance (as measured in the linear region) of their electrodes and ignored the "power consumption" of the lead and saline/tissue resistances which the author believes is more important, and less favourable to Mund et al's electrodes.

The magnitude of $R_{CT(dc)}$ is important as it effects the recovery of the electrode system after the removal of the applied pulse. It was shown in section 5.1.3 that if the electrode system is not able to recover between stimuli, the system is driven into nonlinear behaviour. This will be minimised or avoided if the system's time constant, and hence $R_{CT(dc)}$, is as small as possible.

It is also desirable to inject charge via the nonfaradaic, Z_{CPA} impedance and avoid as far as possible faradaic processes which may generate toxic by-products. In this case it would therefore be advantageous if the system's time constant is sufficiently large to avoid or minimise the flow of faradaic charge throughout the duration of the stimulus pulse.

The above conditions can be met by chosing an electrode which has suitable values of K and $R_{CT(dc)}$ under large signal, transient conditions.

- Other important parameters

There are several others interrelated factors which make an electrode a 'good' one.

Biocompatability - Vitreous carbon is well known to be inert to body tissue (Kingma, 1977; Elmqvist et al, 1983) whereas platinum has been known to cause tissue damage (Mortensen and Bojsen, 1982).

Voltage and current thresholds - These are required to be as small and as stable as possible to enable economic stimulation. The thresholds increase

with fibrotic growth, and, as carbon gives rise to the least fibrotic growth, it has the most stable thresholds with relatively little increase with time (Elmqvist et al 1983). According to Mund et al (1979) carbon also has one of the lowest initial thresholds.

Electrode area - It has been found that reducing the surface area (ie increasing the ratio R_{TISSUE}/R_{LEAD}) decreases the current and voltage stimulation thresholds and consequently minimizes the energy demand on the pulse generator (Ripart and Mugica, 1983). However as pointed out above, increasing R_{TISSUE} beyond R_{LEAD} will increase the voltage threshold. Also, decreasing the electrode area increases the interfacial impedance which will eventually increase the thresholds. This can be overcome by using small, rough surfaced electrodes which minimise both thresholds and Z_{CPA} (ie using porous or activated vitreous carbon electrodes).

Thickness of Fibrosis - Fibrotic growth increases the chronic thresholds by increasing the distance between the electrode and excitable tissue and hence should be avoided as much as possible. Ripart and Mugica (1983) showed that when fibrosis occurred, effects due to original surface area became insignificant and that fibrosis thickness was the dominant factor in chronic thresholds. Fibrotic tissue grows due to mechanical irritation and chemical interaction (Elmqvist et al 1983). An electrode which is well fixed to the heart wall (eg porous electrodes) will minimise movement and mechanical irritation. On

the other hand the vitreous carbon electrode is well known for its biocompatibility and should give rise to little or no chemical interaction and hence little fibrotic tissue growth. The activated vitreous carbon electrode is therefore good on both points. Tests have shown that the vitreous carbon electrode gives rise to the least fibrosis (Elmqvist et al, 1983) and to the smallest percentage rise in chronic current threshold (Mund et al, 1979).

Good fixation - Rough or porous electrodes are held firmly to the heart wall by initial fibrotic tissue in growth. The lead when firmly positioned minimises trauma to heart tissue, and further growth of fibrosis or electrode dislodgement which can lead to pacing failure.

Summary

The activated vitreous carbon electrode appears to be ideal - low fibrotic growth, low stable thresholds, small area, rough surface, biocompatable and small interfacial impedance. However the electrode tested (Siemens-Elema 411S) had too large a lead resistance to enable "economic" stimulation. Presumably this is not the case for all such electrodes on the market.

In chapter 6 the impedances of electrode failures will be investigated in the linear and nonlinear regions.

Chapter 6

Impedance of Electrode Failures in the linear and nonlinear regions

Introduction

There are generally two major sources of electrode failure.

(i) The lead insulation may rupture and thus provide an alternative pathway for the generator output, in parallel with that of the electrode tip. In this case the overall impedance of the lead will decrease. With a voltage-source generator the second pathway allows an additional current through the body but with a current-source generator the pathway competes for some of the limited available output. When the 'active' cardiac electrode is bypassed, the reduction in current may result in failure to stimulate (Hepburn, 1979).

(ii) The lead wire may fracture due to metal fatigue. Where the break is dry and complete, current flow through the lead is prevented. If the dry break makes intermittent contact, the decrease in current will usually fluctuate between slight and complete. This can even happen within the duration of the pulse, causing apparent reduction in artefact duration and ragged shape (Hepburn, 1978; Davies et al, 1969). When the break is bridged by body fluid, the load increase will not be so marked.

The key to interpreting the experimental results for the two kinds of failure studied in this chapter is in understanding the form of the lead wire-electrolyte interfacial impedance. When the lead insulation ruptures, the above impedance is in parallel with that of the electrode tip. When the lead wire fractures,

the electrode tip impedance is in series with two such impedances.

As shown in section 1.2.3.2.2 the impedance locus of an exposed lead wire is similar in form to that of a very rough surfaced electrode. It was suggested that this effect is due to the coiled wire behaving somewhat like a porous surface.

At high frequencies, therefore, the lead wire interface impedance will be small in magnitude and have a phase angle of around 45°. At lower frequencies the impedance magnitude and phase angle should increase.

For a break in insulation the total impedance will decrease relative to that of an intact electrode and the phase angle will decrease.

For a break in the lead wire, the total electrode impedance will increase relative to that of an intact electrode and the phase angle will decrease.

In section 6.1 the electrical impedances of insulation breaks are studied and their effect on the total lead impedance described. After a description of the experimental set-up (section 6.1.1) the above impedances are initially studied in the linear region (section 6.1.2) and then in the nonlinear region (section 6.1.3) in order to determine the relevence of the linear small signal measurements to pacing applications.

The electrical impedances of wire fractures and their effect on the total lead impedance are studied in Section 6.2. Section 6.2.1 describes the experimental set-up. In Section 6.2.2 the impedances

are studied in the linear region, while in 6.2.3 they are investigated in the nonlinear region using pacing pulses.

Section 6.3 is a summary of the experimental findings.

6.1 Electrode Failure due to Ruptured lead insulation

6.1.1 Experimental arrangement

The impedance measurements in the linear and nonlinear regions were carried out as previously described in Chapters 1,2,3 and 5.

Initially, the impedance of an intact lead was measured and the measurement repeated on the same lead after its insulation sheath had been ruptured by a sharpe blade (eg Devices SC(no 1) electrode, Section 6.1.2A). With this arrangement, however, it was difficult to define accurately, or vary, the exposed area of the lead wire.

To overcome these problems the electrode set-up illustrated in figures 6.1.B to 6.1.D was used. Sections of the lead insulation were completely cut away (b and d). The insulation left between the two removed portions (c) formed a movable sleeve enabling the variation of the exposed area of lead wire (b). The overall impedance of the electrode was therefore due to the parallel combination of that of the electrode tip, $Z_{E.T.}$, and that due of the insulation break, $Z_{I.B.}$

ELECTRODE INSULATION RUPTURE

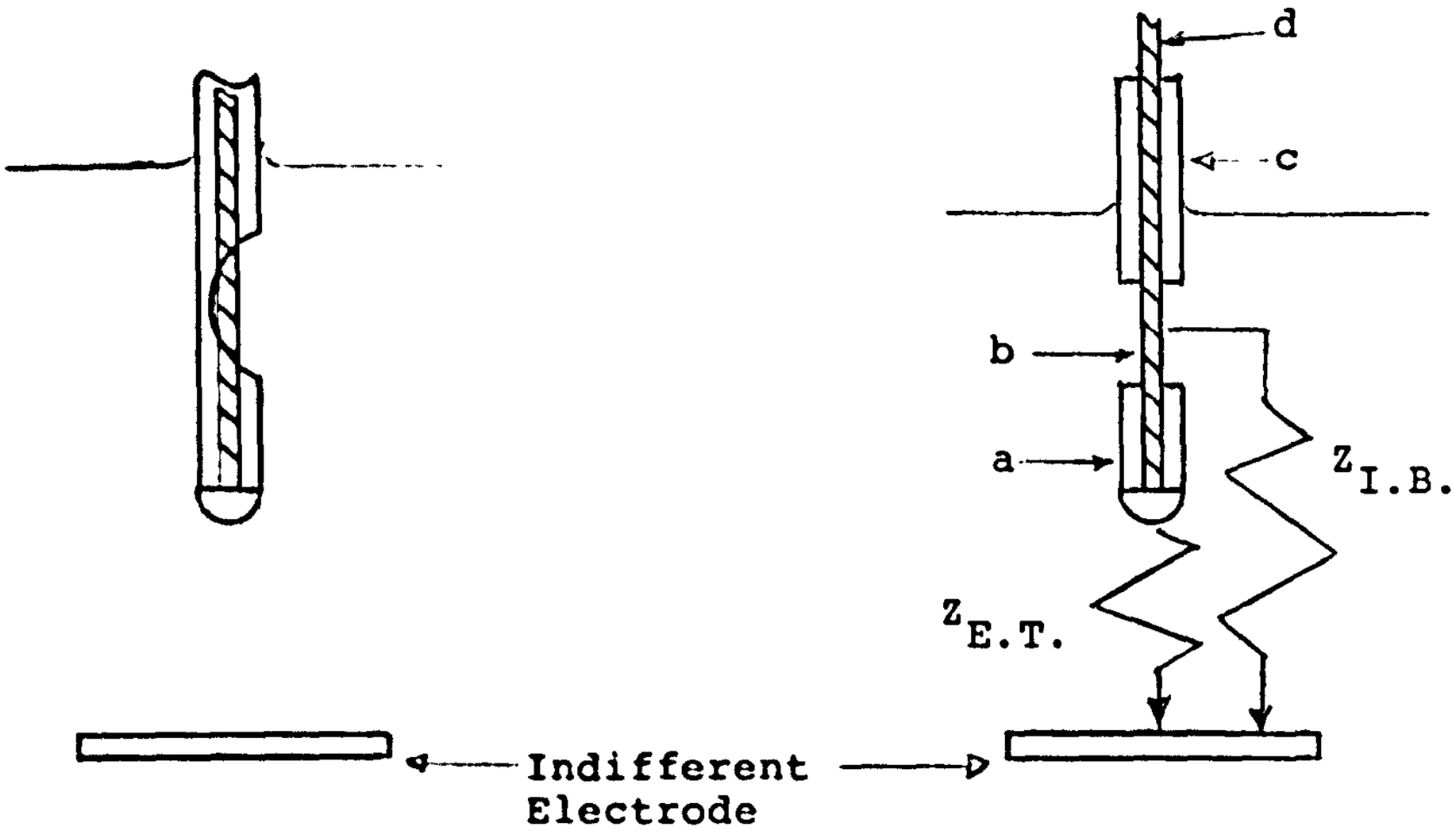

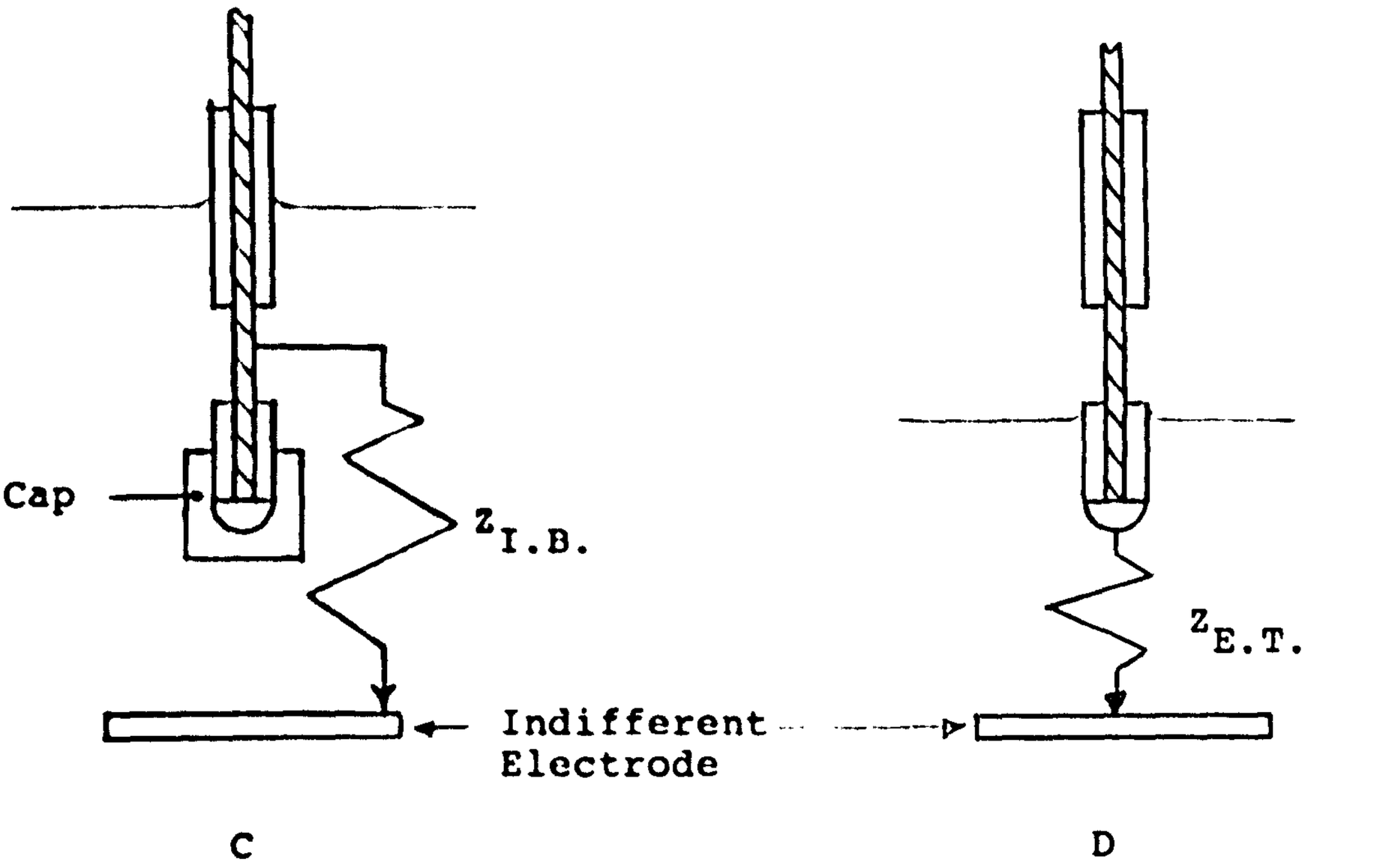

Figure 6.1

6.1.2 Linear Impedance Results

Linear impedance measurements were carried out in both the high and low frequency regions as described in chapters one and two.

6.1.2.A Linear High Frequency Impedance Results

These experiments were carried out on the Devices SC ($21mm^2$ no 1) electrode (figure 6.1.A). The exposed area of lead wire was approximately 1/2 cm^2. The measurements were initially carried out using the Wein Kerr Bridge and later repeated using the Solartron 1250 FRA. Both sets of results are presented below.

- Wein Kerr Bridge measurements

The experimental results are listed on Table 6.1.

TABLE 6.1

	R_{TOT} (Ω)	K ($k\Omega\, s^{-\beta}$)	β_1	β_2
Z_{ET}	180	149	0.9	1
Z_{IB}	233	19.2	0.49	0.5
Z_{TOT}	167	46.6	0.74	0.85

- Solartron 1250 measurements

The experimental results, carried out several months after the Wein Kerr measurements, are listed on Table 6.2

TABLE 6.2

	Exp no	R_{TOT} (Ω)	K ($k\Omega\, s^{-\beta}$)	β_1	β_2
Z_{ET}	53B	178	52.1	.86	.83
Z_{IB}	55	245	10.8	.53	.52
Z_{TOT}	54	166	18.8	.73	.74

The above results are plotted on figure 6.2.

A noticeable decrease in the impedance magnitudes has taken place between the Wein Kerr measurements and those obtained several months later using the Solartron 1250 FRA. This stresses the importance of electrode history on impedance measurements. Relative changes in the impedances are, however, the same. Once the importance of electrode history was appreciated, the electrodes were regularly ultrasonically cleaned. This was found to minimise the above problem.

It is noted (figure 6.2) that the impedance locus of the exposed lead wire, $Z_{I.B.}$, is concave. It was shown in earlier chapters that a wire coil behaves like a porous surfaced electrode.

At high frequencies the form of the over all electrode impedance, Z_{TOT}, is dominated by that of the electrode tip, Z_{ET}. As the frequency is decreased, however, the impedance of Z_{TOT} deviates from Z_{ET} behaviour and approaches that of the insulation break, Z_{IB}.

This behaviour can be explained if one approximates the above impedances by $Z_{CPA's}$ as on Table 6.2.

Letting $Z_{ET} = K(j\omega)^{-\beta}$

and $Z_{IB} = A(j\omega)^{-c}$

the total electrode impedance, Z_{TOT}, due to the parallel combination of Z_{ET} and Z_{IB} is given by (neglecting the series resistances, R_{TOT})

$$Z_{TOT} = \frac{K}{(j\omega)^{\beta} + n(j\omega)^{c}} \qquad 6.1$$

where $n = K/A$

As c is generally smaller than β, and A is generally smaller than K, at frequencies below $\omega_1 = n^{(1/\beta - c)}$ the total impedance is dominated by (though smaller than) that of the insulation break, Z_{IB}. This behaviour is observed on figure 6.2.

6.1.2 B Linear Low Frequency Impedance Results

The low frequency measurements were carried out on a Telectronic 224(no 1) electrode with an exposed lead wire portion 1cm long. The results are plotted on figure 6.3 and the calculated parameter values are listed below in Table 6.3.

TABLE 6.3

	Exp no	K ($k\Omega\, s^{-\beta}$)	β_1	β_2	R_{CT} ($k\Omega$)
Z_{ET}	42	89	0.72	-	671
Z_{IB}(1cm)	46	60.8	0.635	.63	-
Z_{TOT}(1cm)	43	28.2	0.57	.58	-

As the small series resistance, R_{TOT}, has little effect on the measured impedance results at such low frequencies, calculated values of R_{TOT} in this frequency range are very inaccurate and have therefore

Lead Insulation Failure

Dev.S.C.(No.1)

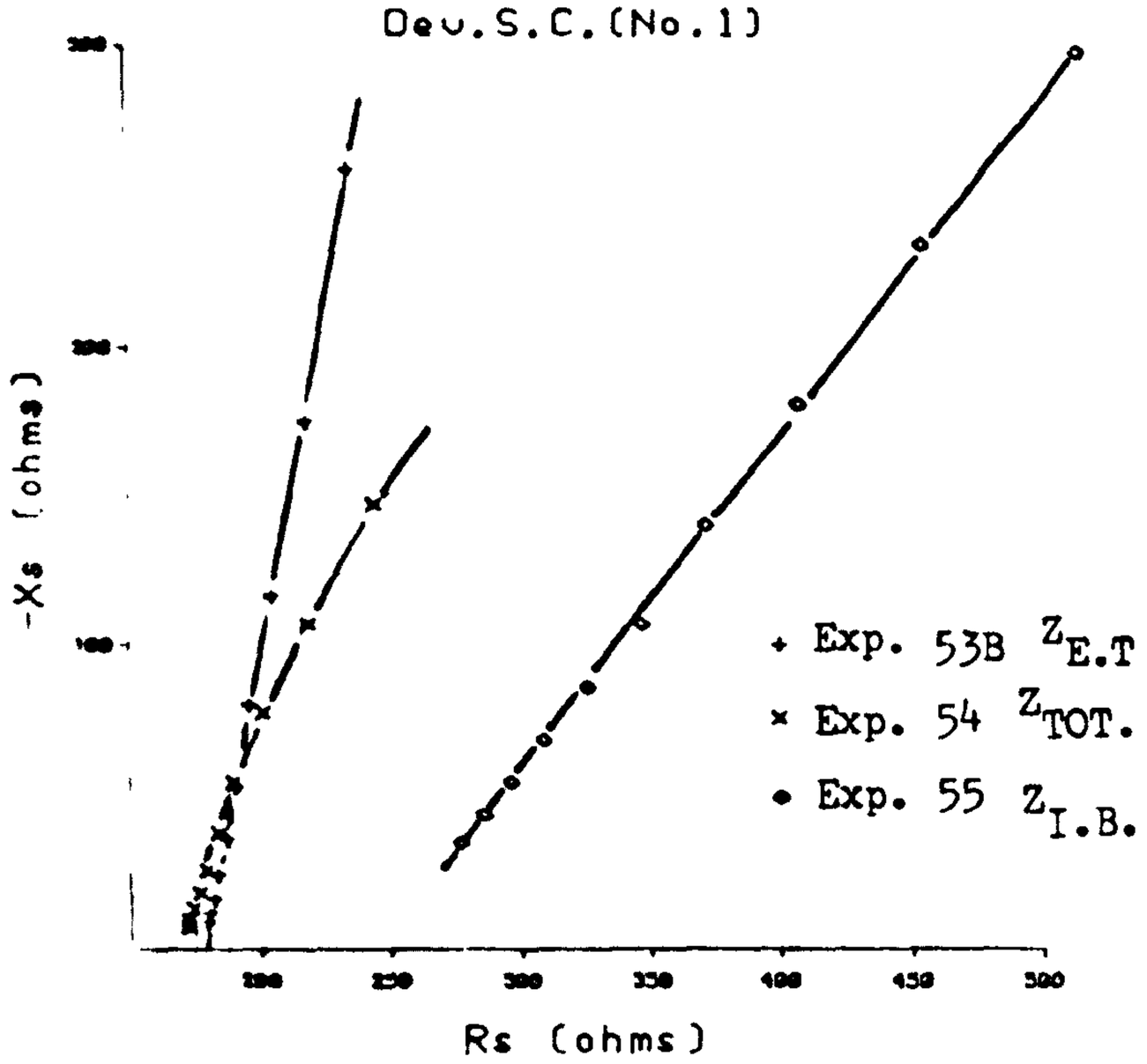

Figure 6.2

Lead Insulation Failure

1cm break in Insulation

Tel. 224 (No.1)

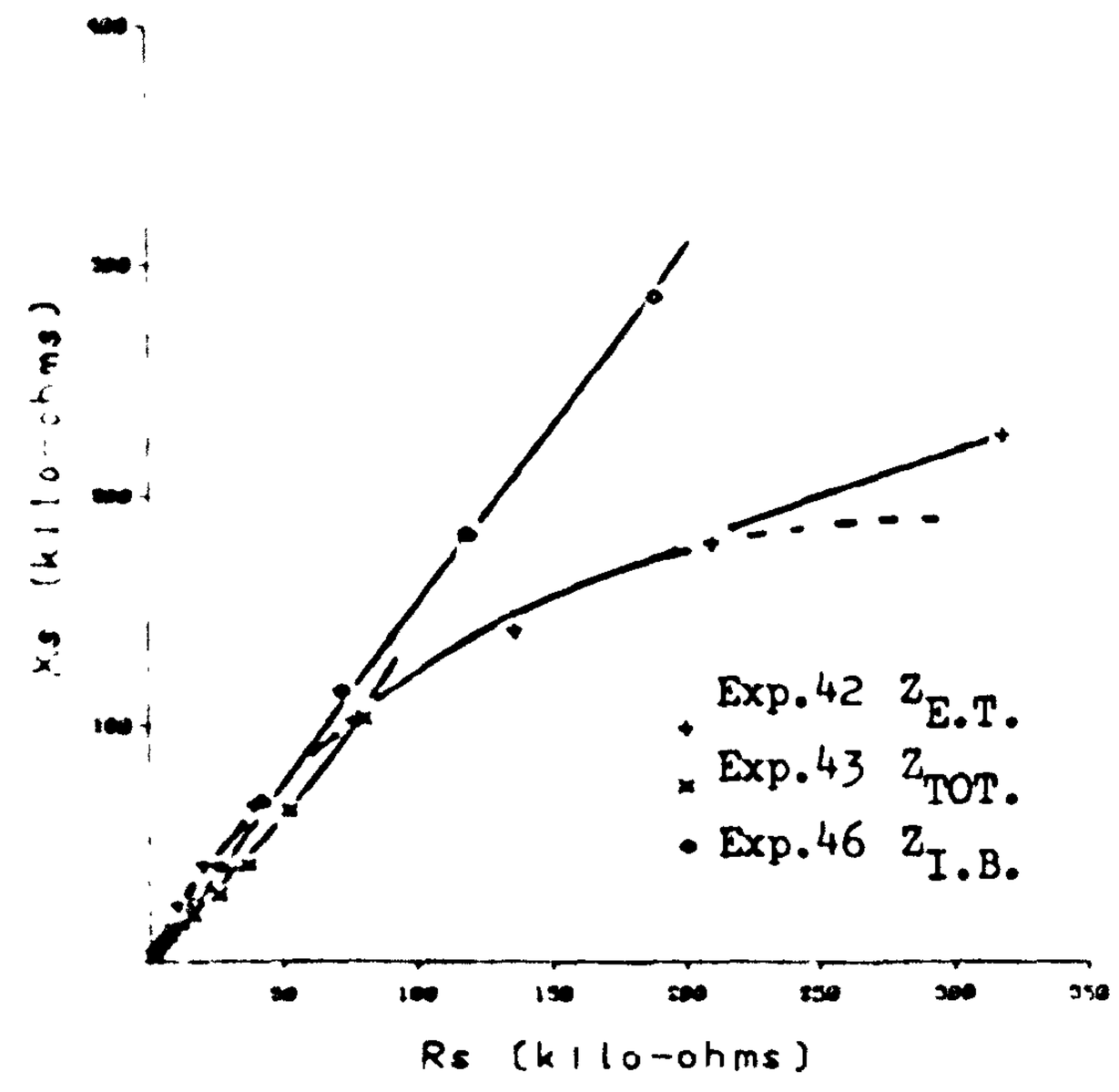

Figure 6.3

been ignored.

The "cross over" frequency, f', calculated from equation 6.1, was approximately $10H_Z$, and hence the overall electrode impedance, Z_{TOT}, is dominated by that of Z_{IB} in this low frequency region. This is evidenced by the low phase angle (β = 0.58) and the form of the impedance locus (figure 6.3). As the overall impedance is due to the parallel combination of Z_{IB} and Z_{ET}, it is smaller than either.

The above experiments were repeated for various lengths of break in electrode insulation.

For a 1/2 cm insulation break, the impedance Z_{IB} (Exp 47) is plotted on figure 6.4. The locus is now no longer a straight line, as was the case for a 1 cm break, and the magnitude and phase angle of the impedance have both decreased. Surface roughness effects appear therefore to dominate to lower frequencies with smaller insulation breaks.

The total lead impedance, Z_{TOT}, for a lead with a 1/2 cm break in insulation is plotted on figure 6.5. At low frequencies the impedance locus has the same form as that due to the insulation break, ie a concave curve. At higher frequencies the influence of the electrode tip's impedance (figure 6.3, Exp.42) is observed and the high frequency points form part of an arc.

For a 1/4 cm long insulation rupture, the impedance $Z_{I.B.}$, (Exp.48) is plotted on figure 6.4. Once again the locus deviates from a straight line, the form of the curve indicating surface roughness effects.

Effect of Insulation Break size
on the insulation break impedance, $Z_{I.B.}$

Tel.224 No.1

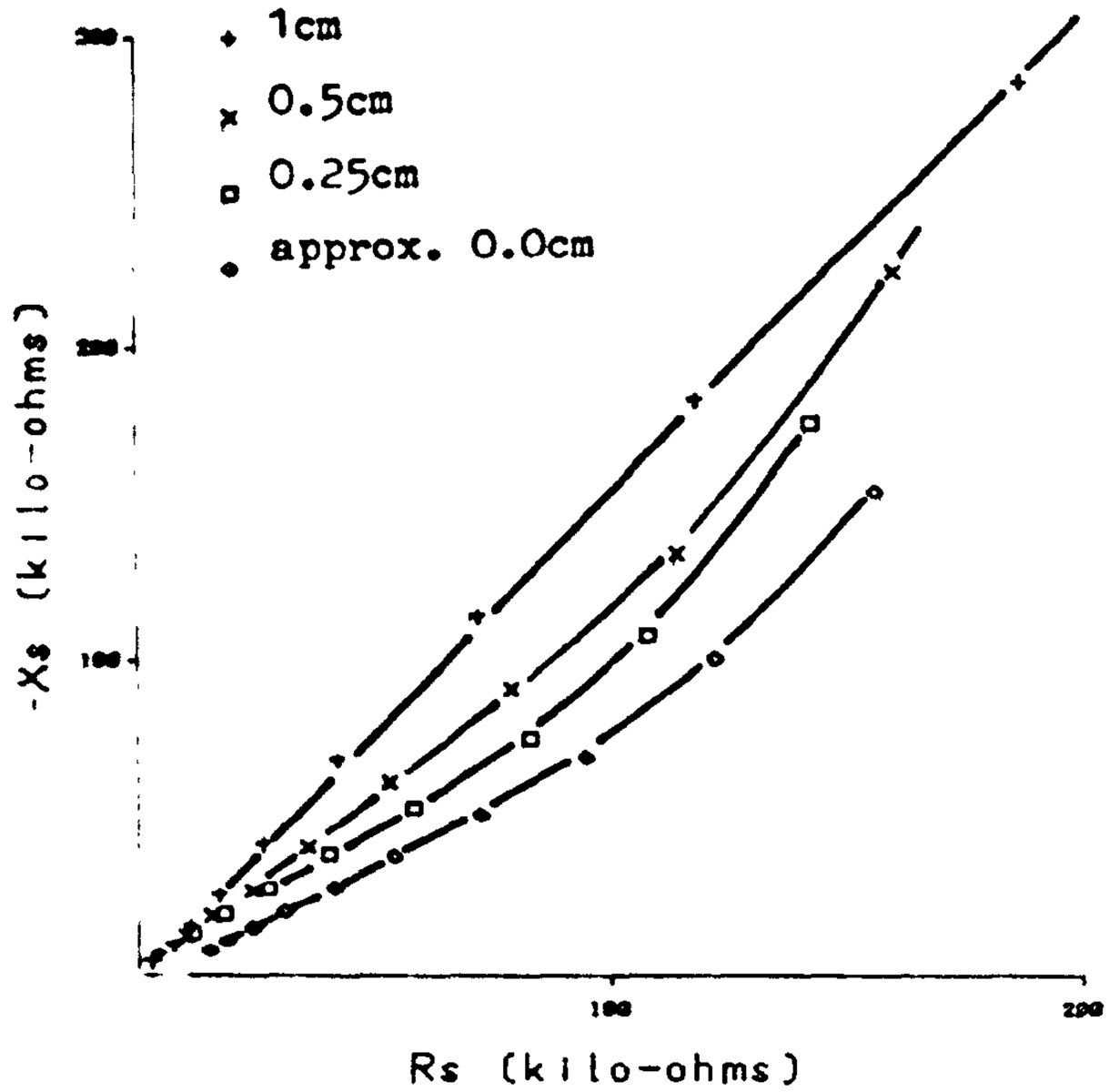

Figure 6.4

Effect of Insulation Break size

on Total Electrode Impedance, $Z_{TOT.}$

Tel.224 No.1

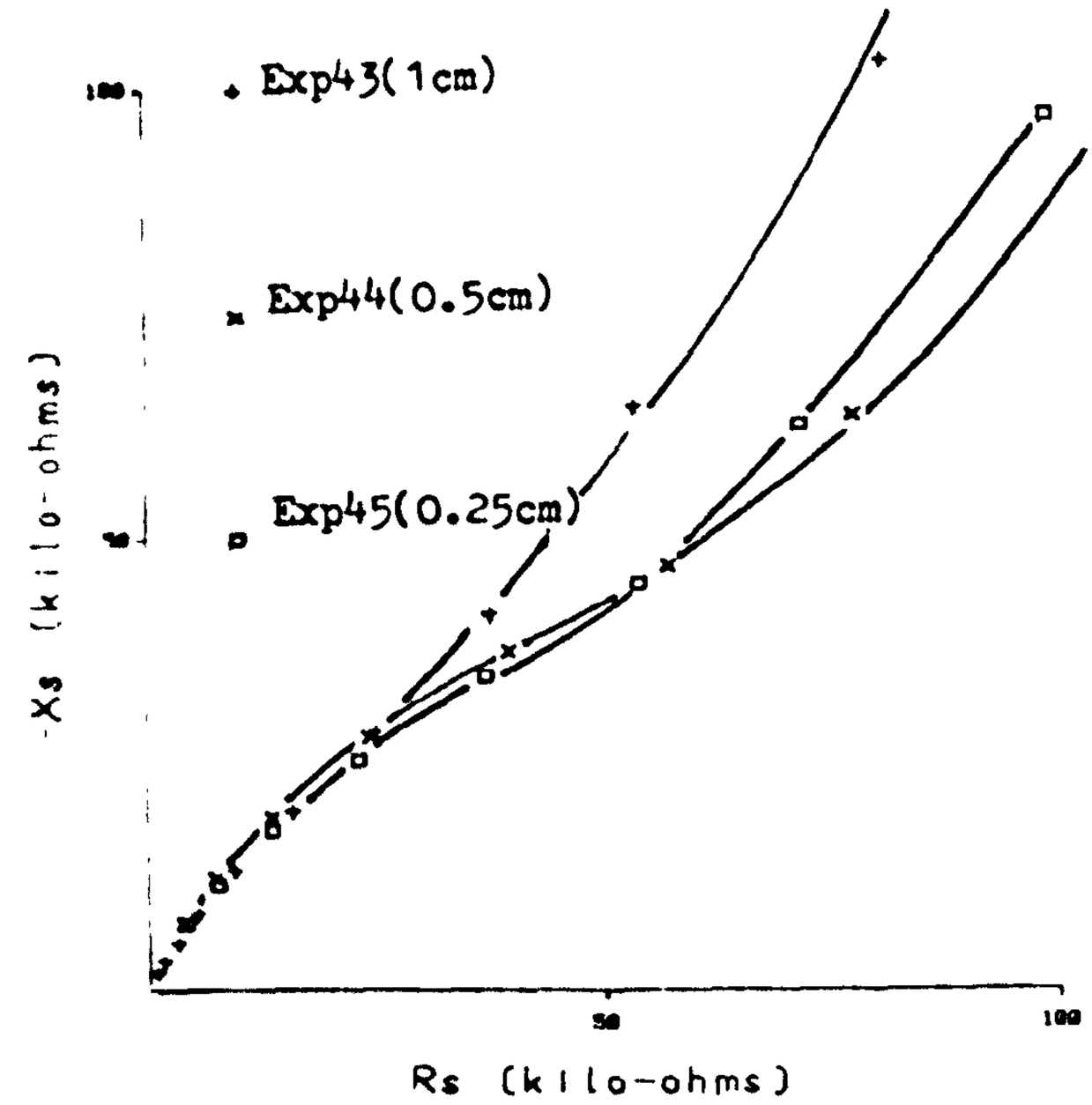

Figure 6.5

The total lead impedance, Z_{TOT} (Exp 45), for an electrode with a 1/4 cm long insulation break is plotted on figure 6.5. The very low frequency impedance is dominated by that of the insulation break, whereas, at high frequencies it is dominated by that of the electrode tip.

- Summary on the impedance of the insulation break, Z_{IB}.

The impedance of the insulation break is plotted on figure 6.4 for varying lengths of insulation breaks. As the exposed wire is coiled, the overall effect is one of surface roughness (section 1.2.3.2.3). When the exposed area is very small the 'pores' between turns in the coil are very large relative to the total exposed surface area. In this case (Exp 48, 1/4 cm exposed length) the surface appears to behave as a very rough one and the impedance locus is a characteristic concave curve. As the exposed area increases the 'surface roughness' effect becomes less pronounced at these low frequencies and the locus tends towards a straight line, as observed on figure 6.4

6.1.3 Nonlinear (Pulse) Impedance Results

The effect of voltage amplitude on Z_{ET}, Z_{IB} and Z_{TOT} was investigated using two different electrodes- the Devices SC (no1) electrode with an exposed lead wire length of approximately 1/2 cm and the Devices LC (no3) electrode where a range of exposed lengths was possible.

The experimental arrangement was as described in chapter 5.

A/ Devices SC electrode (no1)

The results were obtained using a 4 volt pulse and are listed below in Table 6.4

TABLE 6.4

	Exp no	R_{TOT} (Ω)	K ($k\Omega s^{-\beta}$)	β_1	β_2
Z_{ET}	75	181	23	0.84	0.87
Z_{IB}	85	257	18.3	0.72	0.78
Z_{TOT}	76	169	12.1	0.77	0.8

Comparing the nonlinear results with those obtained under 'linear' conditions (section 6.1.2.A.1) it is found that the values of R_{TOT} are very similar, K_{ET} has decreased to 15% of its linear value, whereas K_{IB} has only decreased to 95% of its linear value. As previously pointed out, impedances which are the largest in the linear region are also the most nonlinear and hence rough surfaced electrodes are found to have relatively linear impedances. Z_{ET} has now decreased to almost the same magnitude as Z_{IB}. Z_{IB}, however, still has a relatively low value of β .

The total lead impedance, Z_{TOT}, is now approximately half that of Z_{ET} or Z_{IB}, as it is due to their parallel combination. The values of β for the overall electrode impedance lie, as would be expected, between those for the electrode tip and insulation break impedances.

B/ Devices LC electrode no3

The experimental results are listed on Table 6.5 for an applied pulse height of 4 volts

TABLE 6.5

	Exp no	R_{TOT} (Ω)	K ($k\Omega\, s^{-\beta}$)	β_1	β_2
Z_{ET}	T29	112.6	12.1	.84	.85
Z_{IB}(1cm)	T33	115.3	17.7	.9	.89
Z_{TOT}(1cm)	T30	69.2	7.7	.84	.87
Z_{IB}(1/2cm)	T34	145.7	21.5	.89	.88
Z_{TOT}(1/2cm)	T57	95.9	11.9	.83	.88
Z_{IB}(1/4cm)	T35	190.7	22.1	.78	.83
Z_{TOT}(1/4cm)	T56	101.7	10.7	.82	.84

The experimental results for an applied pulse amplitude of 3 volts are listed in table 6.6.

TABLE 6.6

	Exp no	R_{TOT} (Ω)	K ($k\Omega s^{-\beta}$)	β_1	β_2
Z_{ET}	T67	107.1	22.4	.91	.92
Z_{IB}(1cm)	T64	112	25.5	.8	1
Z_{TOT}(1cm)	T61	86.3	9.6	.85	.84
Z_{IB}(1/2cm)	T55	143.4	30.5	.78	.89
Z_{TOT}(1/2cm)	T62	87.4	13.1	.85	.89
Z_{IB}(1/4cm)	T66	129.8	30.4	.79	.86
Z_{TOT}(1/4cm)	T63	90.2	12.8	.8	.86

- Z_{IB}

From the above tables (6.5 and 6.6) the effect of varying the size of insulation break can be seen. For

very small breaks (1/4 cm, Exp T35 and T66) the magnitude of the impedance, K, is very small due to surface roughness effects. As the break is increased in size (1/2 cm, Exp T34 and T55) the surface roughness effect decreases and the impedance increases. Increasing the break further to 1cm (Exp T33 and T64) causes the impedance to decrease. This is presumably due to the increase in area.

Z_{IB} was found to be relatively linear and at 4 volts had only decreased to approximately 70% of its 3 volt value.

Fitting the results to the exponential

$$K = a \exp(-bV),$$

it was found that

$K = 77\times10^3 \exp(-0.37V)\Omega s^{-\beta}$ for a 1 cm break

$K = 87\times10^3 \exp(-0.35V)\Omega s^{-\beta}$ for a 1/2 cm break

and $K = 79\times10^3 \exp(-0.32V)\Omega s^{-\beta}$ for a 1/4 cm break.

- Z_{ET}

The electrode tip impedance, Z_{ET}, was found to be very nonlinear and at 4 volts it was only 54% of its 3V value (compared to 70% for Z_{IB}).

It was calculated that

$$K = 142{,}000 \exp(-0.62V)\Omega s^{-\beta}$$

Note the large values of 'b' and 'a', both almost double those found for Z_{IB}. The electrode tip impedance is therefore larger in the linear region and is more nonlinear.

- Z_{TOT}

The magnitude of total lead impedance is, as expected, smaller than that of Z_{ET}. Z_{TOT}, like Z_{IB}, increases as the size of the insulation break is increased (1/2 cm, Exp T57 and T62) due to a decrease in the "surface roughness effect". Further increase in the size of the break causes a decrease in both Z_{IB} and Z_{TOT} (1 cm, Exp T30 and T61) due to the increase in exposed area.

Z_{TOT} is relatively linear as demonstrated by the small values of 'b' calculated from the experimental results.

$K = 19{,}100 \exp(-0.23V)\Omega s^{-\beta}$ for a 1cm break

$K = 17{,}500 \exp(-0.1V)\Omega s^{-\beta}$ for a 1/2cm break

$K = 21{,}850 \exp(-0.18V)\Omega s^{-\beta}$ for a 1/4cm break

- Example of an electrode failure

During the initial stages of the research, while carrying out transient experiments on a Devices LC electrode (no1), a break in insulation occured on the indifferent electrode lead. The wire had also corroded causing a partial break. The recorded results (Exp T5) are plotted On figure 6.6 for an applied voltage pulse amplitude of 4 volts.

The impedance locus is concave due to the impedance of the lead wire-electrolyte interface. Fitting the high frequency points to a series R_{TOT}-Z_{CPA} model gave the following parameter values.

$R_{TOT} = 870\Omega$ $K = 10.9\ k\Omega s^{-\beta}$

$\beta_1 = .49$ $\beta_2 = .5$

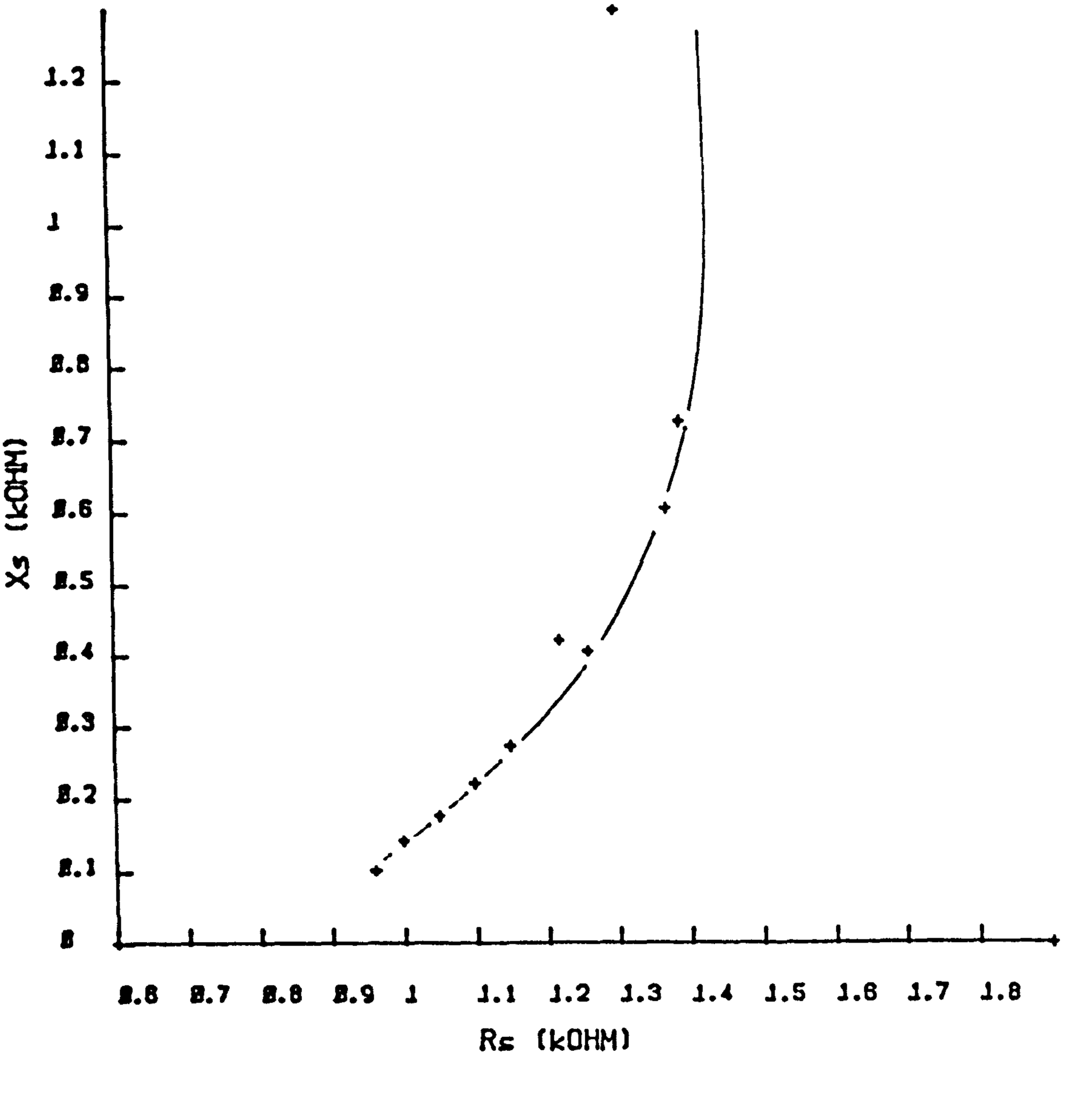

IMPEDANCE LOCUS OF FAILED ELECTRODE

Figure 6.6

These can be compared with the results obtained under the same conditions for an intact electrode (Exp T6)

R_{TOT} = 121Ω K = 23.9 kΩ $s^{-\beta}$

β_1 = .83 β_2 = .86

The break in insulation gave rise to a parallel path for current flow and hence decreased the magnitude, K, of the total lead impedance. The phase angle also decreased as expected. The series resistance, R_{TOT}, increased dramatically due to the corrosion of the lead wire. From the above results and using equation 6.1, the magnitude of Z_{IB} can be estimated at approximately 20kΩ $s^{-\beta}$, which is typical of a small break in lead insulation (see table 6.1).

6.2 Electrode Failure due to wire fracture

6.2.1 Experimental Set-up

In practice, wire fractures are often bridged by body fluids and thus current continues to flow through the electrode system inspite of the electrode failure. The body fluids enter the lead at the electrode tip or at a point where there is a rupture in the insulation. This may be some distance away from the position of the eventual wire fracture. In some instances the presence of such fluid causes the corrosion and fracture of the lead wire.

In our experiments an electrode lead was cut in two and the ends rejoined using a tight rubber sleeve, leaving a variable gap between the two segments of lead

"INTACT" ELECTRODE

LEAD WIRE FRACTURE

Indifferent Electrode

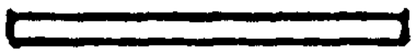

Saline filled gap

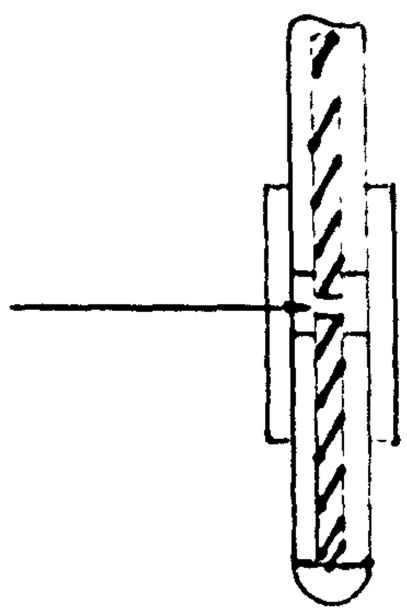

FAILED LEAD WITH "WET" FRACTURE

ELECTRODE WIRE FRACTURE

Figure 6.7

wire (figure 6.7). Prior to rejoining the two segments, the gap was filled with 0.9% saline to enable the flow of current, as found invivo. With this experimental set up it was possible to vary the width of the gap in the lead wire and observe its effect on the total lead impedance.

In order to measure the impedance due solely to the wire fracture, the electrode tip was connected directly to the measuring system thus avoiding the electrode tip-saline interfacial impedance. In order to measure the electrode tip's impedance, Z_{ET}, the two ends of the wire fracture were reconnected together, thus forming an "intact" electrode lead.

6.2.2 Linear Impedance of Fractured Leads

Linear measurements were carried out in both the high and low frequency ranges. The experimental arrangement was as described in chapters one and two.

6.2.2.A. Linear high frequency impedance of fractured leads

These high frequency linear measurements were carried out on a Telectronic 224 (no 2) electrode. The calculated parameter values are listed in table 6.7 and the impedance loci plotted on figure 6.8.

Effect of Wire Fracture

on Total Electrode Impedance

2mm saline filled break

Tel.224 No.2

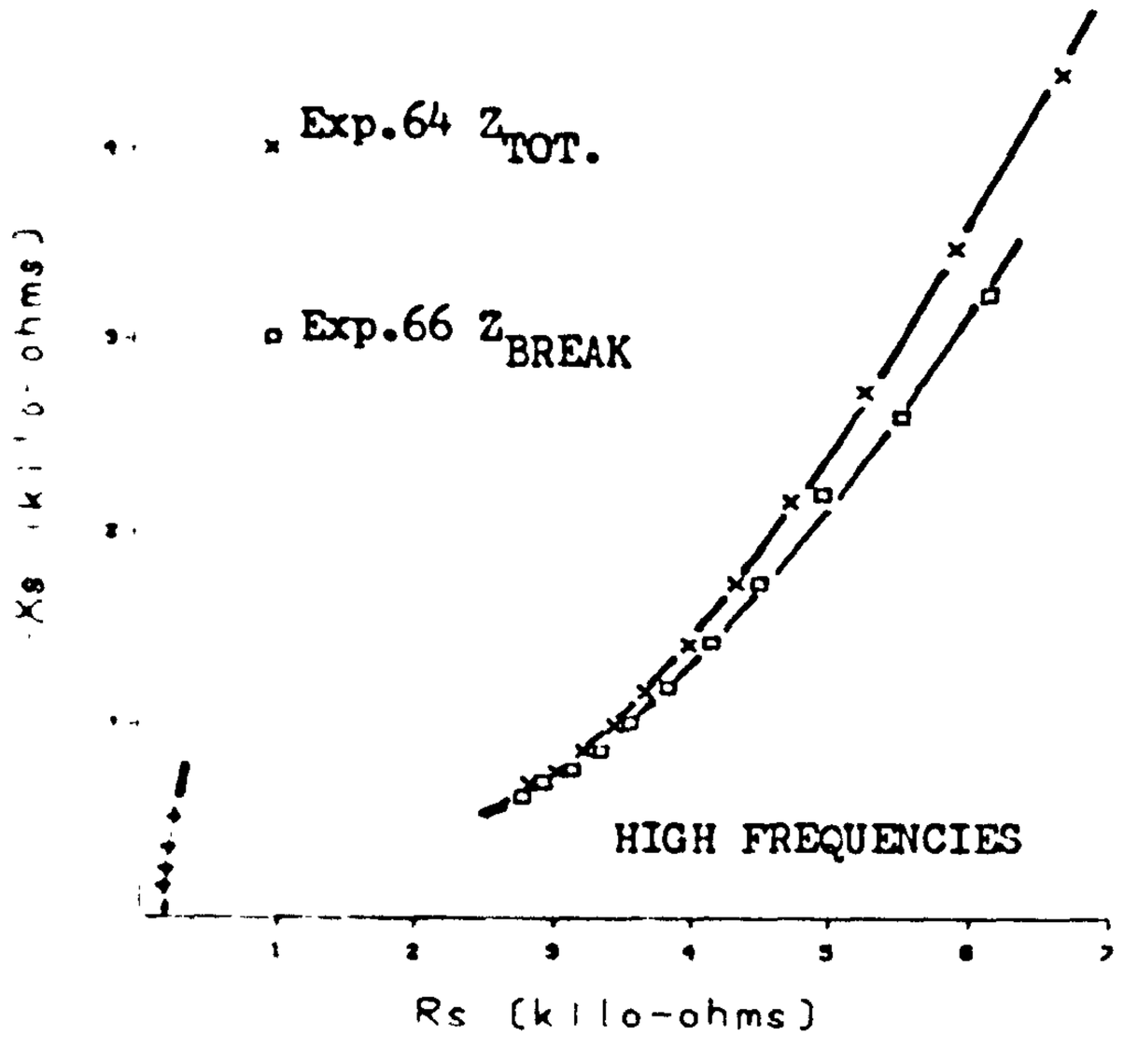

Figure 6.8

Effect of Wire Fracture

on Total Electrode Impedance

2mm saline filled break

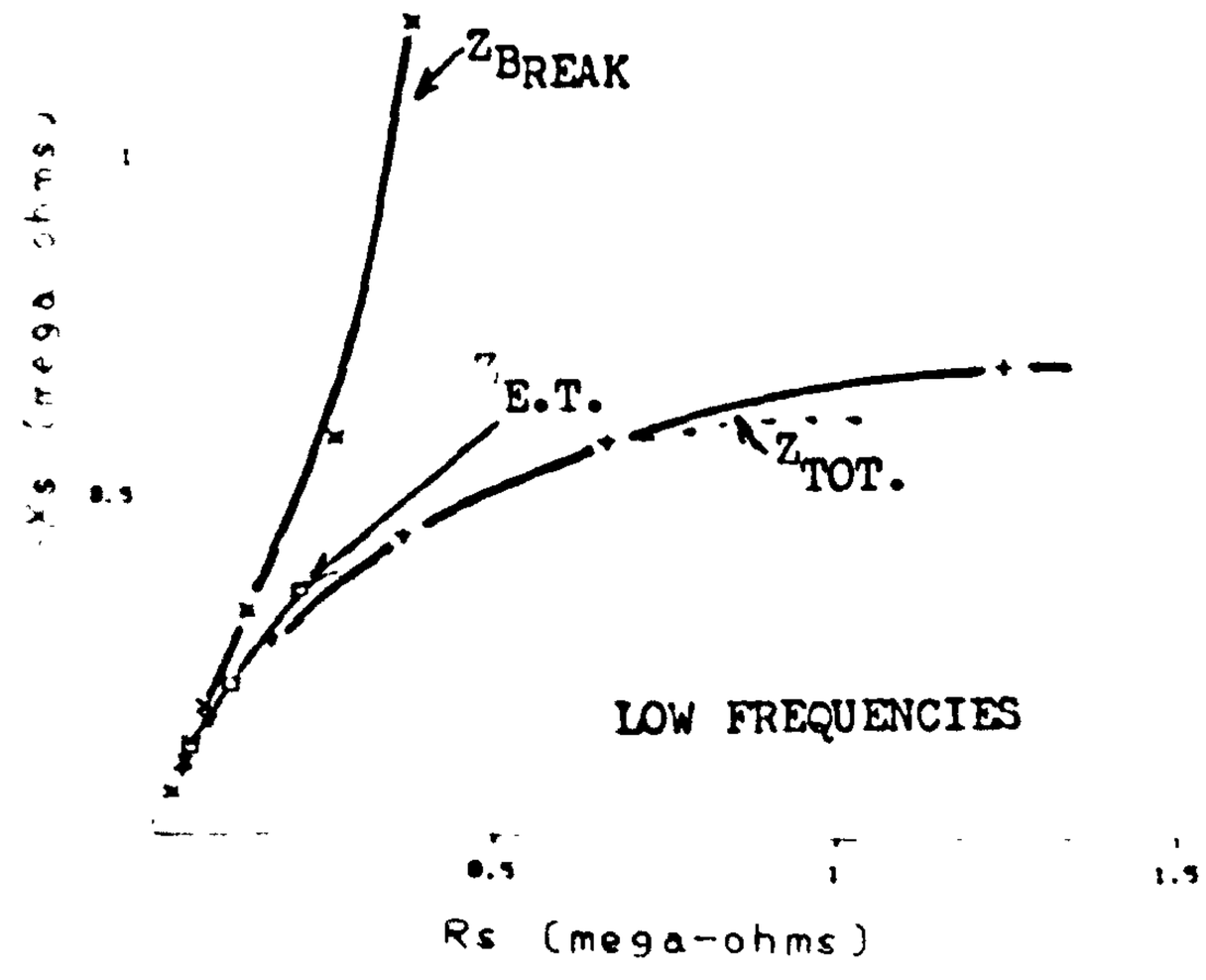

Figure 6.9

TABLE 6.7

	Exp No	R_{TOT} (Ω)	K ($k\Omega s^{-\beta}$)	β_1	β_2
Z_{ET}	50	164.5	121.6	.88	.84
			K_{HF} ($k\Omega s^{-\beta}$)		C_{LF} (μF)
Z_{BREAK}(2mm)	66	2.2K	65.2	.4	5.3
Z_{TOT} (2mm)	64	2.3K	68.0	.4	1.06

As the impedances of the electrode tip and the lead fracture are in series, the total impedance, Z_{TOT}, is simply the sum of the two, with the larger determining the form of the impedance locus.

At these high frequencies the total impedance is therefore dominated by that of the wire fracture as shown on figure 6.8.

The wire fracture impedance locus is concave (characteristic of surface roughness effects) and the results were therefore fitted to a series R_{TOT}-$Z_{CPA(HF)}$-C_{LF} model. The fit was not however very good but did enable comparison of Z_{BREAK} and Z_{TOT}.

6.2.2.B Linear low frequency impedance of fractured leads.

The low frequency, linear measurements were carried out on a Telectronic 224 (no 3) electrode. The impedance loci are plotted on figure 6.9 and the calculated parameter values are listed in table 6.8.

TABLE 6.8

	Exp No	K ($k\Omega s^{-\beta}$)	K_{HF} ($k\Omega s^{-\beta}$)	β	R_{CT} ($M\Omega$)	C_{LF} (μF)
Z_{ET}	74	101	-	.77	2.25	-
Z_{BREAK} (2mm)	67	-	228	.74	-	.3
Z_{TOT} (2mm)	65	430	-	.88	1.72	-

The overall electrode impedance is due to the sum of Z_{BREAK} and Z_{ET}. Z_{BREAK} has an impedance locus typical of a rough surfaced electrode. In this frequency range Z_{ET} makes a significant contribution to the overall impedance, Z_{TOT}, causing the latter to be a distorted arc (figure 6.9).

6.2.3 Nonlinear (Pulse) Impedance of wire fractures

The effect of the applied voltage amplitude on Z_{ET}, Z_{IB} and Z_{TOT} was investigated for two sizes of wire fracture using a Devices LC electrode (no4) and an applied voltage amplitude of 4 volts. The results are listed on table 6.9.

TABLE 6.9

	Exp No	R_{TOT} (Ω)	K ($k\Omega s^{-\beta}$)	β_1	β_2
Z_{ET}	T70	117	14.4	.85	.875
Z_{BREAK}(1mm)	T68	648	29.3	.64	.63
Z_{TOT}(1mm)	T71	1,500	69.6	.64	.59
Z_{BREAK}(2mm)	T69	928	48.4	.71	.68
Z_{TOT}(2mm)	T72	1,850	79.6	.65	.61

The total impedance, Z_{TOT}, in each case is dominated by the large series impedance due to the wire fracture, Z_{BREAK}. As the gap between the two wire ends increases, Z_{BREAK} and hence Z_{TOT} increases. Z_{BREAK} has a small phase angle due to the surface roughness effect of the coil and similar behaviour is observed for Z_{TOT}.

The impedance of one end of the lead wire was measured in 0.9% saline (Exp T25) and the following equivalent circuit parameter values were obtained

$$R_{TOT} = 160\Omega \qquad K = 15.1\ k\Omega\ s^{-\beta}$$

$$\beta_1 = 0.79 \qquad \beta_2 = 0.79$$

The impedance of a wire facture (comprising two wire-electrolyte interfaces in series) should therefore be approximately twice the above, ie $30k\Omega s^{-\beta}$. This was found to be the case for a break of 1mm.

6.3 Conclusions

As mentioned in the introduction, the interfacial impedance between the lead wire and the electrolyte is of major importance in the study of the two modes of electrode failure.

It was shown in section 1.2.3.2.3 that the impedance locus of a lead wire has much the same form as one for a rough surfaced electrode. At high frequencies the impedance and phase angle are very small. As the frequency decreases both these parameters increase in magnitude. These results have been confirmed in figures 6.2, 6.3, 6.4, 6.8 and 6.9.

- Insulation break

In figure 6.2 it was noted that the impedance of an insulation break dominates the total linear electrode impedance at low frequencies, whereas that of the electrode tip dominates at higher frequencies.

In the nonlinear region (section 6.1.3) the impedance of the insulation break is comparable to that of the electrode tip. In this region, therefore, the total electrode's impedance is approximately half that of the electrode tip and the phase angle is slightly less.

- Wire fracture

In the linear region the total electrode impedance of a fractured lead is dominated at high frequencies by that of the fracture. At low frequencies the electrode tip impedance dominates the form of Z_{TOT}.

In the nonlinear region the impedance of the fracture is larger than that of the electrode tip and its phase angle is smaller. The total electrode impedance is therefore dominated by that of the wire fracture.

CHAPTER 7

Diagnosis of electrode failure

- Introduction

The first part of the chapter is concerned with the in-vivo electrode-tissue interface impedance. It's characteristics are compared with those of the electrode-saline interface described earlier. The form of the impedances are found to be substantially the same, differing only in magnitude. Implications for pacemakers with load changes due to electrode failure are discussed in the second half of the chapter.

7.1 In Vivo Impedance

7.1.1. Theory

The principal cations in extracellular fluid are Na^+ (150mEq/litre), K^+ (4mEq/litre), Ca^{2+}(4.5mEq/litre) and Mg^{2+} (2mEq/litre)and the principle anions are Cl^- (103mEq/litre) and HCO^-_3 (26mEq/litre) (Mansfield, 1967; Donaldson and Donaldson, 1986). All the preceding experiments in this thesis were carried out in 0.9% physiological saline (154mEq/litre) and this obviously differs from body fluid/tissue. It is therefore very probable that invivo impedances will differ, at least in magnitude, from those measured in saline. In this section the probable differences in equivalent circuit parameter values between invitro and invivo conditions will be discussed.

- R_{TOTAL}

According to Greatbatch and Chardack (1968) the invivo impedance differs from that invitro

(physiological saline) only in that it has a larger value of series resistance, R_{TOTAL}, due to the increased resistivity of biological fluid. The above is not completely correct as other parameters in the equivalent circuit model are also effected, as will be shown later. The increase in resistivity of biological tissue relative to that of saline should indeed give rise to an increase in R_{TOTAL} as R_{TOTAL} is the sum of the series resistances R_{LEAD} and $R_{SALINE/TISSUE}$, where

$$R_{SALINE/TISSUE} = \rho / 4\pi r_o$$

(r_o is the radius of the electrode and ρ is the resistivity of the electrolyte/tissue.

The increase in resistivity under invivo conditions is of the order of several hundred percent (section 5.2.3) which will result in a sizeable increase in R_{TISSUE} and hence in R_{TOTAL} (by 185Ω according to Greatbatch and Chardack, 1968).

$-z_{CPA}$

In the first two chapters of this thesis it was shown that the magnitudes of K and β are largely determined by the surface condition of the metal electrode and to adsorption effects. The expected changes in K and β due to the increased resistivity of tissue and its differing composition will be deduced from the physical models proposed for surface and adsorption effects.

-K

Delevie (1967) showed that the impedance of a rough surfaced electrode approached the value

$Z_o=(R_e Z_I)^{0.5}$ at high frequencies, where Z_I is the interface impedance in the absence of surface effects and R_e is the solution resistance in the pore (related to ρ).

From the above it follows that the magnitude of the interfacial impedance, K, is proportional to the square root of the solution resistance for very rough surfaced electrodes. K, therefore, should increase under invivo conditions due to the large increase in resistivity.

If surface effects do not dominate, one expects K to be smaller invivo as there is a lower concentration of chloride ions in tissue than in saline. DeRosa and Beard (1977) demonstrated that K decreases as the concentration of halide ions in the electrolyte is decreased.

- β

According to Delevie (1965) surface roughness effects will be more pronounced in solutions of high electrolyte resistivity. A solution of high resistivity should therefore have a lower value of β over a given frequency range.

- R_{CT}

At low frequencies the "transmission line" effect of surface pores will have diminished and surface finish should not affect the value of R_{CT} as much as that of K. If surface finish does affect R_{CT}, one would expect an increase in it's value under invivo conditions, as $R_{CT} \triangleq (R_{CT}' \ R_e)^{1/2}$, where R_{CT}' is the value of the charge transfer resistance in the absence of surface effects.

If surface effects can be ignored then R_{CT} should increase as the concentration of the current carrying ions is decreased. As tissue has a lower concentration of chloride ions than saline, R_{CT} is therefore expected to increase in magnitude.

It is concluded that R_{CT} should be larger invivo, whether surface effects are significant at low frequencies or not.

7.1.2 Experiments

7.1.2.1 Linear Impedance Measurements

Several experiments were carried out comparing the linear ac impedance of a Telectronic 224 electrode (no3) in saline and in laboratory synthesized C.S.F.

C.S.F. (Cerebral Spinal Fluid) is considered to approximate more closely invivo conditions than physiological saline. C.S.F. comprises NaCl, KCl, C_aCl_2 and several other constituents.

The experimental results are listed below on table 7.1. Values of RCT were measured in the low frequency

(10Hz to 10mHz) range.

TABLE 7.1

Electrolyte	Exp.No	$R_{TOT}(\Omega)$	$K(k\Omega s^{-\beta})$	β	$R_{CT}(M\Omega)$
Saline	76	149	144	0.84	2.25
C.S.F.	87	160	238	0.88	2.68

As the lead resistance of the Telectronic (no3) electrode is 77Ω , $R_{ELECTROLYTE}$ has increased from 72 to 83Ω , an increase of 15%. There is a dramatic increase in K (65%) and a slight increase in β (5%). As expected, R_{CT} also increased, by 20% in this case. Similar results were obtained using several other electrodes.

The increase in K is most probably due to the increase in electrolyte resistivity and hence surface effects dominate the form of the Z_{CPA} impedance.

7.1.2.2 Nonlinear Invivo Impedance Measurements

Measurements were made invivo on the nonlinear impedance of a freshly implanted Sorin S80 electrode. A 3.9 volt pulse was applied to the electrode system using a Devices Demand Pacemaker (E4161) and both the applied voltage and resultant current waveforms were recorded and digitized. The data was then transformed and the impedance derived as explained in section 5.2. The results are listed on Table 7.2 and compared with results previously obtained on a similar electrode in saline under similar conditions.

TABLE 7.2

	Exp No	$R_{TOT}(\Omega)$	$K(k\Omega s^{-\beta})$	β_1	β_2
invivo	V2	440	35.8	.85	.85
invitro (saline)	T81	109	22.7	.87	.93

The invivo impedance locus (figure 7.1) is almost a straight line, curving slightly at higher frequencies.

R_{TOT} is found to be much larger invivo than invitro, as observed by Mansfield (1967). This increase is due to the large resistivity of biological tissue compared to that of saline (Geddes and Baker, 1967). Subtracting the resistances of the leads (52Ω), it is found that R_{TISSUE} (338Ω) is nearly six times larger than R_{SALINE}.

The magnitude of the Z_{CPA} impedance, K, is also found to be larger (160%) invivo than invitro. This is attributed to the relatively large resistivity of biological tissue and it is concluded that surface effects largely determine the magnitude of Z_{CPA}.

β is slightly smaller invivo and this would agree with Delevie's observation that β is smaller in solutions of high resistivity.

Although it was not possible to calculate the magnitude of R_{CT}, it is however known that R_{CT} is larger invivo than invitro (Mansfield, 1967). Mansfield, for example, observed an almost two fold increase in the value of R_{CT} in tissue compared to that found in Ringers solution or Plasma. Mansfield also reported that R_{CT} is 600% larger invivo relative to

IMPEDANCE LOCUS OF A FRESHLY IMPLANTED
SORIN S80 ELECTRODE

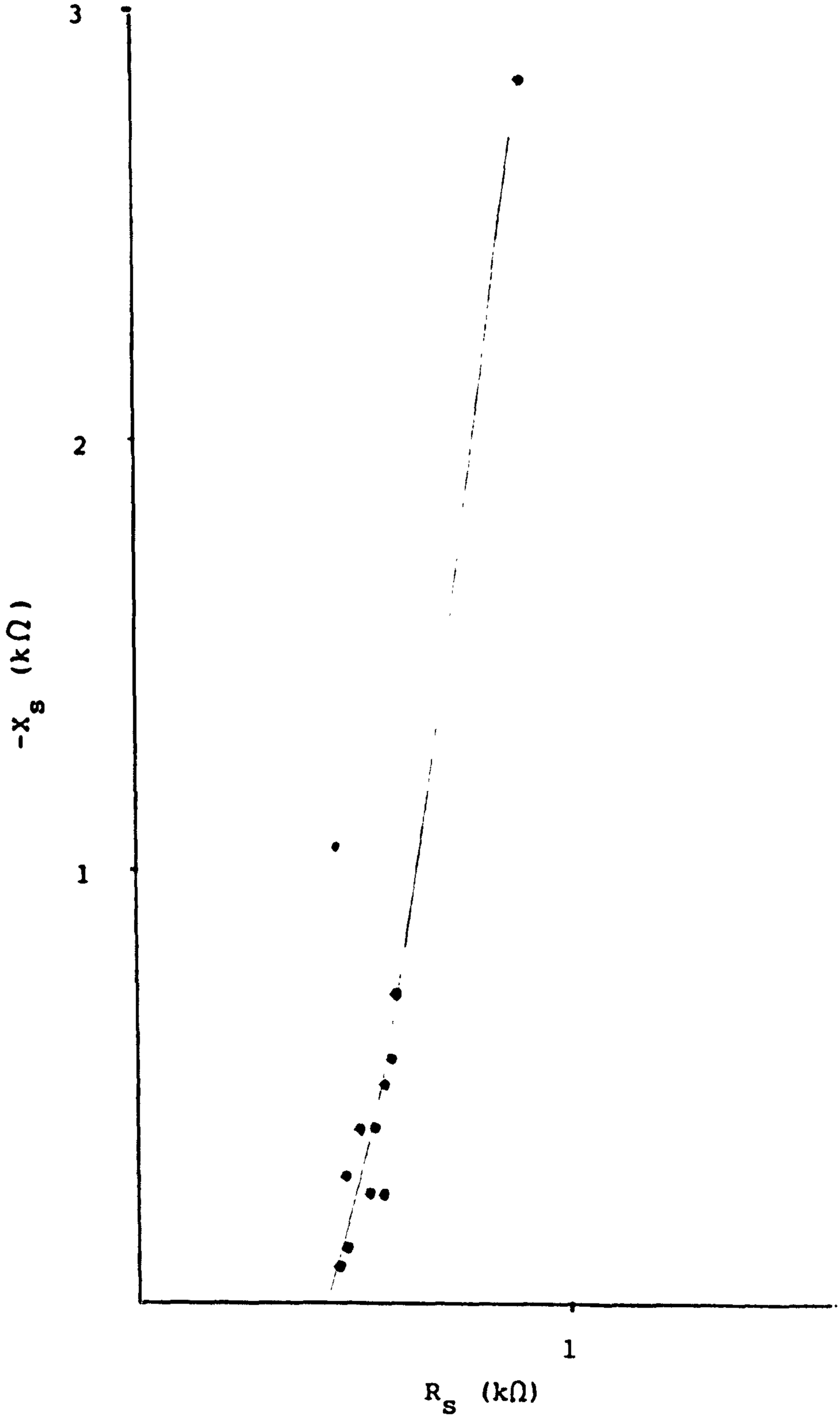

Figure 7.1

values found in saline .

7.1.3 Conclusions

The invivo interface impedance was found to have the same form as that found invitro and can be modelled by the proposed equivalent circuit shown on figure 2.2a. The parameter values differ, however. R_{TOT}, K and R_{CT} are larger and β smaller invivo.

7.2 Pacemaker sensitivities to electrode failures

7.2.1 Review

In chapter 6 it was shown that the two most common modes of electrode failure produce quite different changes in the loading of the stimulus generator. Insultation ruptures decrease the overall electrode impedance, whereas wire fractures give rise to an increase in impedance.

Hepburn (1979) reviewed the sensivity of different pacemakers to changes in their load resistance. His results are plotted on figures 7.2a and 7.2b. It was noted that there is a large variation in load sensitivity between different manufacturers and models. In general it was found that a pacemaker's output rate decreases as the load resistance decreases (insulation breakdown), as does the stimulus duration.

Hepburn (1978), while conceding that the electrode-tissue impedance is not purely resistive,

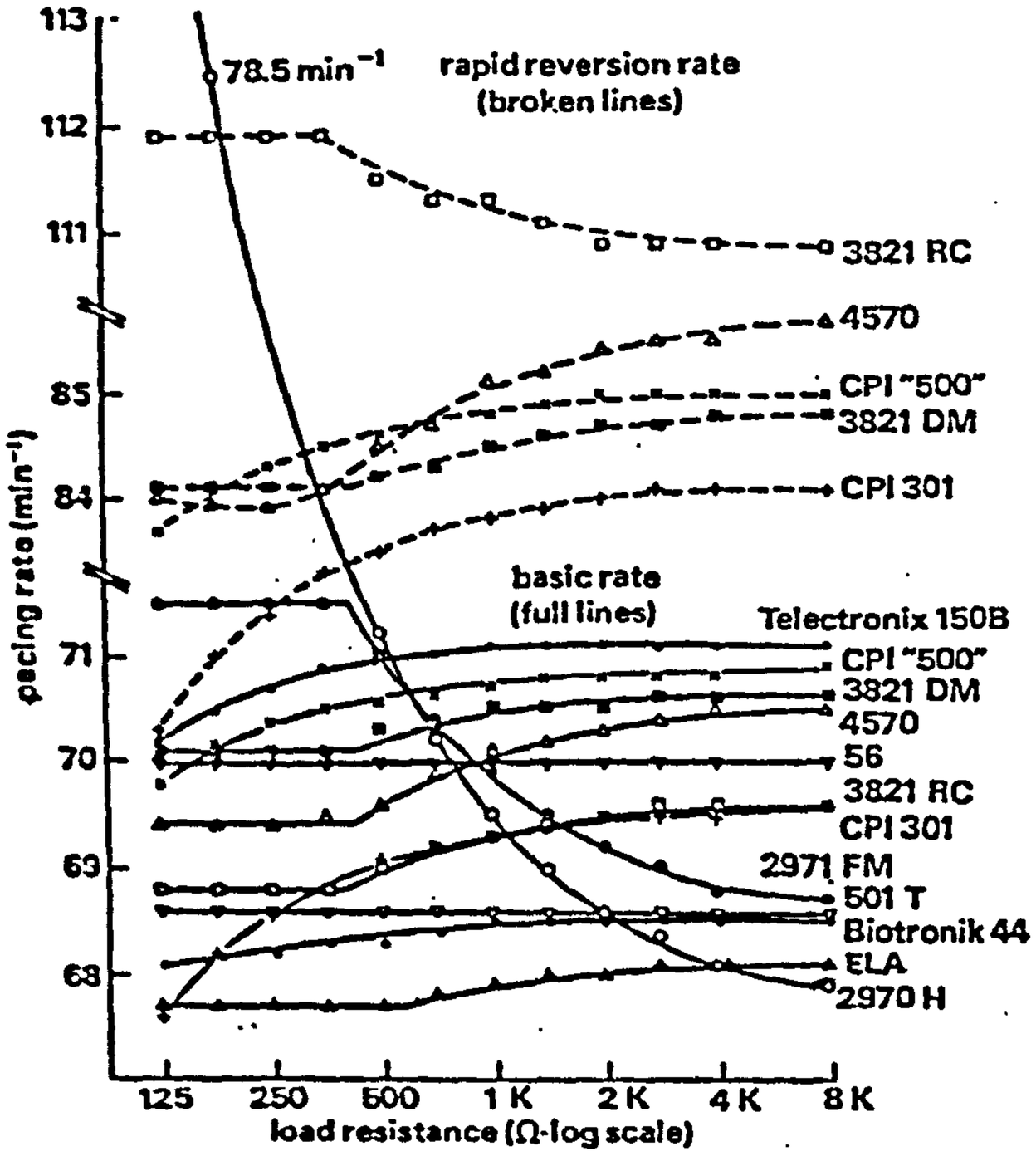

Figure 7.2a

Dependence of stimulus rates on resistive load for various pacemaker models (Devices 2970H, 2971FM, 3821RC, 3821DM, and 4570; ELA Stanium; Vitatron 501T and S6, CPI 301, and 500 series; Telectronics 150 B and Biotronik 44).

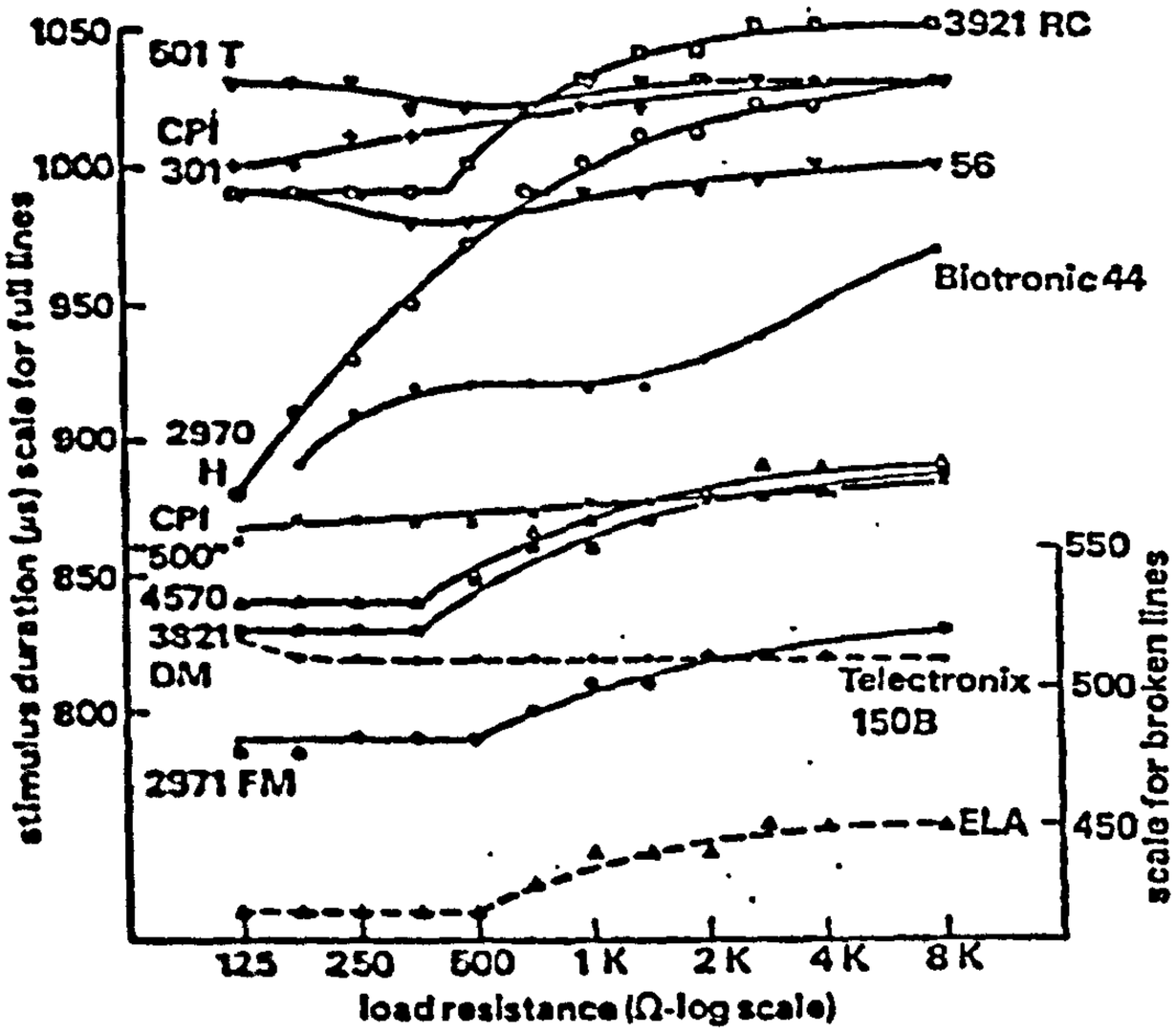

Figure 7.2b

Dependence of stimulus duration on resistive load for various pacemaker models

believed that use of a simple resistance was an adequate approximation to the pacemaker load. Taking the average generator loading (R_{TOT} + R_{CT}) as 1KΩ , Hepburn (1978) represented the effects of insulation rupture by decreasing the load from 1KΩ to 300Ω , while, for wire fracture, the load was increased from 1KΩ to 5KΩ . The effects of these loads on different pacemakers are listed on Table 7.3.

Hepburn observed, however, that the recorded changes in rate and duration are rarely large enough for most pacers to be judged significant, frequently being of the same order as the resolution limit for their detection.

Hepburn found that for a few generators the stimulus duration and rate were sufficiently load-sensitive and the circuit otherwise stable enough to allow measurement of these two temporal features and the indication and classification of electrode failures, often in a latent stage before pacing failure had occurred.

Although Hepburn's observations have proved clinically useful, his use of a simple resistive load for his bench trials was challenged. An investigation was therefore initiated into the form and magnitude of the invitro and invivo inter-electrode impedances and resultant changes in them due to electrode failures. This work led to the present thesis.

Preston et al (1966) simulated the invivo pacer load by a resistance (R_L) in series with a capacitance (C_L). They observed that pulse width increased with

TABLE 7.3

Pacemaker assessed			Basic (and reversion) rate changes (ppm)		Pulse duration changes (μs)	
Brand	Model	Version	Insulation Rupture	Wire fracture	Insulation Rupture	Wire fracture
Devices	2971	C	+ 1.6	- 1.0	- 20	+ 20
	3821	DM	-0.2(-0.4)	+0.2(+0.2)	- 30	+ 20
	4570		-0.7(-0.9)	+0.3(+0.6)	- 40	+ 20
C.P.I.	Maxilith	301	- 0.5	+ 0.2	- 10	+ 10
	Minilith	501	- 0.3	+ 0.1	nil	+ 10
	Minilith	503	- 0.1	nil	- 10	+ 10
E.L.A.	Stanium		- 0.1	+ 0.2	- 10	+ 10
	Stilith	120	- 0.1	+ 0.2	- 10	+ 10
Vitatron	40	RT	+ 0.3	- 0.1	- 20	+ 10
	40	RT	nil	nil	- 20	nil
	41	RT	nil	nil	- 10	nil
	42	RT	nil	nil	- 20	+ 10
	42	R	nil	nil	- 10	+ 10
	151	S	nil.	nil	- 20	+ 10
	251	T	nil	nil	nil	nil
	501	T	nil	nil	- 10	nil
	501	TC	nil(nil)	+0.1(+0.2)	- 20	nil
Telectronics	150	B	- 0.3	nil	nil	nil

CHANGES IN THE RATE AND DURATION OF VARIOUS PACERS OUTPUTS TO CHANGES IN LOADING

increase in R_L. Varying R_L, however, did not change the pulse rate significantly until R_L exceeded 5,000Ω.

Changes in C_L caused a proportionate change in pulse width, and an inverse change in pacemaker rate.

It will be appreciated that Preston et al's R_L - C_L model is a simplification of the R_{TOT} -Z_{CPA} model, the contribution of the relatively large charge transfer resistance, R_{CT}, being ignored. Preston et al observed typical invivo values of R_L and C_L of 300Ω and 47μF respectively, equivalent to values of R_{TOT} and K of 300Ω and above 21kΩ$s^{-\beta}$. These values agree favourably with those calculated from our own invivo experiment (table 7.2) where R_{TOT} = 400Ω and K = 35.8kΩ $s^{-\beta}$ for a Sorin S80 electrode with a 8 mm^2 area. Unfortunately Preston et al did not state the make or area of the electrodes used in their experiments.

An insulation rupture will cause R_{TOT} and K to decrease (section 6.1) hence it is expected that R_L will decrease and that C_L will increase under this condition. A decrease in R_L by itself would result in a decrease in pulse width whereas an increase in C_L would result in an increase in pulse width and a decrease in the rate. The changes in R_L and C_L have therefore opposing effects on the pulse width of the stimulus waveform. As Preston et al observed a decrease in pulse width with no change in the rate for insulation ruptures, one can conclude that the changes in R_L dominate those in C_L.

This should come as no surprise, as the series resistance (R_{TOT}) is much larger than the interfacial,

capacitive impedance (Z_{CPA}) in the nonlinear region for frequencies above 1kHz. It was therefore quite reasonable for Hepburn in his bench tests to approximate the inter-electrode impedance by a simple resistance.

A break in lead wire which is bridged by body fluid will give rise to an increase in R_{TOT} and Z_{CPA} (section 6.2) and hence to an increase in R_L and a decrease in C_L. The changes in R_L would tend to increase the pulse width whereas those in C_L would tend to decrease pulse width and increase the rate. As Preston et al observed an increase in pulse width and rate for invivo wire fractures, it can be concluded that once again the changes in R_L dominate, though the decrease in C_L has an effect on the pulse rate.

7.2.2 Experimental Section

7.2.2.1 Experimental Setup

The sensitivity of three pacemakers to changes in their loading was investigated. These were CPI, Intermedic and Telectronic Pacers.

The pacemakers were kept in a body-temperature thermostated water bath and each pacemaker was in turn connected to an intact Telectronic 224 electrode and the large area indifferent electrode, both emmersed in the saline bath. After the pacers' output characteristics were recorded the pacemakers were then connected to failed electrodes and their output parameters again recorded. The output parameters

monitored included,

I_{max}, the initial current, measured using the digitizing set up (section 5.2)

V_{max}, the peak of the voltage output, measured using the digitizing set up

V_{max}', the maximum voltage, measured using a Devices Pacemaker analyser (Type 4580)

P.W., the pulse width, measured using a Venner Electronics Preset Counter (Type TSA 5545)

P.W.', the pulse width, measured using a Devices Pacemaker analyser

R, the rate, measured using the Venner Electronics Preset Counter

R', the rate, measured using the Devices Pacemaker analyser

R_{TOT}, the series resistance, calculated by dividing V_{max} by I_{max}.

DR, the decay ratio, calculated by dividing the current response after 0.5 msec by I_{max}

β, the fractional power factor of Z_{CPA}, calculated from the gradient of the log $[I_{max} - i(t)]$ versus log (t) plot.

The failed electrodes were as described in chapter 6 and shown on figures 6.1 and 6.6. Three lengths of insulation rupture were used in the tests (i) almost zero cm (ie a fine crack in the insulation), (ii) 0.25 cm and (iii) 0.5 cm. Two degrees of wire fracture were used (i) an almost zero gap and (ii) a 2mm gap between wire segments.

7.2.2.2 Experimental Results

The measured output parameters of the pacemakers under study are tabulated on Tables 7.4, 7.5 and 7.6.

- **Pulse Width**

The pulse width of the Telectronic pacer was insensitive to the changes in its loading due to the electrode failures. The C.P.I. pacer was scarcely "better" with only a slight increase in pulse width for the severest wire fracture (2mm gap). The Intermedic pacemaker's pulse width increased by a measurable 1.6 x 10^{-5} sec for insulation ruptures and decreased by up to $5x10^{-5}$ sec for the 'wet' wire fractures. The Intermedic pacer would therefore be a suitable, load sensitive pacer, enabling external diagnosis of electrode failure. It is noted that the Intermedic pacer's decrease in pulse width with load is the opposite to the general trend observed by Hepburn (1978, 1979) and Preston et al (1966).

- **Pulse Rate**

There was little change in the pulse rate of the CPI pacer with changes in loading. A slight increase was observed for the wire fractures and a slight decrease for the insulation ruptures. For the Intermedic and Telectronic pacemakers, however, the pulse rate decreased by approximately 0.3 ppm for insulation ruptures and increased by up to 2 ppm for wire fractures. These latter pacers can therefore give

TABLE 7.4

CHANGES IN THE OUTPUT CHARACTERISTICS OF THE C.P.I. PACEMAKER INDUCED BY ELECTRODE FAILURES

	Size of Failure	V_{max} (V)	V_{max}' (V)	I_{max} (mA)	R_{TOT} (Ω)	Pulse Width' (msec)	Pulse Width (msec)	RATE' (ppm)	RATE (ppm)	ER	β
INTACT		4.725	4.95	22.39	211	.59	.597	70.2	70.266	.762	.8
INSULATION RUPTURE length	$\simeq$ 0cm	4.875	4.94	24.3	200	.59	.597	70.2	70.266	.731	
	0.25 cm	4.825	4.86	28.47	169	.59	.596	70.2	70.253	.703	.66
	0.5 cm	-	4.84	-	-	.59	.596	70.2	70.243	-	
WIRE FRACTURE gap	$\simeq$ 0cm	4.9	4.94	22.91	214	.59	.597	70.2	70.29	.733	
	2 mm	5.625	5.5	2.35	2400	.61	.600	70.5	70.48	.635	.49

TABLE 7.5

CHANGES IN THE OUTPUT CHARACTERISTICS OF THE INTERMEDIC PACEMAKER INDUCED BY ELECTRODE FAILURES

	Size of Failure	V_{max} (V)	V_{max}' (V)	I_{max} (mA)	R_{TOT} (Ω)	Pulse width' (msec)	Pulse width (msec)	RATE' (ppm)	RATE (ppm)	DR	β
INTACT		3.825	3.72	18.67	205	.67	.681	66	66.26	.539	.723
INSULTATION RUPTURE length	≃0 cm	3.75	3.68	19.07	197	.68	.682	66	66.189	.532	
	0.25 cm	3.675	3.56	21.27	173	.68	.694	65.7	65.926	.488	.675
	0.5 cm	-	3.48	-	-	.69	.697	65.7	65.86	-	
WIRE FRACTURE gap	≃0 cm	3.95	3.72	18.44	214	.67	.683	66.1	66.17	.531	
	2 mm	5.175	5.12	2.07	2500	.63	.63	68.3	68.358	.608	.404

TABLE 7.6

CHANGES IN THE OUTPUT CHARACTERISTICS OF THE TELECTRONIC PACEMAKER INDUCED BY ELECTRODE FAILURES

	Size of Failure	V_{max} (V)	V_{max}' (V)	I_{max} (mA)	R_{TOT} (Ω)	Pulse Width' (msec)	Pulse Width (msec)	RATE' (ppm)	RATE (ppm)	DR	β
INTACT		3.375	3.33	17.54	192	.53	.536	67.9	68.128	.328	.48
INSULATION RUPTURE length	≅ 0 cm	3.325	3.27	17.75	187	.53	.536	67.8	68.146	.344	
	0.25 cm	3.2	3.18	20.05	160	.53	.536	67.7	67.919	.336	.425
	0.5 cm	-	3.13	-	-	.53	.537	67.7	67.843	-	
WIRE FRACTURE gap	≅ 0 cm	3.425	3.3	17.53	195	.53	.536	67.7	67.873	.43	
	2mm	4.9	4.56	185	2650	.54(?)	.530	70.0	70.05	.517	.395

an externally observable indication of electrode damage before total failure to pace occurs.

- Waveform

Analysis of the current response waveform assumes that the applied voltage pulse is a good square wave. Inspection of figure 7.3 shows this is not always the case. The voltage waveforms applied to intact electrodes generally decrease with time hence great care must be used when interpreting the resultant current response waveforms.

Another problem is that the applied voltage waveforms change in amplitude and shape according to loading (see figure 7.4). All of the voltage output waveforms of the pacers evaluated increased in amplitude with increase in loading due to wire fracture and decreased with the decrease in load due to insulation rupture (see tables 7.4 to 7.6).

The CPI pacer was the least sensitive in this respect and hence effects due to change in loading will be reflected mainly in the current response waveform for this pacemaker. As only the current response can be monitored externally, it is desirable that all changes in waveform due to variations in loading occur in the current waveform and that the voltage waveform remains, as far as possible, a good square wave of constant amplitude. As the CPI output voltage waveform is also closest to being a square wave, observations made on the CPI current waveforms should be the most valid.

APPLIED VOLTAGE WAVEFORMS OF VARIOUS PACEMAKERS
TO INTACT TEL. 224 ELECTRODES

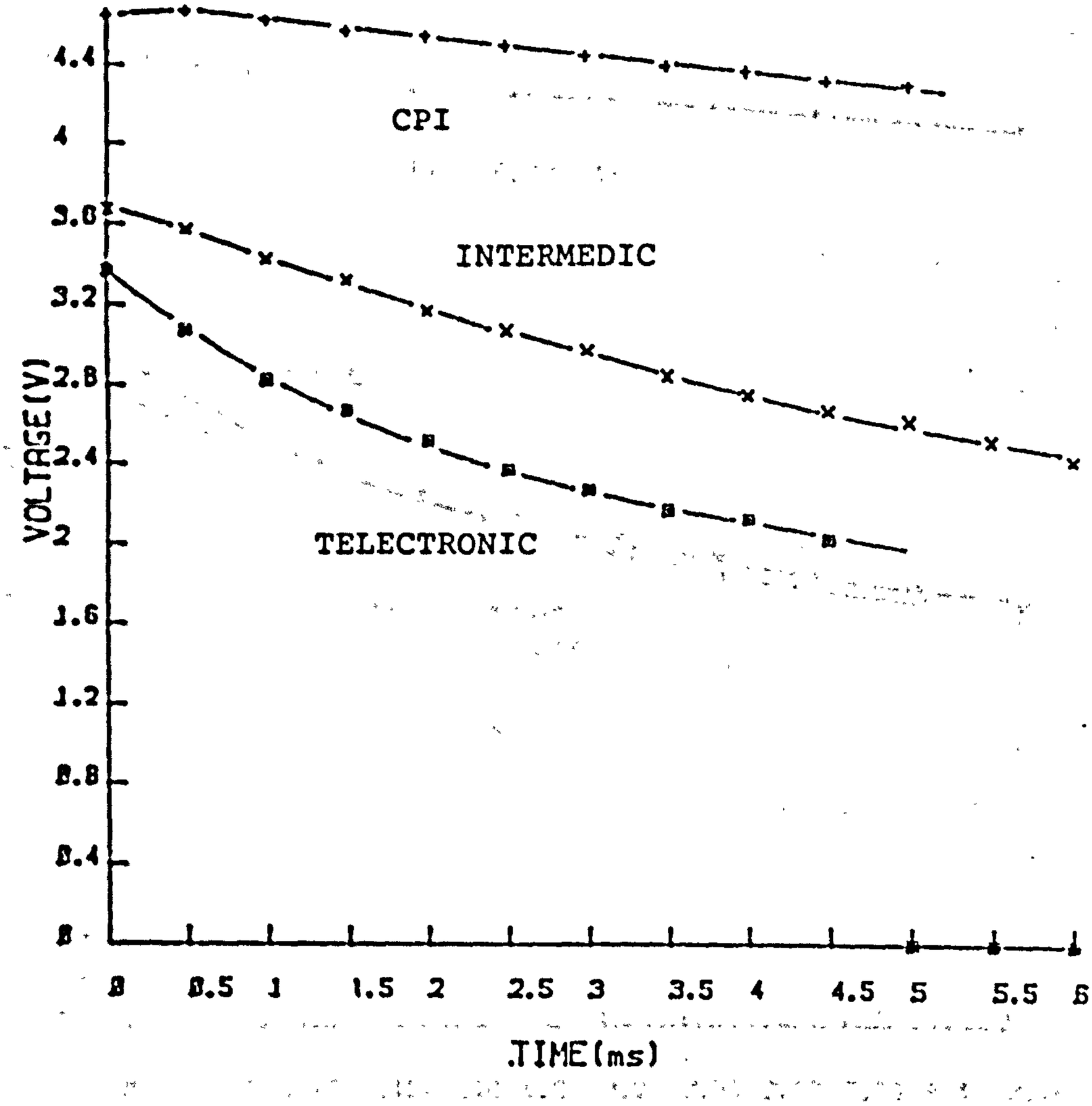

Figure 7.3

TELECTRONIC PACEMAKER

Applied Voltage Waveforms for Various Electrode Conditions

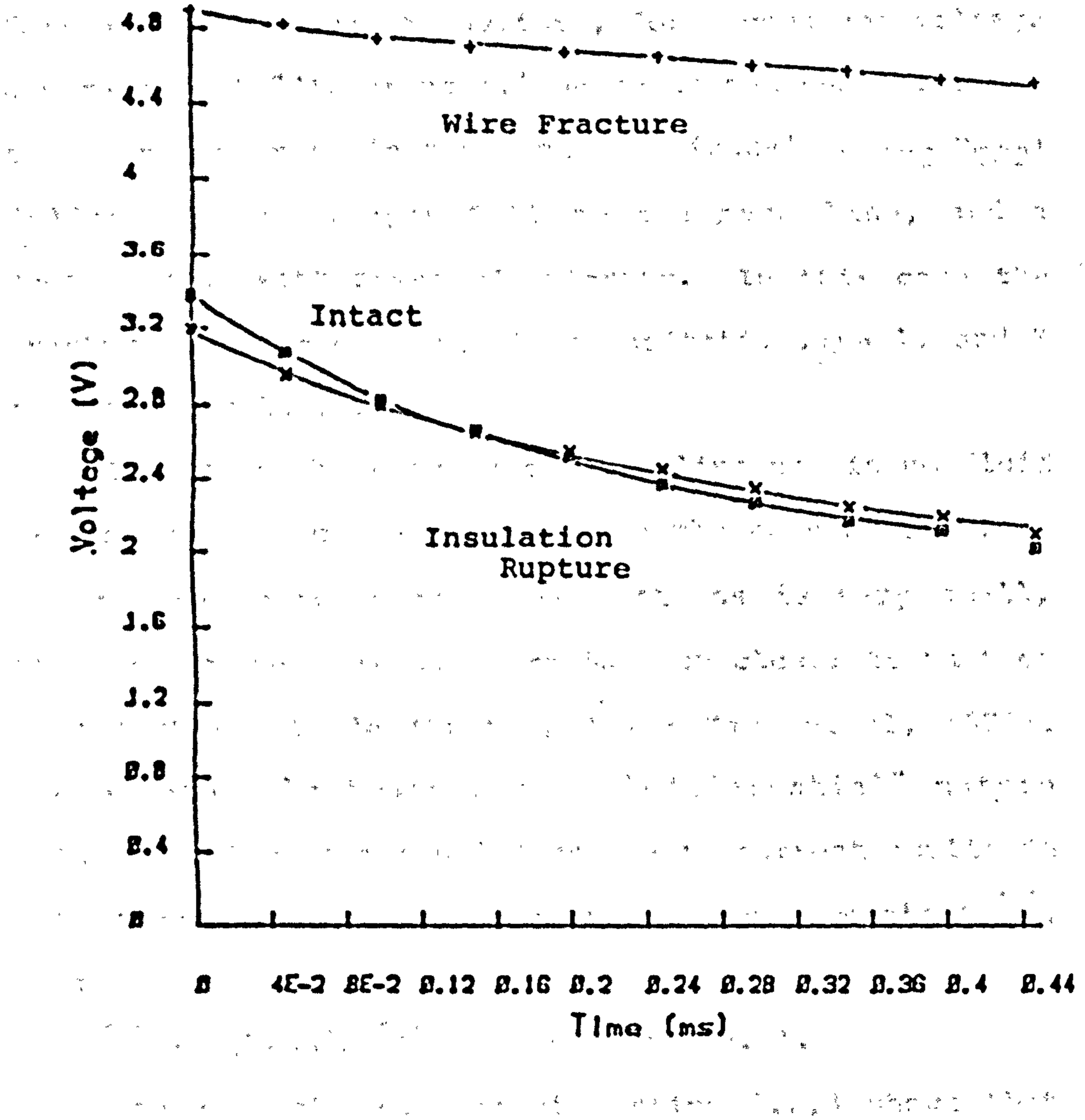

Figure 7.4

The current response waveforms of the CPl pacer for various electrode conditions are shown on figure 7.5.

Wire Fracture

According to Kaul et al (1979) and Davies et al (1969) a 'dry' lead fracture is evidenced by a "differential" current waveform, for a constant voltage generator. A "differential' pulse is one characterised by an initial rise in the amplitude (equal to V_{DC}/R_{TOT}) followed by an abrupt fall to the base line, and a second spike with reversed polarity. In this case the fracture impedance is purely capacitative, $\beta = 1$, and K is extremely large.

If, as in the present case, saline or tissue fluid has entered the catheter lumen via the ends of the lead and the gap between the wire sections is very small, the current response waveform is much closer to that of an intact electrode (Furman, 1977; Kaul et al, 1979). The waveform is however of a "differential" nature (figure 7.5) with a rapid decrease in current amplitude with time due to a decrease in the time, constant, τ, where

$$\tau = (R_{TOT}/K)^{1/\beta} \quad \text{(equation 3.6).}$$

Study of the results of section 6.2.3 shows that the time constant, derived from equation 3.6, for an intact Devices LC electrode is nearly 4msec whereas that of similar electrode with a 'wet' wire fracture is approximately 2msec. Such a decrease in time constant is due to the large decrease in β (from approx .86 to .62) as the ratio, R_{TOT}/K, actually increases due to a

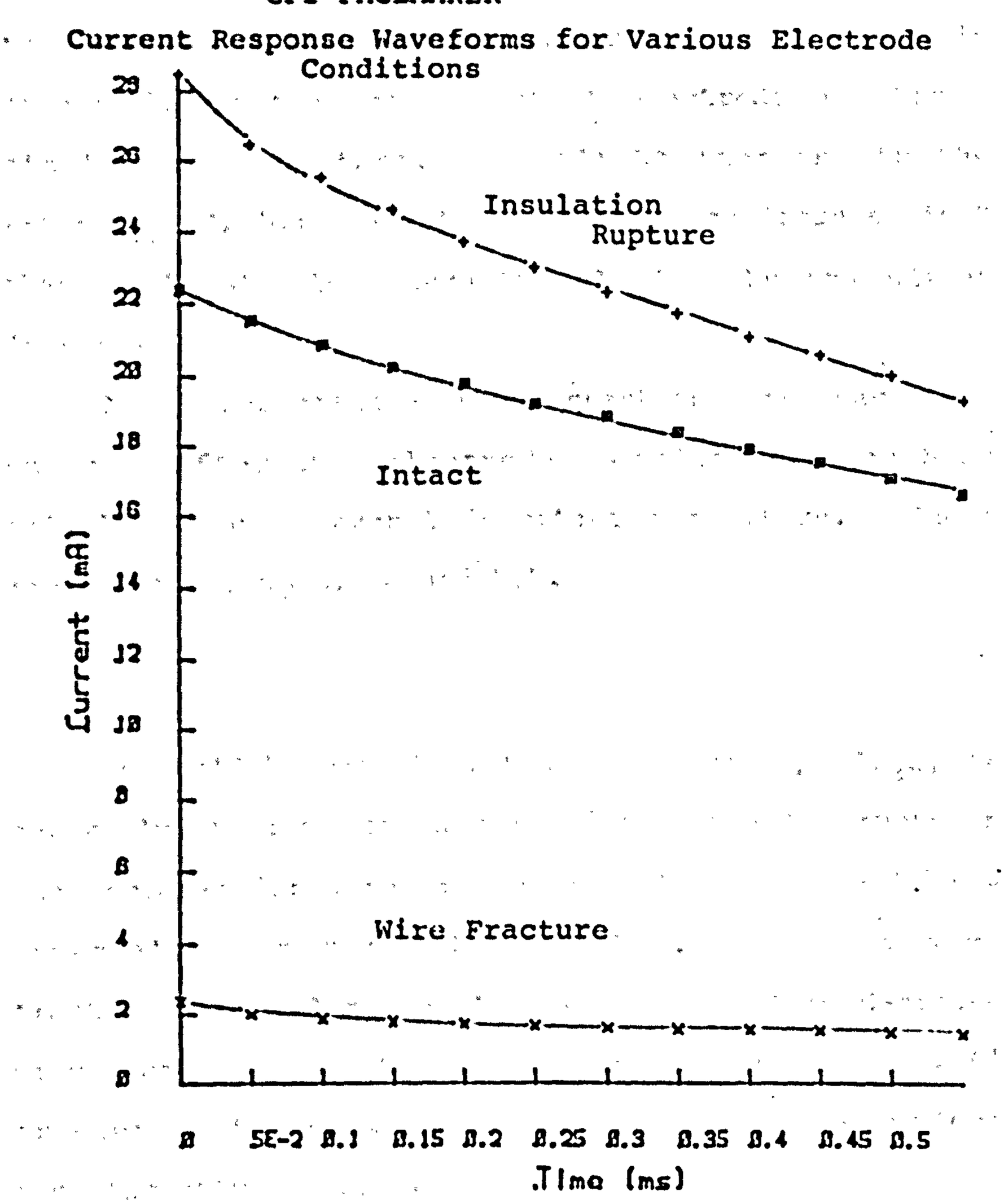
CPI PACEMAKER
Current Response Waveforms for Various Electrode Conditions
Insulation Rupture
Intact
Wire Fracture
Current (mA)
28
26
24
22
20
18
16
14
12
10
8
6
4
2
0
0
5E-2
0.1
0.15
0.2
0.25
0.3
0.35
0.4
0.45
0.5
Time (ms)

Figure 7.5

larger percentage increase in R_{TOT} than in K.

Insulation Rupture

The current response of an electrode with an insulation rupture has a larger value of I_{max} due to the decrease in R_{TOT}. The current decay with time is comparable to that of an intact electrode and has a similar time constant. The slight increase in the ratio R_{TOT}/K, (due to a larger percentage decrease in K than in R_{TOT}) is generally nullified by the slight decrease in β.

Close inspection of the current response waveforms under different electrode conditions enables calculation of serveral important parameters. These include I_{max}, R_{TOT}, β and D.R.

- I_{max}

As would be expected, the peak current, I_{max}, is generally observed to increase for insulation ruptures and decrease for wire fractures (tables 7.4 to 7.6) - especially for the CPI pacemaker. For the wire fracture with a 2mm gap, I_{max} was observed to decrease dramatically for all three pacers. The small 'wet' fracture did not, however, appear to affect significantly the current waveform.

- R_{TOT}

The value of the series resistance, R_{TOT}, was calculated by dividing V_{max} by I_{max}. As expected, R_{TOT} was approximately 200Ω for an intact Tel.224 electrode, 170Ω for one with an insulation rupture 0.25 cm long and 2,500Ω for a 'wet' wire fracture with a 2mm gap

between the lead wire sections. Little change was observed for a 'wet' fracture with a small gap.

Although V_{max} cannot be measured externally under invivo conditions, its value can be estimated and approximate values of R_{TOT} calculated and used as a means of monitoring the condition of the implanted electrodes.

- β

The constant phase angle impedance's fractional power factor, β , can be calculated from the slope of the $\log(i_{decay})$ versus log(time) plot (equation 5.33), where the decay current, i_{decay}, at any time, t, is given by,

$$i_{decay} = I_{max} - i(t).$$

The intercept on the y axis at t = 1sec of the above plot should give an indication of the magnitude of the ratio $V_{dc}K/R_{TOT}^2$.

As the CPI pacer has the voltage output waveform which best approximates a perfect square wave and whose magnitude and shape change the least with loading, one would expect values of β calculated from this pacer's current response to be the most accurate.

Plots of $\log(i_{decay})$ versus log(t) for the different electrode conditions are shown on figure 7.6 for the CPI pacemaker. Calculated values of β are listed on Table 7.4.

The plots form straight lines except for the wire fracture (2mm gap) which shows signs of limiting at longer times. Such behaviour is most probably due to the presence of the parallel charge transfer

CPI PACEMAKER

Log. of Current Decay vs. Log. of Time

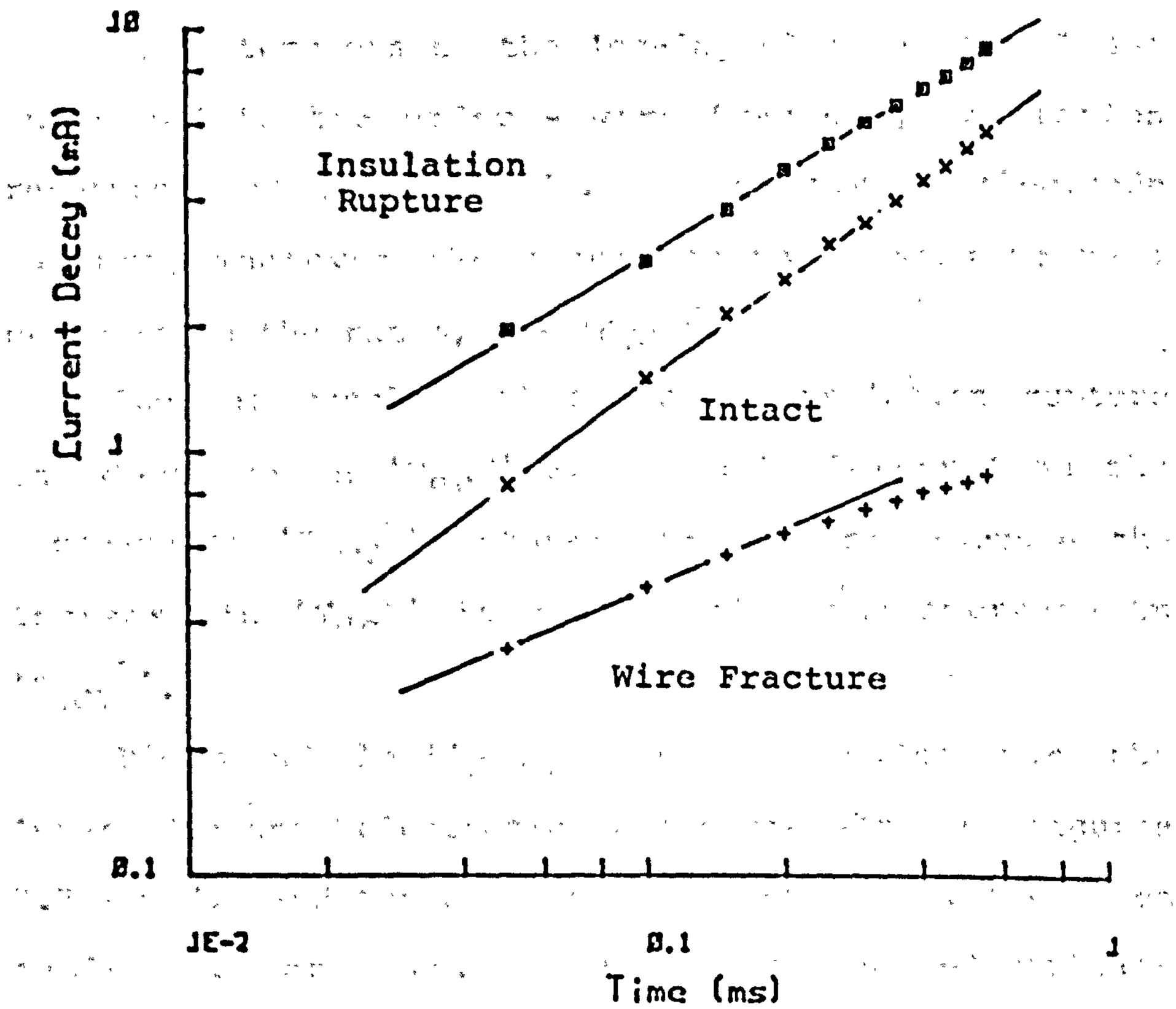

Figure 7.6

resistance, R_{CT}. This would indicate that the time constant of the current response's decay (figure 7.5) is in this case relatively very short.

As expected, β decreases for either form of electrode failure. These decreases are quite significant, from 0.8 to 0.49 for a wire fracture and from 0.8 to 0.66 for an insulation rupture.

The intercepts of the log-log plots at t = 1 sec increased in the order - wire fracture, insulation ruputure, intact electrode. Hence for an electrode failure, whatever the cause, there appears to be a decrease in the ratio, $V_{DC}K/R_{TOT}^2$.

One can conclude that for an insulation rupture the decrease in '$V_{dc}K$' is slightly larger than the decrease in 'R_{TOT}^2', whereas for a wire fracture the increase in '$V_{dc}K$' is smaller than the increase in 'R_{TOT}^2'.

Plots of $\log(i_{decay})$ versus $\log(t)$ for the Intermedic and Telectronic pacers are shown on figures 7.7 and 7.8 and the derived values of β are listed on tables 7.5 and 7.6. Due to the applied voltage waveforms being poor square waves the calculated values of β are not very accurate, e.g. β = 0.48 for an intact electrode according to the Telectronic results. However the qualitative changes in β with electrode failures are as expected - a decrease in β for both kinds of failure, with the largest decreases for wire fractures. As with the CPI Pacer, the intercepts at t = 1 sec were found to increase in the order - wire fracture, insulation rupture, intact electrode.

INTERMEDIC PACEMAKER

Log. of Current Decay vs. Log. of Time

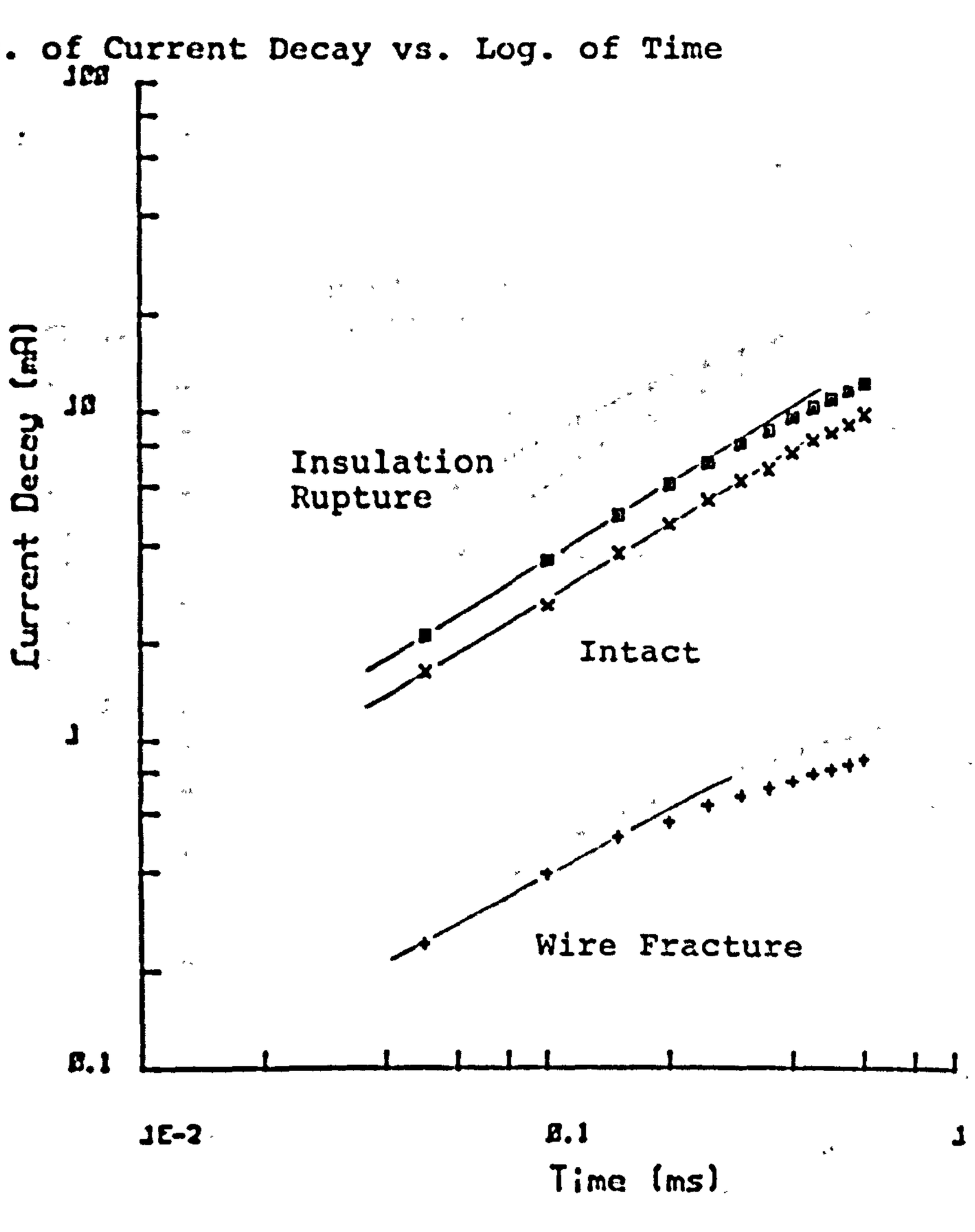

Figure 7.7

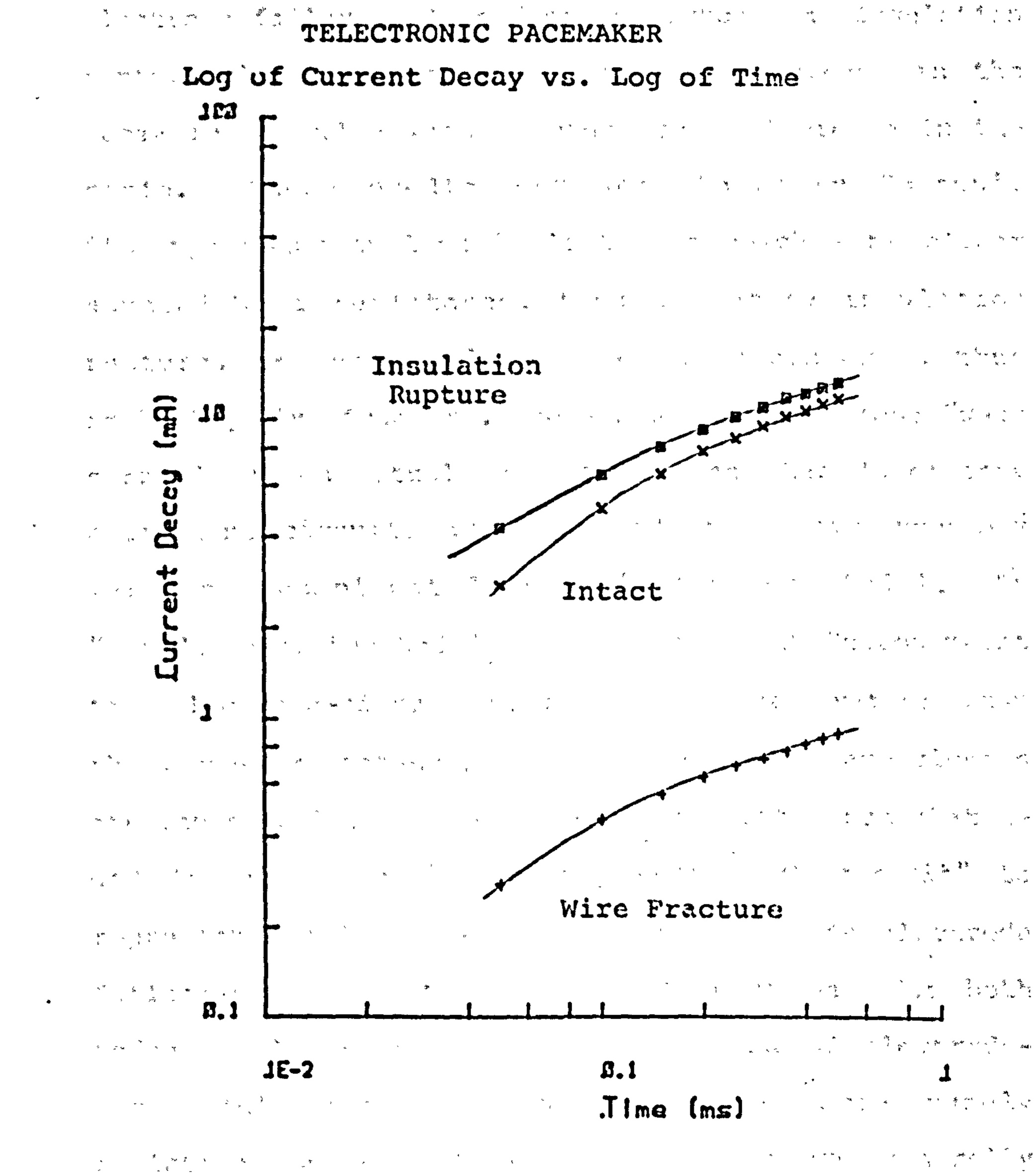
TELECTRONIC PACEMAKER
Log of Current Decay vs. Log of Time
10
1
0.1
1E-2
0.1
1
Current Decay (mA)
Time (ms)
Insulation Rupture
Intact
Wire Fracture

Figure 7.8

- Decay Ratio

Sowton (1967) and Sowton and Gray (1971) suggested that the decay ratio could be used to indicate electrode failure. According to Sowton an insulation rupture should be characterised by a decrease in the decay ratio and a wire fracture by an increase in the ratio. These predictions were based on Sowton's findings using implanted electrodes which were either shunted by a resistance, thus imitating insulation rupture, or connected to a series resistance, thus imitating wire fracture. The above investigations "were carried out on actual patients rather than laboratory equivalent circuits as the impedance of the body may vary in a complicated manner" (Sowton, 1967). By "impedance of the body" it is assumed that Sowton meant the electrode-tissue interface impedance rather than the series resistance, R_{TOT}. His invivo experiments are commendable, However it must be pointed out that he did infact use a "laboratory equivalent circuit" to represent the "impedance of the body" at the electrode failure-body fluid interface. Lead wires, for both modes of electrode failure, form additional electrode-body fluid interfaces which are no more purely resistive, even if their phase angles are generally less, that that at the electrode tip.

In using series and parallel resistances as described above, Sowton was in effect assuming that a wire fracture gives rise only to an increase in R_{TOT} and that an insulation rupture causes R_{TOT}, K and R_{CT} to decrease - the latter being qualitatively correct, the

former being erroneous.

The capacitive component of the electrode failure impedances cannot, in this case, be ignored as it will have a marked effect on the current response waveform and hence on the decay ratio.

In section 5.2.4.2 it was shown that the decay ratio can be expressed as (ignoring the contribution of R_{CT} over the short time duration of 5msec)

$$DR = 1 - \frac{K}{R_{TOT}} \frac{(0.5 \times 10^{-3})^{\beta}}{\sqrt{(1+\beta)}} \quad \text{(equation 5.32)}$$

The decay ratio is therefore a complicated parameter, being a function of several variables. The value of DR is largely determined by the product of the terms 'K/R_{TOT}' and '$(0.5\times10^{-3})^{\beta}$' as the '$\sqrt{(1+\beta)}$' term is relatively constant and has a value of approximately unity.

Insulation Ruptures

All three pacers tested showed a decrease in DR (of up to 10%) for insulation ruptures. This decrease infers either an increase in the magnitude of the ratio, K/R_{TOT}, or an increase in the '$(0.5\times10^{-3})^{\beta}$' term. As the ratio, K/R_{TOT}, generally decreases in magnitude for insulation ruptures (section 6.1.3), the decrease in DR is due to the increase in '$(0.5\times10^{-3})^{\beta}$' and hence to the decrease in β. It is surprising, and generally not appreciated, that β has such a dominating effect on both the decay ratio and the time constant (equation 3.6).

The above decrease in DR for insulation ruptures however agrees with Sowton's predictions.

Wire Fractures

The CPI pacer, contrary to Sowton's postulations, showed a decrease in decay ratio for wire fractures. However this is what one would expect for a "differential" waveform such as that shown on figure 7.5. Sowton and Gray obtained a similar "differential" waveform for an electrode with a fractured lead wire (1971, figure 4b) and yet concluded that the decay ratio increased! Inspection of their figures 4a and 4b indicates that the decay ratio decreased from approximately 0.68 to 0.43. Hence Sowton and Gray's experimental results agree with the author's findings that DR decreases for wire fractures and does not always increase, as predicted by Sowton (1967) based on the results of his unrepresentative "bench test".

The Intermedic and Medtronic pacers showed an increase (up to 15%) in decay ratio for wire fractures. These however are probably due to the applied voltage pulses being poor square waves (figure 7.4) and to the dramatic increase in the applied voltages' amplitudes for wire fractures (figure 7.5) which will change the interfacial impedance.

It should however be pointed out that the decay is very sensitive to changes in β and it is possible for the decay ratio to increase for a wire fracture. For example, the ratio, K/R_{TOT}, decreased by a factor of almost 3 for a Devices LC electrode (section 6.2.3) with a 'wet' fracture relative to a similar intact electrode, whereas the '$(0.5 \times 10^{-3})^{\beta}$' term increased 6 fold due to the decrease in β from 0.86 to 0.63.

The increase in the latter term dominated and DR therefore decreased. However, a smaller change in β, say from 0.8 to 0.67, would have caused DR to increase. It is therefore possible for the decay ratio to increase for some lead wire fractures, as anticipated by Sowton.

It must be concluded that the decay ratio, being largely dependent on the value of β, may either increase or decrease for the two modes of failure reviewed and hence must be used with caution and in conjunction with the analysis of other pertinent parameters.

A further problem is that the above reported changes in DR are probably not significant for clinical use as they could easily be masked by changes due to the gradual drift in the magnitude of the inter-electrode impedance and to variations with time in the output characteristics of the pacer. Sowton and Gray (1977), in defence of the use of the decay ratio, stated that "95% of normal pacemakers have decay ratios which have not changed by more than 20% from the control at any time". This infers, however, that the decay ratio must change by at least 20% due to electrode failure to be significant. This was not the case in the present study.

7.3 Conclusions

Although the invivo interface impedance differs from that found invitro, the difference is only in the magnitude of the equivalent circuit parameters and the same equivalent circuit model applies to both conditions.

The output characteristics of pacemakers do change with change in loading and in a few cases these are sufficiently marked to indicate and classify an electrode failure. Damage to electrode leads is commonly deduced from diminished and distorted stimulus artefacts. These changes, however, may either not occur or may not discriminate between the two modes of electrode failure. The decay ratio, for example, is very sensitive to the parameter 'β' (which decreases for both types of failure) and may not necessarily change in the same direction for a certain mode of failure. Changes in the peak current, I_{max}, may also be masked by changes in the applied voltage amplitude. Care must therefore be used in the interpretation of observed changes in current response waveforms and a pacer should be chosen whose voltage output is as load independent as possible and whose waveform is as close to a square wave as possible.

For some generators the stimulus duration and rate are sufficiently load sensitive to enable positive indentification of an electrode failure, often in a latent stage before pacing failure has occurred (Hepburn 1978, 1979). As the rate and duration of the

stimulus can be measured simply and non-invasively and the two types of lead damage cause opposite changes in these two temporal features, their periodic measurement forms an attractive means of monitoring the condition of the implanted electrodes.

Chapter 8

A review of the contributions made in this thesis to the understanding of the electrical properties of inter-electrode impedance.

Introduction

The initial goal of this thesis was the investigation of the sensitivity of various pacemakers to changes in their loading due to electrode failures. Based on the literature it had been assumed that the inter-electrode impedance of intact and failed electrodes in saline and in tissue could be represented by the "3-component" model (figure 0.2).

At an early stage in the author's research, it was established that this was not, however, the case. It was therefore necessary to determine and account for the form of the inter-electrode impedance under intact and failed conditions and under linear and nonlinear ac and transient conditions. This proved to be an immense, though interesting, task. It was found that many aspects of the inter-electrode impedance involved were either unexplored, insufficiently understood or subject to controversy and hence had to be investigated by the author.

Obviously, due to limited time, resources and abilities, the problem of inter-electrode impedance could not be researched exhaustively by the author. It is believed, however, that several important contributions have been made in this thesis and these are reviewed in this chapter. Also, areas deserving further study have been identified and it is hoped that comments and suggestions made will prove useful to future investigations.

8.1 Chapter 1

It was shown that the inter-electrode impedance is well modelled over a wide frequency range by the series combination of a resistance, R_{TOT}, due to the sum of the lead and electrolyte resistances, and a constant phase angle impedance, Z_{CPA}, where

$$Z_{CPA} = K (j\omega)^{-\beta} \qquad \text{(eqn 1.3)}$$

and generally $0.5 < \beta < 1$.

The Z_{CPA} impedance is, however, only a means of representing the experimental data and has no physical significance in itself.

The fractional power factor, β, was observed to gradually increase towards unity as the applied frequency was decreased, giving rise to a concave impedance locus (figure 1.2). The "constant" phase angle impedance element therefore only applies over a limited, though rather wide, frequency range.

The source of the observed frequency dependence of the inter-electrode impedance has been found to be located at the electrode-electrolyte interface. After an extensive review it has been established that for smooth surfaced electrodes, the deviation from purely capacitive behaviour ($\beta = 1$) is most probably due to specific adsorption effects. However solid electrodes have rough surfaces, at least on a microscopic level, and this surface inhomogeneity further distorts the interfacial impedance from purely capacitive behaviour. With pacing electrodes the surface effects are the major source of the observed "frequency dispersion"

(β < 1) and adsorption plays a relatively minor role. Surface roughness effects dominate the interfacial impedance at high frequencies, causing K and β to decrease. As the frequency is decreased, surface effects diminish and the interfacial impedance gradually returns to 'smooth' surface behaviour ie K increases and β approaches unity. Surface effects therefore give rise to the observed concave impedance locus (figure 1.2).

In the past several attempts at modelling the effects of surface finish on the interfacial impedance have been made and these have been briefly reviewed in this thesis. The relatively simple, "surface pore-transmission line" model of Delevie (1964,1967) gives most insight into the problem and enables qualitative interpretation of results. The problem, however, warrents further study and Delevie's model can be improved upon. These improvements can possibly be achieved by

1) deriving an alternative expression for the interfacial impedance, Z_i, in the absence of surface effects,ie when the form of the impedance is due solely to adsorption effects. Delevie represented Z_i by a simple capacitance, however our results indicate that a Z_{CPA} impedance would be more appropriate. More complex expressions for Z_i should, of course, be essayed;

2) representing the electrode surface grooves with more complex network models, for example, with 'tapered transmission lines' (Delevie, 1965), and with poly-dimensional 'branched ladder networks' (Scheider,

1975); and

3) incorporating distribution functions into the expression for the interfacial impedance which describe the dispersion of the pores over the electrode surface (Edeling et al, 1983) and the range of pore diameters and depths.

It was shown that electrode history has a very important effect on interfacial impedance. The magnitude of K is observed to increase and that of β to decrease with time after immersion of the electrodes into the electrolyte (Gray and Svaetichin, 1951). Cleaning the electrodes, and thus removing the adsorbants, reverses to some extent the above changes. Inspite of such cleaning, experimental results are not reproducable to an acceptible degree (Gray and Svaetichin) and care must therefore be taken in the interpretation of experimental results. Experiments investigating the effect on the interfacial impedance of varying the magnitude of a certain parameter should be carried out over the shortest possible period of time (yet allowing sufficient time for the electrode system to reach a pseudo equilibrium before taking measurements) in order to minimise changes in the impedance due to electrode histroy. The experiments should also be repeated several times where possible and the order of the experiments varied to establish the relative changes in the inter-electrode impedance with changes in the parameter of interest.

A detailed study of the changes in electrode impedance with time is very necessary. Bottelbergh (1976) has suggested that the increase in K is

proportional to the quantity of electricity passed. This statement brings to mind Faraday's law which states that the amount of a product formed at an electrode is directly proportional to the quantity of electricity passed (Denaro, 1971). The observed increase in K is indicative of a gradual decrease in surface coverage of the ions responsible for the capacitive effect. Presumably other ions and impurities adsorb onto the surface and thus displace or block those ions generating the pseudo capacitance. It was observed in later chapters that the change in K was more pronounced after experiments carried out at low frequencies (Chapter 2) or in the nonlinear region (chapters 4 and 5). In these regions the "Faradaic" resistance, R_{CT}, due to the transfer of charge across the interface, plays a more significant role in the interfacial impedance. It is therefore very probable that the passage of faradaic current and the reactions involved in the transfer of this charge at the interface give rise to the observed changes in K and β. This would be in concord with Delahay's (1966) observation that the faradaic and nonfaradaic impedances cannot be assumed to be separate and independent of each other. The investigation of the relationship between the magnitude of K and β and the total faradiac charge passed across the interface should prove rewarding.

The development of a technique which successfully removes the materials adsorbed onto the electrode surfaces and enables experimental results to be

reproduced to a more acceptable level would obviously be most useful. Although several methods for cleaning elctrodes have been suggested in the past, these do not appear to have been rigorously investigated and it is feared that in some cases these may alter the electrical properties of the interface.

It was shown that rough surfaced electrodes are 'better' than smooth, ensuring stable fixation, minimal fibrous tissue growth, low stimulation thresholds and small interfacial impedances. It was, however, pointed out that comparison of electrodes under small signal, linear ac impedance conditions may not be relevent to nonlinear pulse conditions, as the interfacial impedance is known to be very nonlinear.

8.2 Chapter 2

It was established that at very low frequencies the inter-electrode impedance locus deviates from Z_{CPA} behaviour and eventually reaches a purely resistive value at $\omega = 0$. Several physical explanations suggested in the literature have been reviewed and found inadequate.

It was shown that the impedance locus forms an arc describable by equation 2.1. Onaral and Schwan (1982) were however first to publish this observation.

This expression can be represented by a Z_{CPA} shunted by a parallel resistance, Rp, where

$Rp = Ro - R_\infty$ and $Z_{CPA} = (Rp/\gamma^\beta)\ (j\omega)^{-\beta}$

The author has equated the parallel resistance

with that due to the transfer of charge across the electrode-electrolyte interface. This is an important postulation as many aspects of the interfacial impedance can now be physically interpreted for the first time.

It was shown that surface finish affects the magnitude of the parallel charge transfer resistance as well as, though to a lesser degree than, that of the high frequency, constant phase angle impedance. One must therefore take into account these effects and not simply assume that R_{CT} shunts the surface dependent Z_{CPA} impedance.

The expression for Z_1 in Delevie's finite transmission line model was therefore altered to incorporate the charge transfer resistance, shunting the low frequency, surface independent, $Z_{CPA(LF)}$ impedance (or C_{LF}).

This modification resulted in impedance loci similar to those found experimentally in this study. For very rough surfaced electrodes the locus forms two arcs, one at high frequencies which characterises the impedance of the rough surface and one at lower frequencies which is characteristic of the electrode interface in the absence of surface effects. The latter impedance has larger values of β, K and R_{CT} relative to the former, high frequency arc. Generally however, the high frequency arc appears only as a 'kink' at the high frequency end of the low frequency, 'smooth surface' arc. Although such behaviour can be observed on impedance arcs published in the literature,

it has not, to the author's knowledge, been hitherto explained.

Obviously, the improvements to Delevie's model mentioned in section 8.1 apply to the above model. A study of the effects the various parameters of the model have on the form of the resultant impedance locus should prove most enlightening.

The value of the charge transfer resistance was observed to decrease with time thus indicating that the ions adsorbing onto the electrode surface facilitate the flow of faradaic current.

It was pointed out that the magnitude of the charge transfer resistance is a measure of the 'polarisability' of an electrode system. An electrode-electrolyte interface which has a large value of charge transfer resistance is therefore said to be polarisable - ie its potential will deviate from its equilibrium, "reversible" value upon the passage of dc, or faradaic current, thus giving rise to a large "over-potential".

Electrodes which are relatively non-polarisable (ie where R_{CT} is small) are desirable for stimulation purposes. Rough surfaced electrodes were found to have significantly lower values of R_{CT} than those with "smooth" surfaces. It is now common for pacemaker manufacturers to roughen the surfaces of their electrodes in order to exploit this and other advantages.

8.3 Chapter 3

The equivalent circuit models derived from the analysis of transient responses of electrode systems were reviewed and it was shown that the same model as derived under ac conditions applied.

8.4 Chapter 4

It was in this chapter that the major contributions of the thesis to the study of electrode impedance were made. These were largely due to the observation that the parallel resistance in the equivalent circuit model is that due to the transfer of charge across the interface.

The charge transfer resistance is derived from the dc current-voltage characteristic which is describable by the Butler-Volmer expression (eqn 1.19). The derived "resistance" is very nonlinear and is the major source of the overall interfacial impedance's nonlinearity.

The nonlinearities of Z_{CPA} and R_{CT} were derived from first principles and investigated experimentally. It was found that Z_{CPA} (and hence K and β) is relatively linear, only decreasing significantly in magnitude for voltages above approximately 250 mV. In this region the adsorption pseudo capacitance increases rapidly which leads to the observed decrease in K and β. R_{CT} on the other hand, became nonlinear at voltages

around 20 mV and decreased approximately linearly with applied current amplitude and exponentially with applied voltage amplitude.

As low frequency points on an impedance locus are dominated by the parallel resistance, R_{CT}, they become nonlinear before those at higher frequencies which are controlled by the relatively linear Z_{CPA} impedance. It therefore takes progressively larger signal amplitudes to cause higher frequency points to become nonlinear.

An expression for the "limit current of linearity", ie the current required to cause a point of frequency, $f_{10\%}$, to deviate by 10% from its linear value, was derived based on the proposed equivalent circuit model. The expression (eqns 4.79, 4.81, 4.83) was found to have the form $i_L \propto \omega_{10\%}^{\beta}$ for a wide range of frequencies [note that at high and low frequencies i_L will limit at values where Z_{CPA} and R_{CT} respectively become nonlinear].

Such a relationship has been observed empirically in the past by Schwan and his colleagues but this is the first time the relationship has been physically interpreted.

It was shown that the magnitude of i_L is dependent on the axis used to monitor the 10% change in the impedance. This, apparently, has not been previously appreciated. It was also demonstrated for the first time that the value of the series resistive component of the impedance, R_s, initially increases (figures 4.9 and 4.25) before decreasing with applied signal amplitude.

Contrary to Schwan et al's statements, the limit voltage of linearity, V_L, varies with frequency. Very low frequency points become nonlinear at 40/n mV due to the nonlinearity of R_{CT} whereas at very high frequencies V_L tends to a limiting value at which Z_{CPA} becomes nonlinear (generally several hundred millivolts).

It was shown that electrodes which have the largest impedances in the linear, small signal region are the most nonlinear. The impedance of these electrodes decreases rapidly with applied signal amplitude and their relative performance therefore improves. Such electrodes are generally those with smooth surfaces. Rough surfaced electrodes have smaller impedances under linear conditions but these impedances decrease relatively little with signal amplitude. It is therefore incorrect to compare the impedances of pacing electrodes solely in the linear, small signal region - as is common in the literature.

It was demonstrated that the analysis of Lissajous figures prove useful in the study of electrode systems under large signal, low frequency conditions.

It was shown that the i-η curve, from which R_{CT} is derived, has at least two Tafel regions, and that these account for low frequency signal distortion, the form of the Lissajous figures and the deviation of the impedance loci from arcs at low frequencies.

It was pointed out that the flow of faradaic current should, as far as possible, be avoided as the reactions involved tend to give rise to toxic effects.

8.5 Chapter 5

In this chapter two techniques were developed to analyse the inter-electrode impedance under large amplitude, pacing pulse conditions. In the first, both the current and voltage waveforms are transformed into the frequency domain and the ac impedance derived prior to analysis. In the second, the transient responses of electrode systems to large amplitude pulses are analysed directly.

It was shown that the "3 component" model is inadequate in representing the inter-electrode impedance under these conditions. The reported dependence of the elements of this equivalent circuit on pulse duration is simply due to the model being incorrect.

It was demonstrated that K decreases with applied voltage amplitude and β appears to increase. The decrease in K is due to an increase in adsorption effects in this large signal region.

R_{CT} decreases pseudo exponentially with voltage and should decrease linearly with current amplitude.

Distorted arcs were in some cases observed, due to "high" frequency surface effects. This behaviour was anticipated in earlier chapters.

The proposed model succeeds in physically explaining many of the empirical observations of Schwan et al. Using the model it was shown, for example, that the limit current of linearity, $I_{dc}(10\%)$ is proportional to $t^{-\beta}$ and that the limit voltage of

linearity, V(t)10% is almost constant.

Some groups have in the past observed sinal distortion at low frequencies. Such behaviour has been identified with the nonlinear behaviour of R_{CT}.

Direct analysis of the response waveforms proved useful in many cases but was however inferior to the transformation technique.

It was shown that the decay ratio is related to K and β. As both these parameters decrease with surface roughness, the decay ratio proved to be a measure of surface finish. A large decay ratio indicates a 'smooth' surfaced electrode.

Plotting log-log plots of the current decay versus time enables the estimation of K and β for an electrode. The applied voltage should however be a good squarewave and its magnitude should vary little with pacer loading.

It was pointed out that under pacing conditions the interfacial impedance is very small relative to R_{TOT}. It is therefore more important to minimise the resistances of the leads, R_{LEAD}, in an effort to reduce energy loses, rather than further decreasing the already small interface impedance. This apparently is not widely appreciated.

8.6 Chapter 6

It was shown that a coiled lead wire behaves somewhat like a porous surfaced electrode, especially when the exposed area is small. The impedance locus of

the lead wire-electrolyte interface is concave and the values of K and β are relatively small compared to those of the electrode tip interface impedance.

-Insulation rupture

For an electrode with an insulation rupture the electrode tip impedance is shunted by that of the exposed lead wire. The magnitude of the overall impedance therefore decreases, as does its phase angle.

At high frequencies the form of the overall impedance is still, however, dominated by that of the electrode tip. As the frequency decreases, the impedance of the exposed lead wire begins to dominate the form of the overall electrode impedance.

The small impedance of the 'rough surfaced' lead wire is relatively linear and decreases little with applied signal amplitude. In the nonlinear region the magnitude of the electrode tip impedance is found to be comparable with that of the exposed lead wire. The magnitude of the overall impedance is therefore approximately one half of that of the electrode tip interface and its phase angle lies between those of the electrode tip and the insulation rupture.

-Wire fracture

For an electrode with a 'wet' lead wire fracture, two additional lead wire-electrolyte interface impedances are in series with that of the electrode tip. The overall inter-electrode impedance is therefore observed to increase in magnitude and decrease in phase angle. The large fracture impedance dominates the form of the overall electrode impedance

for a wide range of frequencies thus resulting in a concave impedance locus.

In the nonlinear region the impedance of the wet fracture is still considerably larger than that of the electrode tip. The former therefore dominates the overall impedance which is large in magnitude and low in phase angle.

8.7 Chapter 7

It was shown that although the composition of body fluid differs from that of physiological saline, the interfacial impedances have the same form, differing only in the relative magnitudes of the equivalent circuit parameters.

It was established that surface effects largely determine the form and magnitude of the interfacial impedance. In this case the interelectrode impedance is very sensitive to electrolyte resistivity. As body fluid / tissue is more resistive than saline, R_{TOT}, K and R_{CT} are larger invivo and β is smaller.

It was demonstrated that certain pacemakers are sensitive to the changes in their loading due to electrode failure and respond to these changes with characteristic variations in pulse rate and duration. Monitoring of these two temporal features has enabled the detection and classification of electrode failures, sometimes even in a latent stage before pacing failure had occured.

APPENDIX 1

References

REFERENCES

AMUNDSON,D., McARTHUR,W., MacCARTER,D., MOSHARRATA,M. (1979) Proceedings VI World Symp. Cardiac Pacing, Montreal, 29 - 16

ARMSTRONG, R.D. and BURNHAM, R.A. J. Electranal. Chem. 72, 257-266

ARMSTRONG, R.D., RACE, W.P. and THIRSK, H.R. (1968) Electrochimica Acta 13, 215 - 39

J. Electroanal. Chem 16, 517 - 529

BARD, A.J. and FAULKNER, L.R. (1980) "Electrochemical Methods", John Wiley and Sons

BERGVELD, P. (1976) Med. & Biol. Eng. & Comput. 14, 479 - 482

BLOCK, M.T. (1968) Med. & Biol. Eng. & Comput. 6, 517 - 525

BOCKRIS, J. O'M. and CONWAY, B.E. (1958) J. Chem. Phys. 28, 707 - 716

BOCKRIS, J. O'M., GILEADI, E. and MULLER, K. (1966) J. Chem. Phys. 44, 1445 - 1456

BOCKRIS, J. O'M and DRAZIC (1972) "Electro-Chemical Science", Taylor & Frances Ltd,London

BOCKRIS, J. O'M and REDDEY, A.K.N. (1970) "Modern Electrochemistry", Plenum Press, New York

BORISOVA, T., ERSHLER, B. and FRUMKIN,A. (1950) Zh. Fiz. Kim. 24, 337 - 344

BOTTELBERGHS, P.H. (1976) Thesis, University of Austria

BREITER, M.W. (1963) Electrochimica Acta 8, 925 - 935

BRIGHAM, G.O. (1974) "The Fast Fourier Transform" Englewood, Cliffs.

BRILLER, S.A., GESELOWITZ, D.B., ARLINGER, S.D., DANIELSON, G.K., JARON, D. and JOYNER, C.R. (1966) Am. Heart J. 71, 656 - 665

BROWNSTEIN, M. (1982) PhD Thesis, Drexel University, Philadelphia

BRUMMER, S.B. and ROBBLEE, L.S. (1983) Ann. N.Y. Acad. Sci. 405, 159 - 171

BRUMMER, S.B. and TURNER, M.J. (1975) Bioelectrochem. Bioenergetics 2, 13 - 25

BRUMMER, S.B. and TURNER M.J. (1977) IEEE Trans. BME 24, 59 - 63

BUCK, R.P. (1968) J. Electroanal. Chem. 18, 381 - 386

CHAPMAN, D.L. (1913) Phil. Mag., 25, 475

CARIM, H.M., BEARD, R.B. and MILLER A.S. (1977) J. Electrochem. Soc. 124 (5) 680 - 688

CHABLI, A., DIARD, J.P., and LE GORREC. B J. Appl. Electrochem. 12, 585 - 590

CHARDACK, W.M., GAGE, A.A., FREDERICO, A.J., SCHIMERT,G. and GREATBATCH, W. (1964) Ann. N.Y. Acad. Sci. 111, 1075 - 1092

CLYNES, M. and MILSUM, J.H. (1970) in "Biomedical Engineering Systems",McGraw-Hill 133-155

COLE, K.S. (1934) Science. 79, 164 - 165

COLE, K.S. and CURTIS, H.J. (1938) J. Gen. Physiol. 22, 37 - 64

COLE, K.S. and COLE, R.H. (1941)
J. Chem. Phys. 9, 341 - 351

COLE, K.S. and COLE, R.H. (1942)
J. Chem. Phys. 10, 98 - 105

CONWAY, B.E. and GOTTESFELD, S. (1973)
J. Chem. Soc. Farad. T1. 69, 1090 - 1107

CREASON, S.S., HAYES, J.W. and SMITH, D.E. (1973)
J. Electroanal. Chem. 47, 9 - 46

DAVES, J.G. and SIDDONS. H. (1969) Thorax 24, 74

De BOER, R.W. and VAN OOSTEROM, A (1978)
Med. & Biol. Eng. & Comput. 16, 1 - 10

DEBYE, P. (1929) in "Polar Molecules"
Chemical Catalogue Company, N.Y.

DELAHAY. P. (1961)
in " Adv. Electrochem. & Electrochem. Eng."
1, 233 - 318 ; Ed. Delahay & Tobias; J. Wiley & Sons

DELAHAY, P. (1968) J. Electroanal. Chem. 16, 61

DELAHAY, P. and SUSBIELLES, G.G. (1966)
J. Phys. Chem. 70(10) 3150-3157

DELEVIE, R. (1964) Electrochem. Acta, 9, 1231-1245

DELEVIE. R. (1965) Electrochem. Acta, 10, 113-130

DELEVIE. R. (1967)
in "Adv. Electrochem. & Electrochem. Eng."
6, 330 - 397 ; Ed. Delahay & Tobias; J. Wiley & Sons

DENARO, A.R. (1971) "Elementary Electrochemistry"
Butterworths, London - Boston

De ROSA, G.F. and BEARD, R.B. (1977)
IEEE Trans. BME 24, 260 -268

DOLIN, P. and ERSHLER, B. (1940)
Acta Physiochem. URSS 13, 747

DONALDSON, N. deN. and DONALDSON, P.E.K. (1986)
Med. & Biol. Eng. & Comput. 24, 41 - 49

DYMOND, A.M. (1976)
IEEE. Trans. BME 23, 274-280

EDELING, M., MUND, K. and NASCHWITZ, W. (1983)
Siemens Research & Development Reports 12 (2) 85-90

ELMQVIST, H., SCHUELLER, H. and RICHTER, G. (1983)
Pace, 6, 436 - 439

EPELBOIN, I. and KEDDAM, M. (1970)
J. Electrochem. Soc. 117, 1052

ERSCHLER, B. (1947) Disc. Far. Soc. 1, 269-277

FALK, G. and FATT, P. (1964)
Proc. Roy. Soc. B. 160, 69 - 123

FISCHLER, H. (1979) Pace. 2, 403 - 416

FISCHLER, H and SCHWAN, H.P. (1981)
Med. & Biol. Eng. & Comput. 19, 579 - 588

FITZHUGH, R. and COLE, K.S. (1973)
Biophys. J. 13, 1125 - 1140

FURMAN, S. (1977) Am. Heart J. 94 (3) 378 - 386

FRANKLIN, A.D. (1975) J. Am. Cer. Soc.
58 (11 - 12) 465 - 473

FRICKE, H. (1932) Phil. Mag. 7 (14) 310 - 318

FRICKE, H. and CURTIS, H.J. (1936) J.Phys.Chem. 40, 715

FRICKE, H. and CURTIS, H.J. (1937) J.Phys.Chem. 41, 729

FRUMKIN, A.N.(1960) J. Electrochem. Soc. 107, 461

FRUMKIN, A.N. and MELIK-GAIKAZAYAN, V.I. (1951)
Ber. Akad. Wiss. Ud. SSR 77, 855

GEDDES, L.A. and BAKER, L.E. (1967)
Med. & Bio. Eng. & Comput. 5, 271 - 293

GEDDES, L.A., DA COSTA, C.P. and WISE, G. (1971)
Med. & Bio. Eng. & Comput. 9, 511 - 521

GESTELAND, R.C., HOWLAND, B., LETTVIN, J.Y. and
PITTS, W.H. (1959) Proc. IRE. 1856

GIBBS, J.W. (1877-1878) Trans. Connecticut. Acad.

GILEADI, E. and CONWAY, B.E. (1964)
in "Modern Aspects of Electrochem." Vol 3, 347 - 442
Eds. Bockris, J.O'M. and Conway B.E.; Butterworths,
London

GOUY, G. (1910) J. Phys. Radium 9, 457 - 468

GRAHAME, D.C. (1946) J.Amer.Chem.Soc. 68, 301-310

GRAHAME, D.C. (1952) J.Electro.Soc. 99, 370C - 385C

GRAY, J.A.B. and SVAETICHIN, G. (1951)
Acta Physiol. Scand. 24, 278 - 284

GREATBATCH, W. and CHARDACK, W.M. (1968)
Ann. N.Y. Acad. Sci. 148, 234 - 251

GREATBATCH, W., PIERSMA, B., SHANNON, F.D. and
CALHOON, S.W. (1969)
Ann. N.Y. Acad. Sci. 167, 722 - 744

GREEN, G.D., FORBES, W., BAIN, W.H., SHAW, G.B. and
KENMURE, A.C.F. (1969) Brit, Heart, J. 31, 707

GULD, C. (1963) Acta Physiol. Scand. 59, 57

HEPBURN, F. (1977) IEE. Med. Electronics Monographs
5 (24) 30 - 57

HEPBURN, F. (1978) J. Med. Eng. Tech. 3, 130

HEPBURN, F. (1979) Brit. J. Clin. Equip. May, 98 - 113

HOARE, J.P. (1967)
in "Adv. Electrochem & Electrochem. Eng."
Vol 6, 201 - 288. Ed P.Delahay; John Wiley & Sons, N.Y.

HOLUB, K., TESSARI, G. and DELAHAY, P. (1967)
J. Phys. Chem. 71 (8) 2612-2618

HOPKINSON, J. and WILSON, E. (1897)
Phil. Trans. Roy. Soc. Lond. Ser.A., 189, 109 - 135

HYDE, G.R. (1971) J. Am. Ceram. 54 (11) 535

ISEKI, S., OHASHI, K. and NAGAURA, S. (1972)
Electrochem. Acta, 17, 2249 - 2265

JARON, D., SCHWAN, H.P. and GESELOWITZ, D.B. (1968)
Med. & Biol. Eng. & Comput. 6, 579 - 594

JARON, D., BRILLER, S.A., SCHWAN, H.P. and
GESELOWITZ, D.B. (1969)
IEEE. Trans. BME. 16, 132 - 138

KAUL, T.K., GREEN, D.G. and BAIN, W.H. (1979)
Europ. J. Cardiology 10/5, 385 - 394

KINGMA,Y.J.(1977) Med. & Biol.Eng & Comput.15, 327-332

KNUCKEY, L., McDONALD, R., SLOMAN, G. (1965)
Brit. Heart J. 27, 483 - 489

KRAMERS, H.A. (1927) Atti Congr. Fisici. Como. 545

KRONIG, R. de L. (1926) J. Opt. Soc. Amer. 12, 547

LAITINEN, H.A. and RANDLES, J.E.B. (1955)
Trans. Far. Soc. 51, 54

LAXMINARAYAN, S., LAXMINARAYAN, R., LANGEWOUTERS, G.L.,
and VOS, A.V.D. (1979)
Med. & Biol. Eng. & Comput. 17, 623 - 628

LEIKIS, D.I. and KABANOV, B.N. (1957)
Tr. Inst. Fiz. Khim. Akad. Nauk. SSSR 6

LILLY, J.C., HUGHES, J.R., ALVORD, JR. and GALKIN, T.W.
(1955) Science 121, 468 - 469

LITTAUER, E.L. and SCHREIR, L.L. (1966)
Electrochemica Acta 11, 527 - 536

LLOPIS, J., FERNANDEZ-BIARGE, J., and
PEREZ-PERNANDEZ, M.(1959) Electrochem. Acta 1, 130-145

LORENZ, W. (1958) Z. Elektrochem. 62, 192

LORENZ, W. and MOCKEL, F. (1956)
Z. Elektrochem. 60, 507, 939

MANSFIELD, P.B. (1967) Am. J. Physiol. 212(6) 1475-1488

MAYELL, J.S. and LANGER, S.H. (1964)
Electrochemica Acta 9, 1411 - 1416

MELDRUM (1982) Written Communication

MORKRID, L., OHM, O.J. and HAMMER, E. (1980)
Med. & Biol. Eng. & Comput. 18, 223 - 232

MORTENSEN, B.T. and BOJSEN, J. (1982)
J Bio. Med. Eng. 4(2) 103 - 106

MUND, K., RICHTER, G., WEIDLICH, E., VON STURM, F. and
DAVID, E. (1976)
Bielectrochem. & Bioenergetics 3, 272 - 283

MUND, K., RICHTER, G., WEIDLICH, E., VON STURM, F. and
DAVID, E. (1977)
IV Nordic Meet. Med. Biol. Eng. Copenhagen 29 - 6

MUND, K., RICHTER, G., WEIDLICH, E., VON STURM, F. and
DAVID, E. (1979)
Siemens Research & Development Reports. 8(4) 227 - 234

NOVAK, D.M. (1979)
J. Electrochem. Soc. 126(5) 209C - 212C

NOVAK, D.M., TILAK, B.W. and CONWAY, B.E. (1982)
in "Modern Aspects of Electrochem." 14, 195 - 318
Eds Bockris, J.O'M. and Conway, B.E.,Plenum Press, N.Y.

NOWOTNY, R. and NOWOTNY, C.H. (1980)
Med. & Biol. Eng. & Comput. 18, 979 - 782

OHM, O.J. (1979) Pace 2, 465 - 485

OHSAKA, T., SAWADA, Y., YOSHIDA, T and NIHEI, K.(1976)
J. Electrochem. Soc. 123(9) 1339 - 1345

ONARAL, B. and SCHWAN, H.P. (1982)
Med. & Biol. Eng. & Comput. 20, 299 - 306

ONARAL, B. and SCHWAN, H.P. (1983)
Med. & Biol. Eng. & Comput. 21, 210 - 216

ONARAL, B., SUN, H.H. and SCHWAN, H.P. (1984)
IEEE. Trans. BME. 31 (12) 827 - 832

PILLA, A.A. (1970) J. Electrochem. Soc. 117(4) 467-477

POLLAK, V. (1974)
Med. & Biol. Eng. & Comput. 12, 454 - 459, 460 - 464, and 606 - 612

POON, C.S. and CHOY, T.T.C. (1978)
Med. & Biol. Eng & Comput. 16, 633 - 641

PRESTON, T.A., JUDGE, R.D., BOWERS, D.L. and MORRIS, J.D. (1966) Am. Heart J. 71, 92 - 99

RAMALEY, L. and ENKE, C.G. (1965)
J. Electrochem. Soc. 112 (9) 947 - 950

RANDLES, J.E.B. (1947) Disc. Far. Soc. 1, 11 - 19

RANDLES, J.E.B. and SOMERTON, K.W. (1952)
Trans. Fraday Soc. 48, 937, 951

REINMUTH, W.H. (1968) Anal. Chem. 40 (5) 185R - 194R

RICHTER, G.J., WEIDLICH, E., STURM, F.V., DAVID, E., BRANDT, G., ELMQVIST, H. and THOREN, A. (1979)
Proc. VI World Symp. Cardiac Pacing, Montreal
Chapter 29 - 13

RIPART, A. and MUGICA, J. (1983) Pace 6, 410 - 421

SALTER, D.C. (1979) in "Non invasive Physiological measurements" 1, 21 - 64; Ed P. Rolfe; Academic Press

SCHEIDER, W. (1975) J. Phys. Chem. 79 (2) 127 - 136

SCHUHMANN, D. (1966) C.R. Acad. Sc. Paris. 262, 624-627

SCHUHMANN, D., CONTAMIN, O. and LEVART, E. (1977)
J. Electroanal. Chem. 84, 287 - 293

SCHWAN, H.P. (1957) Adv. Biol. Med. Phys. 5, 147-209

SCHWAN, H.P. (1963) Phys. Techn. Biol. Res. 6, 323-406

SCHWAN, H.P. (1968) Ann. N.Y. Acad. Sci. 148, 191-209

SCHWAN, H.P. and ONARAL, B. (1985)
Med. & Biol. Eng. & Comput. 23, 28 - 32

SENDA, M. and DELAHAY, P. (1961)
J. Phys. Chem. 65, 1580 - 1588

SHIGEMITSU, T., MATSUMOTO, G. and TSUKAHARA, S. (1979)
Med. & Biol. Eng. & Comput. 17, 465 - 470

SIMPSON, R.W., BERBERIAN, J.G. and SCHWAN, H.P. (1980)
IEEE. Trans. BME. 27 (3) 166 - 171

SLUYTERS, J.H. (1960) Recl. Trav. Chim. Pays-bas
79, 1092 - 1110

SLUYTERS - REHBACH, M. and SLUYTERS, J.H. (1970)
in "Electroanalytical Chemistry"; 4, 1 - 128
Ed A.J. Bard; Dekker, New York 4, 1 - 128

SOWTON, E. (1967) Israel J. Med. Sci. 3 (2) 260 - 269

SOWTON, E. and GRAY, K. (1971) Thorax 26, 145 - 154

SPADARO, J.A. and BECKER, R.O. (1979)
Med. & Biol. Eng. & Comput. 17, 769 - 775

STERN, O. (1924) Z. Elektrochem. 30, 508 - 516

STIBITZ, G.R. and McCANN, F.V. (1974)
Biophysical J. 14 (2) 75

TAKAHASHI, K. (1968) Electrochemica Acta 13, 1609

THIRSK, H.R. and HARRISON, J.A. (1972)
"A Guide to the study of Electrode Kinetics"
Academic Press, London

THOMAS, A.B. (1964) J. Phy. Chem. 68 (11) 3363

TIMMER, B., SLUYTERS-REHBACH, M. and SLUYTERS, J.H. (1967) J. Electroanal. Chem. 15, 343 - 357

TIMMER, B., SLUYTERS-REHBACH, M. and SLUYTERS, J.H. (1968) J. Electroanal. Chem. 18, 93 - 106

TURNEY, S.Z., NEUMAN, M.R., KO, W.H. and KENNEDY, J.H. (1967) VII Int. Conf. Med. & Biol. Eng. Stockholm, Sweden 2-10

WAPENAAR, K.E.D. and SCHOONMAN, J. (1981) Solid State Ionics 2, 253 - 263

WARBURG, E. (1899) Ann. Physik Und Chemie 67, 493-499

WEIN, M. (1896) Ann. Phys. 58 (2) 37 - 72

WEINMAN, J. and MAHLER, J. (1959) Proc. II Int. Conf. Med. Electronics, Paris Ed C.N. Smyth; Iliffe, London. 18 - 24

WEINMAN, J. and MAHLER, J. (1964) Med. Electron. & Biol. Eng. 2, 299 - 310

WILSON, G.I., McGREGOR, D.C., BOBYN, J.D., LIXFELD, W., PILLIAR, R.M., MILLER, S.L. and SILVER, M.D. (1983) Proc. VI World Sym. Cardiac Pacing, Montreal, 29 - 12

WOLFF, I. (1926) Phys. Rev. 27, 755 - 763

YAMAMOTO and YAMAMOTO (1981) Med. & Biol. Eng. & Comput. 19, 302 - 310

ZEUTHEN, T. (1978) Med.& Biol.Eng.& Comput. 16, 483-488

ZEUTHEN, T. (1978) Med.& Biol.Eng.& Comput. 16, 489-499